Nanostructured hydrogel films for encapsulation and release

Wasbrough, Matthew

Award date:
2011

Awarding institution:
University of Bath

Nanostructured hydrogel films for encapsulation and release.

Matthew John Wasbrough
A thesis submitted for the degree of Doctor of Philosophy
University of Bath
Department of Chemistry
November 2011

Acknowledgements

Firstly I would like to thank Karen Edler for her support and guidance throughout my final year as an undergraduate and during my time as a PhD student. There were times, particularly during the first year, when things were harder than they should have bean, however I hope in hindsight she would agree it was worth it. Along with Karen I would also like to thank Gareth Price for his support and the regular reminders to always try and look at other perspectives.

From with the Edler research group I would particularly like to thank Adrian Hawley, who got me through my experiments and been a great support, and Jim Holdaway, who has been a constant sounding board and fountain of knowledge, even when I only needed a simple answer. I am also especially thankful to Jim for his support on numerous experiments at facilities, I hope I was able to repay this help by helping on enough of his experiments.

As well as these particular people I would like to thank all the other members of the Edler, Price, and Roser research groups who I have had the pleasure of working with throughout my time in Bath. I would also like to thank all other members of the University of Bath Department of Chemistry who have helped me, it has been a lovely department to be a member of.

Outside of the Department of Chemistry I would like to express my thanks and appreciation to all the scientists at ISIS, the ILL, the ESRF, ANSTO and NIST who have helped when performing the various experiments that have given the majority of the results throughout this thesis.

Finally on a personal note I would like to thank my family for their continued support and enthusiasm, particularly my wife Rosie. She has had to put up with my, fairly regular, absences for experiments, and my strange working habits. Her support and encouragement has been the backbone onto which this thesis has been built.

Abstract

We have been investigating solutions of surfactants and polyelectrolytes that are able to spontaneously form micron thick hydrogel films at the air/solution interface. Previous research within the group has shown that the surfactant can act as a templating agent for the polymer hydrogel, leading to well ordered mesostructured films similar to those seen in surfactant templated inorganic materials or polymeric layer-by-layer films, which have both been highly active areas of research over the past 20 years. This project built on the previous research within the group to develop a greater understanding of these films and how they may be controlled and used for real world applications. This thesis concentrates on two areas; the first is films made from a cationic surfactant/polymer system and the second from a cat-anionic surfactant/polymer system.

Using the cationic surfactant/polymer system, we built on the previous research by altering the head group area to tail volume ratio of the surfactants being used to allow control over the final mesostructure within the films. Small angle neutron scattering (SANS) was used to study the bulk solution while neutron and x-ray reflectivity and grazing incidence diffraction were used to study the films. Using this system we have also developed the previous work, studying the incorporation of sparingly soluble species in films, by studying the encapsulation of hydrophobic and amphiphilic species into the surfactant micelles and therefore into the films as a function of micelle and film structure. We have also studied, using Fluorescence spectroscopy, the subsequent release of these species from the films.

The cat-anionic surfactant/polymer system was discovered more recently and therefore has not had as much previous research performed on it. It is of particular interest because it allows films to be formed from a variety of different polymers where the cationic system currently has only been found to form films with one polymer. Using this cat-anionic system we have studied the surfactant interactions in the bulk with SANS, ultra-SANS and spin-echo-SANS to determine the structure over a wide length range. This data is compared to cryo-SEM results. In particular cryo-SEM and USANS have been used to validate modelling from the new technique of SESANS. We then studied the film formation with x-ray and neutron reflectivity. As well as forming from a wider range of polymers, these films are much thicker and more robust, which may be due to the larger scale aggregates formed in solution.

List of Abbreviations

BAM	Brewster Angle Microscopy
BT5	USANS Instrument, NCNR
C_{12}TAB	Dodecyltrimethylammonium Bromide
C_{14}TAB	Tetradecyltrimethylammonium Bromide
C_{16}TAB	Hexadecyltrimethylammonium Bromide
CTEAB	Hexadecyltriethylammonium Bromide
CAC	Critical Aggregation Concentration
CMC	Critical Micelle Concentration
C_nTAB	Alkyltrimethylammonium Bromide
D11	SANS Instrument, ILL
$dC_{16}dTAB$	Fully deuterated C_{16}TAB
$dC_{16}TAB$	Tail deuterated C_{16}TAB
DDAB	Didodecyldimethylammonium Bromide
EGDGE	Ethylene Glycol Diglycidyl Ether
ESRF	European Synchrotron Radiation Facility, Grenoble, France
FIGARO	Neutron Reflectometer, ILL
GIXD	Grazing Incidence X-ray Diffraction
ID10B	X-ray Reflectometer, ESRF
ILL	Institut Laue-Langevin, Grenoble, France
LOQ	SANS Instrument, ISIS
LPEI	PEI with a molecular weight (M_w) of 750,000Da
LPEO	PEO with a molecular weight (M_v) of 100,000Da
NCNR	NIST Centre for Neutron Research
NG7 Reflectometer	Neutron Reflectometer, NCNR
NG7 SANS	SANS Instrument, NCNR
NIST	National Institute of Standards and Technology, Gaithersburg, Maryland, USA
OFFSPEC	SESANS Instrument, ISIS
PAAm	Polyacrylamide with a molecular weight of (M_w) of 10,000Da
PEI	Polyethylenimine
PEO	Poly(ethylene oxide)
PLATYPUS	Neutron Reflectometer, ANSTO
SANS	Small Angle Neutron Scattering
SAXS	Small Angle X-ray Scattering
SDS	Sodium Dodecyl Sulfate
SEM	Scanning Electron Microscopy
SESANS	Spin-Echo Small Angle Neutron Scattering
SPEI	PEI with a molecular weight (M_w) of 2,000Da
SPEO	PEO with a molecular weight (M_v) of 10,000Da
SURF	Neutron Reflectometer, ISIS
USANS	Ultra-Small Angle Neutron Scattering

1 Introduction

1.1 General Introduction

Amphiphilic compounds are all around us and are an essential part of life on this planet. They are characterised by containing two regions that are alternately polar and apolar. Amphiphilic roughly translating as "friendly at both ends".[1] The polar region is often called the hydrophilic region and is directly connected to the apolar hydrophobic region, an example of a simple amphiphilic species is hexadecyltrimethylammonium ($C_{16}TA^+$), which is shown below, Figure 1-1. In this figure the polar region is labelled as the head group and is a quaternary ammonium species while the apolar region is the alkyl chain that makes up the tail. Not included here but usually found with charged amphiphilic species is a counter ion. Some charged amphiphilic species do not have a counter ion, but this is because they have two oppositely charged groups making them overall charge neutral. These species are known as zwitterionic compounds.

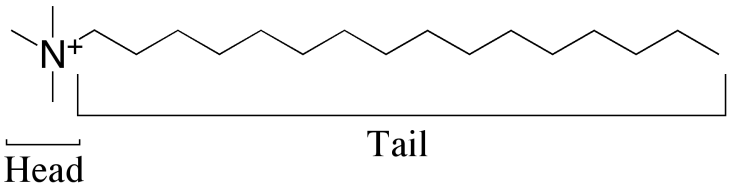

Figure 1-1. Hexadecyltrimethylammonium. Not included in the image is a counter ion.

Due to the different regions, when amphiphilic species are dissolved in a solvent one region will preferentially move to the interface or aggregate in solution. The amphiphilic species that are able to do this are termed surfactants and are known for their ability to lower the surface tension of a solution interface or form self-assembled structures within the bulk solution. The importance of this self assembling property of surfactants is clearly illustrated by lipids, a natural form of surfactants, which form membranes that are the basis for cell membranes in all living things.[2]

Almost as ubiquitous a range of compounds as amphiphiles are polymers. Polymers are characterised by being a chain of multiple repeats of one or more small sub units. Like amphiphiles they are commonly found in some of the building blocks of life, such as DNA. They have also been extensively used by humans for items such as paper, which is primarily made from the biopolymer cellulose. Natives in the Amazonian rainforests also used natural latex from the sap of rubber trees to create waterproof foot coverings prior to contact with western civilization.

Although natural surfactants and polymers are constantly around us, the development of synthetic polymers and synthetic surfactants are both relatively recent discoveries. The oldest of the two fields as a modern science is polymer synthesis which first started growing in the mid 19th century with Charles Goodyear developing the process of vulcanising rubber. Although it wasn't until 1907 when the first fully synthetic polymer was created by Leo Baekeland.[3]

What really drove the polymer industry on next, and what helped the surfactant industry get started was World War 2. For the polymer industry the demand for rubber in the build up and during the war lead to synthesis of synthetic rubber compounds. This was started in Germany but mirrored by the USA, particularly when Japanese occupation of the East Indies constricted supply of natural rubber sources. At the end of the war there was an excess of petroleum and petroleum related products, which meant an excess of cheap small alkane monomers.[3]

These small alkanes were also important to the surfactant industry, as they are also the basis for many, now common, surfactants. As with rubber in World War 2, the availability of the raw materials for soaps, animal and vegetable fats, were scarce during World War 1, which led to the development of synthetic alternatives. However it was the availability of short chain alkanes that helped the surfactant industry grow.[4]

Since this time both the surfactant and polymer industries have grown into strong industries in their own right. The polymer industry is known more for materials, such as food packaging and clothing while the surfactant industry is mainly known for soaps and detergents. In reality however the two industries are very closely linked with surfactants used in a lot of polymeric materials and polymers used in many surfactant industries. Examples of this are surfactants used in food packaging to help disperse clays within the polymeric material to improve its performance.[5] The opposite example is the use of polymer as thickening agents along with surfactants in cosmetic products.[6]

Due to the range of uses for systems involving mixtures of polymers and surfactants this has become a large area of research over the past few decades. This area of research has remained so big due to the diversity of systems that can be studied thanks to the differences available within surfactants or within polymers and the variety of molecular interactions that can play a role in forming their composites. The most common studies involve either oppositely charged surfactants and polymers or a charged species with a neutral species.[7]

In 2003 Edler et. al. published results from a study of a cationic surfactant with a weakly charged cationic polyelectrolyte.[8] This paper was the first to report the formation of thin, solid structured films formed from the interaction between the surfactant and the polymer. This paper is interesting as it appears to contradict the current understanding of polymer/surfactant interactions where like charged species would be expected to repel.

1.1.1 Surfactant Solution Behavior

In a pure solution the individual molecules feel attractive forces to the other molecules in the solution. If the molecules are in the bulk solution then these attractive forces are equivalent in all directions. However if the molecule is near the surface then these forces will only be in the direction of the bulk solution drawing the molecule into the solution. This inward pull of molecules causes the solution to minimise the surface area for a given volume, thus causing solutions to tend towards spherical when possible. This is known as the surface tension, γ, which defined as the force acting at right angles to any line of unit length on the surface of a solution, however it can also be defined as the energy required to increase the area of a surface isothermally and reversibly by a unit amount.[9, 10]

Using the definition of the surface tension as the energy required to increase the area of a surface by a unit amount, it is possible to directly measure the surface tension by measuring the force, F, required to alter the surface tension. This can be done using a flat plate, known as a Wilhelmy plate, of known width, x, and thickness, y, dipped into the surface of a solution. The surface tension can then be determined using Equation 1-1. It is important to note in this equation a correction to the force is important to account for the buoyancy of the Wilhelmy plate.

$$F = \gamma\, 2(x+y) \qquad \text{Equation 1-1}$$

When a solute is added to this solution the solute-solvent interactions will alter the forces within the solution. If the solute-solvent attraction is greater than the solvent-solvent interaction, as is the case in salt solutions, then more solvent will be forced to the interface surface causing an increase in the surface tension. However in many cases the solvent-solute interaction is not as strong as the solvent-solvent interaction meaning the addition of the solute causes the solute to concentrate at the surface, which leads to a decrease in the surface tension. In some miscible liquids, such as ethanol in water, the surface is more similar to ethanol than water as there is an

excess of ethanol at the surface caused by the strength of intermolecular forces in water. In an aqueous surfactant solution not only does the hydrophilic part get pushed to the interface due to weaker interactions between itself and the water, but also the hydrophobic part drags the surfactant to the interface where it can be out of solution while the hydrophilic part is still in solution.

In sufficiently dilute surfactant solutions it is possible to follow the amount of surfactant at the interface by slow addition of surfactant to the solution while measuring the surface tension of the solution. A theoretical plot of the change in surface tension as the concentration of surfactant is increased is shown in Figure 1-2. This plot is known as an adsorption isotherm, which is a plot of the adsorption at a constant temperature plotted against a measure of the bulk phase concentration of the adsorbing substance.

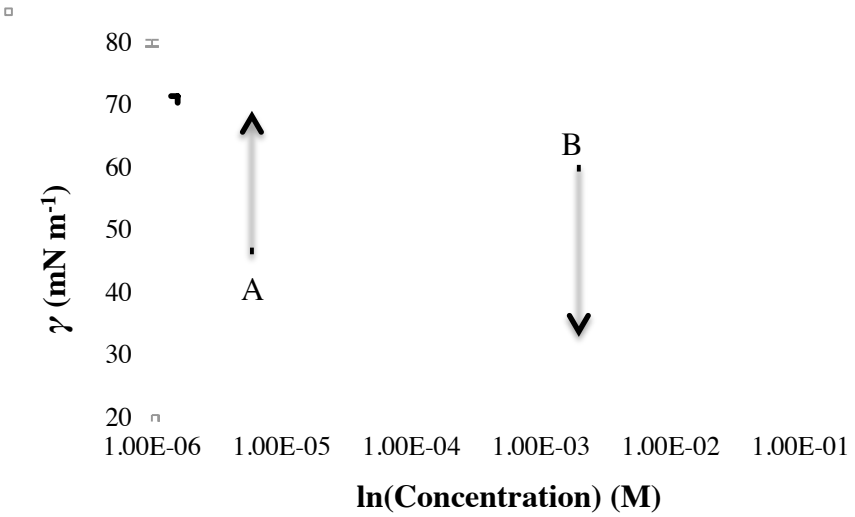

Figure 1-2. A theoretical adsorption isotherm.

Before the adsorption isotherm can be understood it is important to define the surface. Mathematically the surface is an infinitely thin line that separates the liquid phase from the gaseous phase. This however is not realistic, particularly in the case of surfactants being adsorbed to the surface, because molecules have a finite thickness. This is shown more clearly in Figure 1-3 where the mathematical surface between the phases a and b is given as SS. In a real surface the concentration of components varies between XX and YY giving a surface phase σ. Any difference between the concentration of the components in the interface phase, σ, compared to the concentration in the bulk phase, b, is then termed the surface excess concentration. The surface excess concentration is mathematically given in Equation 1-2, where Γ_i is the surface excess concentration of component i, n_i^{σ} is the number of molecules of component i in phase σ, and A is the area of the surface.

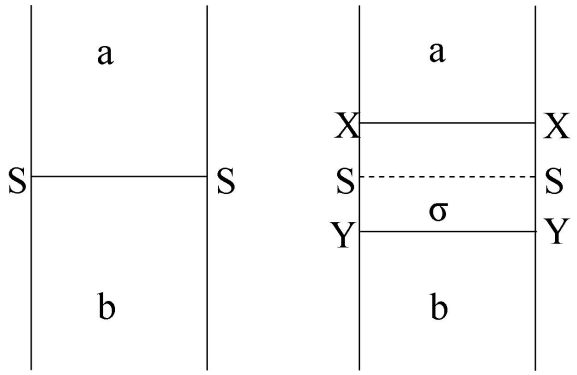

Figure 1-3. Representation of a mathematical (left) and real (right) surface between phases a and b, modified from Shaw.[9]

$$\Gamma_i = \frac{n_i^\sigma}{A} \qquad \text{Equation 1-2}$$

The surface excess is very dependant on where the surface SS is chosen. If the surface SS is chosen such that the surface excess concentration of the solvent is 0, then the surface excess concentration of the adsorbate will be positive indicating an increased concentration of adsorbate at the interface. The alternate is true if the surface SS is chosen such that the surface excess concentration of the adsorbate is 0 then the surface excess concentration of the solvent will be negative indicating a lower concentration of solvent at the interface.

The surface excess concentration of a substance adsorbed to the interface would be interesting to know but it cannot be measured. However in the 19th century J. W. Gibbs suggested that the major component, usually the solvent, should be chosen for the surface excess concentration to be 0, called the Gibbs dividing surface. He then went on to derive an equation, from the surface excess internal energy, to relate the surface excess concentration to the surface tension and the surface activity of the component, the full derivation is given by Barnes.[10] Making the assumptions that the system is a two component system, that the Gibbs dividing surface is used, and that the concentration of the adsorbate is approximately the same as the surface activity of the adsorbate, it is then possible to write the Gibbs equation as shown in Equation 1-3. In this equation R is the gas constant, T is the temperature and c_i is the concentration of adsorbate. The surface excess concentration can then be calculated from a plot of $d\gamma$ vs. $d\ln c_i$, which is shown in Figure 1-2.

$$\Gamma_i = -\frac{1}{\mathrm{RT}} \quad \frac{d\gamma}{d\ln c_i} \qquad \text{Equation 1-3}$$

Using the Gibbs equation, Equation 1-3, and studying the plot in Figure 1-2 two important transitions can be seen. Before point A the surface tension is constant, indicating that there is no surfactant at the interface, this is due to the concentration of surfactant being too small. Between point A and point B there is a decrease in the surface tension therefore there must be an increase in concentration of surfactant at the interface. Above point B the surface tension is again independent of the concentration of surfactant and this is due to saturation of the surface by the surfactant forming a monolayer. As the surfactant can no longer tend to the interface at point B it remains in the bulk where the hydrophobic tails interact to form micelles, therefore the concentration of point B is called the critical micelle concentration (CMC).

If the surfactant is charged then as the surface tension decreases and the concentration of free surfactant in the bulk solution increases then electrical conductance of the solution will also increase. As the concentration of surfactant increases past the CMC the electrical conductance of the solution will continue to increase but at a slower rate, this is due to two reasons. The first is that concentration of free surfactant molecules will remain roughly constant and therefore give the system a base electrical conductance. Secondly the concentration of unbound counter ions will continue to increase. The electrical conductance of the solution can be measured and where the gradient of the increase in electrical conductance changes this is then the CMC.[11] This is shown in Figure 1-4. This method of measuring CMCs may be more reliable than the surface tension method since it measures the formation of micelles directly rather than by inferring a connection with the surfactant packing at the interface.

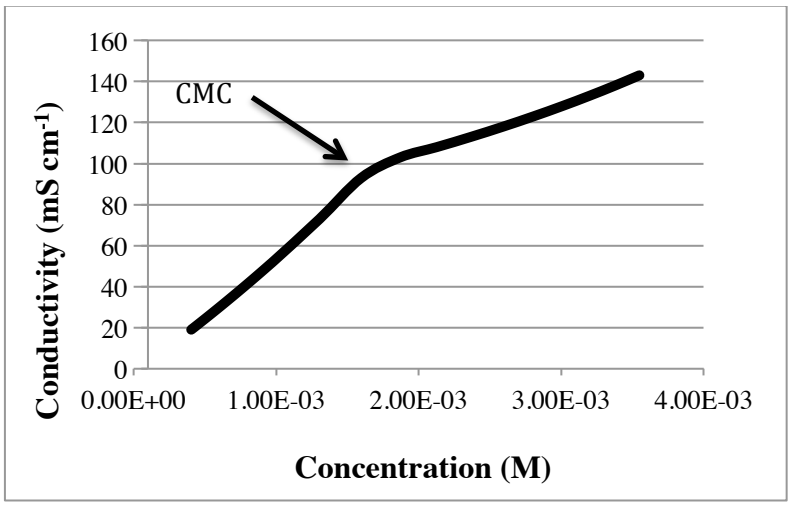

Figure 1-4. An idealised electrical conductivity plot showing the CMC.

1.1.2 Polymers

Polymers are macromolecules made up of repeating smaller units, known as monomers. The simplest polymer is a chain of repeating units, such as polyethylene, or can be more complex involving a chain cross-linking with other polymer chains to make a large network, such as DNA.[2] In this thesis the focus will be on fairly simple water-soluble polymers, which comprise a large range of compounds in their own right.[12-14]

One of the most important characteristics of a polymer is dependent on the chemical nature of the monomers that it is made of. A simple polymer such as polyethylene is made up of repeating ethane units $[-CH_2-CH_2-]_n$. Given the monomer unit cannot be charged, polyethylene in a neutral polymer in solution. When a polymer is made up of ionisable monomers, it can also be called a polyelectrolyte. There are also two types of polyelectrolytes; weak and strong polyelectrolytes. A strong polyelectrolyte will dissociate completely in solution leaving the polymer chain charged, while a weak polyelectrolyte will only partially dissociate giving the polymer a partial charge.[2] It is also possible to make polymers that have a permanent charge, a common example of this is polydiallyl dimethyl ammonium chloride (PDADMAC).

Although the chemical nature of the monomer determines factors such as the charge of the polymer chain and the solubility, some monomers are also able to respond to stimuli to change the fundamental properties of the polymers. Two of the most common stimuli that polymers can respond to are temperature and pH.[15] A well studied polymer that responds to temperature stimuli is poly(*N*-Isopropyl acrylamide) (PNIPAM).[16] In microgels below 32°C PNIPAM has a swelled structure, however above 32°C it undergoes a lower critical solution temperature phase transition to a dehydrated shrunken state. An interesting example of pH responsive polymers is a di-block copolymer of poly[methacrylic acid-block-2-(diethylamino)ethyl methacrylate] (P(MMA –b- DEA)). At high pH, >9, the anionic DEA block is solvated, while at low pH, <3, the cationic MMA block is solvated. As the two blocks are attached, when a block is not solvated it aggregates meaning at high pH there are micelles with anionic surface and at low pH the micelles have a cationic surface.[17]

It is not only the chemical nature of the polymers that is important to the solution behaviour but also their molecular architecture. There are three main types of structure in polymer systems, which are known as linear polymers, branched polymers and cross-linked polymers.[18] Linear polymers are single chains of polymers, which are able to pack closely together in concentrated systems and as

solids in which they often crystallise. Branched polymers contain a linear backbone with polymer chains attached to it. These branches can have a range of molecular weights and have branches of their own. The main backbone of the polymer is the longest single chain present in the polymer therefore any side chains will be shorter than the main chain. If there are lots of short side chains on the backbone the branched polymer can also be called a comb polymer. If there are lots of long branches with side chains on them then the polymer is known as a hyper-branched polymer. There are no definitive rules about the separating all branched polymers into categories. If a branched polymer has branches that are connected to each other, usually though a side chain off one of the branches, then these polymers are also called cross-linked polymers. These cross-linked polymers are usually very high molecular weight polymers that appear as though they are branches connecting multiple different main chains.

Branched polymers can be characterised by two factors, degree of branching and compactness. A linear polymer could be described by these factors with the degree of branching at 0 and the compactness also very low. Assuming the ability of a polymer to interact with other species is determined by the ability of an individual monomer to interact with the species it can be said that an increase in the degree of branching will increase the steric hindrance around the monomers on the main chain. If the compactness is also increased, creating a hyper-branched polymer, then the steric hindrance around the branches will also increase.[19]

An increase in compactness and degree of branching, and the fact that linear polymers are more able to pack together, means that the physical properties of the polymer solution are also affected. Molecular dynamics simulations[20] have shown that an increase in the degree of branching causes an increase in the shear viscosity of the solution. This can be explained by the higher the branching of the polymers leading to a greater interaction. The same simulations also studied the normal stress, which is a study of the tensile force on a polymer under shear, and the results show that a decrease in polymer length, which is similar to an increase in compactness, decreases the normal stress. This is explained as more compact polymers not being able to stretch, while the branches on a comb polymer are able to flatten and so act as a linear polymer.

1.1.3 Polymer/Surfactant interactions

One area of study that strongly utilises surface tension measurements and electrical conductivity is the area of polymer/surfactant interactions. Due to the size of this

field numerous books and reviews have been written.[7, 21-25] The systems studies can be split into two distinct groups. One is the study of an uncharged species with a charged species, while the other is the study of two charged species.

In the area of one uncharged species with a charged species, one of the early studies that has shaped our understanding was published by Jones in 1966.[26] This study looked at the sodium dodecyl sulfate (SDS) with polyethylene oxide (PEO) using surface tension and electrical conductivity. The conductivity results show some variation in the CMC value derived with the addition of polymer, indicating the polymer and the surfactant are interacting, however it is the surface tension measurements that of particular interest. The surface tension measurements show that the surface tension decreases with increasing surfactant concentration. However, as shown on Figure 1-5, at a concentration lower than the CMC, labelled T_1, the surface tension plot levels out for a short interval before decreasing further, at point T_2', and levelling out again, at T_2, to the same final surface tension seen with no polymer. This is shown with the dashed line in Figure 1-5, as compared to the surfactant only surface tension plot, solid line.

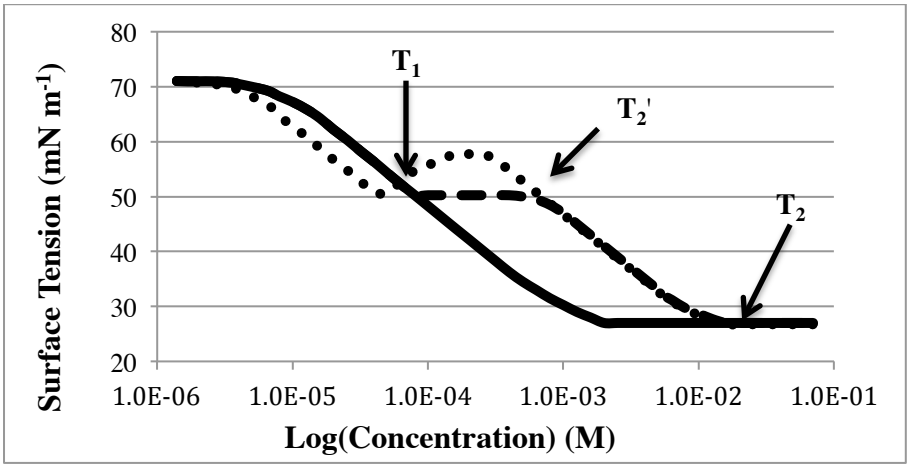

Figure 1-5. Idealised surface tension plots of surfactant only (solid line), surfactant and polymer according to Jones[26] (dashed line), and surfactant and polymer according to Lange[27] (dotted line).

The labels T_1 and T_2, as seen in Figure 1-5 were described by Jones, however T_2' was a later refinement.[23] These points are of interest as they describe when the surfactant and polymer first start interacting, at T_1, then between T_1 and T_2' any additional free surfactant preferentially binds to the polymer both at the surface and in solution. When the polymer is saturated with surfactant, at T_2', the surface tension resumes decreasing as it did previously until the CMC at T_2. This decrease in surface tension between T_2' and T_2 is due to the build up of free surfactant molecules in solution causing pressure at the interface displacing the surfactant-polymer complex. Due to the aggregation between the surfactant and polymer at T_1 this point is also

referred to as the critical aggregation concentration (CAC) or the critical association concentration, and is viewed as the point at which surfactant molecules begin to attach to the polymer forming bound micelles, which occurs generally at lower concentrations than the formation of free micelles in solution.

The dashed line in Figure 1-5 is an idealised situation and recent studies have found it be inaccurate. Therefore the dotted line shows an exaggerated surface tension plot of what could theoretically happen in real systems. The first difference is in the initial gradient of the surface tension. At this point, if the polymer is surface active then it will cause an increase in the rate of surface tension lowering, and the more surface active the polymer the higher the gradient will be. The next difference is between the T_1 and T_2' points, where an increase in surface tension has been observed[28] which has been attributed to the strength of the polymer/surfactant interaction causing a decrease of surfactant at the solution interface to preferentially bind with the polymer.

The cause of the points at T_1 and T_2 are mainly bulk related effects, such as desorption of surface active component due to stronger bulk interactions or competitive adsorption of the different species. These can be seen in the surface tension plot therefore it is expected that the same break points would be visible in the electrical conductivity plots. A schematic of the surface and the bulk solution is shown in Figure 1-6. This has been seen to be correct[29] with two break points being visible in the plots that are in good agreement with the T_1 and T_2 positions, therefore corresponding to the CAC and the CMC.

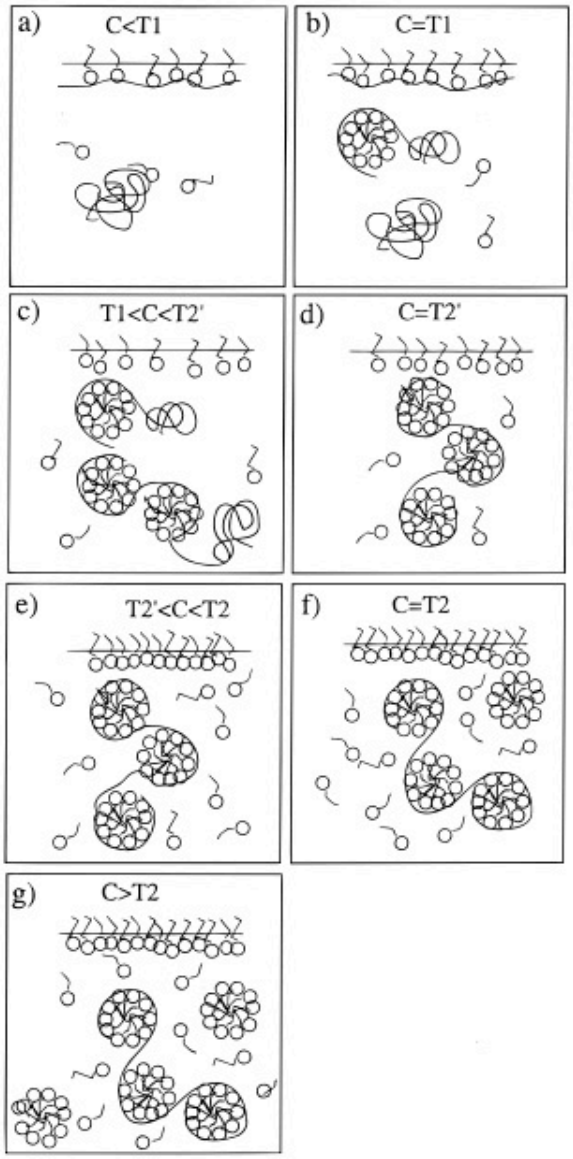

Figure 1-6. Schematic of a polymer/surfactant solution at various points on the surface tension curve. Reprinted with permission from B. M. Folmer and B. Kronberg, Langmuir, 2000, 16, 5987–5992. Copyright 2011 American Chemical Society.

In systems with an uncharged polymer and charged surfactant it is mainly the hydrophobic or hydrophilic interactions that drive the association of the surfactant and the polymer. In systems where both species have opposite charges then the interaction is an ionic interaction, therefore it can be expected that the effects discussed above will be much more exaggerated. An idealised version of the surface tension plot seen is shown in Figure 1-7, dashed line, in comparison to surfactant alone, solid line.

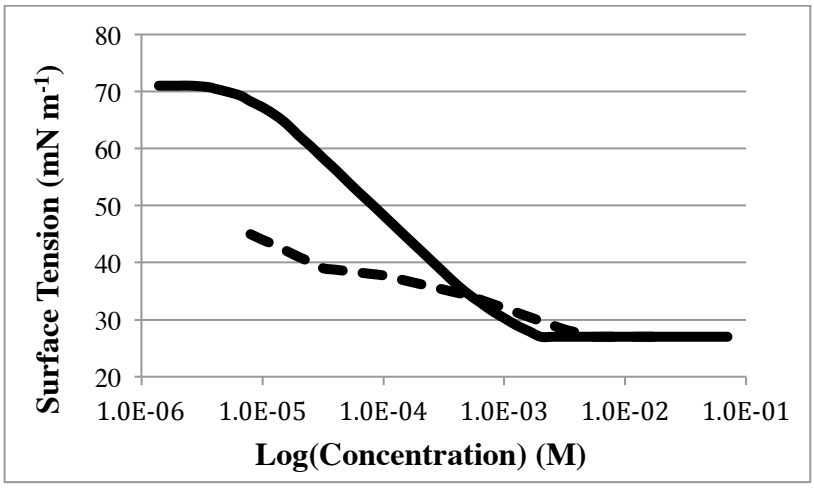

Figure 1-7. Idealised surface tension plots of surfactant only (solid line) and strongly interacting surfactant and polymer (dashed line).

The results reported[30] are very similar in nature to the results seen for highly surface active, non-ionic polymers, even when the charged polymers are not surface active. The initial surface tension is much lower than seen in the surfactant case alone suggesting a strong interaction between the surfactant and the polymer even at very low surfactant concentrations. As the surfactant concentration increases the surface tension decreases, as expected, however prior to the CMC the interaction between the polymer and surfactant is strong enough to cause precipitation. During this time the surface tension still decreases but at a slower rate suggesting that the polymer/surfactant aggregates are highly surface active. As with the uncharged/charge polymer/surfactant system the surface tension decreases to the same level as the uncharged polymer before levelling out.[22]

As discussed in the overview of polymer systems, there are polymers that are only charged under certain conditions, also known as polyelectrolytes. Strong polyelectrolytes completely dissociate, therefore they can be thought of as a charged polymer/surfactant system. However the weak polyelectrolytes behave very differently, as seen in a system like SDS with polyethylenimine (PEI). These systems are interesting to study because the charge on the PEI can be controlled by changing the pH of the solution. At a pH of 3, PEI is a fully charged polyelectrolyte, while at a pH of 12 it is an almost neutral polyelectrolyte.[19] At the same time Penfold et al also studied the effect of branching of the polymer. With linear PEI the surface tension behaviour is as expected from the previously discussed results. At a high pH, where the polymer is neutral, there is very little seen in the surface tension plot, suggesting limited interaction between the polymer and the surfactant. At lower pH where the charge on the polymer is much higher the surface tension shows a plot similar to the dashed line in Figure 1-5, suggesting a polymer surfactant interaction in the bulk solution increasing the surface tension until the polymer is saturated

therefore allowing free surfactant to return to the interface. This study was coupled with neutron reflectometry that showed that there was little more at the surface than a surfactant monolayer throughout these experiments. Although it appears that a small amount of extended polymer does interact with the surfactant head groups.

The branched polymer however is different, which is of particular interest in this thesis as this is similar to the main polymer used. At low pH where the polymer is charged, the surface tension is similar to the non-charged polymer/charged surfactant. As the pH is increased the surface tension trend tends towards the oppositely charged polymer/surfactant systems with a large increase in the middle of the surface tension plot, shown in Figure 1-8, corresponding to T_1. As the polymer at high pH is effectively neutral the interaction between the polymer and surfactant must be due to hydrophobic interactions. The link between the surface tension and the complex formation in the bulk is still unclear, however it appears that the surfactant and the polymer populate the interface gradually decreasing the surface tension. At the CAC, point A on Figure 1-8, the polymer and surfactant tails start interacting leading to a plateau in the surface tension plot. As the polymer/surfactant complex reaches saturation, the surface tension decreases from an increase in complex solubility leading to a partial surfactant monolayer, point B to point C on Figure 1-8. The addition of further surfactant to the solution increases the pressure of SDS at the interface leading to a decrease in surface tension.

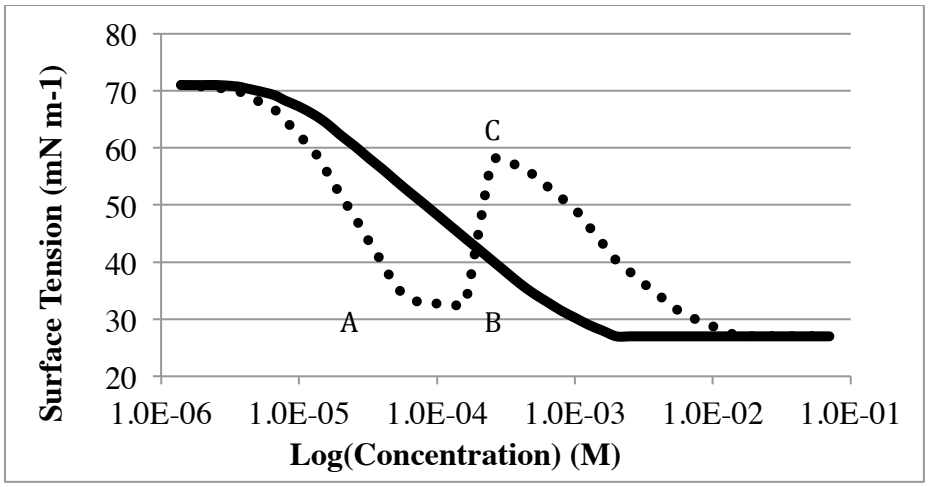

Figure 1-8. Idealised surface tension plot showing the interaction of SDS with branched PEI at high pH (dashed line) in comparison to a pure surfactant solution (solid line).

Although this topic has been studied for some time there is still not a single model that explains all the results seen in the literature. In numerous cases the literature results and explanations can be contradictory suggesting these systems are highly complex.

As expected, the oppositely charged polymer/surfactants interact very strongly while the uncharged polymer with charged surfactant only moderately interact. From these two systems it would therefore be expected that similarly charged polymer and surfactants would repel each other resulting in no interaction. In his review of charged polymer/surfactant systems[22] Goddard states that "when the respective charges are of the same sign, association between the polymer and the surfactant can be expected to be feeble or absent as has been reported between sodium carboxymethylcellulose (NaCMC) or DNA with SDS."

Given this, it is therefore it is surprising that not only are the interactions seen by Edler et al[8] appear to be of considerable strength, leading to solid thin films at the air solution interface and, even more intriguing, that they are composed of the cationic surfactant hexadecyltrimethylammonium bromide (C_{16}TAB) and the partially cationic polyelectrolyte PEI, which is about 3% charged under the experimental conditions used.

1.1.4 Polymer/Surfactant Thin Films

Surface tension has been the main tool for studying polymer/surfactant interactions at the air/solution interface. While the surface tension is able to give information relating to the composition of components at the surface and, by comparison with electrical conductivity, it is possible to infer how this is linked to the bulk solution the surface tension, it does not give information about the structuring of the components at the surface. Complementary techniques that can also study the interface of solutions are Brewster Angle Microscopy and neutron reflectometry, details of which are given in chapter 2. Both techniques use the reflection, either of neutrons or light, from the surface of a solution, however it is neutron reflectometry that has the resolution to describe the structure at and near the solution surface.[7] This can be very valuable as the interaction of the surfactants and the polymer is not limited to the interface but can cause structuring into the bulk solution, which gives further insight into the strength of the polymer/surfactant interaction.

An example of the information gained from neutron reflectivity in the case of an uncharged polymer with a charged surfactant is from studying SDS with PEO.[31] By using contrast variation available with neutron reflectometry it was possible to determine that as the concentration of surfactant was increased from below the CAC to the CAC and the amount of PEO at the surface decreased, while the amount of SDS increased. This is an expected result as PEO is surface active on its own[32] however at the CAC the amount of PEO decreases to almost zero. Although this can

be explained partially by the complexation of the SDS to the PEO, making it more soluble therefore causing it to leave the interface, this would not completely explain this result because the surface activity of the polymer is so high. Therefore the explanation is that it must also be related to an increase in the amount of free SDS at the surface forcing the PEO into the bulk. Interestingly the thickness of the surface layer above the CAC is only slightly thicker than would be expected for SDS on its own. This indicates that the PEO does not complex strongly with the SDS at the solution surface and is instead separated to the bulk solution.

It is in the study of oppositely charged polymers and surfactants where neutron reflectometry is most valuable. Thomas et. al.[7, 33] have classified two types of interactions for oppositely charged polymers and surfactants. Type 1 consists of strongly interacting pairs of polymers and surfactants that form more complex structures than simple monolayers at the solution interface. Type 2 systems consist of interactions that are more like the neutral polymer with charged surfactant systems in that they only form fairly simple monolayers at the solution interface, however they are separated from the uncharged polymer with charged surfactant systems by different surface tension behaviour.

The type 1 behaviour has been described in a system composed of dodecyltrimethylammonium bromide (C_{12}TAB) and sodium poly(styrene sulfonate) (NaPSS). This system shows a surface tension plot similar to, but more exaggerated than, the dashed line in Figure 1-7. In this sample the polymer is not surface active therefore the surface tension is not complicated by excess polymer at the surface. However studying the amount of polymer at the surface of the solution using neutron reflectometry with contrast variation shows that above the CAC the amount of polymer at the surface increases rapidly. This increase in polymer at the surface is coupled with an increase of thickness of the surfactant layer at the surface. This increase in layer thickness has been modelled as a surfactant monolayer on the interface with a surfactant bilayer slightly below the surface with polymer intercalating between the head groups, and partially into the tail regions, of both structures holding them together. The thicker surface layers have also been seen with C_{12}TAB with DNA,[34] or polyacrylamide (PAAm)[35] and SDS with PEI at pH=10,[36] or poly(vinyl pyridinium iodide) PVPmI.[33] These thicker layered systems suggest that the strength of the interaction between the polymer and the surfactant is great enough that the complex can bind to the surface monolayer and in some cases produce a multi-layered system, a detail that cannot be inferred from surface tension.

The type 2 behaviour on the other hand, in samples such as SDS with poly(dimethyldiallylammonium chloride) (PDMDAAC) is very different.[37] The

surface tension plots show a sudden sharp rise in surface tension half way through the measurement followed by a return to a slow decrease in surface tension, similar to the dashed line in Figure 1-8. This sharp rise is coupled with a slight drop of the amount of SDS at the surface, as determined by neutron reflectometry. At the same time as the amount of SDS drops so does the amount of polymer suggesting that the increase in surface tension is due to removal of surfactant and polymer from the interface. This is likely to occur at the point when the polymer becomes saturated with surfactant and therefore becomes either more soluble in the bulk or more insoluble and precipitates. Above this point the decrease in surface tension is due to the increase in SDS at the interface with only a small amount of polymer remaining just under the surfactant monolayer.

As with the surface tension results, the neutron reflectometry results show that there is a weak interaction between non-charged polymer and charged surfactants, mainly due to hydrophobic interactions, while there is a strong interaction between charged polymer and charged surfactants. This strong interaction is even able to produce simple multi-layered systems of surfactant bilayers bound together by intercalated polymer. Therefore once again the results reported by Edler et. al.[8], showing thick multi-layered films in systems that should either have no interactions or very weak interactions, are of some interest.

So far only structures formed by adsorption to the air/solution interface have been discussed however there are other ways of creating structured thin films at an interface. A number of techniques are known more generally by the title of layer-by-layer (LbL) assembly. Again this has been a growing area of research over the past two decades.[38] The LbL technique relies on sequentially adsorbing layer after layer of different materials onto a surface.[39]

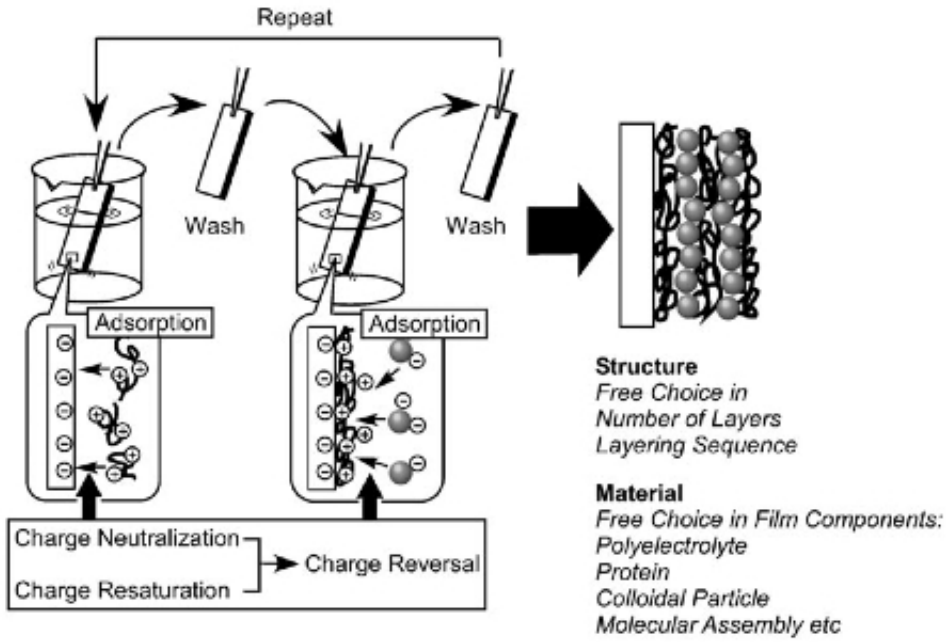

Figure 1-9. Schematic of the layer-by-layer dip coating technique for creating thin films. K. Ariga, J. P. Hill, and Q. Ji, Phys Chem Chem Phys, 2007, 9, 2319–2340 - *Reproduced by permission of the PCCP Owner Societies*.

Of the techniques under the title of layer-by-layer assembly probably the most common and one of the simplest is dip coating. Dip coating starts with a charged substrate, which is dipped in a solution containing a component with an opposite charge. If the substrate is left in the solution the component in the solution will interact with the substrate and become attached to it. The substrate is then removed from the solution, rinsed then placed in a second solution containing the oppositely charged species. Once again the solution interacts with the substrate through electrostatic charges and becomes attached to it. The substrate is removed from the second solution and rinsed then the process is repeated until a film has been created with the desired thickness of the application, as shown in Figure 1-9.

Although relatively simple, this technique is very labour intensive to produce films of any substantial thickness. One report states that the substrate is dipped into the alternate solutions for 20 minutes per solution with a brief wash in between immersion steps for n cycles to achieve desired thickness.[40] The substrate does not have to be flat as it can also be more complex as has been shown by Caruso et al who have used a colloidal core, which when dissolved produced hollow spheres.[41]

Two alternate versions of layer-by-layer assembly have recently been developed are spin and spray coating.[38, 42-48] Both of these techniques effectively cast the components onto the surface of the substrate, however attractive interactions between the species forming the layers are still very important for final film

structure. The advantages of spin and spray coating are that it is much quicker per application of solution and that the amount of solution used per application is much smaller; which is of particular benefit if the components are toxic or expensive. As well as being faster to apply each layer, they also dry much quicker, because the layers use only a small amount of solution, making them ready for the following application.[43]

Many LbL systems are made up of two components, usually two polyelectrolytes.[49] In these systems the main role of both components is to form the film with any other functionality being included in the film by modifying one of the components.[50] Recently however there have been studies into including subsidiary components that are not part of the film forming process but increase the film functionality. One of these studies is the incorporation of phospholipid vesicles into a multilayer film made up of two polyelectrolytes.[46] What is particularly interesting about this study is that it is performed using dip coating, however Michel et al have also created these films using spray coating.[45] These spray-coated films show that there is very little disruption to the phospholipid vesicles during the spraying process meaning that even complex soft materials can be used in LbL assembly of thin films.

A final method of forming structured thin films to be discussed here is that of polymerisation around a surfactant template. This is a relatively small field of study but it has a certain advantage over adsorbed films and LbL films. This advantage is the 3-dimensionality of the structure of the formed film. Taylor reports[7] that the adsorbed polymer-surfactant films discussed above have been studied with grazing incidence x-ray diffraction to study the off-specular scattering to determine if there is any 3-dimensional structure in the films. The results of this were that there was no indication of any further structure, so it was reported that the sub-surface layers of surfactant are probably large bilayers aligned with the surface. Similarly, so far there are no reports of long-range 3-dimensional order in LbL systems.

A brief summary of the different techniques shows us that adsorbed films, similar to those studied by Taylor et. al.[7], are simple to form as they arrange spontaneously at the solution interface. However these films are liquid-like, do not contain long range ordered structures and their thickness is limited to the strength of the polymer/surfactant interactions. The LbL films, discussed by Ariga et. al.[38], are more versatile with the components that can be used and the thickness of the films is dependent on how many layers are deposited giving these films more potential application than adsorbed films. However the LbL films still suffer from the lack of long range 3D ordering and structure, which may improve the characteristics of the film for any potential application and also can be prepared as free standing films

only by use of a sacrificial layer which allow them to be floated off the surface after preparation. The surfactant templated polymerised films show this long-range order and the knowledge of the use of different surfactants to produce different templated structures is well known from surfactant templated inorganic films. These polymerised films however are still very early in their development and the polymerisation conditions may seriously affect the long-range order of the final film. Therefore it is proposed that the surfactant templated adsorbed films previously created by Edler et. al.[8] show the simplicity of adsorbed films that can be as thin as, or much thicker than, LbL films and have long-range order similar to the polymerised films and templated silica films. These films may therefore find uses in many places LbL films currently have applications. In biomedical coatings[51] thin film, up to 1000nm thick, can be created as coatings using biocompatible polyelectrolytes to contain many different species such as enzymes, drugs and anti-fouling materials. The films discussed here should be able to be biocompatible and contain all these things and because their fabrication is by self-assembly they are much easier to prepare. Another use of these films could be in multi-layered enzyme supports on for use in ultra-filtration[38] where the films discussed in this report should be able to incorporate the enzymes and the filtration properties will be controllable by controlling the mesostructure within the multi-layer.

1.1.5 Surfactant properties in concentrated solutions

To be able to control the structures of the films then it is important to have an understanding of the factors that affect surfactant micellization. As discussed previously surfactants have a hydrophilic part and a hydrophobic side. For simplicity here an aqueous solvent is assumed and the surfactants have a hydrophilic head and a hydrophobic tail. Above the CMC the strength of the hydrophobic interactions cause the surfactant molecules to aggregate together into micelles.

The structure of the micelles is dependent on a number of parameters that describe the effective shape of each surfactant molecule. For instance a surfactant with a large head group and a relatively short tail can be viewed as a cone while a double tailed surfactant with smaller head group can be viewed as a cylinder. An equation to describe the shape of a surfactant has been developed[52] and is shown below, Equation 1-4.

$$\text{Packing Parameter} = v/a_0 l_c \qquad \text{Equation 1-4}$$

In this equation v is the volume of the hydrocarbon tail, a_0 is the surface area of the head group, and l_c is roughly equal to but slightly less than the fully extended length of the tail. The resultant packing parameter can then be used to estimate the structure of the micelles that a surfactant will form in solution. A simplified version of the potential micelle structures is given below, Figure 1-10.

$$\text{Sphere} < 0.33 < \text{Globule} < 0.38 < \text{Toroid} < 0.44 < \text{Cylinder} < 0.5 < \text{Bilayer}$$

Figure 1-10. Micelle shape relation to the packing parameter as given by Israelachvili[52]

More recently these shape assignments have been studied using computational methods which have confirmed the importance of the molecular geometry of the surfactants and have proposed that tuning of the surfactant structure can control the micelle structure and size.[52] A list of the parameters for some of the surfactants used in this thesis is given in Table 1-1, a complete list of packing parameters can be found in Chapter 2. Included in this list is didodecyldimethylammomnium bromide (DDAB) for comparison with a double tailed surfactant.

	v	a_0	l_c	Packing Parameter
SDS	351.90	57.8	16.68	0.37
C_{16}TAB	460.05	64.0	21.74	0.33
DDAB	703.70	68.0	16.68	0.62

Table 1-1. Surfactant molecular parameters for calculating the packing parameters. Values for v and a_0 are taken from Warr et. al.[53] except the SDS value for a_0 which is taken from Garg et. al.[54] Values for l_c are calculated using Tanford's formula, lc = 1.50 + 1.26(no of carbons).[55]

From these results it can be concluded that SDS will form globular micelles, C_{16}TAB will be on the boarder of spherical and globular micelles and DDAB will form bilayer sheets. With these parameters it is also possible to say that if an equi-molar mixture of C_{16}TAB and DDAB were made then calculation of the respective average values of the parameters would lead to a packing parameter of 0.46, modifying the micelle structure to produce infinitely long cylinders. The use of packing parameters to control film structures is discussed further in chapter 3.

Mixing of two surfactants in a solution can be thought of in the same way.[56-59] If the surfactants mix ideally then the enthalpy of mixing will be, zero which means the CMC of the mixed surfactant micelle (CMC*) can be calculated as a sum of CMCs of all components in the system, weighted by their macroscopic mole fractions, α, as shown in Equation 1-5. Mixtures of non-ionic surfactants tend to behave ideally, however ionic surfactants are able to depart from ideality. This is due to interactions between the surfactant molecules, in this case each surfactant is given an activity

coefficient, which describes the interaction between the different surfactant species. Including this activity coefficient in Equation 1-5 leads to Equation 1-6.

$$\frac{1}{\mathrm{CMC}^*} = \sum \frac{\alpha_i}{\mathrm{CMC}_i} \qquad \text{Equation 1-5}$$

$$\frac{1}{\mathrm{CMC}^*} = \sum \frac{\alpha_i}{f_i \mathrm{CMC}_i} \qquad \text{Equation 1-6}$$

Using a regular solution approximation, Rubingh[60] was able to express the activity coefficients as a function of an interaction parameter, β_{ij}, which is related to the net pair interactions within the micelle.[58, 60] In a binary mixture this means Equation 1-6 can be written as Equation 1-7.

$$\frac{1}{\mathrm{CMC}^*} = \frac{\alpha}{f_1 \mathrm{CMC}_1} + \frac{1-\alpha}{f_2 \mathrm{CMC}_2} \qquad \text{Equation 1-7}$$

$$f_1 = \beta(1-x)^2 \qquad \text{Equation 1-8}$$

$$f_2 = \beta x^2 \qquad \text{Equation 1-9}$$

From Equation 1-7, if CMC*, CMC_1, and CMC_2 are known then it is then possible to work out the interaction parameter, β, by substituting in Equation 1-8 and Equation 1-9. Knowing the interaction parameter it is then possible to compare the interactions of different surfactant mixtures. It is also possible to determine x, which is the mole fraction of component 1 in the mixed micelle.

1.1.6 Surfactants used for encapsulation and release

One important feature of surfactants that comes out of the dual hydrophilicity and hydrophobicity of surfactants is their ability to encapsulate an insoluble species while themselves being dissolved in the same solvent.[2] This is the basis for detergents where the surfactants are able to encapsulate oil based "dirt" within the tail group region making it soluble in the water allowing it to be washed away instead of being left on the clothes.

In cleaning products as well as having surfactants for cleaning purposes there are also surfactants for encapsulation of fragrances.[61] Although it is hard to imagine these films being used for cleaning purposes the encapsulation potential of the

surfactants lead to a wide variety of potential applications. One potential application is for use as a drug delivery system, a potential bandage that releases the drug into the wound as it breaks down. In this situation the structure of the film is highly important because micellar structures have a much lower capacity for the drug encapsulation than liquid crystalline phases.[62] Although the films discussed in this report have yet to reach a stage where any applications can be properly tested the idea of thin films being used for drug delivery is a growing area of research within the LbL community. This research has already shown that it is possible to make thin films that release the drug load at a steady rate over 20 days from a supramolecular complex incorporated in a polyelectrolyte multi-layered system.[63, 64]

1.2 Previous research within the Edler group.

As mentioned previously these films were first reported by Edler et. al.[8] in 2003 and were based on previous research in surfactant templated silica films at the air solution interface. It was proposed that during synthesis of surfactant-silica films the silica formed an intermediate that resembled a polymeric material in structure and this intermediate has an important role in the formation of the structured thin films.[65] This was confirmed by replacing the silica species with a polymer of similar structure and charge. In this experiment the surfactant used as the template was C_{16}TAB and the polymer used to represent the silica was hyperbranched PEI. The creation of films at the interface was plainly visible by eye but also confirmed with Brewster Angle Microscopy (BAM). Neutron reflectivity and grazing incidence x-ray diffraction (GIXD) were also used to determine the extent of mesoscale ordering within the films.

From this work it was shown that ordered films could be formed at the air solution interface from mixtures of C_{16}TAB and PEI at pH >8. Two molecular weights of branched polymer were used and it was determined that using a high molecular weight of polymer produced thicker films which were less well ordered than when using a low molecular weight polymer. The molecular weights of the polymer were nominally 750,000Da known as LPEI and 2,000Da known as SPEI. Addition of NaOH was also studied and it was shown that increasing the NaOH concentration increased the thickness of the film, decreased the film formation time and promotes the formation of well-ordered structure. Suggesting that the film formed via interactions between C_{16}TAB and the neutral rather than charged form of PEI.

Following on from this work the study was developed into a project which started by studying alkyltrimethylammonium bromides (C_nTAB) with different tail lengths to

try and control the film structure, with the first results published in 2005.[66] In this study while the surfactants were being varied the polymers used were the same as before, and their concentration was studied. The results from this work confirmed that higher molecular weight polymers produce thicker but less well ordered films when compared to low molecular weight polymers and also showed that there is an optimum polymer concentration, dependant on the surfactant concentration, for forming well-ordered films. In this study, three surfactants were used, C_{12}TAB, C_{14}TAB and C_{16}TAB, and from these surfactants it was shown that as the tail length of the surfactant is decreased the ordering of the film also decreases. The ordering within the films suggests the structure is predominantly made up of cylinders packing parallel to the solution surface. A study of the effect of pH showed that this structure could be partially controlled by altering the pH. As the pH of the solution is decreased from ~pH 9, the natural pH of the polymer solution, the charge on the PEI is increased resulting in no film formation. However an increase in pH to above pH 12 leads to increased ordering and thickness of the films. This was attributed to the PEI being more neutralised and therefore more able to interact with the charged micelles allowing the micelles to pack closer together. A final important finding from this work was a study into the formation of films in a closed system. It was found that film formation does not occur when there is a lid on the formation dish, leading to the conclusion that an evaporative process of water leaving the surface of the solution plays an important role in film formation.

Once it had been shown that polymer charge played an important role on film formation, the next step was study the effect of changing the charge on the micelle. This was done by mixing the C_{16}TAB with a non-ionic surfactant.[59] Two non-ionic surfactants were used octaethylene glycol monohexadecyl ether ($C_{16}E_8$) and Brij56 (polydisperse $C_{16}E_{10}$) and they were mixed with C_{16}TAB by varying the mole ratios of ionic to non-ionic surfactant and therefore keeping the surfactant concentration constant. Only SPEI was used in this study and the concentration series was a shortened version of that used previously. The results from this study indicate that as the ratio of ionic surfactant is decreased the ordering and thickness of the films also decreases and that no film is formed with non-ionic surfactant alone. This has been attributed to a decrease in interaction between the polymer and the surfactant caused by decrease in overall charge on the surfactant micelle. This result suggests that the charge on the surfactant is important and causes a cation-dipole interaction with the polymer that allows these films to form.

The following paper to be published[67] contained two parts to it. The first reported work that had continued on from the initial work reported in 2005,[66] the second reported an extension to the original work that was a study of the polymer molecular

weight and branching and whether the use of a cross-linker had any effect on the film structure. The important difference to the initial work and the first part of this paper was that it contained GIXD patterns that give more information about the structure in the films than reflectometry alone. The GIXD data on the films supported the previous conclusion that the SPEI films contained a more ordered structure, indicated in the GIXD patterns by diffraction spots instead of the rings observed for the LPEI films. In the second part of this paper two types of LPEI were used. According to Sigma Aldrich the difference between the polymers is in the synthesis that leads to a hyperbranched polymer (L1-PEI) or a comb-like copolymer that had only short pendant branches (L2-PEI). Also used were a single type of SPEI (also comb-like) as in previous experiments and an extra molecular weight polymer, 25,000Da (MPEI) (hyperbranched). The cross-linker used was ethylene glycol diglycidyl ether (EGDGE). In the study relating to the polymer molecular weight and branching the results suggest the branching of the polymer plays very little role in the formation of the films and it is the molecular weight that is the important factor for thickness and structure, the MPEI films showing similar behaviours to both SPEI and LPEI and the two types of LPEI behaving the same way. The results from the addition of cross-linker showed this caused an increase in thickness of the films allowing them to be removed from the solution surface. Studying a range of concentrations, it was determined that there was an optimal amount of EGDGE above which the thickness of the film does not change. An increase of the concentration of EGDGE too far above this optimal limit also causes the whole solution to gel instead of just a strengthening of the film. The mesostructure of the films was also reported and this was seen, in a majority of cases, to be the same as the films without cross-linker. Also published in this paper was a short study on using another quaternary ammonium bromide surfactant, the surfactant chosen was hexadecylpyridinium bromide (CPB). This study was important as it showed, for the first time, ordered film formation with surfactants other than the C_nTABs.

Once it had been shown that the thickness of these films could be increased it was found that it was possible to recover them from the solution surface. These recovered films still contained the well-ordered structure allowing consideration of potential applications. The most obvious application uses the inherent properties of the surfactant to incorporate small hydrophobic molecules into the micelle and therefore be taken up into the film.[68] In this study the hydrophobic species were cyclohexane, cyclohexanol, and decane. Study of the surfactant solutions confirms that hydrophobic species were incorporated in the surfactant micelles, however the concentrations were much lower than expected. Also the shapes of the surfactant micelles are not altered from the micelles without hydrophobic species. Study of the films also shows similarity between films with and without additive, when using

either cyclohexane or cyclohexanol as the additive, the only difference seen is that the films appear to be more stable and show slightly better structure with additive. The use of decane however gives films a very different structure to those seen without additive, in some cases forming a well-ordered cubic phase instead of the hexagonal phase previously seen and reported.

Although the Edler group was the first to report studies on these films and it is this group that has the majority of publications, there have been other groups who, in collaboration with the Edler group, have reported studies on the same or very similar systems. The main collaborators have been Aurora Pérez-Gramatges and Hansel Comas-Rojas at the Higher Institute of Applied Sciences and Technologies, Havana, Cuba who have worked with the same C_{16}TAB/PEI system but at much lower concentrations. In their first paper in 2007[11] they reported three regions at low surfactant concentration and varying polymer concentration that correspond to below the critical aggregation concentration (CAC^*), between the CAC^* and the critical micelle concentration (CMC^*), and above the CMC^*. It is important to note here that the CAC is usually a bulk phase property however in this case it is where films start to be observed at the interface. Corresponding shrinking of the PEI coils in these dilute solutions due to C_{16}TAB binding in solution was also observed between the CAC* and the CMC*, with the polymer then swelling again as micelles formed demonstrating the interaction between these species in solution as well as at the air-solution interface. Studies of the effect of short chain alcohols on the micellization of C_{16}TAB in the presence of PEI also demonstrated that the polymer had little effect on the hydrophobic interactions causing micellization, since these were affected in the same way by alcohol in the presence or absence of PEI. Thus the hydrophobic interaction is not a strong component of the interaction between polymer and surfactant in this system.

This study was continued with further results being published in 2009[69] looking at the concentration of surfactant in solution during single film formation then also during multiple film formation from the same solution using a surfactant selective electrode. The results of measuring surfactant concentration during single film formation showed that the surfactant starts interacting with the polymer very quickly and within five minutes has reached a metastable equilibrium state that does not change over the course of one hour. This suggests that the surfactant-polymer interactions occur immediately and film formation also occurs within the first five minutes of the experiment. The results of surfactant concentration during multiple film formation were studied by removing the film from the solution surface after one hour then observing whether another film was formed in its place. The results showed that multiple films could be formed from a single polymer surfactant

solution down to a limiting factor that is thought to be a surfactant concentration near the CAC*. It is even shown that structure is also present in these films below the CMC and that this structure is more ordered than structure from the films above the CMC, the structure formed however is the same in both cases, a 2D hexagonal phase with the long axis of the cylinders lying parallel to the interface.

As well as performing experimental studies there has been a theoretical study published from a recent collaboration.[70] In this study theoretical predictions were made with regards to forming multilayer systems at the air solution interface, they were then compared to experimental data collected from a dioctyl sodium sulfosuccinate (AOT)/water system. This model states that evaporation from the surface of the solution causes a net transport of material to the surface leading to a concentration gradient. If the system has a low energy for phase separation then phase separation can occur forming an interfacial phase whose properties are dependent on the magnitude of this energy barrier and the rate of evaporation from the solution surface. This model is supported by the experimental results from the AOT/water system and agrees with the conclusions that have been made by Edler et al from the PEI-surfactant system.

Although the C_{16}TAB/PEI system has been the main focus for the study of these films, it is not the only system that has been found to produce films like this. While studying the effect of mixing C_{16}TAB with non-ionic surfactant the effect of mixing C_{16}TAB with anionic surfactant was also studied. The anionic surfactant used was sodium dodecyl sulfate (SDS) and this mixture of C_{16}TAB/SDS was found to give much thicker more robust films than C_{16}TAB alone. These results were published in 2007.[71] Not only were these films thicker and more robust than previously seen films but they were also capable of being formed with a wide variety of polymers while PEI had previously been the only polymer found to form films with C_{16}TAB.

1.3 Motivation

The aim of this project was to further our understanding of these films by building on the work discussed above. This effectively split the project into two related yet separate areas, the first the cationic surfactant/polymer system and the second the cat-anionic surfactant/polymer system.

Building on the work done on the cationic surfactant/polymer system the motivation was to try and accomplish one of the aims that was set out in the 2005 paper. [66] In that paper it was attempted to control the film structure by altering the surfactant tail

length. As the molecular properties of the surfactants used were so similar, very little difference in structure was seen. Therefore the first part of this thesis aimed to show whether by altering the surfactant molecular properties more dramatically different film mesostructures would result, discussed in chapter 3. Following this, a comparison study to the original data could then be carried out with a study into encapsulation of hydrophobic species similar to that published in 2008.[68] This could also be taken one step further to include a study of the release of these hydrophobic species, discussed in chapter 4.

Another area of this first system that needs work is the role of the polymer. Although not discussed in detail in any paper, work within the group has been unable to replicate film formation with C_{16}TAB alone with any other polymer. Well-controlled polymers with various architectures (graft, comb, star) were therefore synthesised by a post-doctoral researcher within the group carried out in conjunction with the work reported in this thesis. As part of this thesis film formation using these polymers was carried out by the candidate and is reported in chapter 6, and their implications for the film formation mechanism are discussed.

The cat-anionic surfactant/polymer system has had a lot less work done on it, however the communication published in 2007[71] did pose a number of questions. Firstly what is the effect of the surfactant and how does changing the ratio of C_{16}TAB to SDS alter the structures in solution and in the films? Secondly, what is the interaction between the surfactant and the polymer that allows films to be formed with multiple different polymers? Thirdly, given films have been seen with different polymers are the structures of these films different due to the polymers or is the structure only dependent on the surfactant? The first two questions will be answered by studying the bulk solutions, in chapter 5, while the third question will be answered by studying the film itself, in chapter 6.

Stepping slightly away from the previous work there are still studies to run. Looking again at potential applications, thin films are already created industrially using other techniques. If these films are ever going to be used commercially then the ability to use multiple film formation techniques may prove beneficial, the other technique studied here is spray coating. The 6C_{16}TAB:4SDS system with polymer was used to study this and the results are reported in chapter.

2 Techniques, Theory and Methods

2.1 Experimental

2.1.1 Surfactant Synthesis

A range of different surfactants and chemicals has been used during this thesis. The most important of these are given as a concise list in Table 2-6, Table 2-8 and Table 2-9 at the end of this chapter. All of these chemicals were purchased, as stated, apart from hexadecyltriethylammonium bromide. Chemical structures of all of the common chemicals used are shown in appendix 1.

All the surfactants were available for purchase from various suppliers except CTEAB, which was synthesized. The synthesis procedure has been reported by Kim et al[72] and has been modified as follows. Equi-molar amounts of 1-bromohexadecane (97% Sigma) and triethylamine (99%, Sigma) were combined in absolute ethanol (Fisher) and refluxed for 24 hours. The ethanol was removed by evaporation using a rotary evaporator until a white paste was obtained. A minimal amount of chloroform (Fisher) was used to dissolve the paste, and then cold ethyl acetate (Fisher) was used to precipitate the solid. The sample was re-crystallised a minimum of three times using chloroform and ethyl acetate to increase the purity and ^{1}H-NMR was used to confirm the synthesis. The peaks in the ^{1}H-NMR are CH_3, t, 0.9ppm, $14CH_2$, s, 1.2ppm, $3CH_3$, t, 1.4ppm, CH_2, 3.3ppm, 3CH2, q, 3.5ppm.

2.1.2 Film Preparation

All purchased chemicals were used without further purification.

Test films were created on the bench top in 6cm diameter polystyrene petri dishes from 30ml polymer/surfactant solutions. The polymer/surfactant solutions were prepared by making individual solutions of the surfactant and polymer in ultrapure water (purified to 18 MΩ cm using an Elga PURELAB system) then mixing them together making the final solution a 1:1 volume mixture of the two preliminary solutions. This final polymer/surfactant solution was then poured into the petri dish and allowed to stand until a film was formed. The ambient conditions were monitored but not controlled, the temperature varied between 17 and 24°C, and the relative humidity varied between 10% and 60%.

When making solutions of two surfactants with a polymer, three initial solutions were created. These are one for each surfactant, and one for the polymer. Both surfactants were dissolved to have the same concentration and the correct ratio of surfactants is achieved by mixing the correct volume ratio, this final solution was then allowed to come to equilibration at room temperature before addition of the polymer. The polymer was then added making a 1:1 volume ratio of the final surfactant solution and the polymer solution. This final polymer/surfactant solution was then poured into the petri dish and allowed to stand until a film formed.

Before pouring the surfactant/polymer solutions into the petri dish a plastic mesh was placed in the petri dish. This mesh was on average $3cm^2$, with diamond shaped holes roughly 1cm by 0.5cm at the points, and helped with recovery of the films. When a film has formed and believed to have reached equilibrium a square is cut into it and the mesh was picked up with tweezers. If the film were not cut into a square then as the mesh was lifted the film left on the surface would drag the film off the mesh and back into the petri dish. Once a film had been removed from the surface of the solution and was on the mesh, the mesh was hung to allow the film to dry.

Only films encapsulating Nile red were studied in the lab for encapsulation and release. When performing these studies the Nile Red was dissolved in a minimal amount of acetone and then mixed into the surfactant solution. This solution was allowed to stand room temperature for at least 10 minutes allowing the Nile Red to be incorporated into the surfactant micelles. This additive/surfactant solution was then mixed with the polymer before the addition of ethylene glycol diglycidyl ether (EGDGE). The EGDGE was added to the solution to cross-link the polymer making the films thicker and more robust, as was previously shown by O'Driscoll et al.[67] After the EGDGE is added to the solution the whole solution was gently agitated to mix all the components before being poured into the petri dish. The rest of the film formation details were the same as described above and the films were allowed to dry before being studied for encapsulation or release, described in chapter 4.

The use of EGDGE has previously been shown to crosslink these films to make them more robust to allow them to be removed from the solution surface.[59] The EGDGE has been used as a cross linker for these polymer due to its common use in cross-linking amine based polymeric materials.[73, 74] Figure 2-1 shows the reaction mechanism leading to cross-linking of the polymer chains.

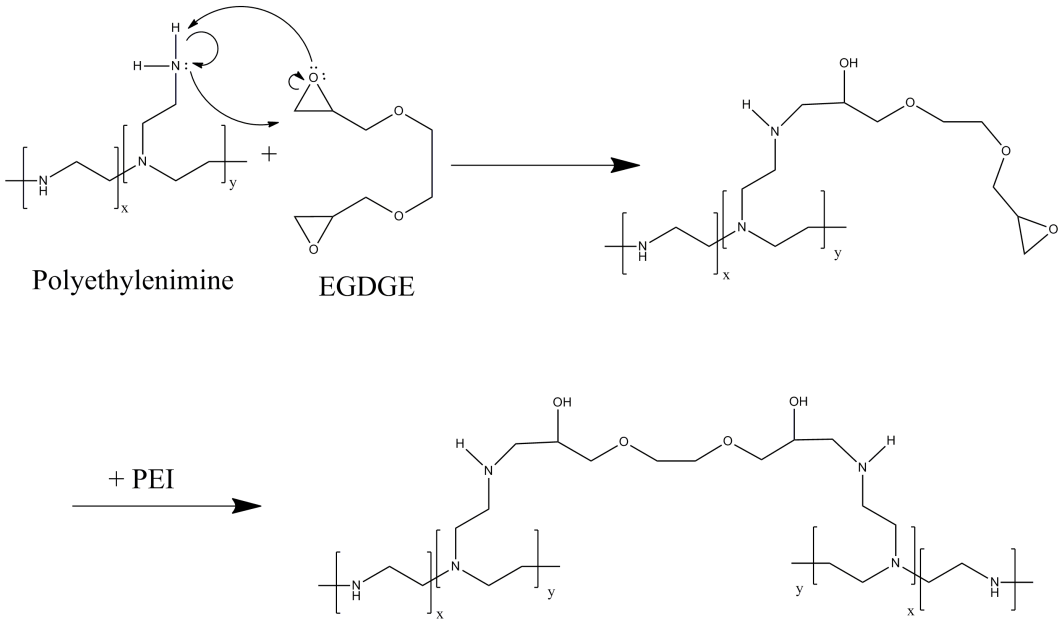

Figure 2-1. Reaction mechanism of EGDGE with PEI

2.1.3 Spray Coating

The solution preparation was exactly the same as for solution films except in spray coating the final solution was sprayed onto a substrate instead of being poured into a petri dish. The substrate used was either a glass microscope slide, or more commonly a 100mm diameter circular silicon wafer. The silicon wafers were purchased from www.universitywafer.com and were orientated with the [100] plane of the crystal at the surface. The spray bottle consists of a plastic bottle with an atomiser in the lid. The lid also contains a one-way valve allowing pressure to be applied by "pumping" air into the sealed container with the hand pump provided. Surfactant/polymer solutions were not stored under pressure, instead only put under pressure immediately prior to deposition. Pressure in the containers was not measured however 20 "pumps" were always used to maintain continuity. After application the wafer was placed on the bench top allowing the layer to dry. Figure 2-2 shows the silicon wafer prior to spray deposition (left) showing the reflection of the ceiling, and showing the coverage of four layers of spray coated film (right).

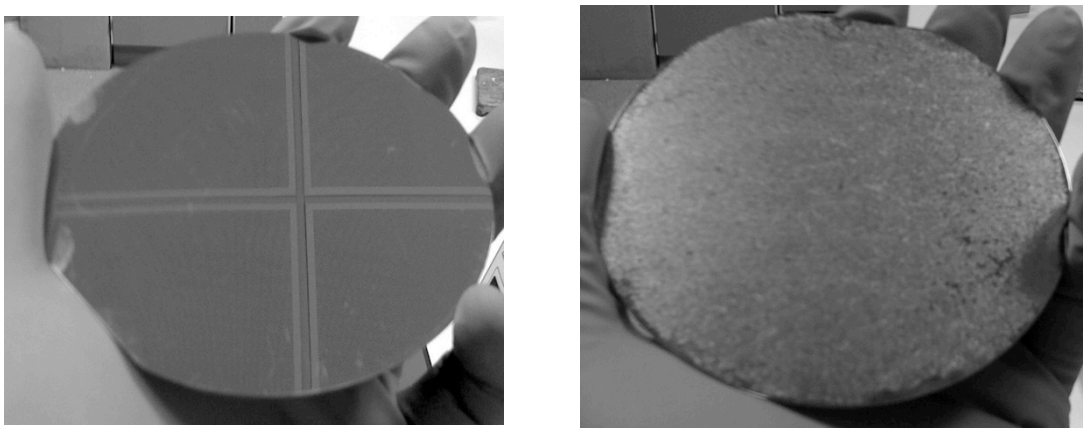

Figure 2-2. Silicon wafer prior to (left) and post (right) sprayed film deposition.

2.2 Characterization Techniques

2.2.1 Scattering

The main techniques used in this research are based on the interaction of radiation with matter, particularly x-rays and neutrons although visible light is also used. Due to the wave particle duality of matter it is possible to consider all of these forms of radiation together and use the properties of waves to build up an understanding of these techniques. There are a number of books and articles that have been written that cover this in more detail[75-78] so what follows is an overview designed to give enough detail to understand the results that follow.

If the sample is considered as a single point in space and if it is assumed there is no energy transferred during the interaction then it is possible to represent the scattering of radiation diagrammatically as shown in Figure 2-3.

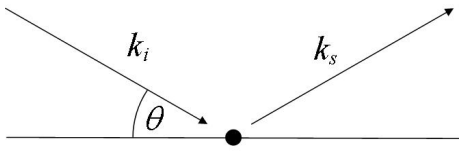

Figure 2-3. Scattering from a point in space.

In this diagram the incoming radiation is defined as the wave vector k_i and the scattered radiation as wave vector k_s, which have magnitude defined as:

$$|k| = \frac{2\pi}{\lambda} \qquad \text{Equation 2-1}$$

The vectors can then be rearranged to give the scattering vector Q by defining Q as in Equation 2-2, as shown diagrammatically in Figure 2-4.

$$Q = k_s - k_i \qquad \text{Equation 2-2}$$

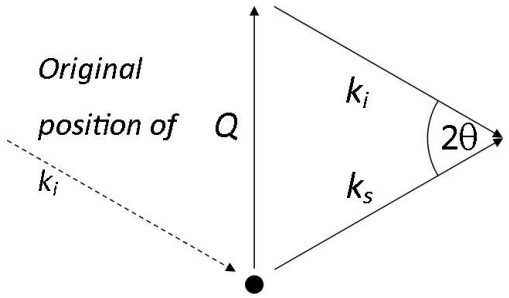

Figure 2-4. Definition of Q.

From Figure 2-4 Q can be calculated using trigonometry giving the result in Equation 2-3, which can then be transformed using Equation 2-1 to give Equation 2-4, which is a form of Bragg's Law.

$$\frac{Q}{2} = k\sin(\theta) \qquad \text{Equation 2-3}$$

$$|Q| = \frac{4\pi}{\lambda}\sin(\theta) \qquad \text{Equation 2-4}$$

A scattering experiment is the measure of the intensity of scattered radiation as a function of Q. This definition shows that Q varies with both angle and the wavelength of the incident radiation. This is an important factor that affects the set up of an experiment to measure scattering. If the equipment is set up to have a fixed angle of incidence then Q is varied by varying the wavelengths of the incoming radiation, this is known as an energy dispersive setup. This is commonly done by creating a pulse of many wavelengths of radiation, then measuring the scattering as a function of time after the pulse was created. As described by Equation 2-5 this time can be converted to a velocity, given the source to detector distance is known, which can then be converted wavelength and finally to a scattering vector Q. The other experimental setup is known as angular dispersive and to perform this experiment a fixed wavelength of radiation is used and the experimental geometry is altered to alter the incoming and scattered angles and then directly convert these angles to a scattering vector Q. Both techniques have been used in this report and will be discussed later.

$$E = h\nu = \frac{hc}{\lambda}$$ Equation 2-5

After defining the independent variable, the scattering vector, it is important to understand how the dependant variable, the scattered intensity, arises from the interaction. To do this the interactions of the radiation with the sample needs to be understood. X-rays interact with the electron cloud of the sample while neutrons interact with its nucleus.

Firstly considering the case of interaction of x-rays with the sample. As stated previously the x-rays interact with the electron cloud of the sample, therefore the scattering is dependant on the electron density of the sample. To simplify the problem the sample is considered as a single atom allowing the scattering to be defined according to a parameter called the scattering length, as Zr_e, where Z is the atomic number of the atom in question and r_e is the classical electron radius. From this it is clear that scattering increases linearly with increasing atomic number.

A similar definition can be used for neutrons, and the scattering length for neutrons is given symbol b, and has previously been measured for different atoms in the periodic table.[79, 80] As stated earlier the neutrons interact with the nucleus of the sample which means that, whereas x-ray scattering length increases linearly across the periodic table, neutron scattering length appears to be almost random.

This apparent randomness is one of the main reasons for performing neutron scattering but before that can be discussed another term needs to be defined. This new term is scattering length density, N_b, and, as the name suggests, it is directly related to the scattering length just discussed. Previously the system was simplified to scattering from a single atom. In this report scattering from larger objects in the main focus of interest, such as aggregates of molecules, therefore the scattering length has to take into account all of the different atoms within a particular molecule and the number of molecules in a given volume. Fortunately this can be done by using an average scattering length for the aggregate and this is the scattering length density, which is related to the scattering length by the following equation, Equation 2-6

$$N_b = \frac{\sum_{i=1}^{n} b_i}{v_m}$$ Equation 2-6

Here b_i is the coherent scattering length of the i^{th} of n atoms in the molecule and v_m is the molecular volume of that molecule. Although shown here is the calculation for the neutron scattering length density it is possible to replace b_i with $Z_i r_e$ where Z_i is

the atomic number of the i^{th} of n atoms and then calculate the x-ray scattering length density.

So far only one type of scattering has been discussed, this is scattering where there is no energy transferred between the incoming radiation and the scattering body, $|k_i| = |k_s|$, this is called elastic scattering. However as atoms are able to move in a sample if the atom moves due to the interaction of the radiation then there will be an energy transfer, this is called inelastic scattering. This can be precisely explained mathematically as shown by Van Hove in 1954.[81] From Van Hove's formalism two other types of scattering are revealed, these are coherent and incoherent scattering. Coherent scattering is when the phase of the scattered radiation is consistent throughout the sample therefore the scattering from different scattering bodies will interfere. Incoherent scattering is when the phase of the scattered radiation is different for the different scattering bodies within the sample.

Of importance to this study is elastic coherent scattering. As there is no energy transfer during the interaction and the phase of the scattered radiation is the same the resulting interference pattern can be used to determine the position of the different scattering bodies within the sample. This is more clearly shown in Figure 2-5, which is a diagram of Bragg's Law given in Equation 2-7. It is also possible to use Equation 2-7 along with Equation 2-4 to show how the scattering vector Q is related to the distance between the scattering bodies, d, shown in Equation 2-8, because of this inverse relationship Q is known as a reciprocal space measurement.

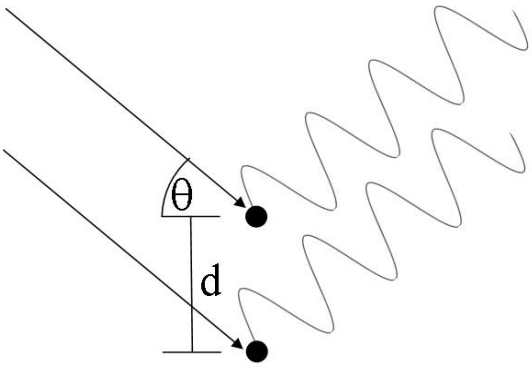

Figure 2-5. Coherent Scattering

$$n\lambda = 2d\sin(\theta) \qquad \text{Equation 2-7}$$

$$Q = \frac{2\pi}{d} \qquad \text{Equation 2-8}$$

While elastic coherent scattering is the most important form of scattering used in this study inelastic coherent scattering and incoherent scatter still occur however these are seen as "noise" in the scattering patterns. Inelastic coherent scattering can be used to give information about collective motion of atoms within a sample such as a crystal while incoherent scattering can be used, for instance, to give information about atomic diffusion.[77]

The neutron coherent and incoherent scattering lengths of hydrogen and deuterium are shown in Table 2-1.[79] The important thing to notice from these values is the hydrogen is not a good coherent scattering body but a very good incoherent scattering body, where-as deuterium is a good coherent but a bad incoherent scattering body. Due to this when performing a neutron scattering experiment it is advisable to minimise the amount of hydrogen in the system therefore it is common to use heavy water (D_2O) instead of regular water for systems that have an aqueous solvent.

	Coherent Scattering Length (fm)	Incoherent Scattering Length (fm)
Hydrogen	-3.741	25.274
Deuterium	6.671	4.04

Table 2-1. Scattering Lengths of Hydrogen and Deuterium

In real world situations instead of scattering off a point, as described above, scattering actually occurs at the interface of two regions of different scattering length density, this can be roughly compared to reflection off a solution where the refractive indices are different. The difference between two regions of different scattering length density is called the contrast and it plays a major role in neutron and X-ray scattering. In x-ray scattering, studying a surfactant micelle with water as the solvent gives scattering length densities of water as 9.46×10^{-6} Å^{-2}, of a surfactant as 7.3×10^{-6} Å^{-2} and this gives a contrast of 2.13×10^{-6} Å^{-2}. As the x-ray scattering length increases linearly across the periodic table many hydrocarbon surfactants will have very similar scattering length densities.

In neutron scattering things are very different, as alluded to earlier. The neutron scattering length varies almost randomly across the periodic table, which means some atoms that are next to each other in the periodic table have very different coherent scattering lengths. This is not just true for similar atoms it can also be true for isotopes of the same atom, as shown with hydrogen and deuterium in Table 2-1. As well as replacing hydrogen for deuterium in water a similar substitution is possible for any hydrogenated chemical; this alters the scattering length density of

the chemical and therefore the amount of scattering from the sample. For example a molecule of hexadecyltrimethylammonium bromide (C_{16}TAB) that has hydrogens attached will have a scattering length density of -0.34×10^{-6} Å^{-2} and a fully deuterated C_{16}TAB molecule 6.53×10^{-6} Å^{-2}. Given the neutron scattering length density of D_2O is 6.37×10^{-6} Å^{-2} the contrast of D_2O to hydrogenated C_{16}TAB is 6.71×10^{-6} Å^{-2}, while the contrast for D_2O to deuterated C_{16}TAB is -0.15×10^{-6} Å^{-2}.

The use of isotopic variation in neutron scattering is very important as it alters the scattering from a sample without significant alteration of the physical properties of the sample. This allows specific areas of the sample to be highlighted while hiding other areas without altering the structure of the sample. In Table 2-2 scattering length densities are shown for both hydrogenated and deuterated tails and head groups of C_{16}TAB where the head and tail of C_{16}TAB is defined as in Figure 2-6. Also included are the scattering length densities of water and D_2O. To completely hide certain areas of a sample it is possible to mix water and D_2O to give a scattering length density that is exactly the same as the part of the sample to be hidden. For example the use of C_{16}TAB with a hydrogenated head, a deuterated tail and D_2O as a solvent would give the majority of scattering from the C_{16}TAB head with very little from the tails.

	Scattering Length Density (Å^{-2})
Water	-0.56×10^{-6}
D_2O	6.37×10^{-6}
Hydrogenated Head Group	-0.29×10^{-6}
Deuterated Head Group	5.79×10^{-6}
Hydrogenated Tail Group	-0.35×10^{-6}
Deuterated Tail Group	6.74×10^{-6}

Table 2-2. Scattering length densities of different hydrogenated and deuterated components.

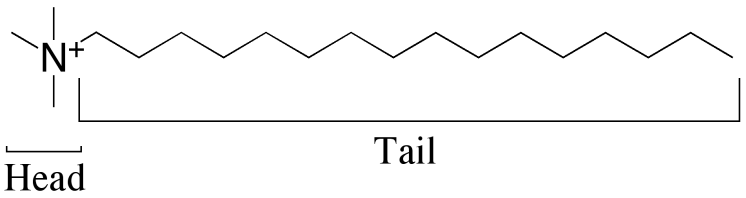

Figure 2-6. Diagrammatic definition of a surfactant head and tail group used to calculate the SLDs in Table 2-2

2.2.2 Small Angle Scattering

2.2.2.1 Theory

Small angle scattering is a transmission measurement of the sample this means that the incident angle is at 0° therefore the diagrammatic representation is the same as Figure 2-3 except that it is rotated anti-clockwise by the angle θ as shown in Figure 2-7.

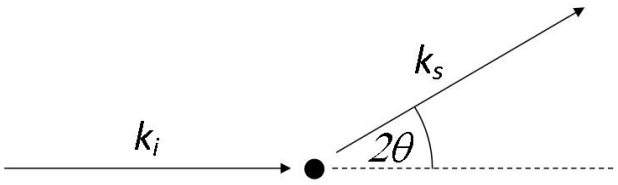

Figure 2-7. Small-angle scattering

If the sample has a well-ordered arrangement of scattering centres then the scattering pattern will show an array of discrete spots that could be used to determine the position of the scattering centres in relation to each other. This is usually done at wide angles to determine the structure of single crystals however it is possible to do this with larger molecules and aggregates in the small angle region. In this report the samples discussed are large micellar structures that are not ordered enough to show spots however they do show scattering from intra-micellar distances and also from average inter-micellar distances.

In small angle scattering the scattered intensity caused by intra-micellar scattering is known as the form factor, $P(Q)$, and the intensity caused by inter-micellar scattering is known as the structure factor, $S(Q)$. Together the structure factor and form factor combine to give the total scattered intensity, $I(Q)$, as shown in Equation 2-9. As well as the form factor and the structure factor in Equation 2-9 there is a term for background, this is a value for the incoherent background and instrumental noise associated with small angle scattering experiments.

$$I(Q) = P(Q)S(Q) + \text{background} \qquad \text{Equation 2-9}$$

In dilute systems it is possible to make the assumption that there will be no scattering from inter-micellar interactions therefore the $I(Q)$ is entirely dependant on the form factor. The simplest form factor is that of a sphere and is shown in Equation 2-10.[82]

$$P(Q) = \frac{scale \times (\Delta\varrho)^2}{V} \left[\frac{3V(\sin(Qr) - Qr\cos(Qr))}{(Qr)^3} \right]^2 \qquad \text{Equation 2-10}$$

In this equation V is the volume of a sphere given by $\frac{4}{3}\pi r^3$, r is the radius of the sphere, $\Delta\varrho$ is the scattering length density contrast between the micelle and the solvent. This equation also contains a term called the scale, which is a multiplicative factor related to the amount of scattering per unit volume of the sample therefore if the scattering is on an absolute scale then the scale will be equal to the particle volume fraction. All the small angle neutron scattering data reported herein is normalised to an absolute scale by comparison with a standard having known scattering. An example of the scattering pattern created using this equation is shown in Figure 2-8 where the scale is set to 0.005, the radius is 40Å, the contrast is 5.3×10^{-6} Å^{-2} and the background is 0.001.

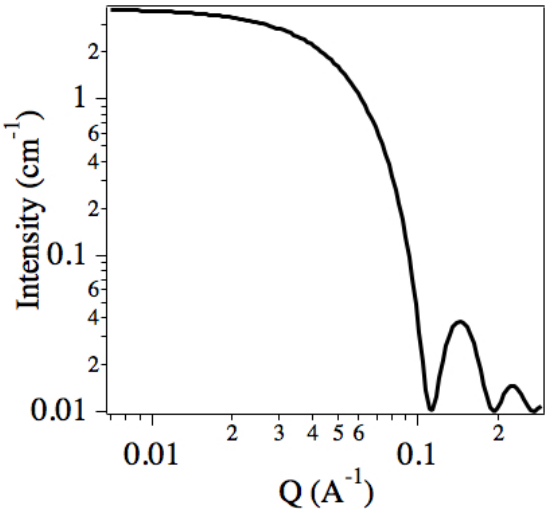

Figure 2-8. Scattering from a model sphere

As this data is from a theoretical monodisperse sphere there are a number of details about this graph that would not appear in real data. In reality the dimensions of the neutron beam are not infinitely small therefore there is a range of incident angles around 0, at the same time the detector pixels are not infinitely small therefore there is a small range of scattering angles in both the vertical and horizontal axis. Both of these details, and others, lead to an effect called smearing, which simply means that there is inaccuracy in the Q value and in the intensity, this flattens out the peaks and troughs seen in the high Q region of the graph. Also in the systems discussed in this report there is usually a degree of polydispersity in the micelle size similarly leading to flattening out of the peaks and troughs at high Q.

Although dilute systems are common in many cases it is important to also consider the structure factor. Given the systems studied in this report the most useful structure factor is the Hayter Penfold Mean Spherical Approximation[83] (HPMSA) that describes the interference effects caused by interacting charged particles in a dielectric medium. The HPMSA uses the same scale and diameter as the form factor but also includes terms for the charge on the micelle, the dielectric constant of the solvent, the temperature of the system, and the concentration of any component that may interfere with interaction between two micelles. The effect of the HPMSA can be graphically represented as shown in Figure 2-9. Figure 2-8 and Figure 2-9 can then be combined to show the theoretical scattering pattern from a sample of monodisperse 40Å spheres that are interacting in solution, Figure 2-10.

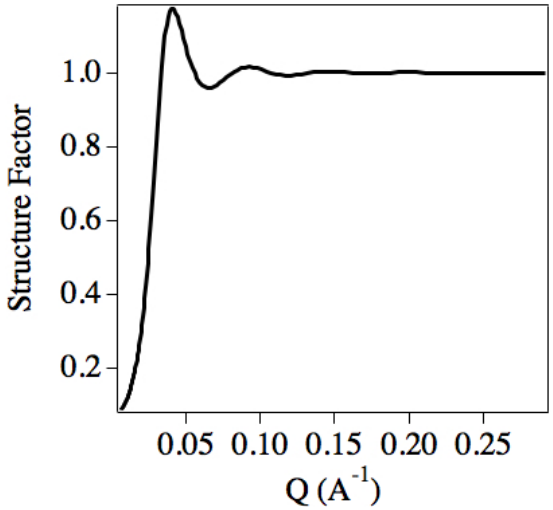

Figure 2-9. The Hayter Penfold Mean Spherical Approximation (HPMSA).

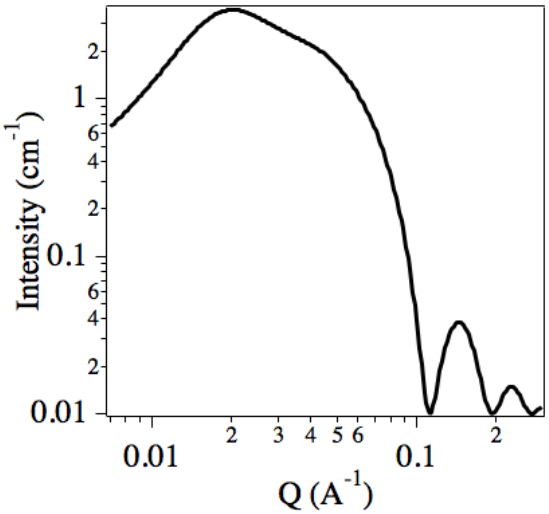

Figure 2-10. The combination of the of the HPMSA with the scattering from a model sphere.

2.2.2.2 Small Angle Neutron Scattering (SANS)

Small angle neutron scattering (SANS) has been performed at various locations during the course of this research project. The main instrument used was LOQ on Target Station 1 at the ISIS Pulsed Neutron Source, Chilton, UK. The other neutron instruments used were D11 at the ILL, Grenoble, France and NG7 at the NIST Centre for Neutron Research (NCNR), Gaithersburg, Maryland, USA. Both the NCNR and the ILL are reactor based neutron sources that start with a continuous beam of neutrons with a variety of wavelengths. To perform SANS both sites monochromate the neutron beams and vary the scattering angle making them angular dispersive instruments.

LOQ is a slightly strange case as it is a mixture of both angular and energy dispersive instruments. ISIS creates a pulse of neutrons, which, as described above, can be converted to a neutron wavelength as long as the source to detector distance is well known, therefore LOQ can be described as an energy dispersive instrument. However LOQ also has an area detector, which due to its ability to detect position and time, can be used as an angular dispersive detector with computer reduction to produce a proper intensity vs. Q map.

In all cases the neutron beam is collimated to achieve a narrow circular beam with low divergence through the sample and onto the detector. If the beam divergence were high then the scattered intensity at the lowest scattering angles would overlap with the direct beam meaning the intensity would be inaccurate. By creating as near to a point as possible, and by correcting for any overlap during the data reduction process, the scattering pattern can be described well by the mathematical functions described above.

The Q range and the related size range of the instruments used are shown in Table 2-3. These values are the reported values on the respective instrument websites however they will vary depending on the sample being studied and the instrumental set-up.

	Q Range ($Å^{-1}$)	Size Range (Å)
LOQ	0.006 – 0.24	30 – 1,000
D11	0.0003 - 1	10 – 10,000
NG7	0.0008 – 0.7	10 – 5,000

Table 2-3. Instrumental Characteristics, as reported on the instrument websites.

2.2.2.3 Ultra Small Angle Neutron Scattering (USANS)

As mentioned earlier the size of the structure being studied is inversely proportional to the scattering angle therefore to view larger structures, smaller angles must be used. Using a standard SANS setup there is a lower limit on the Q range due to the dimensions of the beam, below which it is the direct beam that is studied. When collimating the beam making the dimensions of the beam smaller leads to a decrease in the flux of neutrons on the sample therefore dimensions of the beam are dependant on the required flux for the experiment. It is possible however to use a different collimation setup for experiments that require very small angles, this setup is called USANS. Where as in SANS the beam of neutrons is collimated by cutting out divergent neutrons in USANS the neutrons are reflected off multiple crystals that separate out divergent neutrons leaving a highly collimated beam of neutrons. This technique, known as the Bonse-Hart technique, has been used since 1965[84] and is shown in Figure 2-11.

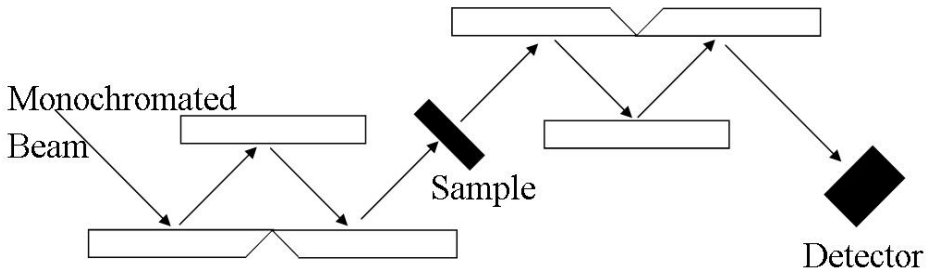

Figure 2-11. Bonse-Hart camera for USANS measurements.

Although the beam of neutrons is highly collimated because it is being bounced off a number of crystals it is better collimated in one axis than the other, in effect making it a narrow slit instead of the point collimation typical of SANS instruments. This is a form of smearing and important for data analysis and is discussed later. Also important is the fact that with the highly collimated beam of neutrons comes a significant reduction in the flux therefore USANS experiments are usually much longer per sample than SANS experiments.

The USANS instrument used in the research is called BT5[85] and is based at the NCNR in Gaithersburg, Maryland, USA. The *Q* range and size range of BT5 are shown in Table 2-4 in comparison to NG7, the SANS instrument at the same facility. Between the two instruments the measurable size rage is substantial.

	Q Range ($Å^{-1}$)	Size Range (Å)
BT5	0.00003 – 0.01	100 – 200,000
NG7	0.0008 – 0.7	10 – 5,000

Table 2-4. Instrumental characteristics of USANS vs. SANS

2.2.2.4 Experimental

Samples for SANS and USANS were prepared at the facility where the experiments were being performed using chemicals transported from the University of Bath or purchased specifically for use at the facility. For all neutron experiments D_2O was used as the solvent or in a mixture of 70% D_2O and 30% H_2O. While working at ISIS the D_2O used was purchased from Sigma (99%) by the facility for use by all experimenters. At D11 the D_2O provided on request by the facility to individual research groups. At the NCNR D_2O was provided on request from supplies purchased from CDN Isotopes (99% D).

As much as possible samples were prepared from pre made stock solutions of chemicals to avoid inconsistencies within an experiment. Stock solutions were made no more than 24 hours before the start of an experiment and the longest experiments lasted 7 days, and except where mentioned were kept at ~30°C throughout the experiment. All solutions were prepared in containers with lids and were also para-filmed to limit deuterium/hydrogen exchange. All experiments were performed in 1mm thick quartz glass double stopper sample holders with a volume of 0.6ml purchased from Hellma. Samples were held at 28C during data collection as this is above the Krafft point of C_{16}TAB.[86]

2.2.2.5 Data Treatment and Fitting

SANS data reduction is performed separately for each instrument using software developed by the facility. The raw data is corrected for scattering caused by the sample holder, the solvent, and by the instrument by subtracting the scattering from the sample holder and solvent as a background and an empty beam run. The raw data is also scaled pixel by pixel for detector efficiency to correct for detector abnormalities, and then the intensity is normalised by comparison to a standard, which is different at each instrument. The standards are samples that have known scattering to which all experimental samples can be normalised to. On LOQ the standard is a block copolymer, on D11 the standard is water and on NG7 the standard is air. The data is corrected for the beam size then radially averaged to produce an intensity vs. *Q* plot for further analysis.

USANS data reduction is similar in theory however the detector is a point detector instead of an area detector therefore there is no detector efficiency correction and there is no radial averaging. Data correction is still corrected for empty cell scattering and background scattering and then normalised to an absolute scale therefore making it comparable to scattering from the SANS experiments.

All data fitting was performed using the SANS Analysis Package for Igor Pro (Wavemetrics) developed by NIST.[87] This package provides an easy to use interface for comparison of mathematical models to the collected data. Building on the backbone of the IgorPro software has allowed access to built-in routines such as global fitting, for fitting the models to multiple different data sets. Also having the models written in the IgorPro programming language allows access to the underlying maths within the models and therefore allows further refinement of the models to suit particular fitting purposes. Any alteration of the mathematical models used will be discussed further with discussion of the results.

As mentioned briefly above the SANS instruments scatter from a point of neutrons while the USANS instrument scatters from a narrow beam of neutrons. This has to be taken into account when analysing data from any of the instruments. Although it is possible to use a mathematical algorithm to remove this effect, called desmearing, this can adversely affect the data therefore it is more common to mathematically model the effect and then include this in the model being fit to the data. Included with all the models in the SANS Analysis package is a smeared version where the effect of smearing is taken into account. In reality the smearing effect from the SANS instruments is very low or corrected for during the data reduction therefore it is common to use the point scattering models when analysing the data, for USANS however the smeared models are always used.

2.2.3 Spin-Echo Small Angle Neutron Scattering (SESANS)

2.2.3.1 Theory

As described earlier to study structures larger than are visible using SANS it is possible to perform USANS, however there are two drawbacks, the first is that it is a very time consuming experiment, the second is that it is a growing field with limited available instruments around the world. Over the past 10 years an alternative instrumental setup has been developed for the study of very large structures at the Delft University of Technology called Spin-echo small angle neutron scattering

(SESANS). Recently a new instrument, called OFFSPEC, has been built at ISIS Target Station 2, which has the ability to perform SESANS experiments.

Although SESANS and USANS give very similar information the theory behind how the two instruments work is very different. Since SESANS is a recent development (first published 1996[88]) there has been relatively little published on the subject. The following is an overview of the technique to explain the differences between USANS and SESANS.[89, 90]

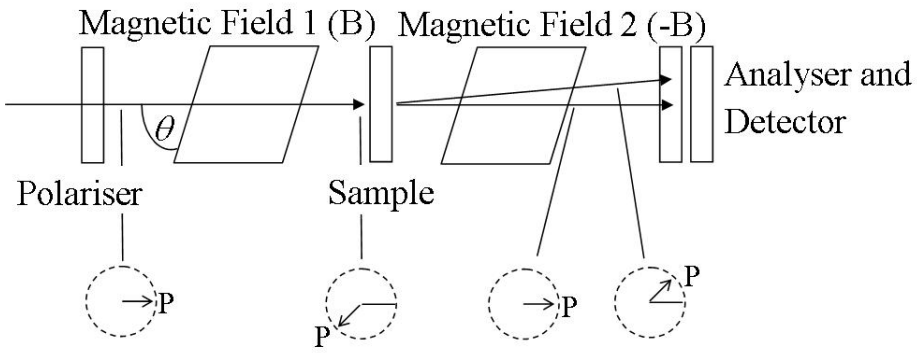

Figure 2-12. Schematic of the polarisation of a neutron beam through a SESANS instrument. Adapted from reference[91]

The SESANS instrumental setup is shown in Figure 2-12. It works on the principle that the spin of neutrons will precess in a magnetic field. As a neutron passes through the first magnetic field the neutron is depolarised before hitting the sample. If there is no sample in the beam then the neutron will pass through into the second magnetic field that has the exact opposite field strength. Assuming there is no scattering between magnetic field regions the path length of the second magnetic field region will be exactly the same as the first, this will lead to a repolarisation of the beam exactly cancelling out the depolarisation caused by the first magnetic field region. If there is a sample in the beam a scattered neutron will have a different path length in the second magnetic field than in the first therefore there will be a net depolarisation of the beam.

As the magnetic field regions are identically shaped if a neutron passes through the instrument to the detector, assuming no scattering from a sample, the depolarisation caused by magnetic field 1 will be cancelled out by magnetic field 2 regardless of angle of entry. Due to this the collimation of the incoming radiation is far less important than in SANS or USANS. This means a wide beam can be used maximising the flux on the sample making SESANS a relatively fast experiment. In USANS to get a well-collimated beam the majority of neutrons are discarded, thus seriously limiting the flux on the sample.

The net depolarisation of the neutron beam is caused by a difference in path length between magnetic field regions 1 and 2 therefore it can be said that it is the interaction between the neutrons and the magnetic field that define the experiment. The parameters that are important in a SESANS experiment are the wavelength of the neutron beam, λ; the magnetic field strength, B; and the angle of the magnetic field, or pole shoe angle, θ, shown in Figure 2-12. These parameters combine, in Equation 2-11, to give the spin-echo length, z.

$$z = \frac{m_N \gamma_N \lambda^2 BL \cot\theta}{2\pi h} \qquad \text{Equation 2-11}$$

In Equation 2-11, m_N is the neutron mass, γ_N is the neutron gyromagnetic ratio, L is the path length of the magnetic field and h is Planck's constant. It is the amount of depolarisation as a function of spin echo length that leads to determination of the size of the particles in the sample. As ISIS Target station 2 is a pulsed source the spin echo length is varied by varying the wavelength, while the magnetic field strength and pole shoe angle are held constant. It is important to note here that z is proportional to λ therefore SESANS is a measurement in real space rather than reciprocal space.

2.2.3.2 Experimental

Sample preparation for a SESANS experiment is exactly the same as for the SANS and USANS experiment. Samples were prepared no earlier than 24 hours before an experiment and stored in sealed containers to minimise hydrogen exchange in the sample. The longest experiment was 3 days. The experimental sample holders were quartz Hellma cells however they were 5mm and 2mm thick instead of the 1mm used in SANS and USANS. As there was no temperature control of the sample holder the samples were at the temperature of the experimental chamber which is ~20°C.

2.2.3.3 Data Treatment

During a SESANS experiment to get a depolarisation from the instrument it is the polarisation of the sample, $P(z)$, that is measured and compared to the polarisation of an empty beam, P_0, which is the maximum polarisation for the instrumental settings. Due to this the experiment is performed in a loop with a number of samples and an empty beam. Each sample is measured for 15 minutes and the number of loops

through all the samples was decided by the quality of the data and the amount of time left for the experiment.

Data reduction is performed using Mantid, a data reduction and analysis program developed at ISIS to handle all the new data reduction and analysis needs created by the more complex instruments at ISIS Target Station 2. The python scripts to perform data reduction of OFFSPEC data were written separately by the instrument scientist. The data reduction adds the raw data from each sample from each loop, converts the wavelength to spin echo length then divides the *P(z)* of the sample by the P_0 measurements before writing the data to a useable file type.

As SESANS is still a relatively new technique there is no publicly available analysis software, however a recent publication has calculated the mathematical solutions of *G(z)* for commonly studied structures.[92] A selection of these solutions has since been converted into fit functions using the programming routines in Igor Pro. Creation of these fit functions will be explained and shown with the relevant data in chapter 5.

2.2.4 Reflectometry

2.2.4.1 Theory

To study the structure of thin films one of the best techniques available is reflectometry, which is a measure of the intensity of reflected radiation from an interface. The general theory of scattering, as described above, is very adaptable to understanding reflectivity. In reflectometry it is the specular reflection from an interface that is studied, which is defined such that in a monochromatic beam the incident angle of the radiation is equal to the reflected angle as shown in Figure 2-13.

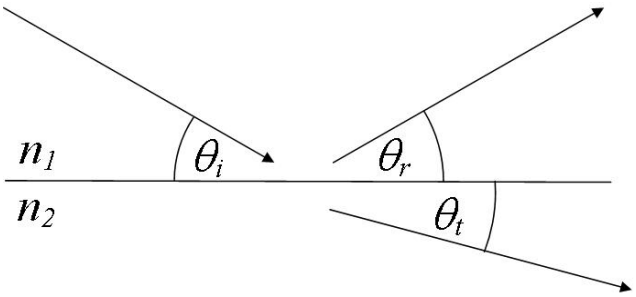

Figure 2-13. Reflection and transmission of radiation at a surface.

Also shown in Figure 2-13 is a refracted wave because in reflectometry refraction, as described by the Fresnel equation, also has to be considered, Equation 2-12.

$$R = \left[\frac{n_1 \sin\theta_i - n_2 \sin\theta_t}{n_1 \sin\theta_i + n_2 \sin\theta_t} \right]^2 \qquad \text{Equation 2-12}$$

Here R is the fraction of reflected light, n_1 and n_2 are the refractive indices of the materials, and θ_i and θ_t are the angles of incidence and transmittance respectively, as shown in Figure 2-13. If θ_t is unknown then it can be calculated from Snell's Law, Equation 2-13. For neutron and x-ray experiments the refractive index can be calculated from Equation 2-14, where N_b is the scattering length density as discussed earlier.

$$n_1 \cos\theta_i = n_2 \cos\theta_t \qquad \text{Equation 2-13}$$

$$n = \frac{\lambda^2}{2\pi} N_b \qquad \text{Equation 2-14}$$

In this research reflectometry is performed at the air/solution interface therefore n_1 refers to the refractive index of air which is 1, therefore simplifying Equation 2-13 to Equation 2-15.

$$\cos\theta_i = n_2 \cos\theta_t \qquad \text{Equation 2-15}$$

When the refractive index of the solution is less than 1 there is a point at which $\theta_t = 0$ while $\theta_i > 1$ leading to total reflection. This point is known that the critical angle below which there is total reflection. This point can be seen clearly in Figure 2-14.

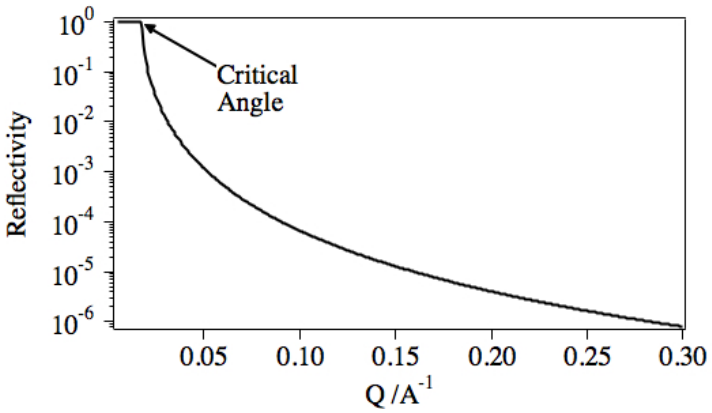

Figure 2-14. Theoretical reflectivity from a clean D_2O surface.

The plot shown in Figure 2-14 is a theoretical plot from a clean D_2O surface that has a critical angle, $Q_c = 0.01739 Å^{-1}$. Above the critical angle the drop off in reflectivity

is proportional to $^{1}/_{Q^4}$. However a clean solution surface is rarely measured therefore it is important to understand the effect of adding layers to a system. Figure 2-15 illustrates a simplified model of what occurs in a system with multiple layers.

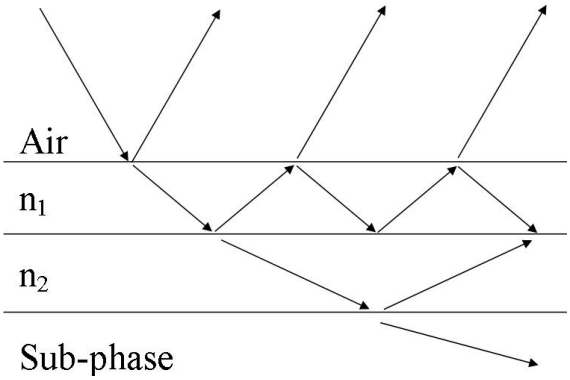

Figure 2-15. Reflection and refraction from a multi-layered surface.

As well as reflecting from the surface, some of the incident radiation is transmitted. This transmitted radiation will then interact with the second interface where some radiation will be reflected and some transmitted. The reflected radiation will then interact with the surface where it can either be reflected or transmitted, the transmitted radiation emerging from the sample and being collected by the detector, while the reflected radiation will re-interact with the second interface. At each interface the same calculations can be performed as described above until a value for the total reflectivity is obtained.

The reflection and transmission of multiple layers will alter the reflectivity pattern shown in Figure 2-14, however if the layers are well defined then the resulting pattern will be indicative of the structure formed, as shown in Figure 2-16.

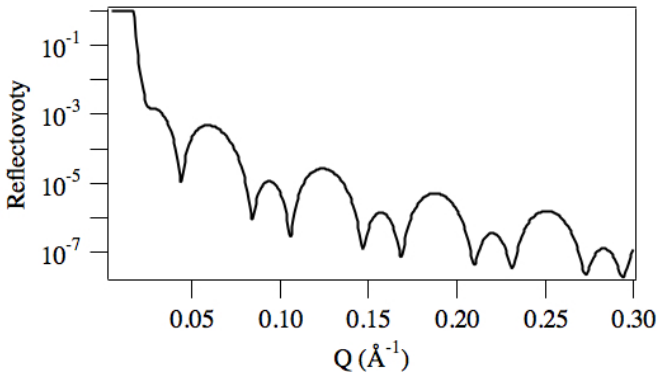

Figure 2-16. Reflectivity pattern from a two-layered surface.

Figure 2-16 is the theoretical reflectivity from a system with two 100Å layers, the top layer having a scattering length density of 2×10^{-6} Å^{-2} and the bottom layer

having a scattering length density of 4×10^{-6} Å^{-2} while the sub-phase is D_2O with a scattering length density of 6.37×10^{-6} Å^{-2}.

From the definition of Q in Figure 2-3 and Figure 2-4 and from Figure 2-15 it is possible to say that reflectivity is a perpendicular probe of the structure parallel to the interface. This is very useful for lamellar structures however for more complex structures it is often useful to study scattering away from the specular reflection known as either off-specular reflection or diffuse scattering.

Although many variations of off-specular reflectometry exist only two will be discussed here, as they are two that relate to the work discussed later, they are time resolved off-specular reflection and grazing incidence diffraction.

Time resolved off-specular reflection uses the divergence of a monochromatic beam with a wide footprint on the sample, shown in Figure 2-17. Normally the detector only measures over a small angle range, D_s, where $\theta_i = \theta_r$, however using a wider detector, D_w, it is possible to simultaneously measure higher angles, $\theta_{ih} = \theta_{rh}$, and lower angles $\theta_{il} = \theta_{rl}$. This technique utilises the high flux of the x-ray beam to measure structure formation by following the growth of strong diffraction peaks in the scattering pattern with minute time resolution.

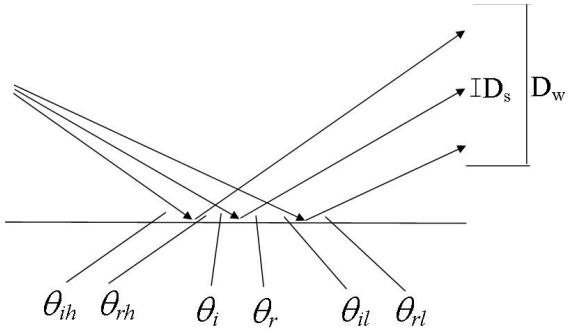

Figure 2-17. Diagram of the scattering angles for time-resolved off-specular reflection

Grazing Incidence X-ray Diffraction (GIXD), also known as grazing incidence SAXS or near surface SAXS however in this report it is called GIXD. As with time resolved off-specular reflection a wide detector is used to give a broad Q range over a short period of time however GIXD also moves the detector in an arc in the plane of the sample, δ, as shown in Figure 2-18. When $\delta = 0$ the experimental set up is very similar to the time resolved measurement except it is performed when the sample structure is not changing. At $\delta = 0$ the pattern only shows the specular reflection from the incident radiation. When $\delta > 0$ the scattering vector is rotated so that reflections that are not parallel to the surface are visible. This is represented for

an array of cylinders packed parallel to the surface in Figure 2-19, where Q_z is visible in specular reflection and Q_{xy} is visible in GIXD.

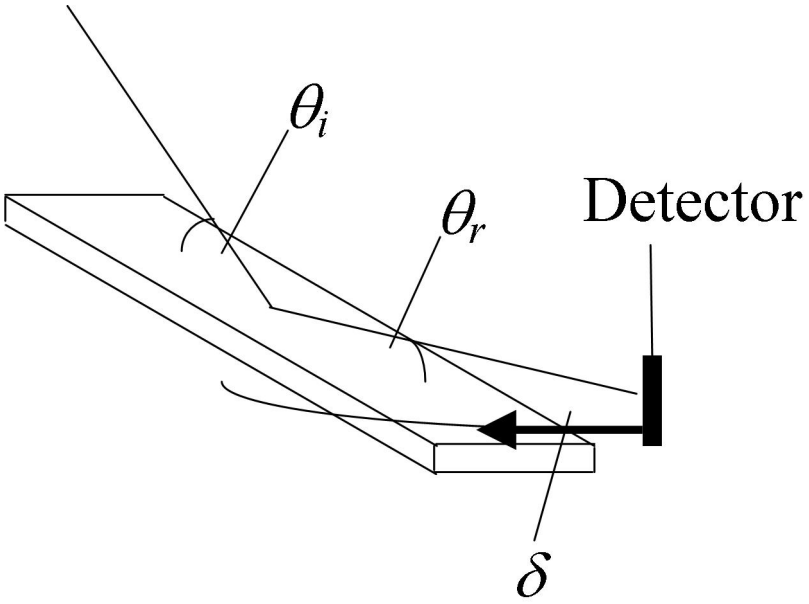

Figure 2-18. Diagram of the grazing incidence x-ray diffraction experiment.

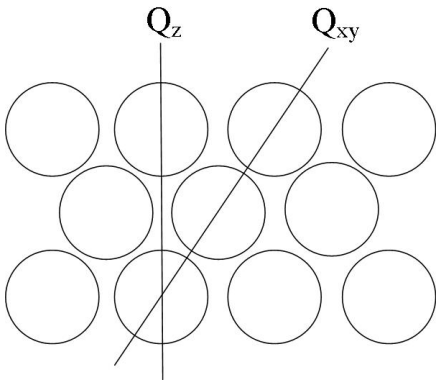

Figure 2-19. Comparison of Q_z measured in reflectometry and Q_{xy} measured in GIXD.

During these experiments two incident angles are used. The first angle is less than the critical angle for the system. At this incident angle an evanescent wave is formed, which when re-radiated, gives structural information about the top 100Å of the sample. The second incidence angle used in these experiments is greater that the critical angle and therefore give rise to structural information from deep within the sample. However the higher the incidence angle the more likely there will be transmission, which when re-emitted from the sample will lead to interference effects which slightly shift the position of features in the scattering as a function of Q.

2.2.4.2 Experimental

In this report two neutron reflectometers have been used, these are SURF at ISIS and FIGARO at the ILL. All of these instruments use a time of flight method to perform energy dispersive experiments. One x-ray reflectometer has also been used; this is Troïka II, on the ID10B beamline at the European Synchrotron Radiation Facility (ESRF), Grenoble, France. Troïka II is an angular dispersive instrument with a much higher flux than the neutron instruments. Reflectometry has been performed on all the instruments mentioned above however due to the higher flux and the versatility of Troïka II it is the only instrument to perform the time resolved off-specular experiments and the GIXD experiments.

As with the other facility based experiments the samples were prepared no longer than 24 hours before the start of the experiment. The solvent for all neutron experiments was D_2O, which was obtained from the sources mentioned previously. Also similar to the other experiments samples were made and stored in sealed containers to limit hydrogen exchange.

Sample holders are custom-made Teflon troughs with dimensions of 152mm, 42mm, 3mm and hold 20 - 30ml of solution with a meniscus well above the side of the trough. These sample holders give flat solution surface area for study with approximate dimensions of 110mm, 30mm. For the neutron experiments these sample holders sit within the facilities own heat controlled sample holders allowing temperature control of the solution during each experiment. For the Troïka II experiment the sample holder has a very thin base is held in place by a custom-made copper heat sink that is attached to the instrument and heated by a temperature controlled water bath. Samples were held at 28-30°C for all experiments as this is above the Krafft temperature of C_{16}TAB.[86]

Any variations for specific experiments will be discussed with the results they relate to.

2.2.4.3 Data Treatment

Each facility has its owns data reduction routines. In all cases no background subtraction is performed on the data. The data is normalised by comparison to scattering from a clean D_2O surface. ESRF data reduction corrects the data for use of attenuators and for any variation of the beam, by normalising it to the monitor.

The structure observed from the reflectivity patterns is composed of diffraction peaks so strong that standard reflectivity data analysis is rarely performed, where is has been performed the Motofit Package for IgorPro is used.[93] The usual data analysis performed in this report has been done by determining the peak positions within the data. The relative peak positions from the data are then compared to tables of calculated relative peak positions to try and identify the structure formed. Where possible relative intensities of peaks have been studied to further identify the structural formation, this has been done by comparison to models determined by Garstecki and Holyst.[94, 95]

2.2.5 Crystal Structural Determination

In the SANS experiments described in this thesis the structures being studied are micelles and the interactions between individual micelles. In these systems there is usually no long-range order. In the films however there is evidence of long range ordering in the structures. This is shown in Figure 2-20, which are the simulated reflectometry patterns from a series of thin films. The model used to create these patterns is a surfactant monolayer, of 15Å and a SLD of -0.35×10^{-6} Å^{-2}, at the surface of the sample, followed by a multi-layered system made up of a 10Å aqueous polymer layer with a SLD of 6×10^{-6} Å^{-2} and a 30Å surfactant bilayer with a SLD the same as the monolayer at -0.35×10^{-6} Å^{-2}. Apart from the pure D_2O surface the only variable changed in these patterns is the number of repetitions of the polymer/surfactant bilayer multilayer.

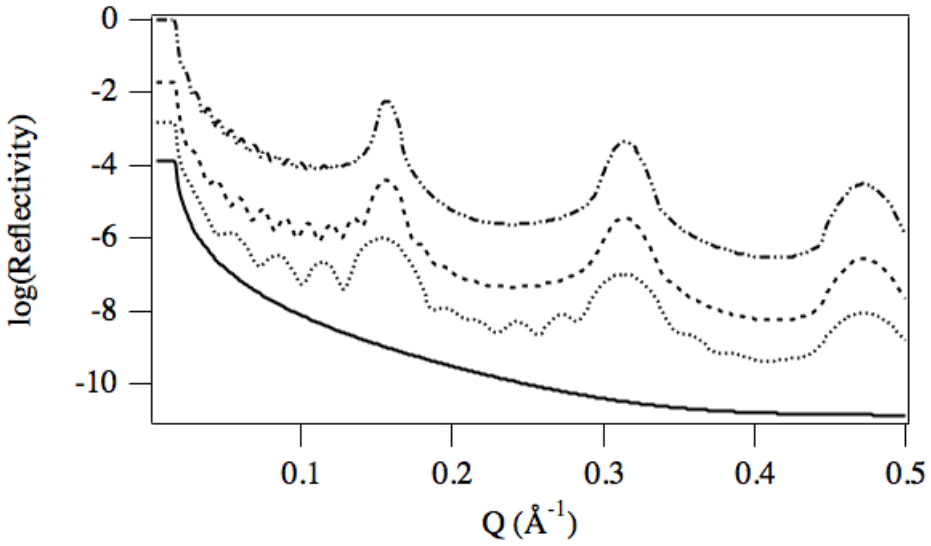

Figure 2-20. Theoretical reflectivity patterns from a multi-layered system as described in the text. The solid black line is a pure D_2O surface for reference. From bottom to top the dotted line is a 5 repetition multi-layer, the dashed line is a 10 repetition multi-layer and the top dashed and dotted line is a 20 repetition multi-layer.

Although Figure 2-20 has the lines off set for clarity it is still clear to see that the more layers in the systems the sharper the peaks become. Due to this the intensity and sharpness of the peaks is an indication of the ordering within a system. The systems with the best ordering and most layers will give the sharpest peaks while the loss of either the ordering or the number of layers will lead to a decrease in both the peak intensity and its sharpness.

If this explanation is taken to the extreme to find the most well ordered systems with an almost infinite number of layers then you end up in the realms of crystallography. This is because single crystals are made up of an array of atoms in specific positions within a lattice. When studying well-ordered systems at least a basic understanding crystallography is therefore required.

Crystallography is a technique where radiation, most commonly x-rays, is scattered from individual atoms in a crystal and the interference pattern is studied to determine the position of the atoms within the lattice. If a simple cubic structure with atoms at each corner, Figure 2-21, is irradiated with x-rays, scattering will occur. Using the points marked on Figure 2-21 the scattering can be explained in relation to an origin, which is defined as atom A. From the origin the directions are defined such that A to B is the *x* direction, A to C the *y* direction, and A to D the *z* direction.

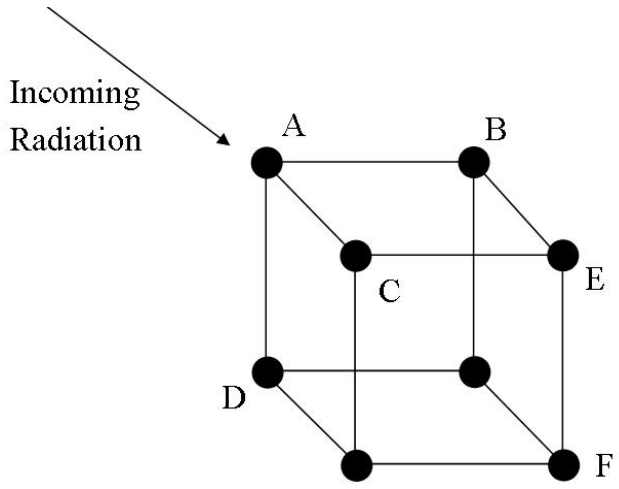

Figure 2-21. Diagrammatic explanation of crystallography.

If the radiation is scattered from the origin and any of the other atoms then the scattered radiation will interfere with each other. At a certain incident angle and radiation wavelength the scattering from the origin and from another atom will be in phase, which will lead to constructive interference and therefore a peak on the detector, this is explained earlier with Figure 2-5. If the wavelength of the incoming radiation is kept constant but the angle of the incident and scattered radiation is

varied then the full scattering pattern can be detected with spots at positions representing the constructive interference from scattering off two atoms. Once the scattering pattern is collected it is possible to calculate the positions of the atoms within the lattice.

To do this Bragg's Law, Equation 2-7, is used to determine the distance between atoms and the origin. For instance in a perfect cube atoms B, C, and D, in Figure 2-21, are all exactly the same distance from the origin, this distance is defined as 1, however they are in different directions. In crystallography the directions are defined as h, k and l which represent the axis x, y and z as defined earlier, these directions are then written as (hkl). Using this notation scattering from atoms A and B can be denoted as (100), A and C as (010), and A and D as (001). As these reflections are all the same distance from the origin the corresponding spot positions will also be the same distance from the origin. Reflections can occur from other atoms, such as the atoms marked as E and F on Figure 2-21. To get from the origin to the atom marked E the distance is one unit on the *x*-axis and one unit of the *y*-axis but none on the *z*-axis therefore it is denoted as (110). Atom F however is one unit along all axis therefore it is denoted as (111). The distance the spot, S_d, in the scattering pattern is from the origin is related to the distance the atom is from the origin atom. This distance can be calculated using trigonometry as shown in Equation 2-16

$$S_d = \sqrt{(h^2+k^2+l^2)} \qquad \text{Equation 2-16}$$

Although relatively simple to understand the description above is not entirely accurate. As mentioned previously scattering is a reciprocal space measurement therefore the (110) spot should be closer to the origin in the scattering pattern than the (100) spot because it is further away. However scattering is actually from reflection planes. The (100) plane is orthogonal to the *x*-axis, and the same is true for the (010) refection and the *y*-axis and the (001) reflection and the *z*-axis. The (100), (010), and (110) reflection planes are all shown in Figure 2-22, atom labels A, B, C, and E are the same as in Figure 2-21 for clarity. Therefore to explain how the (110) spot in the scattering pattern is further from the origin than the (100) spot, it can be seen that the (110) reflection plane is closer to the origin than the (100) plane therefore the spot in the scattering pattern is further away. The exact distance between the origin and the (110) reflection plane in the direction of atom E is the reciprocal of the distance between the origin and atom E. Given scattering is in reciprocal space then distance between the origin at the (110) spot is therefore directly related to the distance from the origin atom to the atom E.

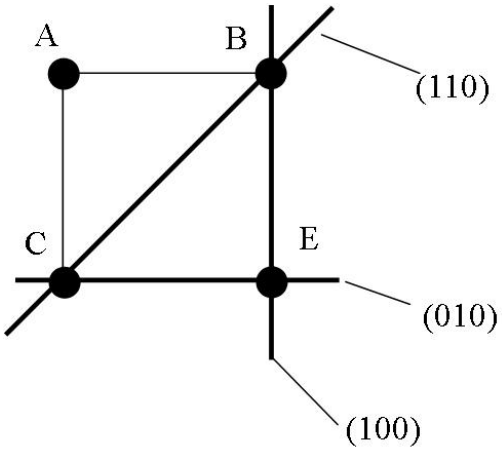

Figure 2-22. Reflection planes in a cubic structure.

Finally to put this into real systems the distance between the atoms A and B is defined as the unit cell parameter, *a*. This parameter is a real length and is dependant on the system being worked with, for instance a micellar cubic pattern may have a unit cell parameter $a = 119$Å.[96] For simplicity when performing these calculations however the relative distances are used therefore the indices h, k, and l are always integers. Not all crystals however are made up atoms sitting on the corners of a perfect cube; therefore it is the positions of the spots and the presence or absence of certain spots that confirms the structure of the crystal lattice. Knowing the geometry of the possible structures allows the derivation of rules for the different cubic structures, these are shown in Table 2-5.

Crystal Lattice Type	Allowed Reflections	Forbidden Reflections
Primitive Cubic	Any h, k, l	None
Body Centred Cubic	$h+k+l$ even	$h+k+l$ odd
Face Centred Cubic	h, k, l all odd or even	h, k, l mixed odd and even
Diamond F.C.C.	h, k, l all odd or h, k, l all even and $h+k+l=4n$	h, k, l all odd and even or h, k, l all even and $h+k+l\neq4n$
Hexagonal (HCP)	l even, $h+2k\neq3$	l odd and $h+2k=3n$

Table 2-5. Selection rules for Miller indices of different cubic structures.[97]

So far it has been assumed that a single, perfect crystal is being studied, however there is also the possibility of seeing powder patterns. Powder patterns describe the scattering of a large number of randomly orientated small crystals. Within the samples the distance between the origin and the reflection planes stays constant however the angle that the radiation is being scattered is being altered because the not all the crystals are aligned with the same orientation. The final pattern therefore,

instead of showing discrete spots, shows rings at the same distance from the origin at the spots where previously seen. In some systems where there is long range order it is sometimes possible to get rings with discrete areas of higher intensity relating to where spots would appear if the sample was slightly better ordered.

In this thesis a number of systems have been studied. The two simplest systems to determine are that of the lamellar and the 2D hexagonal films. These are the simplest due to the limited number of reflections. Hillhouse et al have reported the possible variations within aligned 2D hexagonal systems.[98] The possible cubic structures are however more complex for a number reasons, first is the number of potential cubic systems with similar reflections makes exact determination of structure difficult. On top of this simulations performed for studying thin-films have shown that reflections that should not be visible in certain structures are and that certain areas of peak suppression limit the intensity of other peaks that should be visible.[99]

To help determine the structures within the films, as well as studying the positions of the reflections modelling has been attempted using calculations performed by Garstecki and Holyst.[94, 95] The mathematical models detailed in these papers have been coded for use in Igor Pro, as shown in appendix 2, and as well as giving relative peak positions for different structures they also give relative intensities of the peaks.

Throughout this thesis the there are three specifically mentioned cubic patterns. The $Pm\bar{3}n$ structure, Figure 2-23 left, has previously been seen from templated CTEAB.[100, 101] The $Pn\bar{3}m$ and $Ia\bar{3}d$ structures have previously been reported as potential structures in C_{16}TAB/SDS templated thin films.[102] In the figures the grey areas represent either micelles or surfactant bilayers joining areas of minimal curvature within the structures. The channels between micelles or bilayers are filled with polymer/water mixtures.

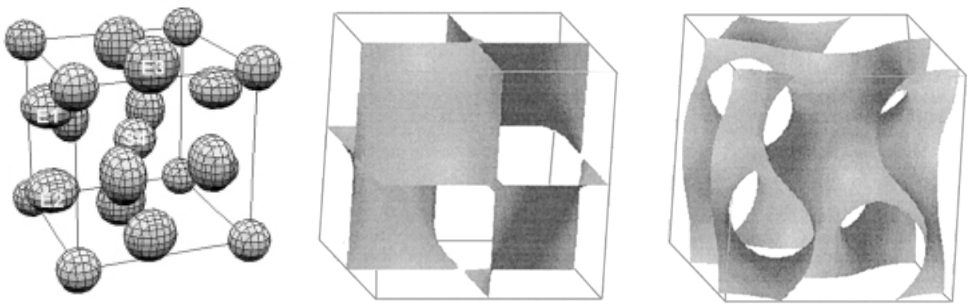

Figure 2-23. From left to right $I^3{}_1$ micellar cubic structure with $Pn\bar{3}m$ symmetry, Double Diamond structure with $Pn\bar{3}m$ symmetry, Gyroid structure with $Ia\bar{3}d$ symmetry. The I_1^3 structure is reprinted with permission from M. W. Anderson, C. C. Egger, G. J. T. Tiddy, J. L. Casci and K. A. Brakke, *Angew Chem Int Edit*, 2005, **44**, 3243-3248.[100] Copyright 2011 Angewandte Chemie. The Double

2.3 Other Techniques

2.3.1 Electrical Conductivity

Electrical conductivity is a measure of the ability of a solution to conduct electrical charge.[2] Conductivity, K, is the inverse of the solutions resistivity, R, which is calculated from the voltage, V, and the current, I, as shown in Equation 2-17.

$$K = \frac{1}{R} = \frac{I}{V} \qquad \text{Equation 2-17}$$

$$C = K \frac{l}{a} \qquad \text{Equation 2-18}$$

In practical terms the conductivity is measured by placing two electrodes in the solution, which create a circuit through the solution. The conductivity measurement is dependant on the distance between the two electrodes and the surface area of the electrodes therefore to standardise the measurement Equation 2-18 is used to define the specific conductance, C, where l is the distance between the electrodes and a is the surface area of the electrodes. However it is not necessary to know l and a for the experimental set up as it is common to use solutions of known specific conductance to calibrate the measurement prior to performing the measurement. The units for the specific conductivity are Siemens per cm (Scm^{-1}), however as the conductivity also depends on the number of ions in solution it is also common to use the molar conductivity, Λ_m ($S\ cm^2\ mol^{-1}$), which is defined as the specific conductance per mole.

The conductivity of a given solution is dependant on the number of charged species within the solution. In a solution of pure water there are very few charged species therefore the conductivity is very low, $0.055 \mu Scm^{-1}$.[103] The addition of an ionic species such as sodium chloride leads to a linear increase in the conductivity of the solution. The same trend can be seen with the addition of low concentrations of surfactant to a solution of pure water. As the surfactant is added to the solution it will partition to the interface and to the bulk solution. As the concentration of surfactant increases so does the specific conductance up to a certain point. At this

point it becomes more energetically favourable for the micelles to aggregate in solution than float around as free molecules. This point is known as the critical micelle concentration (CMC).

At this point the surface of the solution is covered in a monolayer of surfactant and in solution there are a small number of micelles and a concentration of free surfactant molecules that are not interacting. As the surfactant concentration is increased there is a continuation of the upward trend of the electrical conductance however the rate at which the conductance is increasing is much lower than below the CMC. This increase in conductivity is in part due to two reasons, the first is a base level of free surfactant molecules in solution, as this concentration is relatively constant this will ensure the conductivity does not increase. The second reason the conductivity continues to increase above the CMC is the increase in concentration of unbound counter-ions that are part of any ionic surfactant.

By fitting the linear plot of conductance vs. surfactant concentration before the CMC and the separate linear plot above the CMC the intercept will then be the CMC. An example of this is shown in Figure 2-24.

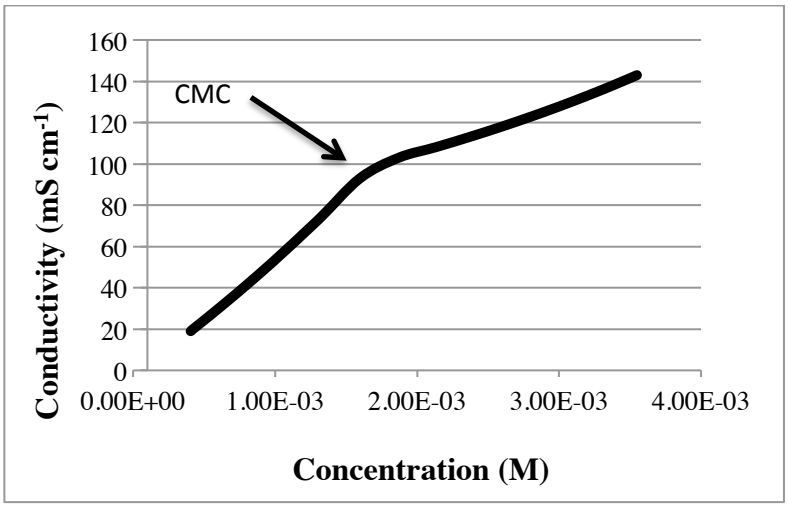

Figure 2-24. An example conductivity plot

In this report electrical conductivity was measured by step-wise addition of a concentrated surfactant solution, both in the presence and absence of PEI, to water or polymer solution. When PEI was used its concentration was held constant. The equipment used was a Mettler Toledo FiveEasy and the solution was held at 30°C using a water bath during the measurement. The solution was stirred thoroughly and allowed time for temperature equilibration before conductivity was measured.

2.3.2 Surface Tension

It is more energetically favourable for liquid molecules to interact with each other than with the air around them or solid surfaces. If a small amount of liquid were floating in the air it would therefore tend to a spherical shape that limits the surface area for the volume of the droplet. Due to gravity when a liquid is placed in a container its surface will tend to be flat as this is the lowest energy state. To change the surface area of the liquid work must be put into the system and the amount of work, δw, is proportional to the amount the surface area is changed, $\delta\sigma$. The constant of proportionality that relates these factors is the surface tension, γ, as shown in Equation 2-19.

$$\delta w = -\gamma \delta\sigma \qquad \text{Equation 2-19}$$

By raising a small wire ring through the surface of a liquid it is possible to change the surface area of the liquid, and if the force required to do this is measured then the surface tension can be calculated. Due to their surface-active nature the effect of surfactants on liquids is very important. As the concentration of surfactant in a liquid is increased the surfactant will partition between the surface and the bulk solution. The surfactant molecules will float around on the solution until the concentration at the solution becomes high enough for the surfactant molecules to start interacting. As the surfactant molecules have their hydrophobic tail away from the surface the tails can interact, which is a more favourable interaction than the surface of the solution interacting with itself. This leads to a decrease in the surface tension, seen as point A in Figure 2-25.

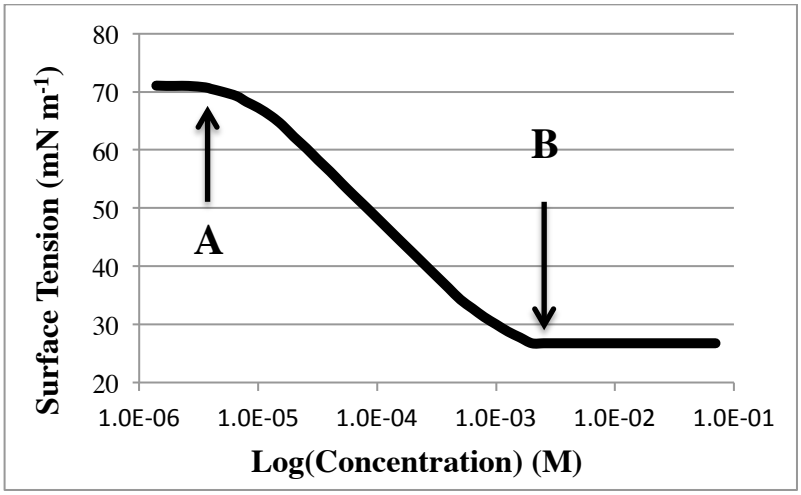

Figure 2-25. An example surface tension plot

The current understanding states that as the surface tension decreases there is a monolayer at the interface and it is interactions with the increasing concentration of surfactant in the bulk that leads to the decrease in the surface tension. As discussed in chapter 1 at the CMC the concentration of free surfactant in the bulk reaches a limit and that the addition of any more surfactant leads to micellization while the concentration of free surfactant stays constant. At this point as micellization is occurring and the concentration of free surfactant is constant then the surface tension becomes stable, point B in Figure 2-25. By calculating slope of a tangent to the curve over the last few points of the curve marked A to B and also the linear fit after point B then the intercept will tell you the concentration at which the surface tension levelled off which is also the CMC.

The surface tension of the solutions was measured using an Attension Sigma Force Tensiometer using a platinum du Noüy ring. The du Noüy ring was rinsed with methanol and flame dried between experiments. Surface tension measurements were carried out both in the presence and absence of polymer. When polymer was absent the surface tension measurements provide comparison to the conductivity experiments for determination of the CMC. When polymer is present the surface tension provide details of the critical aggregation constant (CAC*), reported previously.[11] The CMC or CAC* were determined by calculating the intersection of the lines fitted to the surface tension profile.[11, 22, 104]

2.3.3 Fluorescence Spectroscopy

Fluorescence is the re-emission of light from a compound that has previously absorbed light. The conjugated ring system that is at the centre of the Nile red compound allows adsorption of electromagnetic radiation that will then cause re-emission of the radiation. Nile red is a common fluorophore for studying amphiphilic species due to its low solubility in water and strong fluorescence in a range of organic solvents. In this thesis the Nile red was studied as a solution in chloroform to standardise the measurement. The reason chloroform was chosen is because Nile red is much more soluble in chloroform than water, the chloroform/water partition coefficient, which is the measure of the relative concentration of a solute in two immiscible solvents, at 4°C is 196.[105] Also the fluorescence of Nile red in chloroform is stronger than Nile red fluorescence in a number of other organic solvents allowing determination of very low concentrations of Nile red in the chloroform.[105] Chloroform itself does not fluoresce.

Fluorescence spectroscopy was performed on a Perkin Elmer LS 50B Spectrometer. A wavelength of 543nm was used as the excitation wavelength and a spectrum was recorded between 550nm and 700nm. The emission maximum was confirmed at 590nm ±2nm from the spectra and the intensity at the maxima was recorded. This intensity was then converted to concentration by comparison to a calibration curve made previously. The Fluorescence spectra collected for the calibration curve are shown in Figure 2-26 as an example of the spectra collected.

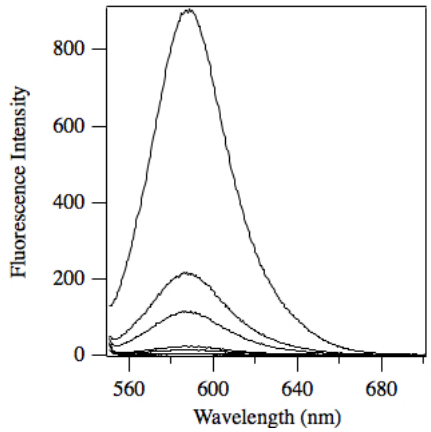

Figure 2-26. Fluorescence spectroscopy spectra for Nile red in chloroform.

2.3.4 Brewster Angle Microscopy (BAM)

Brewster angle microscopy is a similar technique to neutron and x-ray reflectometry in that it studies the reflection of radiation from the surface of a solution or substrate. According to Brewster's law at a given angle related to the refractive indices of the two media there is an angle where polarized light will not be reflected from the surface. This angle is given by Equation 2-20. As a comparison with reflectometry Brewster's angle is $90° - \theta_i$ as given in Figure 2-13. In Equation 2-20 θ_B is Brewster's Angle for a given substrate and n_1 and n_2 are the reflective indices of the media above and below the interface respectively.

$$\theta_B = \arctan\left(\frac{n2}{n1}\right) \qquad \text{Equation 2-20}$$

Experimentally a substrate with known Brewster angle is placed under the Brewster angle microscope and the Brewster angle is set. The polarisation of the light is then altered until there is no reflection from the substrate. The sample can then be deposited on the substrate and when there is sample under the area of study reflection will occur and therefore the sample will be visible. This is represented in Figure 2-27.

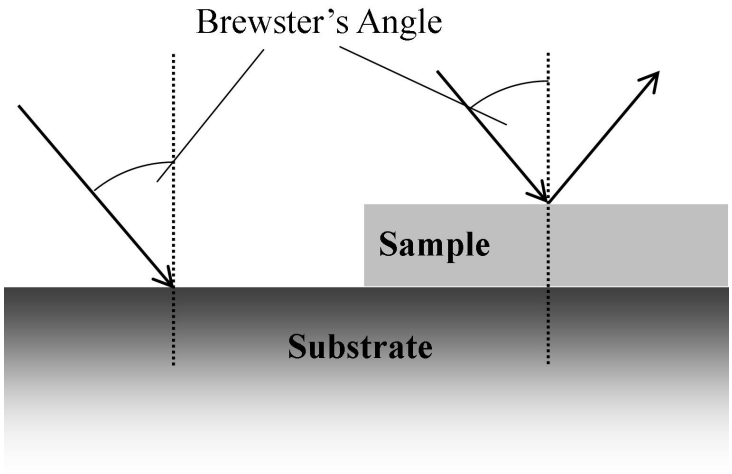

Figure 2-27. Diagrammatic representation of a Brewster Angle microscopy experiment.

A Nanofilm Technologies (NFT) I-Elli 2000 Imaging Ellipsometer was used as a Brewster angle microscope for measurements reported in this thesis. The films studied using BAM were prepared on a silicon wafer substrate, with a $\theta_B = 74°$. BAM works by nulling any reflected polarized light from the substrate surface. Any addition to the substrate will have a different refractive index than the silicon and therefore will cause reflection of light, which is then imaged using a camera connected to a PC.

2.3.5 Scanning Electron Microscopy (SEM)

SEM micrographs were collected using a JEOL JSM6310 scanning electron microscope with an Oxford Instruments Cryotrans1500 low temperature system attached. The structures in solution were visualized by rapidly freezing a droplet of solution onto an aluminium stub, which was mounted in the cryostage. Once in situ the uppermost layer of water was sputtered away from the snap-frozen samples and then a gold layer was deposited, by plasma deposition to prevent, charging during imaging.

2.3.6 Gas Chromatography (GC)

Gas chromatography was performed using an Agilent 6890N Network Gas Chromatography System with an Agilent 19091J-413 HP-5 5% Phenyl Methyl Siloxane 300m x 320μm x 0.25μm column. The temperature ramp was designed to allow separation of either the cyclohexane, boiling point 81°C, or cyclohexanol, boiling point 161°C, from the hexadecane solvent 287°C. All other components were in very small quantities and were non-volatile.

2.4 Chemicals

The commonly used chemicals are listed here along with their suppliers and purities. Other information that is important in this thesis is also included. All molecular structures can be found in appendix 1.

2.4.1 Surfactants:

2.4.1.1 Names, Suppliers and Purities

C_nTAB	Alkyltrimethylammonium Bromides
$C_{16}TAB$	Hexadecyltrimethylammonium Bromide (Acros, 99%)
$d42C_{16}TAB$	D_{42} (Fully) Deuterated $C_{16}TAB$ (CDN or Oxford Isotopes Facility)
$d33C_{16}TAB$	D_{33} (Tail) Deuterated $C_{16}TAB$ (CDN or Oxford Isotope Facility)
$C_{14}TAB$	Tetradecyltrimethylammonium Bromide (Acros, 99%)
$C_{12}TAB$	Dodecyltrimethylammonium Bromide (Acros, 99%)
CTEAB	Hexadecyltriethylammonium Bromide (Synthesised, see text)
dCTEAB	D_{33} (Tail) Deuterated CTEAB (Oxford Isotope Facility)
DDAB	Didodecyldimethylammonium Bromide (Acros, 99%)
d25DDAB	D_{25} (Partial Tail) Deuterated DDAB (Oxford Isotope Facility)
dDDAB	D_{50} (Tail) Deuterated DDAB (Oxford Isotope Facility)
SDS	Sodium Dodecyl Sulfate (Acros, 99%)
dSDS	Deuterated (D_{25}) SDS (CDN or Oxford Isotope Facility)

Table 2-6. Surfactant acronyms, names, suppliers and purities

2.4.1.2 Scattering Length Densities and Packing Parameters

	Scattering Length Density ($Å^{-2}$)			Packing Parameter
	Total	Head	Tail	
C_{16}TAB	-0.34×10^{-6}	-0.30×10^{-6}	-0.35×10^{-6}	
dC_{16}dTAB	6.53×10^{-6}	5.79×10^{-6}	6.74×10^{-6}	0.33
dC_{16}TAB	5.11×10^{-6}	-0.30×10^{-6}	6.74×10^{-6}	
CTEAB	-0.34×10^{-6}	-0.30×10^{-6}	-0.35×10^{-6}	0.29
dCTEAB	4.47×10^{-6}	-0.30×10^{-6}	6.74×10^{-6}	
DDAB	-0.32×10^{-6}	0.02×10^{-6}	-0.37×10^{-6}	
d25DDAB	2.75×10^{-6}	0.02×10^{-6}	3.15×10^{-6}	0.62
dDDAB	5.50×10^{-6}	0.02×10^{-6}	6.25×10^{-6}	
SDS	0.28×10^{-6}	3.01×10^{-6}	-0.37×10^{-6}	0.37
dSDS	5.92×10^{-6}	3.01×10^{-6}	6.60×10^{-6}	
	Mixed Surfactant System Parameters			
DDAB:20C_{16}TAB	-0.34×10^{-6}	-0.28×10^{-6}	-0.35×10^{-6}	0.34
DDAB:20dC_{16}TAB	4.85×10^{-6}	-0.28×10^{-6}	6.41×10^{-6}	
DDAB:2C_{16}TAB	-0.33×10^{-6}	-0.19×10^{-6}	-0.36×10^{-6}	0.43
DDAB:2dC_{16}TAB	3.30×10^{-6}	-0.19×10^{-6}	4.37×10^{-6}	

Table 2-7. Surfactant SLDs and packing parameters. Packing parameter values are calculated from values given by Warr et al and Garg et al.[53, 54] Details about determination of packing parameters discussed in chapter 3.

2.4.2 Polymers:

		SLDs
PEI	Polyethylenimine	
SPEI	Mw 2,000 (Sigma)	
MPEI	Mw 25,000 (Sigma)	5.69×10^{-7}
LPEI	Mw 750,000 (Sigma)	
PEO	Polyethylene oxide	
SPEO	Mw 10,000 (Sigma)	5.82×10^{-7}
LPEO	Mw 100,000 (Sigma)	
PAAm	Polyacrylamide	
PAAm	Mw 10,000 (Sigma)	1.43×10^{-6}
PNIPAM	Poly(*N*-isopropyl acrylamide)	
PNIPAM	Mw 25,000 (Sigma)	Not Used

Table 2-8. Polymer acronyms, names, suppliers and SLDs

2.4.3 Additives:

	Supplier and Purity	SLD
Cyclohexane	Acros, 99+%	-0.28×10^{-6}
Deuterated (D_6) Cyclohexane	Goss, 99.5%D	6.70×10^{-6}
Cyclohexanol	Fluka, 99%	0.05×10^{-6}
Deuterated (D_6) Cyclohexanol	Goss, 99.5%D	7.15×10^{-6}
Nile Red	Sigma, Technical Grade	1.81×10^{-6}

Table 2-9. Additive names, suppliers and SLDs.

3 Control of Cationic Surfactant Film Structure

3.1 Aims of studying cationic surfactants

As discussed in the introduction, the study of the cationic surfactant system and the cat-anionic surfactant system are effectively two sub-projects of the study of nanostructured hydrogel films. The study of the cationic surfactant system builds on previous work performed by O'Driscoll et al[8, 59, 66-68] based around the surfactant hexadecyltrimethylammonium bromide (C_{16}TAB).

The main aim of this project was to see whether careful choice of the components used to form the films was able to give control over the structure of the films. If structural control is then possible a secondary aim of this project is to compare these films with the films formed by O'Driscoll,[68] specifically in their ability encapsulate sparingly soluble species, as this may lead to potential applications, as will be discussed in more detail later. There are two benefits to studying the cationic surfactant system in comparison to the cat-anionic surfactant system. The first benefit is the prior knowledge about the films from the previous work by O'Driscoll et al, as discussed in the introduction. The second benefit is that the system is composed of only two components, which limits the potential complexity.

3.2 Control of cationic surfactant film structure

As mentioned above the main aim of this study into cationic surfactant films was to determine the ability to control the structure of the film. O'Driscoll et al[66] suggested that the film structure is due to the incorporation of surfactant micelles in a polymer matrix at the solution interface. In this study the C_{16}TAB micelles, that are ellipsoidal in solution, undergo an elongation at the interface caused by the high local surfactant concentration at the solution interface. From these results it can be concluded that the structure of the film is related to the surfactant micelle structure. Therefore to study whether it is possible to control the film structure, the starting point is to alter the surfactant micelle structure.

$$\text{Packing Parameter} = \frac{v}{a_0 l_c} \qquad \text{Equation 3-1}$$

As shown by Israelachvili et al[52] the structure of a micelle is dependant on three factors related to the surfactant molecule. These factors are the molecular volume of

the surfactant, v, the surface area per surfactant molecule, a_0, and the surfactant tail length, l_c, as shown in Equation 3-1. Variation of the surfactant properties leading to different film structures has previously been seen by O'Driscoll et al.[66, 67] In this study the surfactants used were C_{16}TAB, tetradecyltrimethylammonium bromide (C_{14}TAB), and dodecyltrimethylammonium bromide (C_{12}TAB). According to the packing parameter equation this shortening of the surfactant tail should lead to a change in the packing parameter and therefore the shape of the micelles. However as well as altering the tail length, the molecular volume of the surfactant is also altered meaning the effect on the packing parameter is not immediately clear. Calculation of the packing parameters of these three surfactants shows that they are all around 1/3, which is the transition point between spherical and ellipsoidal micelles, shown in Table 3-1. In this study the structure of the films was predominantly a hexagonal array of micelles however there were indications of a cubic structure in one sample.

Surfactant	Packing Parameter
C_{16}TAB	0.329
C_{14}TAB	0.325
C_{12}TAB	0.335

Table 3-1. Packing Parameters for different surfactants. Taken from Warr. et. al[53]

As C_{16}TAB had previously been seen to give the most well ordered films it was chosen as the comparison point for any other surfactant chosen. Then using the packing parameter, surfactants could then be chosen to give a range of different micelle structures, which should then lead to a range of film structures.

As C_{16}TAB is on the transition between spherical and ellipsoidal micelles the first surfactant needed to have a lower packing parameter than 1/3. As mentioned previously, altering the surfactant tail length also alters the surfactant molecular volume, meaning that a change in either will not necessarily have the desired affect of decreasing the packing parameter. However an increase in the surfactant head group area will not have a significant change on the molecular volume and therefore can reliably decrease the packing parameter. To keep the new surfactant comparable to C_{16}TAB, the hexadecyl tail remained the same while the head group was altered to have ethyl groups instead of methyl groups. This surfactant is hexadecyltriethylammonium bromide (CTEAB), and has previously been used to template mesoporous silica giving it a cubic structure made up of spherical and ellipsoidal micelles.[101]

After choosing the surfactant with the lowest packing parameter the surfactant with the highest packing parameter was chosen. As it is not possible to create a smaller

quaternary ammonium head group than the trimethyl head group of C_{16}TAB, it was decided to alter the tail. However the basic structure of a quaternary ammonium head group surfactant was still used to keep continuity of interactions between the surfactant and the polymer. Also because a wide range of quaternary ammonium surfactants are commercially available. As discussed previously, an increase in the surfactant tail length leads to an increase in surfactant molecular volume, however this does not necessarily lead to an increase in the packing parameter. It is possible to increase the surfactant molecular volume without increasing the surfactant tail length by using a double tailed surfactant. The initial surfactant chosen was dihexadecyldimethylammonium bromide however the viscosity of the solutions at the required concentrations made handling this surfactant difficult. Therefore it was decided to use didodecyldimethylammonium bromide (DDAB), which has previously been reported as giving lamellar structures in solution.[53]

As well as studying the two extremes of micelle curvature two further surfactant systems were used to study the intermediate packing parameters. However, in these systems, instead of using different surfactants it was decided to create mixed surfactant systems. In a binary surfactant solution the structure of the micelle can be determined as an average of the packing parameters of the two surfactants weighted to their mixing ratios within the micelle. The high packing parameter surfactant used for these mixtures was DDAB while the low packing parameter surfactant was C_{16}TAB. The molar ratios of the two mixtures used for study were 1:20 and 1:2 DDAB:C_{16}TAB, which due to the double chained nature of the DDAB can also be thought of as 1:10 and 1:1 C_{12}:C_{16} tails. The packing parameters of all the surfactants and mixtures are shown in Table 3-2.

	v, Å^3 [a]	a_0, Å^2 [b]	l_c, Å [a]	Packing Parameter
CTEAB	457.8	72 [d]	21.74	0.292
DDAB:20C_{16}TAB [c]	469.4	64	21.50	0.341
DDAB:2C_{16}TAB [c]	538.7	65	20.05	0.413
DDAB	700.4	68	16.68	0.618

Table 3-2. [a] Calculated from Tanford.[55] [b] Given by Warr et. al.[53] [c] Data calculated as a molar average of the two components assuming ideal mixing. [d] a_0 for CTEAB was calculated to be 71 Å by comparison with CTAB a_0=64 Å[53] and hexadecyltributylammonium bromide a_0=88Å^2.[106]

Using Table 3-2 and how the packing parameter corresponds to the micelle structures given by Israelachvili et al[52], it is possible to say that the CTEAB should give spherical micelles, where the packing parameter is less than 1/3, the two mixed surfactant systems should give ellipsoidal structures, where the packing parameter is

greater than 1/3 but less than 1/2, and the DDAB should give a bilayer structure, where the packing parameter is greater than 1/2. These predictions are supported by the previous research mentioned above[53, 101] for the single surfactant systems and by Ono et al[107] who report spherical micelles for DDAB:C_{16}TAB at mole fractions of DDAB less than 0.2 and rod like micelles for mole fractions of DDAB between 0.2 and 0.4. Furthermore, Ono also detected an increase in viscosity suggesting that an elongation of the rods also occurs as the mole fraction of DDAB is increased from 0.2 to 0.4.

From this previous work the aim was to confirm the literature results for the shapes of the micelles in solution for the single and mixed surfactant systems. As the main aim of this study is to produce structured films the effect of polymer on the surfactant solutions is also important. Finally films will be produced and their mesostructure studied to determine whether the structure in the films is related to that in the surfactant solution and therefore whether the structure can be reliably controlled.

3.3 Determination of surfactant critical micelle concentration

One of the main characteristics that define surfactant systems is the concentration at which it is more energetically favourable to form micelles than having individual surfactant molecules in solution, known as the critical micelle concentration (CMC). The CMC for the single surfactants, CTEAB, C_{16}TAB, and DDAB, have previously been reported[106, 108, 109], however the CMC of the mixed surfactant systems is unknown. Also unknown is how the addition of the polymer will affect the CMC.

Previous work related to this research has been performed on C_{16}TAB in the presence and absence of polyethylenimine.[11] It was shown that the addition of polymer to the surfactant decreased the CMC and a critical aggregates concentration (CAC^*) was also reported. The CAC is normally reported at the point at which the polymer and surfactant interact allowing micelles to form on the polymer chain[110] however, here it was defined as the point at which film formation is first visible, indicating there is an interaction between the polymer and the surfactant.

	No Polymer		SPEI	LPEI
	CMC	Literature	CAC*	CAC*
CTEAB	0.74	0.73[a]	0.043	0.013
CTAB	0.93	1.00[b]		
DDAB:20C_{16}TAB	0.47		0.032	0.011
DDAB:2C_{16}TAB	0.049		0.0084	0.014
DDAB	0.06	0.05[c]	0.00034	0.00033

Table 3-3. CMC and CAC values, in mM, determined by surface tension. Literature values for surfactant CMCs were from (a) Buckingham et. al.[106], (b) Berr et. al.[108], (c) Soltero et. al.[109] Uncertainties in the reported values are ±10%.

The surface tension values are similar to the values reported in the literature. The values in the mixed surfactant system can then be used to determine if the surfactants mix ideally. Using Rubingh's theory for ideal mixing[60] beta values of -0.61 and -6.00 are calculated for DDAB:20C_{16}TAB and DDAB:2C_{16}TAB respectively. These negative values suggest a strong interaction between the two surfactant species that lead to non ideal mixing with calculated DDAB mole fractions of 0.45 and 0.63 respectively. Interestingly contrast variation in the SANS experiments, discussed later, indicates that at the experimental concentration the surfactant mixing in the micelles is ideal. This is attributed to ideal mixing occurring at surfactant concentrations well above either surfactant CMC.

The results obtained on the addition of polymer are lower than the CMC suggesting a favourable interaction between the surfactant and the polymer at a CAC*, similar to that reported by Comas-Rojas et al.[11] A full determination of the CAC and CMC for the different surfactant solutions, as performed by Comas-Rojas et al,[11] has not been performed here. The concentration of polymer used in these experiments was set at 1.5wt% as this is the concentration of the polymer used during previous film formation experiments. The aim of this research is not a full study of the surfactant polymer interactions that lead to film formation; instead it is to show whether control of film mesostructure is possible. Therefore the experimental parameters have been controlled to show results from particular points on the phase diagram, instead of studying the whole phase diagram.

3.4 Film formation solutions

The original work performed by O'Driscoll et al[66] used a surfactant concentration of 0.037M and a polymer concentration ranging from 6wt% to 0.375wt%. In these experiments the optimal polymer concentration was 1.5wt% therefore this is the concentration of polymer used for this study. Although using the same surfactant concentration was considered, due to the high viscosity of the DDAB solution above

0.02M it was decided to perform experiments at a total surfactant concentration of 0.01M.

The first structural studies were performed on the surfactant solutions in the absence and presence of polymer. The solutions were studied using SANS on the LOQ instrument at ISIS. The mathematical models used to fit to the data were either for a uniform ellipse[111] or for a bilayer system.[112, 113] The uniform ellipse model can model prolate (rod like), oblate (disk like) micelles and spheres, therefore all of these micelle types can be compared using the same model removing any user influence. The ellipse shape is modelled by two axis as shown in Figure 3-1, if R(a) > R(b) the micelle is prolate and if R(b) > R(a) the micelle is oblate. Also included in the model for the uniform ellipse is a structure factor for the interaction of charged particles. The parameters used to fit the model are given in Table 3-4 and Table 3-5.[83]

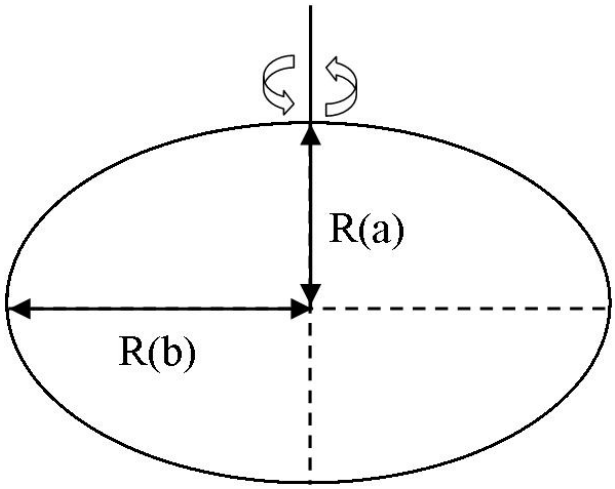

Figure 3-1. Diagram of the two axis defining an ellipse.

Parameter	Uniform Ellipse		Dilute Lamella		Lamellar paracrystal	
1	Scale	Fitted	Scale	Fitted	Scale	Fitted
2	R(a)	Fitted	Bilayer Thickness	Fitted	Bilayer Thickness	Fitted
3	R(b)	Fitted	Polydispersity of thickness	Fitted	Number of Layers	Fitted
4	SLD of the Ellipse	Held	SLD of the Bilayer	Held	Layer Spacing	Fitted
5	SLD of the Solvent	Held	SLD of the Solvent	Held	Polydispersity of Spacing	Fitted
6	Incoherent Background	Held	Incoherent Background	Held	SLD of the Bilayer	Held
7					SLD of the Solvent	Held
8					Incoherent Background	Held

Table 3-4. Parameters used to fit the form factors of the fitting models and whether they were usually held of fitted during the fitting process.

Parameter	HPMSA	
1	Charge	Fitted
2	Temperature (K)	Held
3	Salt Concentration (M)	Held[a]
4	Solvent dielectric constant	Held[b]

Table 3-5. Parameters used to fit the structure factor used with the uniform ellipsoid form factor and whether the parameters were held or fitted during the fitting process. (a) unless otherwise stated this value was held at 0M. (b) unless otherwise stated this value was held at 78 as this is the dielectric constant of water at 25°C.[114]

Two different bilayer models were used in this report. In the absence of polymer the structure can be modelled with a dilute lamellar[113] system where the bilayer is not interacting with another bilayer. In the presence of polymer the model used is a lamellar paracrystal[112] model that not only models the bilayer but also the effect on scattering from multiple interacting bilayers.

To perform modelling some prior knowledge about the system is required. Here that knowledge is the scattering length densities (SLDs) of the different components, which have been previously calculated and are shown in Table 3-6. These SLDs are for the surfactant tail region. Due to the small size of the surfactant head group region and the ability for the solvent and polymer to mix with the surfactant head group the head group SLD is difficult to calculate. Test fitting was performed

treating the head group as a shell and the tails as the core of the micelle. These fits showed that the tail region in contrast to the solvent dominates the scattering; therefore the head groups have been ignored and the fitting performed assuming the tails form the main component of the structure in contrast with the solvent.

Component	Scattering Length Density ($Å^2$)
CTEAB	-0.35×10^{-6}
C_{16}TAB	-0.35×10^{-6}
Deuterated d33-C_{16}TAB	6.74×10^{-6}
DDAB	-0.37×10^{-6}
D_2O	6.37×10^{-6}
H_2O	-0.56×10^{-6}
PEI	0.57×10^{-6}

Table 3-6. Calculated scattering length densities for different components studied in this report.

In all experiments at least two SLD contrasts were measured. Lack of deuterated CTEAB and DDAB available at the time of the experiments meant that in some experiments the solvent provided the second contrast, using a mixture of 70% D_2O and 30% H_2O as the solvent instead of pure D_2O. For the mixed surfactant systems, of DDAB with C_{16}TAB, the second contrast used deuterated C_{16}TAB instead of hydrogenated C_{16}TAB in the mixture.

3.4.1 Solutions without polymer

The first solutions studied were surfactant without polymer. As stated previously these solutions could be used to confirm the predictions made with the packing parameter as to the shape of the micelles in solution. Also these results could be compared to the literature studies. Once the solutions were analysed in the absence of polymer then this would provide a base line for comparison when polymer is added to see the effect on the micelles. Figure 3-2 shows the SANS patterns from the different surfactant solutions along with lines of best fit. The results from this data fitting are given in Table 3-7.

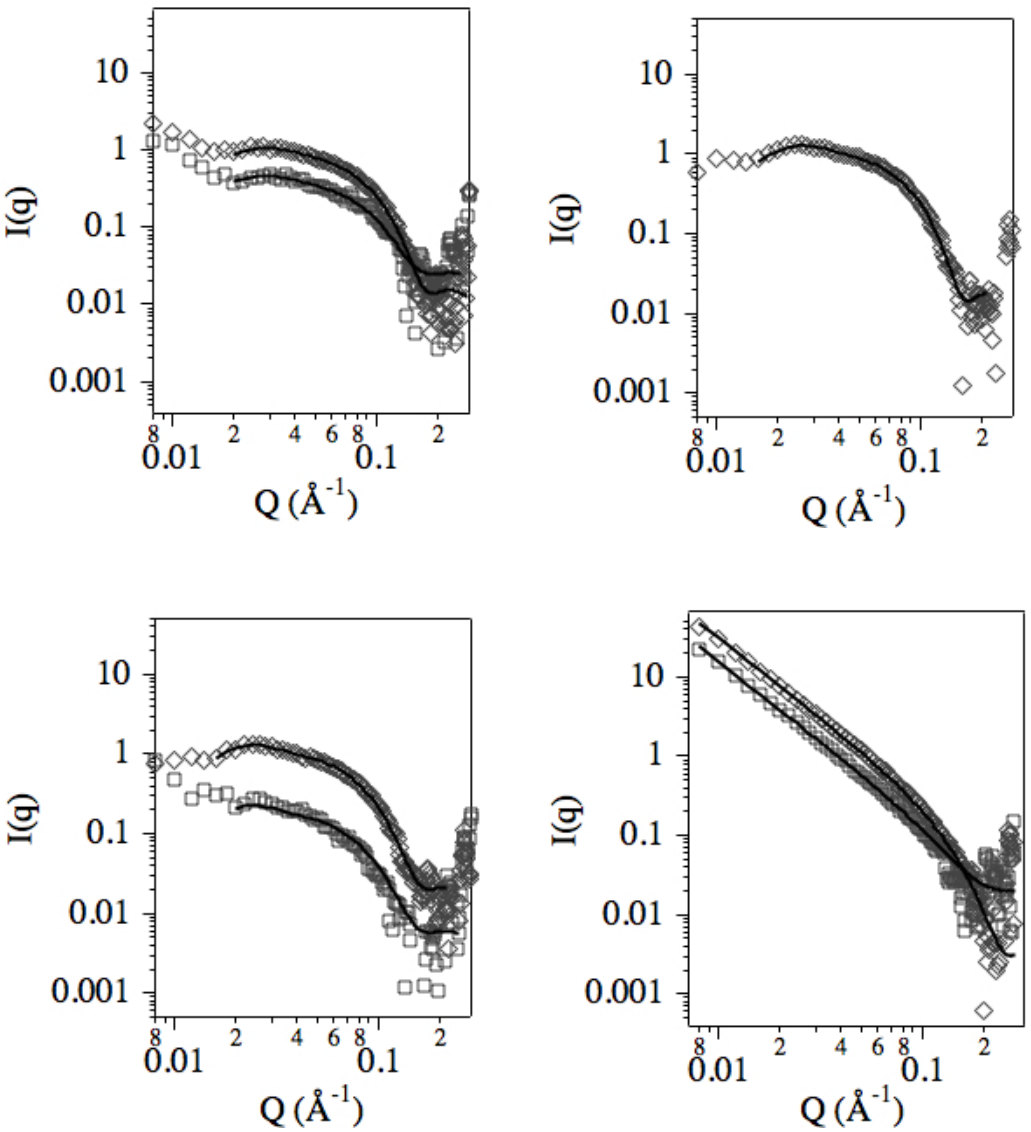

Figure 3-2. From left to right CTEAB and DDAB:20C_{16}TAB (top row) and DDAB:2C_{16}TAB, and DDAB (bottom row). Diamonds indicate the first contrast, hydrogenated surfactant in D_2O. Squares indicates the second contrast as described below.

	CTEAB		DDAB:20C_{16}TAB		DDAB:2C_{16}TAB	
	Fit	Uncertainty	Fit	Uncertainty	Fit	Uncertainty
Scale	3.47×10^{-3}		3.36×10^{-3}		3.04×10^{-3}	
R(a) (Å)	34		34		39	
R(b) (Å)	23		25		24	
Charge	11.5	1.1	14.0	1.1	15.2	1.3

	DDAB
	Fit
Scale	4.71×10^{-3}
Lamellar Thickness (Å)	24

Table 3-7. Fitting results from SANS patterns taken from surfactant solutions. Uncertainty in scale is $\pm5\times10^{-5}$. Uncertainty in dimensions is ±2Å.

The second contrast for CTEAB and DDAB was measured with 70% D_2O and 30% H_2O as the solvent instead of pure D_2O. The contrast for DDAB:2C_{16}TAB was measured with deuterated C_{16}TAB instead of hydrogenated C_{16}TAB in pure D_2O. The contrast for DDAB:20C_{16}TAB was measured with deuterated C_{16}TAB in pure D_2O as well, however this gave such a low SLD contrast that it could not be fitted.

Both oblate and prolate micelle structures were tried for the CTEAB and the two mixed surfactant systems. In all cases the quality of the fits, as determined by minimisation of the chi squared value, were very similar. The fits shown in Table 3-7 are all for the prolate case for easy comparison of dimensions, however fitting does not distinguish between prolate and oblate ellipses with both giving very similar chi squared values and suitable micelle dimensions.

The DDAB results agree with predictions and with the literature, with the solution scattering showing non-interacting lamellar bilayers. The other results however are very similar and therefore do not agree with the predictions. The two surfactant mixtures are very similar in composition therefore it can be expected that they will give similar structures. The structures of the micelles given in the literature are ellipses and rods therefore the fit to a prolate ellipse agrees well with the literature and the more elongated nature of the DDAB:2C_{16}TAB ellipses is in keeping with predictions based on the packing parameter. The CTEAB results however do not agree with the predictions or with the literature. Both the predictions and the literature suggest the micelles should be spherical however the scattering results show ellipsoidal micelles. This result however is not completely unexpected and has previously been seen by Anderson et al[100] who suggest that an impurity of 1-bromohexadecane would cause this change in structure. Interestingly even in the presence of these impurities a cubic phase is still seen in silica templated with this surfactant.

Although the micelle structure is the main point of interest in this research it is also important to note the details from some of the other fitted parameters. The uniform ellipsoid model is normalised to give the scale equal to the particle volume fraction. The volume fraction can then be used to calculate a molecular volume of the scattering body. As the head group region of the micelle contains both surfactant head groups and solvent it is difficult to determine an exact SLD therefore the fitting is performed using the SLD of the tails. This means that the calculated molecular volume should be comparable with the molecular volume of the surfactant tail region. This comparison is straightforward for the CTEAB sample, however it is more complicated for the mixed surfactant system. Using the molar ratios of the surfactants and treating the DDAB as two C_{12} surfactant tails instead of a single

molecule it is possible to calculate a value for the molecular volume of the individual surfactants. These results are shown in Table 3-8 and are compared to the molecular volumes calculated using Tanford's formula.[55]

	Calculated from Experimental Data ($Å^{-3}$)	Calculated from v=27.4+26.9(carbons)[55] ($Å^{-3}$)
CTEAB	551.8	457.8
C_{16}TAB	547.5	457.8
DDAB	400.4	350.2[a]

Table 3-8. Calculated molecular volumes for the surfactant tail. (a) Assuming a single C_{12} carbon chain as when studying just the tails, DDAB can be thought of as two C_{12} tails.

The values calculated from the experimental data are very similar to those calculated using Tanford's formula,[55] except they are all slightly higher. This is most likely due to scattering from the head group region as well as the tails. In all cases, the SLD of the tails is similar to that of the head group therefore the results are still valid. The similarity of the experimental results with the calculated values supports the validity of the fitting.

The scale factor for the lamellar model is not mathematically well defined. Therefore the model is not normalised meaning the scale is not equal to the volume fraction, however it should be on the same order of magnitude. Performing a similar calculation as shown above would give a molecular volume for DDAB 833.5$Å^{-3}$. Although this value appears very large it is because the molecular volume is that of the full DDAB molecule instead of a single C_{12} tail. The calculated molecular volume of the full DDAB molecule is 800.4$Å^{-3}$, which gives a similar discrepancy to that seen in the other results.

Another result of note from Table 3-7 is the charge on the surfactant micelle. Comparing the two mixed surfactant systems, they are relatively similar with the slightly larger micelle having a slightly higher charge. Although DDAB:20C_{16}TAB and CTEAB are similar sized micelles the CTEAB has a lower charge, which can be attributed to a larger head group area meaning there are less surfactant molecules in a CTEAB micelle.

3.4.2 Solutions with polymer

After studying the surfactant solutions in the absence of polymer the next step was to add polymer to observe any effect of the interaction between the two species. Due to

the solubility of the polymer the only contribution the polymer makes to the scattering is to alter the SLD of the solvent. The current understanding of the interactions of PEI with the surfactant micelles is that the PEI is able to wrap around the micelles but does not get incorporated into the core of the micelle. The results of fitting this SANS data for multiple contrasts are shown in Table 3-9 and Table 3-10.

	CTEAB		DDAB:20C_{16}TAB		DDAB:2C_{16}TAB	
	Fit	Uncertainty	Fit	Uncertainty	Fit	Uncertainty
R(a) (Å)	34		35		121	
R(b) (Å)	21		23		20	
Charge	6.2	0.8	4.1	0.4	0.02	0.001

	DDAB	
	Fit	Uncertainty
Lamellar Thickness (Å)	24[a]	
Number of Layers	1.6	0.01
Layer Spacing (Å)	148	5
Polydispersity of layer spacing	0.11	0.03

Table 3-9. SANS results from Surfactant solutions with SPEI. (a) due to the errors on the point fitting the lamellar thickness is very difficult therefore it is done manually. Uncertainty in dimensions is ±2Å.

As with the surfactant solutions without polymer, when SPEI was added the contrast for the CTEAB and DDAB was measured using 70% D_2O and 30% H_2O as the solvent. The DDAB:2C_{16}TAB and DDAB:20C_{16}TAB were both measured with deuterated C_{16}TAB and, as before, a third contrast was also measured using 70% D_2O and 30% H_2O as the solvent. This meant the contrasts used to fit the DDAB:20C_{16}TAB sample were the fully hydrogenated sample and a sample with hydrogenated surfactant in the partially hydrogenated solvent. The contrasts to fit the DDAB:2C_{16}TAB sample were the fully hydrogenated sample, a sample of hydrogenated DDAB with deuterated C_{16}TAB in D_2O, and a sample of fully hydrogenated surfactant in the partially hydrogenated solvent. All contrasts were simultaneously fitted for each sample to give the results shown in Table 3-9.

The CTEAB and DDAB:20C_{16}TAB micelle appear to be unaffected by the addition of SPEI to the solution. The DDAB:2C_{16}TAB however shows a large increase in the R(a) value indicating an elongation of the prolate ellipse. As this change was so great, the sample was repeated and the result found to be reproducible. Due to the difference between R(a) and R(b) in this sample it is also only possible to fit a prolate ellipse, using the uniform ellipsoid model, to this structure, confirming the result seen in the literature that the structure of these micelle is rod like.

Although the micelle dimensions for the CTEAB and DDAB:20C_{16}TAB solutions did not show any change from the addition of SPEI, an effect could be seen in the charge parameter in the model. In fitting the structure factor the charge and the salt concentration act in very similar ways. In the sample without polymer the salt concentration is 0M, however as the polymer is charged it can act like a salt by screening the micelle charges allowing the micelles to pack closer together. As the two parameters are very similar in this system it was decided to hold the salt concentration at 0M and any effect of the polymer acting like a salt would then be seen as an effective lowering of micelle charge. Doing this gives an indication of the interaction of the polymer with the micelle as the better the polymer can interact to help the micelles pack together the lower the micelle charge will appear.

With no polymer, the charge on the micelles increases from CTEAB to DDAB:20C_{16}TAB to DDAB:2C_{16}TAB, which can be attributed to better surfactant packing in the micelle due to the smaller head groups of DDAB and C_{16}TAB. If the polymer had the same effect on all the surfactant micelles then the same trend should be visible, however with SPEI the there is a decrease in surfactant charge from CTEAB to DDAB:20C_{16}TAB and to DDAB:2C_{16}TAB. This indicates that the SPEI is able to interact with the mixed surfactant systems better than the CTEAB and particularly well with the DDAB:2C_{16}TAB, which is also supported by the elongation of the DDAB:2C_{16}TAB micelles.

A structure factor similar to the HPMSA is not available for bilayer structures however two models do exist for determining an interaction between bilayers. The model used in this report is called the lamellar paracrystal model. This model calculates the scattering from N_L bilayers interacting, where N_L is defined in Equation 3-2.[112] In this equation N is an integer number of layers while x_N is the fraction of those layers.

$$N_L = x_N N + (1-x_N)(N+1) \qquad \text{Equation 3-2}$$

The interaction between the DDAB and the SPEI can be seen simply by the fact that the bilayers are interacting causing ripples in the scattering. However calculating the percentage of single bilayers, x_N, suggests 37% of bilayers are not interacting while the rest are only interacting with one other bilayer.

	CTEAB		DDAB:20C_{16}TAB		DDAB:2C_{16}TAB	
	Fit	Uncertainty	Fit	Uncertainty	Fit	Uncertainty
R(a) (Å)	48		45		77	
R(b) (Å)	20		22		22	
Charge	3.2	0.75	8.7	0.60	6.89	0.35

	DDAB	
	Fit	Uncertainty
Lamellar Thickness (Å)	22	
Number of Layers	1.46	0.007
Layer Spacing (Å)	276	10
Polydispersity of layer spacing	0.08	0.002
2nd Contrast		
Layer Spacing (Å)	256	

Table 3-10. SANS results from Surfactant solutions with LPEI. Uncertainty in dimension is ±2Å.

The contrasts when LPEI was added to the surfactant solutions were the same as when SPEI was added to the surfactant solutions. As with the addition of SPEI the SLD contrast using deuterated C_{16}TAB in the DDAB:20C_{16}TAB system was too low therefore the second contrast used 70% D_2O with 30% H_2O as the solvent. Deuterated C_{16}TAB was also used as part of the DDAB:2C_{16}TAB system however a different structure was seen. Fitting just the DDAB:2C_{16}TAB with deuterated C_{16}TAB gives a structure of a cylinder which has an undefined length, this suggests that the DDAB is mainly found in the low curvature area of the cylinder, meaning the end-caps are predominately C_{16}TAB.

The addition of LPEI appears to affect the dimensions of the micelles more than SPEI. Both the CTEAB and the DDAB:20C_{16}TAB micelles are more elongated, although they are still very similar to each other, as seen previously. The DDAB:2C_{16}TAB is not affected as much by the LPEI as the SPEI, as the micelle is less elongated than when in the presence of SPEI. Although, the DDAB:2C_{16}TAB micelles are still more elongated in the presence of either polymer than they are in the absence of polymer.

Interestingly the charge on the micelles is lower for CTEAB than for the surfactant mixture, indicating the LPEI does not interact with the mixed surfactant micelles as well as the SPEI was able to. However the DDAB:2C_{16}TAB micelles have a lower charge than the DDAB:20C_{16}TAB micelles therefore suggesting the LPEI is still more able to interact with the DDAB:2C_{16}TAB. For the DDAB sample there is no charge parameter, however more layers are able to interact and the layers are closer

together in the SPEI sample than in the LPEI sample suggesting the LPEI is less able to interact with the DDAB than the SPEI, as seen with the other surfactant solutions.

Throughout, the fitting of the uniform ellipsoid model R(b) has stayed constant around 21Å. This value corresponds well to expected length of the surfactant tail, as calculated in Table 3-2, which provides extra confidence in the fitting results. The lamellar thickness in the two lamellar models for DDAB is slightly lower than expected at 22Å, as it is a thickness instead of a radius, while the expected value is 33Å,[115] suggesting that there is a high degree of intercalation of the surfactant tails in this phase. However the agreement between the models and the difficulty of fitting this value due to an increase in error in the data suggests that the models can be relied upon and give reasonable results.

3.5 Films

The first prediction was that DDAB would form a multi lamellar thin film. The DDAB:2C_{16}TAB system could also be predicted to form a 2D hexagonal structure with cylinders running parallel to the solution surface. The other two surfactants were harder to predict, however given that previous results had shown C_{16}TAB on its own formed 2D hexagonal structures, it was likely that DDAB:20C_{16}TAB would follow this and also form 2D hexagonal structures. CTEAB was the hardest to predict as the SANS results suggest it should form a hexagonal film like DDAB:2C_{16}TAB, however Anderson et al.[100] have shown that even with ellipsoidal micelles caused by the impurities from the surfactant synthesis this surfactant promotes formation of a cubic $Pm\bar{3}n$ structure in surfactant-templated silica materials that is made up of a mixture of close packed ellipsoidal and spherical micelles. Given these predictions, film formation and final structure was studied using neutrons and x-rays on the SURF and Troïka II beamlines respectively.

3.5.1 Neutron Reflectometry

The reflectivity patterns, shown in Figure 3-3, all show two peaks, suggesting the films are made up of a repeating layered structure; these peaks are highlighted by the two dotted lines. It can be seen that from DDAB to CTEAB the general trend is for the peak position to move to lower Q and become narrower. The repeat values obtained from the peak positions in the plots are given in Table 3-11. Using the calculated surfactant tail lengths, in Table 3-2, would give a polymer layer of 9Å ± 2Å. This trend is in good agreement with the SANS results and predictions and the similar polymer thickness calculated suggests the formation mechanism is similar in

all systems and that the apparent charge on the micelles (and so repulsion between them) also does not vary greatly between systems once the micelles are in the films. This reflects previous results where the concentration of the polymer was the important factor in determining the size of polymer filled regions in the films. Here the concentration of the polymer is constant for all samples so the extent of screening between micelles is similar.[66]

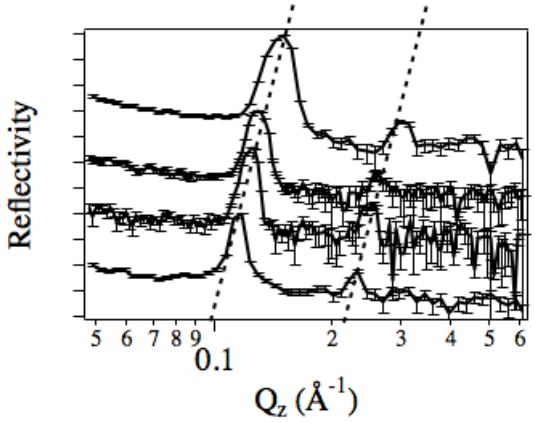

Figure 3-3. From top to bottom DDAB, DDAB:2C_{16}TAB, DDAB:20C_{16}TAB, and CTEAB films with SPEI. Plots are offset for clarity. Dashed lines are guides for the eye.

	1st Peak Q (Å^{-1})	2nd Peak Q (Å^{-1})	d spacing (Å)
DDAB	0.148	0.302	42
DDAB:2CTAB	0.129	0.260	49
DDAB:20CTAB	0.126	0.249	50
CTEAB	0.115	0.230	55

Table 3-11. Peak positions for surfactant/SPEI films. Errors in peak positions are ±5% of reported values.

From these results it would appear that there is no further structure and the films are formed from a multi layered system with layers parallel to the interface. However there are indications of more complex structure from these films, which is visible as the films form. As the film formation takes 1-2 hours as well as studying the final "stabilised" structure it is also possible to the formation of the film by taking a reflectivity pattern at regular intervals during the formation process. On the SURF instrument due to the flux available the time it takes to collect a single reflectivity pattern, with reasonable confidence, is 15 minutes. The five reflectivity patterns from formation of the CTEAB/SPEI film are shown in Figure 3-4 and indicate a more complex film structure is possible.

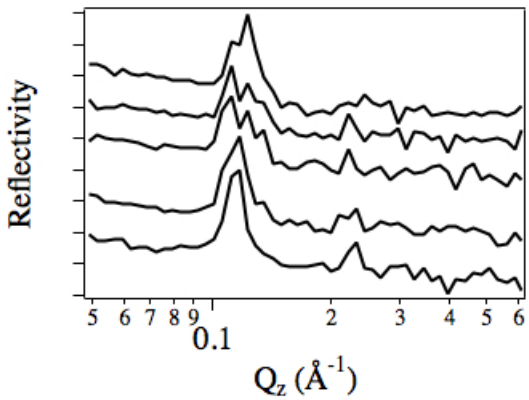

Figure 3-4. Time resolved formation of CTEAB/SPEI film. From top to bottom 12-27mins, 27-42mins, 42-57mins, 57-72mins, 72-87mins. Plots are offset for clarity.

From this data it is possible to see that although a single peak is formed within the first 10 minutes after pouring the solution, the structure goes through a transition to a triple peaked structure before returning to a single peaked structure after roughly 60 minutes. The $Pn\bar{3}m$ structure previously seen with this surfactant is characterised by three reflections close to each other, which in a powder pattern would be visible in the same angular orientation. This data however does not have a high enough resolution in this region to give accurate peak positions for proper structural determination. The reason for the loss of the triple peak leaving a single peak is the growth in structure parallel to the interface. The growth of the film structure is likely to be from the interface down into the solution meaning the layers parallel to the interface will be much more ordered than in any other orientation. Reflectivity is sensitive to layers ordered parallel to the interface therefore the reflections from these layers will be much stronger than any other reflections.

All of the data shown so far is for the surfactants in the presence of SPEI. For the surfactants in the presence of LPEI only one peak is seen. The peak in the CTEAB/LPEI plot is at slightly higher Q, 0.117Å^{-1}, than the first peak in the CTEAB/SPEI films. In the DDAB:2C_{16}TAB and the DDAB films with LPEI the peak is also shifted to lower Q, 0.119Å^{-1} and 0.132Å^{-1} respectively, in comparison to the first peak in the equivalent SPEI films. These results agree with the SANS data where a stronger interaction was seen with CTEAB and LPEI than SPEI and a weaker interaction was seen with DDAB:2C_{16}TAB and DDAB with LPEI than SPEI. Given the stability of the R(b) values determined during SANS fitting this difference in peak position is probably due to a decrease, for CTEAB, or an increase, for DDAB:2C_{16}TAB and DDAB, of polymer in between the layers of surfactant. It is also important to note that the peaks in the LPEI data are much broader than those in the SPEI data suggesting greater polydispersity in the layer thickness in LPEI films.

The DDAB:20C_{16}TAB film was too rough to give a reflectivity signal therefore no comparison is available.

Normally neutron experiments are performed with the use of multiple contrasts to help understand the sample structure. In this case it was hoped that fitting of the multiple contrasts could indicate the number of layers at the surface, or the hydration of the polymer layers within the film. Unfortunately the peaks in the hydrogenated samples are too intense and sharp to be accurately fitted with the current fitting software. Even in the case of the deuterated samples, which only show the single peak, the peak is still too intense and sharp to be fitted realistically. The best fits so far, which still do not accurately represent the data, suggests at least 20 layers of surfactant, being roughly 32Å thick (in the CTEAB sample) with a 20Å thick layer attributed to the polymer which is similar to the results reported by O'Driscoll et al.[66]

3.5.2 X-ray Reflectometry

As only limited structure was seen in the neutron reflectivity patterns it was decided that more detail could be seen using grazing incidence x-ray diffraction (GIXD) to probe the in-plane structures, which are not visible with reflectometry. These experiments are performed on the Troïka II beamline at the ESRF and involve taking a reflectivity pattern, taking approximately 40 minutes, followed by a GIXD pattern, taking approximately 90 minutes, and finally a second reflectivity pattern to study any change in structure over the time of the experiment.

3.5.2.1 X-ray Reflectometry

The reflectivity patterns from the second reflectivity measurement of CTEAB, DDAB:20C_{16}TAB and DDAB:2C_{16}TAB with SPEI are shown in Figure 3-5. The second reflectivity pattern from the DDAB/SPEI film is very unclear, probably due to roughness, (this was noted during the experiment as the sample appearing to have fractal crystallites at the surface) therefore the first reflectivity pattern is shown instead in Figure 3-6. The Q values of the peaks in the reflectivity patterns are given in Table 3-12. Of the three films shown in Figure 3-5, the film with the sharpest critical angle is that of CTEAB which is also the film with the least intense diffraction peaks. It also happens to be the film which is expected to form a cubic structure and it has been previously seen in silica films that the films containing more spherical micelles tend to give much smoother films than those made up of arrays of elongated micelles.[116]

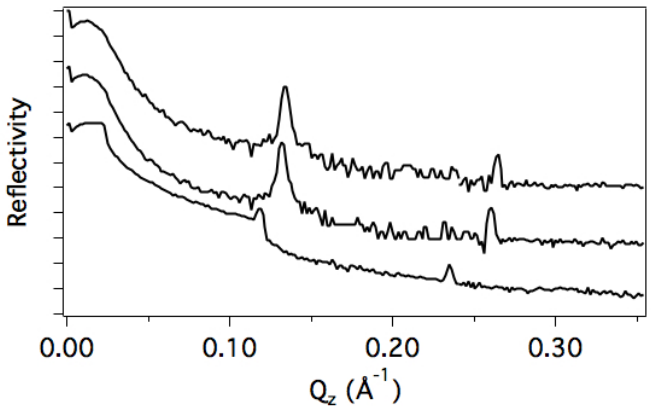

Figure 3-5. X-ray Reflectivity patterns of SPEI with, from top to bottom, DDAB:2C_{16}TAB, DDAB:20C_{16}TAB, and CTEAB. Plots are offset for clarty

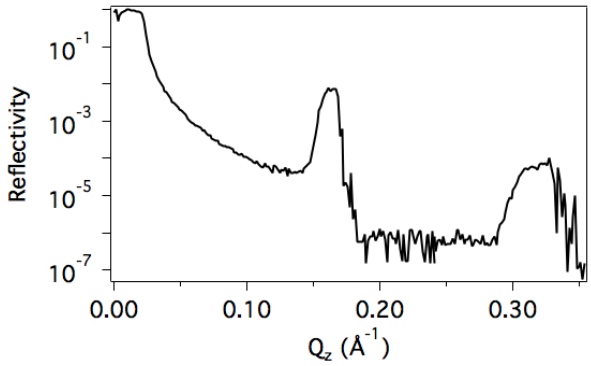

Figure 3-6. X-ray Reflectivity pattern of DDAB/SPEI film

	1st Peak Q (Å^{-1})	2nd Peak Q (Å^{-1})	d spacing (Å)
DDAB	0.163	0.320	39
DDAB:2C_{16}TAB	0.134	0.264	47
DDAB:20C_{16}TAB	0.132	0.260	48
CTEAB	0.118	0.235	53

Table 3-12. Peak positions and calculated d-spacing from surfactant films with SPEI. Errors in peak positions are ±5% of the reported value

As with the neutron reflectivity patterns, all the patterns show two peaks. The CTEAB peaks in both the neutron and x-ray data are in similar position. The difference between the first and second CTEAB reflectivity patterns is a slight shift, of 0.01Å^{-1} in the position of the first peak, furthermore in the first reflectivity pattern there is no second peak suggesting the film requires substantial time to complete ordering into the final structure. The DDAB:20C_{16}TAB and DDAB:2C_{16}TAB films with SPEI are very similar to each other, and both have peak positions at a lower Q than the corresponding peaks in the neutron data. As with the CTEAB/SPEI film over the course of the experiment there is a slight shift, of 0.005Å^{-1}, in the position of the first peak. In both films there are two peaks in both the first and second reflectivity patterns. The film of DDAB with SPEI also has the same trend with the

first peak at a lower Q position than seen with neutrons. As can be seen in Figure 3-6 the peaks from the DDAB/SPEI film are quite broad, similar to those seen in the neutron reflectivity. As time elapses these peaks get broader and less intense, although the centre of the peak shifts by 0.13$Å^{-1}$ the highest Q edge of the peak stays in the same position suggesting that although some of the structure is changing over time there are other parts of the structure that do not change.

Overall this data suggests that there is a slight change in the structure of the films over time. This could be due to a rearrangement of the internal structure of the films from a kinetic structure to a more stable thermodynamic structure where the surfactant layers are slightly further apart. The fact that the peak positions are different between the neutron and x-ray data suggests that there are uncontrolled factors such as humidity that affect the final structure of the film. If the humidity were lower it could cause faster evaporation leading to a thinner polymer/water layer in the structures.

The surfactant films with LPEI also follow the trend shown in the neutron data. All reflectivity patterns only show one peak and this peak is a lot lower intensity than the corresponding SPEI peak, indicating the structure is not as well formed. As seen in the neutron data the CTEAB peak shifts to higher Q, 0.125Å-1, while the other three shift to lower Q; DDAB:20C_{16}TAB to 0.129$Å^{-1}$, DDAB:2C_{16}TAB to 0.132$Å^{-1}$, and DDAB to 0.142$Å^{-1}$.

3.5.2.2 Grazing incidence x-ray diffraction

Like the neutron data, the x-ray reflectivity data did not show much structural information about the films, assuming they have more complex structures as predicted. However this may just be because the structure is aligned parallel to the z-axis meaning that reflectivity would not show the reflections. The GIXD patterns however were able to probe the off-specular reflections giving information reflections from these in plane structures.

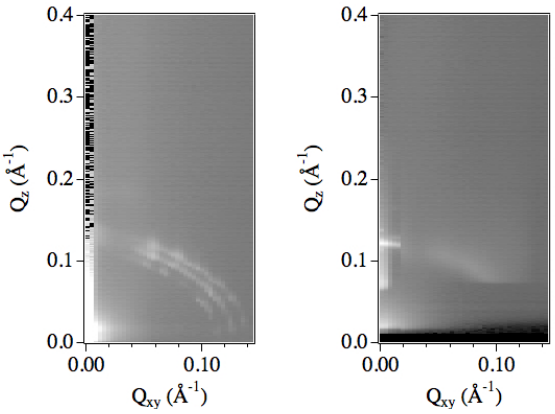

Figure 3-7. GIXD patterns of CTEAB with SPEI with incidence angles of 0.13, left, and 0.9, right.

The GIXD patterns collected for CTEAB are shown in Figure 3-7. The 0.13° angle of incidence pattern, showing structure from right at the top of the system, shows an ordered structure indicated by three rings of spots, magnified in Figure 3-8. The resolution of the detector blurs the position of the spots however it is possible to see discrete areas of lighter colour, indicating higher intensity, particularly in the lowest Q ring. As the spots are not discrete and given there are so few rings, an exact structural determination is not possible, however the best determination achieved is that the rings correspond to the 221, 311, and 321 reflections of a $Pn\bar{3}m$ which is closely related to the $Pm\bar{3}n$ seen previously for cubic structures from this surfactant. It can be seen in the 0.9° incident angle pattern in Figure 3-7, that this structure becomes more disordered as the X-rays probe deeper into the film structure.

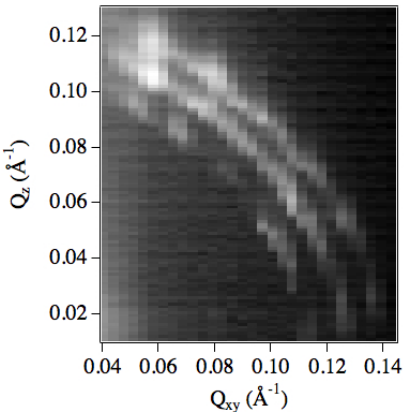

Figure 3-8. Magnified part of a GIXD pattern from CTEAB with SPEI at an incidence 0.13°

A close look at Figure 3-8 shows that the rings are not perfectly spherical as would be expected from a square cubic pattern. Instead the ring positions tend to higher Q as the angle increases away from the Q_z axis. It has been suggested that because evaporation only occurs at the top surface, as the sample dries it will compress more at the top of the film causing uni-axial compression. The spots seen in the off-specular region of the GIXD plots are slightly further from the origin than expected which would support the suggestion of uni-axial compression.

The DDAB:20C_{16}TAB/SPEI and DDAB:2C_{16}TAB/SPEI films can be considered together as they are very similar, as can be seen in Figure 3-9. Both low incidence angle patterns show a spot on the Q_z axis, around 0.13 and a spot at around Q_z=0.06 and Q_{xy}=0.12. These spots can be seen in the high incidence angle patterns as well along with spots at Q_z=0.26 Q_{xy}=0, and Q_z=0.2 Q_{xy}=0.12. All these spots can be indexed to a 2D hexagonal pattern with the 10 and 01 spots visible in the low incidence patterns and the 10, 01, 20, and 21 spots visible in the high incidence angle patterns. The clarity and discreteness of the spots in both the low and high incidence angle patterns suggests this is a very well ordered structure throughout the film with the cylindrical micelles lying parallel to the solution surface.

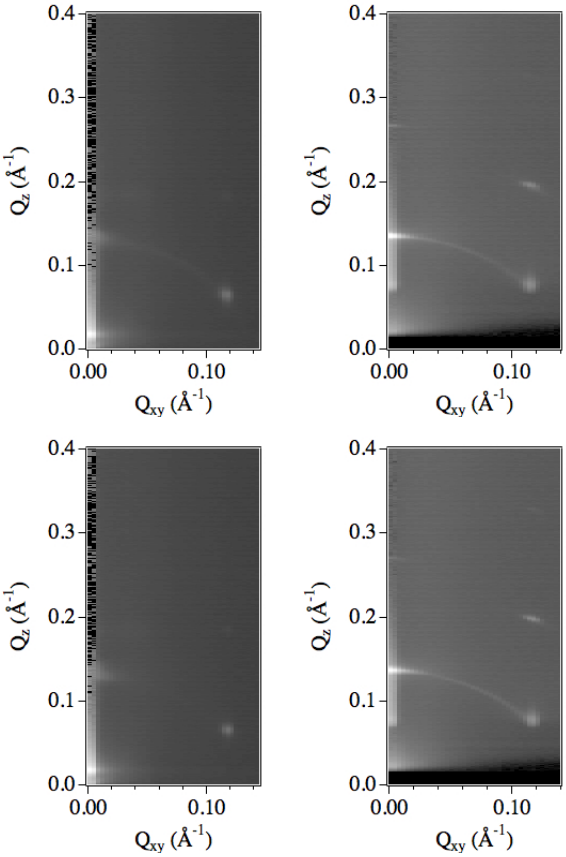

Figure 3-9. GIXD patterns of, top, DDAB:20C_{16}TAB/SPEI with incidence angles 0.13°, left, and 0.96°, right, and, bottom, DDAB:2C_{16}TAB with incidence angles of 0.13°, left, and 0.97°, right.

The GIXD patterns, for the DDAB/SPEI films shown in Figure 3-10, show two rings corresponding to a multi-layered system as predicted for this film. The 0.13° angle of incidence pattern shows faint rings indicating there is not much structure right at the top of the system. This is not surprising as with a repeat distance of 38Å only 5 layers would be able to scatter in the top 200Å, which is beyond the range of an evanescent wave. The high incidence angle pattern shows two more intense rings

however they are both broader suggesting that as the depth into the film increases so does the polydispersity of the layer thickness. This is unsurprising as the deeper the layers are the more hydrated they are likely to be, meaning that they are also more likely to be thicker. A third peak at around Q=0.45Å^{-1} should be expected however given the faint appearance of the 0.3Å^{-1} ring it is unsurprising that a third ring is not visible. In all cases the d-spacings in the GIXD patterns match those seen in the reflectivity patterns.

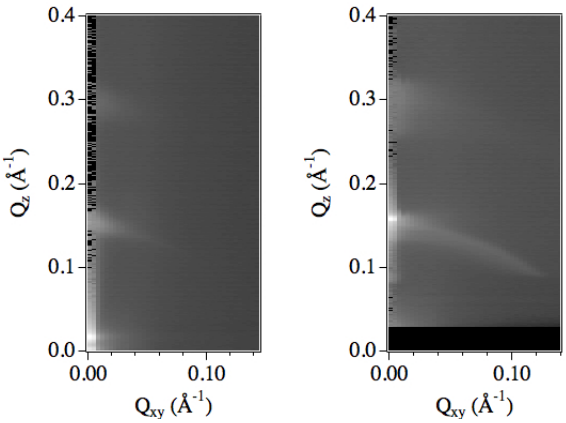

Figure 3-10. GIXD of DDAB/SPEI films with incidence angle 0.13°, left, and 1.15°, right.

3.5.2.3 LPEI films

As mentioned for the neutron reflectivity of the surfactant films made with LPEI only a single peak is seen in the x-ray reflectivity data. The same result is seen in the GIXD patterns where only a single ring of intensity, as seen in Figure 3-11. In both these cases the peak, or ring, is not very intense and quite broad suggesting a high degree of polydispersity. As the x-ray data is mainly interested in structural information about the films and only one peak is visible in the GIXD patterns no further analysis of these films was performed, however it is worth noting that this peak is in a similar position to the primary peak seen in the SPEI data.

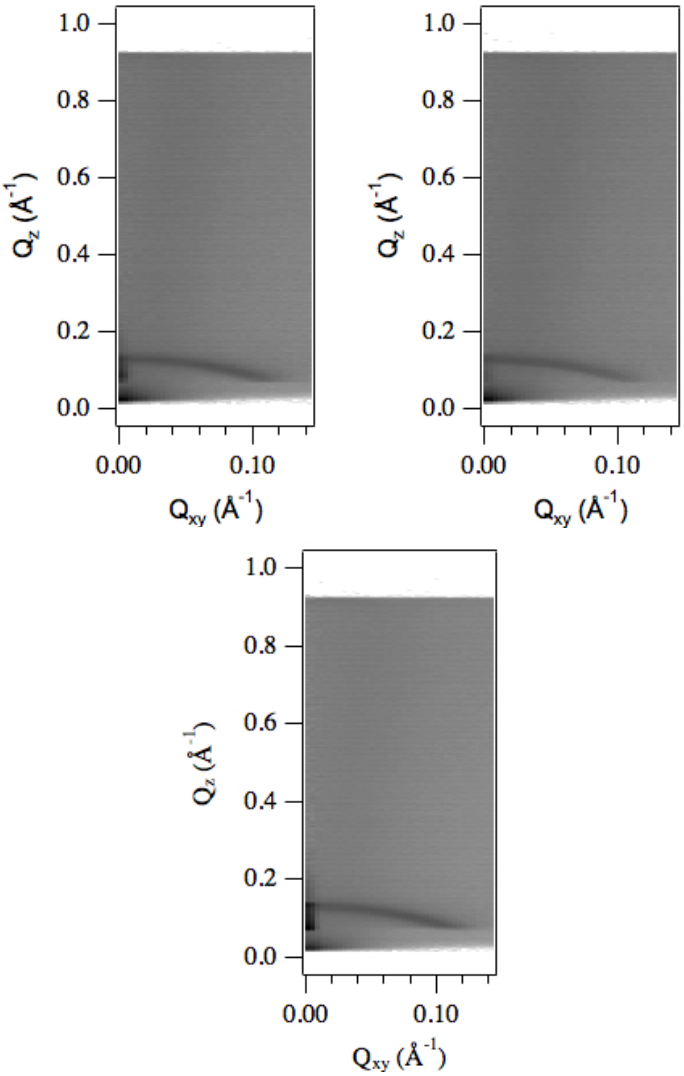

Figure 3-11. GIXD patterns of CTEAB (left), DDAB:20C_{16}TAB (middle), and DDAB:2C_{16}TAB (right) films with LPEI.

3.6 Conclusions and discussion

As stated at the beginning of this chapter, the main aim of this study was to determine whether it was possible to control the structure of these surfactant/polymer films. Previously it had been seen that the films of C_{16}TAB/PEI were made up of an array of hexagonal rods, which has been attributed to rod like C_{16}TAB micelles held in a polymer matrix.[67] From this it was decided that variation of the surfactant could lead to control over the structure of the films.

With the results discussed here it is possible to say the aim has been achieved and it is possible to reliably control the final structure of these films. Furthermore it is possible to say that rational choice of surfactant, based on packing parameter, can

directly lead to specific structure within a film, in a similar fashion to previous research into surfactant templated inorganic materials.[117]

Here it has been shown that a single surfactant that is able to form spherical micelles, and has been seen to template cubic structure in templated silica, is able to form a cubic pattern in a polymeric film. Also a single surfactant that forms bilayer structures in solution creates a multi-layered film. Two mixed surfactant systems showed that hexagonal films could be made from elongated, rod like, ellipses. From these results the difference in elongation between the two mixed surfactant systems does not appear to have an effect on the film structure. It must also be noted here that so far all the surfactants have contained a quaternary ammonium head group and the polymer has always been PEI.

These surfactant systems were chosen using the packing parameter to predict the micelle shapes. SANS was then used to study the surfactant solution in the absence and presence of polymer to determine the shape of the micelles and the effect the polymer had on the micelles. The micelle shapes, as determined by the packing parameter, were fairly accurate with the DDAB sample producing a bilayer structure. The DDAB:20C_{16}TAB samples was also accurately predicted by the packing parameter giving a slightly elongated ellipse. The CTEAB sample was expected to be spherical, while the DDAB:2C_{16}TAB sample was expected to be more elongated than the DDAB:20C_{16}TAB sample, however the results showed both samples were actually similar to the DDAB:20C_{16}TAB sample. All these results, although not exactly predicted by the packing parameter, were still in line with previous research in the literature.[53, 101, 107]

On the addition of polymer to the surfactant solutions there was very little change in the SANS patterns in all samples, except of DDAB:2C_{16}TAB, indicating what appeared to be limited interaction between the surfactant and the polymer. The elongation of micelle shape seen in the SANS patterns of the DDAB:2C_{16}TAB samples with polymer showed the micelles were considerably different than in the absence of polymer. This may indicate that there is more of an interaction between the DDAB and the polymer than the C_{16}TAB, as the pure DDAB solution in the absence of polymer produced bilayers the addition of polymer to this solution would not produce any more elongated structures.

As in the studies by O'Driscoll et al.[66] there are no additional indications of larger aggregates in solution suggesting that the film formation is an entirely surface related process. In fact the solutions in this report show even less evidence than

O'Driscoll had of an interaction between the surfactant and the polymer as he saw a change in micelle structure on the addition of polymer.

A comparison of the neutron reflectivity profiles with previous work shows that, as with C_{16}TAB/PEI interactions, these films show a much greater level of interaction than has previously been seen, even for strongly interacting oppositely charged surfactant/polymer systems.[7] Interestingly even when compared to the original C_{16}TAB/PEI work the films reported here appear much better ordered and visually they are thicker particularly with increasing the level of DDAB.

The best results showing the extent of the structure formed were collected by GIXD. The films expected to be the most reliable for producing structure was the DDAB film, and this was shown to be correct with the most intense peaks and two well-defined rings. The DDAB:2C_{16}TAB films were also expected, from the elongated micelles in solution, to reliably form a hexagonal pattern, and once again this was found to be correct. The DDAB:20C_{16}TAB films were slightly more uncertain as the micelles had not appeared to be elongated cylinders. However once again the pattern showed a clear well ordered hexagonal system. O'Driscoll had reported for the C_{16}TAB films that in the hexagonal systems only a single peak was visible in the off-specular region[67] however in this report at least two spots were seen, once again confirming that these films are more well structured than the C_{16}TAB only films. Finally, as had been hoped, the CTEAB film had produced a pattern with three rings of smeared spots, which have been attributed to an as yet unidentified cubic pattern.

The effect of polymer molecular weight was also studied on these films however due to lack of structure in the films for high molecular weight PEI it was impossible to tell if the polymer affects the structure of the film. In all cases however GIXD patterns showed a single ring of intensity in the pattern suggesting a there is some ordering of micelles in the films. Interestingly this peak is in the same position as the peak seen in the SPEI system therefore it is thought that the polymer does not have a similar affect on the film structure as was seen in the C_{16}TAB/PEI system.

In summary it is confirmed that macroscopic thin films can be formed from certain surfactants that contain a quaternary ammonium head-group. These films contain well-ordered structure that can be easily controlled by the shape of the surfactant micelles that are used to make the films.

4 Encapsulation and Release in Cationic Surfactant Films

In chapter 3 it was shown that it was possible to control the structure of the cationic surfactant/polymer films by altering the surfactant used. The next step was to build on this work by showing how the control of the film structure could influence a potential application. Specifically the potential application is the use of a film as a storage and release device for partially soluble species.

As discussed in the introduction one of the major uses of surfactants is their ability to solubilise apolar solutes in polar solvents. In the detergent industry alone surfactants are used for solubilising the oil based "dirt", increasing the effectiveness by wetting the substrate, enhancing the feel by making the products foam and introducing insoluble species such as small alkanes that are used for fragrance in the product.[61]

One potential storage and release device is the storage and release of therapeutic agents for medical purposes. Studies using the layer-by-layer technique to build up thin films have shown that it is possible to make thin films that contain regions for solubilising partially soluble species.[38, 63, 118] The species can then be released from the film by degradation of the film, which can be tuned by the choice of components in the films. Although these systems do not use surfactants as the drug carrier, further work by Michel et. al. have shown that it is possible to embed phospholipid vesicles into layer-by-layer created films with the potential as drug delivery devices.[45, 46]

Surfactants as drug delivery devices are not just confined to thin films as they are used in a wide variety of aggregate forms.[62, 119] As noted by Bramer et. al.[119] the ability of surfactant micelles to encapsulate drugs is relatively limited. Lawrence[62] however states that in micellar solutions drug encapsulation is limited, although in liquid-crystalline phases the encapsulation is much greater. As discussed in chapter 3, the films in this report potentially have the ability to be tailored to produce liquid crystalline nanostructures for a particular purpose. Therefore these films have the potential for much greater drug loadings than the layer-by-layer films, which can only incorporate micelles into their structure.[45, 46]

Previous work by O'Driscoll et al[68] started this study on the films made from C_{16}TAB and PEI. In this work the use of different sparingly soluble species were used to study the effect of swelling the surfactants and the impact of this on the film

structures. In that study four additives, cyclohexane, cyclohexanol, decane and benzene, were used to study their effect on the micelle structure as well as the amount of additive encapsulated in the micelle. For this report it is the amount of additive that is encapsulated that is of interest and this will be studied, as in the work by O'Driscoll et al, by using cyclohexane and cyclohexanol.

Cyclohexane and cyclohexanol is a good pair of species to study as they are both of similar size and molecular structure. The major difference of course is the alcohol group on the cyclohexanol making it more amphiphilic than the completely hydrophobic cyclohexane, so these two molecules act as highly simplified models of two classes of potential drug molecules for encapsulation. The effect of adding cyclohexane has previously been studied in C_{16}TAB micelle and it has been postulated that it preferentially mixes with the surfactant core[120] which is a sensible conclusion given its hydrophobicity. Cyclohexanol has not been extensively studied however other complex alcohols exhibit similar behaviour to the equivalent 1-alcohol therefore it is expected that the cyclohexanol will be solubilised near the head group region of the micelle.

One addition to the previously studied system has been made; this is the use of the dye Nile red. Nile red is a small organic molecule made up of four benzene rings, as shown in Figure 4-1, and the reason for using it is two-fold. One reason is due to its size, being made up of four benzene rings it is similar in size to steroids, some of which are common drugs. The second reason for using Nile red is due to it fluorescence properties. Nile red is commonly used as a fluorescent probe with amphiphilic species.[105, 121] In this study however the intended use of Nile red is to monitor its fluorescence as it is released from the films.

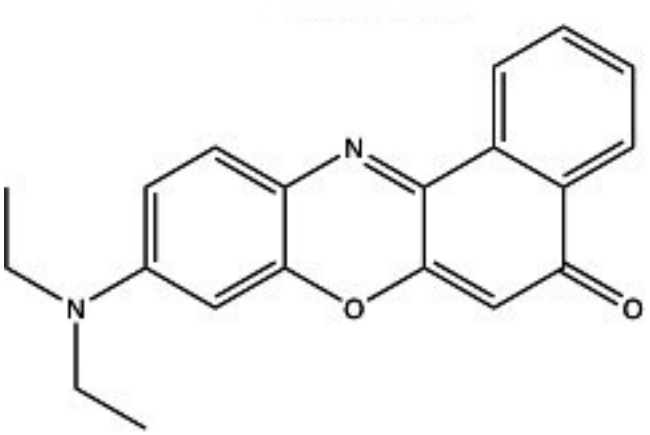

Figure 4-1. Nile red

4.1 Encapsulation of Cyclohexane and Cyclohexanol

In the previous studies[68] the amount of cyclohexane and cyclohexanol detected in the micelle core was much lower than the amount added to the initial solution. In the case of the cyclohexanol this may be explained by its amphiphilic nature, which means that instead of residing in the micelle core it will preferentially be in the head group region, or even potentially more soluble in the water or even evaporated due to its volatility. The encapsulation of the additive was measured by SANS using contrast variation with hydrogenated and deuterated additive. The resolution of the instrument makes it hard to detect the micelle head groups therefore the scattering length density (SLD) contrast is measured between the solvent and the micelle core. If the cyclohexanol was in the core it would affect the SLD of the surfactant tails, however if it was in the head group then its effect may not be noticed. If the cyclohexanol was more soluble in the solvent, then it is in such small quantities compared to the solvent that it would have no effect on the SLD.

Therefore, in this work to confirm that the cyclohexane and cyclohexanol would partition into the micelle core, gas chromatography (GC) was used. A two-phase system of water and hexadecane was used to mimic the surfactant solution with the hexadecane mimicking the surfactant tail region and SPEI and sodium bromide being added to mimic the conditions in the aqueous phase. In separate samples cyclohexane and cyclohexanol were added to the solutions to give calculated amounts of 20vol% and 30vol% of the total additive in the hexadecane. Due to its hydrophobicity it is expected that the cyclohexane will partition completely into the hexadecane. With the amphiphilicity of the cyclohexanol, it is expected that the cyclohexanol will partition into the hexadecane but possibly form an interfacial layer instead of mixing in the bulk hexadecane solution.

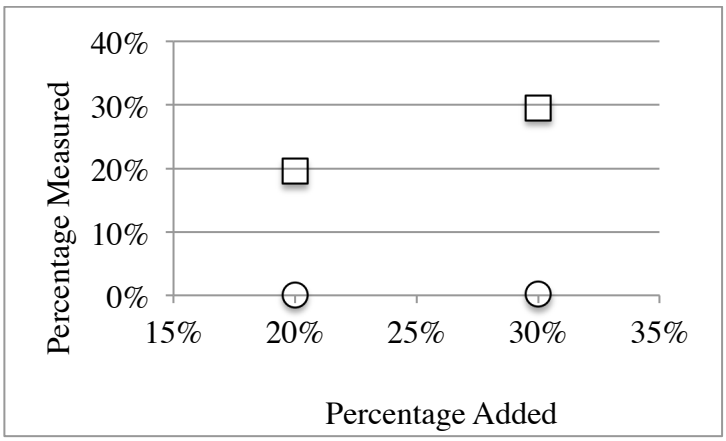

Figure 4-2. GC results determining the partitioning of cyclohexane (squares) and cyclohexanol (circles) in hexadecane. Errors in the percentage measure are the same size as the markers. Uncertainties are ±0.5%

The results from the GC show that the cyclohexane partitions into the hexadecane as expected therefore there is no cyclohexane left in the water or at the hexadecane/water interface, cyclohexane is <1% soluble in water. The cyclohexanol results do not detect any cyclohexanol in the hexadecane. This suggests either the cyclohexanol is all at the hexadecane/water interface or dissolved in the water. As cyclohexanol is much more soluble in the hexadecane than in water, soluble and 3.6% soluble respectively, it is therefore likely that the cyclohexanol is at the water/hexadecane interface and thus not detected because the GC sample was taken from the bulk solution. To confirm the cyclohexanol is at the interface, the interfacial tension between the water and the hexadecane could be measured. If the cyclohexanol is active at the interface then the surface tension will be affected. Unfortunately there was not time to complete this experiment during this work.

4.1.1 Encapsulation into surfactant solutions

As stated above the main hydrophobic species to be used were cyclohexane and cyclohexanol. As the previous study was interested in the effect of swelling the micelles, the additive quantities were calculated such that the reported percentages were the percentage of methylene groups in the micelle core belonging to the additive. For simple comparison with this data the same quantities were used in this report, therefore the percentages reported as 20%, 30% and 40% represent theoretical volume percentages of the micelle core which are equivalent to 70mol%, 114mol% and 178mol% respectively.

The solutions were prepared by making the surfactant and polymer stock solutions. The required amount of surfactant solution was then pipetted, using an auto-pipette, into a vial followed by the polymer solution. The additive was then added in one batch, also by auto-pipette, to the mixed polymer surfactant solution. Auto pipetting may lead to inaccuracies in volume of additive being added to the solution, however every attempt was made to minimise this by making up all the solutions at the beginning of each experiment and manually adjusting the amount pipetted by checking the pipetted weight of ultra pure water. The alternative was weighing the additives out for each sample however would have not been possible due to the small size of the solutions being prepared for the SANS experiments and the high rate of evaporation of the additives. As soon as the additives had been added to the surfactant solutions the vials were closed and a para-film wrapping on top of the cap was used to try and limit evaporation of the additives. The solutions were then gently

agitated and left for at least 15 minutes to equilibrate before being transferred to the measurement cells.

To determine the extent of encapsulation surfactant solutions were measured with both hydrogenated and deuterated cyclohexane and cyclohexanol, C_6H_{12}/C_6D_{12}, and $C_6H_{11}OH/C_6D_{11}OD$ respectively. The surfactants were always hydrogenated and the solvent was always D_2O. By doing this any change in the scattered intensity would be related to the amount of hydrophobic species in the micelle. To calculate the percentage of hydrophobic species encapsulated, simultaneous fitting of the two contrasts using the NIST SANS Analysis package in IgorPro was performed. The difference between the SLDs in the two samples was then related to the difference in percentage of hydrogenated and deuterated methylene groups, which is directly related to the vol% added to the solutions.

To increase accuracy the uniform ellipsoid model and both the dilute lamellar bilayer and lamellar paracrystal fitting models were adjusted so that the percentage was calculated directly during the simultaneous fitting. Equation 4-1 shows the change to the total contrast SLD to take into account fitting the percentage of hydrophobic species. More detail about the changes to the model code can be found in appendix 3.

$$\text{Contrast} = SLD_s - [(1 - PA)\, SLD_M + PA \times SLD_A] \qquad \text{Equation 4-1}$$

In Equation 4-1, SLD_S is the solvent SLD; PA is the percentage additive encapsulated; SLD_M is the micelle scattering length density, which is the SLD of the surfactant tails; and SLD_A is the SLD of the additive which is either the hydrogenated or deuterated additive depending on the curve during the simultaneous fitting. Although mentioned here that the SLD_M is the SLD of the tails this is not entirely accurate as for each methylene group from a surfactant tail there includes an extra $1/16^{th}$ of a hydrogen atom from each end of the surfactant tail. At the same time SLD_A, in the case of cyclohexanol is a methylene with $1/6^{th}$ of the scattering length of an oxygen atom from the alcohol group. The SLDs used are shown in Table 4-1.

	Molecule	SLD ($Å^{-2}$)
	D_2O	$6.37x10^{-6}$
Surfactant Tails	CTEAB	$-0.35x10^{-6}$
	DDAB:20C_{16}TAB	$-0.35x10^{-6}$
	DDAB:2C_{16}TAB	$-0.36x10^{-6}$
	DDAB	$-0.37x10^{-6}$
Additive	Hydrogenated Cyclohexane	$-0.28x10^{-6}$
	Deuterated Cyclohexane	$6.70x10^{-6}$
	Hydrogenated Cyclohexanol	$0.04x10^{-6}$
	Deuterated Cyclohexanol	$7.15x10^{-6}$

Table 4-1. List of scattering length densities used to determine the encapsulation of additives in different surfactant micelles.

Due to the change in fitting the contrast, instead of having two parameters in the fitting models for the SLDs, as shown in Table 3-4, there were four parameters. These were the SLD of the surfactant, the SLD of the additive, the SLD of the solvent and the percentage of the additive in the surfactant. In chapter 3 the h-surfactant in D_2O sample SLDs are held constant during fitting, while the other contrast SLDs are allowed to fit freely. In this chapter all the SLDs are held constant during fitting however the percentage additive is allowed to fit as long as simultaneous fitting is being performed. Any change to this is reported with the fitting results.

Throughout this study the same surfactant systems used were as discussed in chapter 3. This allows comparison with results collected for the addition of additives to the C_{16}TAB solutions and C_{16}TAB/PEI solutions and films.[68] This then allows us to study whether enhanced encapsulation can be achieved with changes to the micelle shape.[62]

4.1.1.1 Solutions without polymer

As with the surfactant solutions data discussed in chapter 3 the same mathematical models were fitted to the scattering data to determine the micellar shape. The models were the uniform ellipsoid[111] with the included Hayter-Penfold mean spherical approximation as the structure factor.[83] This was used to fit the CTEAB, DDAB:20C_{16}TAB and DDAB:2C_{16}TAB data. To fit the DDAB data the model used was the dilute lamellar bilayer.[113] As mentioned previously the form factor models have been adjusted to allow simultaneous fitting of multiple contrasts to give a percentage of additive encapsulated as shown in Equation 4-1. Details of the changes made to the code can be seen in appendix 3. The fitting results are shown in Table

4-2 and sample fits can be seen in Figure 4-3 below. As with the data fitted in chapter 3, the parameters for the models are shown in Table 3-4, except for the SLDs as discussed above.

Cyclohexane Amount of additive added (vol%)		R(a) (Å)	R(b) (Å)	Measured Additive
CTEAB	20%	32	24	9%
	30%	33	24	7%
	40%	33	23	0.4%
DDAB:20C_{16}TAB	20%	33	26	6%
	30%	35	24	5%
	40%	35	26	8%
DDAB:2C_{16}TAB	20%	62	23	2%
	30%	43	25	2%
	40%	-	-	-

Cyclohexanol		R(a) (Å)	R(b) (Å)	Measured Additive
CTEAB	20%	31	23	1%
	30%	32	22	2%
	40%	30	23	4%
DDAB:20C_{16}TAB	20%	32	23	5%
	30%	32	21	11%
	40%	31	24	9%
DDAB:2C_{16}TAB	20%	38	22	11%
	30%	35	21	9%
	40%	39	22	7%

		Bilayer Thickness (Å)	Polydispersity	Measured Additive
DDAB	20%	27	0.20	1%
	30%	28	0.15	3%
	40%	26	0.02	4%

Table 4-2. Fitting results from SANS data with different amounts of cyclohexane and cyclohexanol in CTEAB, DDAB:20C_{16}TAB, and DDAB:2C_{16}TAB solutions with no polymer present. Errors in micelle dimensions are ±2Å. Error in bilayer polydispersity is ±0.05. Error in additive measured is ±2%.

Results not included in Table 4-2 are the samples of DDAB with added cyclohexane and DDAB:2C_{16}TAB with 40% cyclohexane. This is due to the samples giving anomalous results therefore they need to be repeated.

Results for additive encapsulation were calculated, however in none of the systems is the amount of additive equal to the amount expected from the volume added to the solution initially. The manufacturer states a 1% error in volumes added from the pipette used,[122] however due to the small amounts of liquid, particularly the cyclohexanol which is viscous, it may be slightly higher, however this does not account for the discrepancy in the measured value. Unlike the previous results,[68] where as the additive was added the measured value increased, the measured value in these systems fluctuates. Interestingly apart from the CTEAB sample with 40% cyclohexane all the fluctuations are with ±3% of each other. Given this it is therefore likely that this is fluctuation about an ideal surfactant micelle loading. This is similar to the reported 7.9vol% of glucose encapsulated by a DDAB/SDS solution as reported by Kondo et. al.[123]

Figure 4-3 shows the fits for the four different surfactant mixtures in the presence of 30% cyclohexanol. This figure is to show the quality of fit over the Q range studied.

Assuming the values are fluctuating around an ideal surfactant micelle loading then an average of these fluctuations will approximate the ideal surfactant loading for that additive and this value can be compared to study how the different micelle structures encapsulate the different species. This comparison is shown in Figure 4-4, the CTEAB sample with 40% cyclohexane however has not been included because it is considerably lower than expected. This plot clearly shows a trend of cyclohexane being encapsulated more into more spherical micelles such as CTEAB micelles and cyclohexanol being more encapsulated into more elongated structures such as the DDAB:2C_{16}TAB micelle. Given the shapes of the micelles do not differ much, except in the case of DDAB:20C_{16}TAB in the presence of cyclohexane, this trend is not due to larger micelles encapsulating more therefore it is probably due to packing within the micelle. The larger head group of CTEAB could interfere with the cyclohexanol sitting near the micelle solvent interface, or the double tailed DDAB could cause the core of the micelle to be more crowded preventing cyclohexane from packing there. There is no current literature explaining this however Warr et. al.[53] have determined the surface area for the surfactants to be 64Å^2 for the C_{16}TAB and 68Å^2 for the DDAB, this compares with an approximated head group area of 72Å^{-1} for CTEAB, as given in Table 3-2.

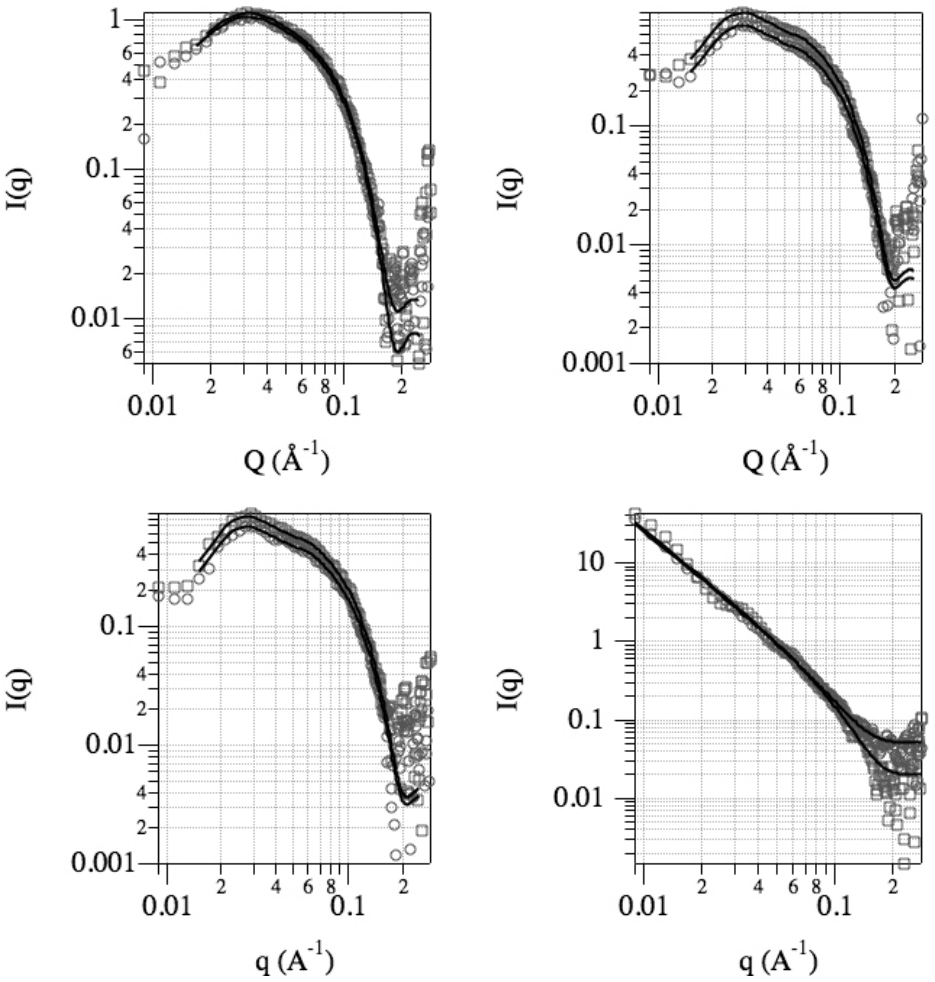

Figure 4-3. Fitted data from solutions of 30% cyclohexanol in, top row, CTEAB (left), DDAB:20C_{16}TAB (right), and bottom row, DDAB:2C_{16}TAB (left) and DDAB (right). Markers are squares for the hydrogenated cyclohexanol and circles for the deuterated data, lines are lines of best fit. Errors bars are not shown as they are much smaller than the markers over the majority of the Q range.

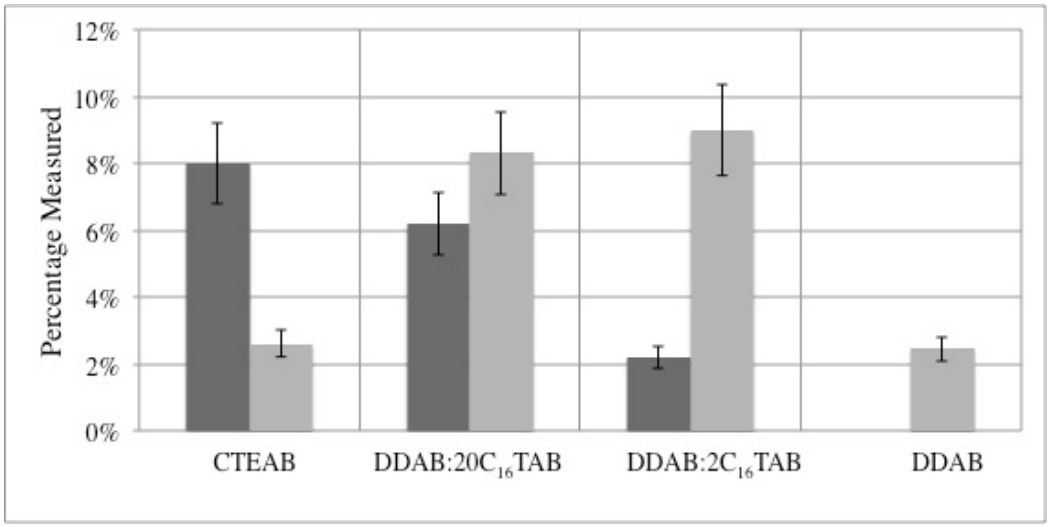

Figure 4-4. Encapsulation of cyclohexane (dark grey) and cyclohexanol (light grey) into different surfactant systems with no polymer.

The trend discussed above for cyclohexanol falls apart when the DDAB samples are considered. These samples show the most elongated structure but show least encapsulation of cyclohexanol. It is unclear why this is but it is probably due to efficiency of packing with the bilayer. Unfortunately due to the lack of results for the cyclohexane sample it is impossible to say whether the trend for the cyclohexane samples would be continued or reversed.

One final difference between some of the samples is the apparent swelling of the micelles as compared to the samples without additive, Table 3-7. The samples that appear to show swelling are the most elongated structures of DDAB:2C_{16}TAB and DDAB. This is surprising given the lack of swelling seen in the other samples and the previously reported data.[68] In the case of the DDAB:2C_{16}TAB samples it was expected that these samples would be more likely to form elongated cylindrical structures and the fact that this wasn't seen was attributed to non-ideal mixing of the surfactant species. The addition of additive here appears to have altered the surfactant mixing allowing the formation of more elongated structure. The same cannot be said for the DDAB samples although these are now more in line with expected bilayer thicknesses for this surfactant. The difference in this case is more likely due to the difficulty in accurately determining the point at which the scattering becomes background, which is an important factor in fitting bilayer thicknesses with the model used here.

4.1.1.2 Solutions with SPEI

After studying the samples in the absence of polymer the next step was to include polymer in the solution, as these are the solutions that will eventually make up the loaded films. Overall the effect of adding SPEI to the majority of the systems appeared to stabilise the samples allowing simultaneous fitting of all but two plots with very little variation between fits of the same surfactant solutions. The results for the fitting of the cyclohexane data are shown in Table 4-3 while the results for the fitting of the cyclohexanol data are shown in Table 4-4, examples of data fitting are shown in Figure 4-5.

	Amount of additive added (vol%)	R(a) (Å)	R(b) (Å)	Measured Additive
CTEAB	20%	31	22	6%
	30%	31	23	4%
	40%	31	23	5%
DDAB:20C_{16}TAB	20%	32	25	3%
	30%	34	24	5%
	40%	35	23	8%
DDAB:2C_{16}TAB	20%	181	21	7%
	30%	56	21	6%
	40%	(A)	23	8%

	Bilayer Thickness (Å)	Number of Layers	Layer Spacing	Measured Additive
DDAB 20%	23	1.82	112	10%
DDAB 30%	-	-	-	-
DDAB 40%	18	1.49	170	14%

Table 4-3. SANS fitting of the surfactant systems with cyclohexane as the additive. (A) The prolate ellipse in this system is so long that changing R(a) has no effect on the χ^2 value of the fit, a value of 400 was held during fitting to reflect this. Errors in micelle dimensions and layer spacing are ±2Å. Error in number of layers ±0.05. Error in additive measured is ±2%.

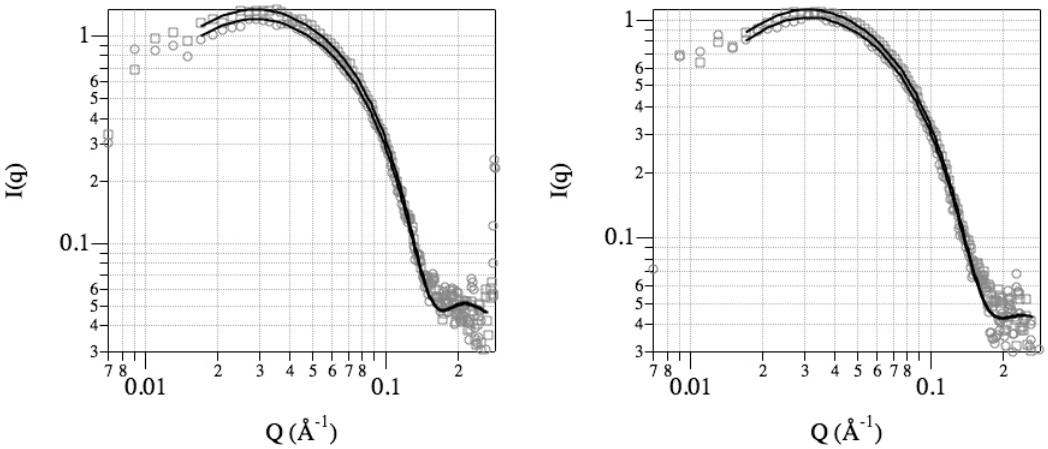

Figure 4-5. Simultaneous fitting of DDAB:20C_{16}TAB with SPEI and cyclohexane (left) or cyclohexanol (right). Squares are from hydrogenated additive and circles are from deuterated additive. Lines are lines of best fit from the fitting. Error bars are not included because they are smaller than the markers.

	Amount of additive added (vol%)	R(a) (Å)	R(b) (Å)	Measured Additive
CTEAB	20%	30	21	2%
	30%	29	22	5%
	40%	29	22	4%
DDAB:20C_{16}TAB	20%	32	22	6%
	30%	34	22	4%
	40%	33	22	8%
DDAB:2C_{16}TAB	20%	-	-	-
	30%	81	18	10%
	40%	136	20	7%

		Bilayer Thickness (Å)	Number of Layers	Layer Spacing	Measured Additive
DDAB	20%	-	-	-	-
	30%	20	1.83	130	0%
	40%	20	1.35	230	5%

Table 4-4. Surfactant systems with cyclohexanol as the additive. Errors in micelle dimensions and layer spacing are ±2Å. Error in number of layers ±0.05. Error in additive measured is ±2%.

In these two tables the only samples not to give results are the DDAB:2C_{16}TAB with 20% cyclohexanol and DDAB with 20% cyclohexanol and 30% cyclohexane. The sample of DDAB:2C_{16}TAB showed significant variation between the hydrogenated sample and the deuterated sample therefore could not be fitted. The DDAB samples on the other hand gave a result of a large negative encapsulation. As this is physically impossible, however in this case it is possible that an error was made with sample preparation. These samples should therefore be repeated to complete the picture.

Similarly to the previously discussed results, the addition of additive does not really affect the size of the CTEAB and DDAB:20C_{16}TAB micelles. Also the DDAB bilayers are not affected in the same way as seen in the samples without polymer. Once again this is more likely due to the fitting as the addition of polymer causes the background level to be noisier making bilayer thickness determination difficult. The one sample that does still show swelling is the DDAB:2C_{16}TAB sample, particularly in the case with the addition of cyclohexane the variation is more obvious and appears correlated to the amount of cyclohexane encapsulated, although this may only be coincidence. To fully understand the system, repeats of these experiments should be performed to confirm how reproducible they are. Along with these repeats,

a further set of experiments using selective deuteration of the different surfactants would also increase the understanding by further correlating the additive encapsulated with the ratio of DDAB to C_{16}TAB in the micelles.

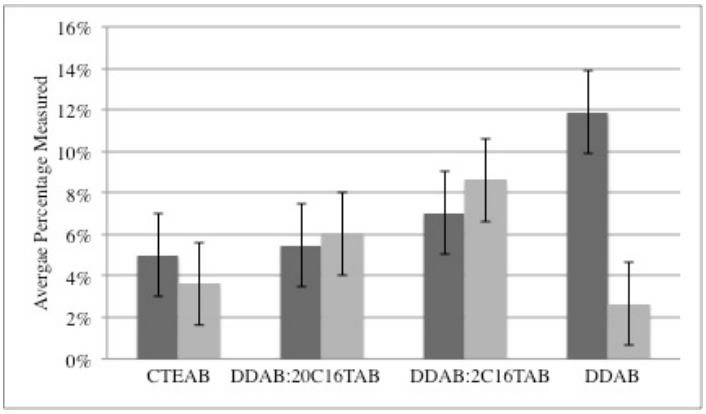

Figure 4-6. Encapsulation of cyclohexane (dark grey) and cyclohexanol (light grey) into different surfactant systems in the presence of SPEI

A similar study of the apparent trend in encapsulated additive is performed and the result is shown in Figure 4-6. The percentage-measured values are an average across all samples assuming they represent an ideal amount of additive to be encapsulated. Instead of having more cyclohexane encapsulated in CTEAB and more cyclohexanol in DDAB:2C_{16}TAB, as seen with no polymer present. It appears that the more elongated the structure the more additive can be encapsulated. This is hard to be certain about however because the DDAB encapsulation of cyclohexanol bucks the trend and actually only encapsulates the same amount as when polymer is not present.

To explain these results it is best first to discount the DDAB cyclohexane results. This is done because the results cannot be compared with a polymer free sample therefore it is unclear what affect the polymer has. In the other samples the trend is most likely due to packing within the micelle. The molecular strength of the interactions leading to the micelle shapes in the absence of polymer obviously cannot be overcome by the addition of small hydrophobic species to the sample, except in the case of DDAB:2C_{16}TAB, which is shown by the lack of swelling of the surfactant micelles. Therefore the addition of hydrophobic species to the micelle is controlled by the ability of the micelle to internally rearrange. It has previously been seen that in a constrained system that there is more movement possible if there are surfactants with different tail lengths, this is due to the ability of the longer tailed surfactants to allow the micelle to expand through.[124] Due to the small amount of additive encapsulated in the micelles this swelling is probably too small over the full size of the micelle to be obvious in the fitting results. This would then also explain

the larger change seen in the DDAB cyclohexanol results, as it is a single length tail surfactant system.

4.1.1.3 Solutions with LPEI

As the film structures with LPEI with no additive did not show good structure it was decided only to investigate solutions containing one additive amount, therefore only samples with 30% additive were measured. The results from this fitting are shown in Table 4-5 and the encapsulated amounts are compared in Figure 4-7, an example of the fitting is also shown in Figure 4-8. The DDAB:2C_{16}TAB results are not included in either the table or figure. Fitting has been attempted however the results are anomalous therefore repeats should be performed.

		R(a) (Å)	R(b) (Å)	Measured Additive	
CTEAB	Cyclohexane	42	21	2%	
	Cyclohexanol	41	21	1%	
DDAB:20C_{16}TAB	Cyclohexane	36	26	7%	
	Cyclohexanol	36	21	9%	
		Bilayer Thickness (Å)	Number of Layers	Layer Spacing	Measured Additive
DDAB	Cyclohexane	27	1.81	256	5%
	Cyclohexanol	18	1.77	254	3%

Table 4-5. Fitting results for Surfactant/LPEI solutions in the presence of additives. Errors in micelle dimensions and layer spacing are ±2Å. Error in number of layers ±0.05. Error in additive measured is ±2%.

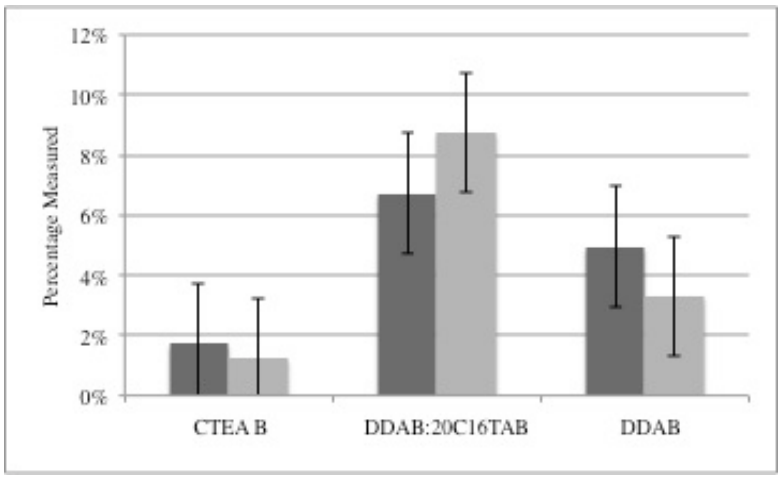

Figure 4-7 Encapsulation of cyclohexane (dark grey) and cyclohexanol (light grey) into different surfactant systems in the presence of LPEI

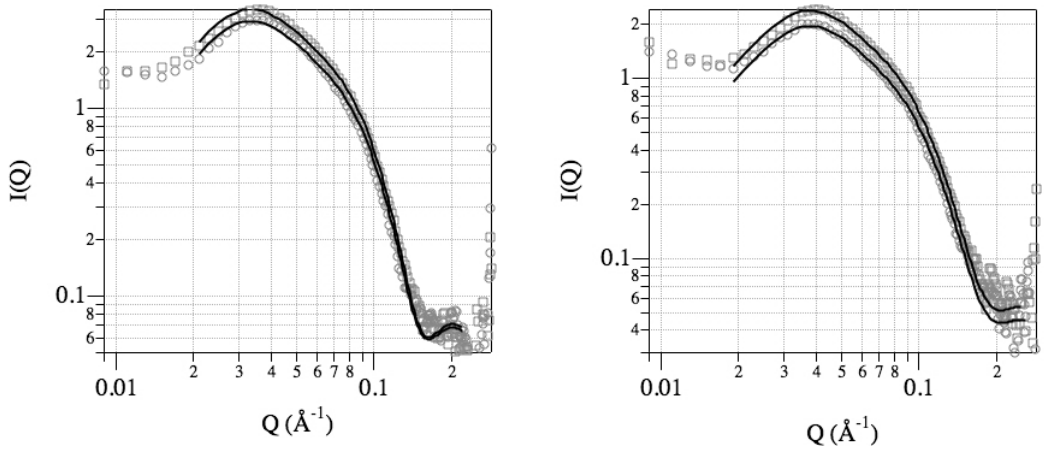

Figure 4-8. Simultaneous fitting of DDAB:20C_{16}TAB with LPEI and cyclohexane (left) or cyclohexanol (right). Squares are from hydrogenated additive and circles are from deuterated additive. Lines are lines of best fit from the fitting. Error bars are not included because they are smaller than the markers.

The results are very similar to those seen with SPEI, as is expected. CTEAB is able to encapsulate slightly less while DDAB:20C_{16}TAB is able to encapsulate slightly more of both hydrophobes. DDAB with cyclohexanol encapsulates the same roughly the same amount irrespective of polymer or whether polymer is present. The only point that disagrees with the SPEI results is that of DDAB with 30% cyclohexane, which is lower than expected. All of this data is just taken from one point however and not an average as seen previously therefore it is possible that any of these results may be anomalous but this cannot be determined from this data.

4.1.2 Encapsulations in surfactant films

4.1.2.1 Simulation of data to produce a correction factor

As in the previous studies and in chapter 3 the films were studied by neutron and x-ray reflectometry and grazing incidence x-ray diffraction (GIXD). Of these the technique best suited to determining the amount of additive in a film is neutron reflectometry. This is because, like SANS, the scattering is dependant on the SLDs of the components therefore by changing only the additive it should be possible to determine the amount of additive in the films.

To quantify the effect of a change in the SLD of the layers, a theoretical model was created using the Motofit procedures[93] for IgorPro. Motofit allows the simulation of neutron and x-ray reflectometry data given a specific model or the fitting of the model to multiple real data sets. Given the direction of the scattering vector for x-ray

and neutron reflectometry is perpendicular to the interface, the model that is created is based only on a repetitive layered structure. The basic theory of the model used is that the sample has a surfactant monolayer on the surface; this monolayer then interacts with a hydrated polymer layer that is interacting with surfactant bilayer that contains the additive, as shown in Figure 4-9. This dual layer of hydrated polymer interacting with a surfactant bilayer is then repeated to build up a sharp diffraction peak as seen in the real reflectometry patterns.

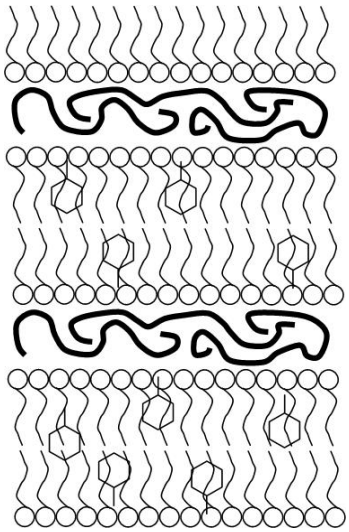

Figure 4-9. Diagram of the top part of the model used to simulate the reflectometry profile of a thin film.

Simulations were performed using this model by altering the SLD of the bilayer to represent a loading of 10-90% hydrogenated additive. These simulations were then compared to simulations representing bilayers with10-90% deuterated additive. In all these simulations the additive loading is like that of the solution additive loading therefore 10% loading means that in the bilayer 10% of the methyl groups belong to the additive while 90% belong to the surfactant. Each corresponding hydrogenated/deuterated pair of patterns was then analysed by determining the peak intensity and the peak area, as these are related to the number of layers and the difference in the SLD between the layers. As well as studying the change in the peak intensity and peak area with relation to the amount of additive in the bilayer, both the roughness and the number of layers in the model were also studied. An example of a simulated pattern is shown in Figure 4-10. This pattern represents a 20 layer model of a CTEAB/polymer system with 30% deuterated cyclohexanol. The inset graph shows the variation of SLD as a function of distance from the interface.

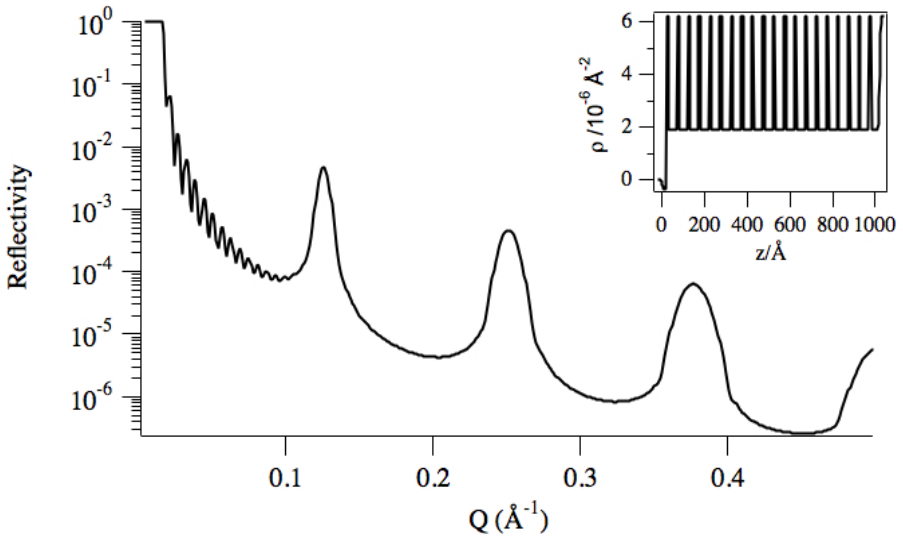

Figure 4-10. Simulated reflectivity pattern of 20 repeat film of CTEAB and 30% deuterated cyclohexanol. Inset is a graph of the variation in SLD as a function of distance from the interface.

As stated previously comparing either the peak intensity of the peak area of the peaks in the comparable hydrogenated and deuterated additive simulations, it is possible to determine the percentage additive incorporated into the surfactant bilayer. The value calculated for the amount of additive in the simulations is not exactly the same as the value expected however there is a linear relationship between the two values allowing for determination of a correction factor. The correction factor values determined are shown in Table 4-6, and correspond to the equation y=mx+c.

	m	c
Cyclohexane	1.30	0.025
Cyclohexanol	1.32	0.033

Table 4-6. Correction factors calculated by modelling for use determining percentage of additive in surfactant polymer films.

Importantly while studying the effect of changing the roughness and the number of layers in the model it was determined that as long as both these parameters are the same in both the hydrogenated and deuterated simulations then this analysis works. As soon as one or both of these parameters is altered, then without fitting it is not possible to determine the amount of additive in the system.

4.1.2.2 DDAB:20C_{16}TAB and DDAB:2C_{16}TAB films

Due to time constraints all the encapsulation experiments could not be performed at the same time therefore the DDAB:20C_{16}TAB and DDAB:2C_{16}TAB experiments were performed separately on the FIGARO instrument at the ILL, while the CTEAB

and DDAB experiments were performed on the SURF instrument at ISIS. FIGARO is a newer reflectometer and has been developed with a much higher flux than SURF. Due to this it was possible to study these films with 5-minute time resolution, the previously discussed SURF experiments have used a 15 minute time resolution. Due to the lack of structure previously seen in the films of LPEI, in chapter 3, it was decided, to save time, not to study encapsulation into these films. An example of patterns collected using DDAB:2C_{16}TAB and SPEI with 20% hydrogenated cyclohexane is shown in Figure 4-11. With each pattern representing a 5-minute period this plot shows the film structure over one hour of experimental time.

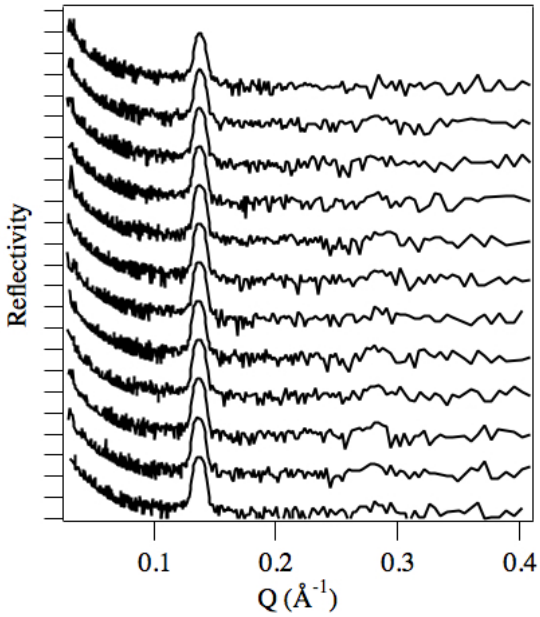

Figure 4-11. Twelve, 5 minute, patterns collected over the course of a single experiment to study the encapsulation of additive into the films. The sample pictured is DDAB:2C_{16}TAB and SPEI with 30% hydrogenated cyclohexane.

Due to the number of patterns produced from the samples, instead of showing a table of numbers, the results are shown in graphical format in Figure 4-12 and Figure 4-13. If the values of encapsulation are discounted initially and the trends studied, it is possible to see that in the majority of patterns there is significant variation over the first 20-30 minutes of the experiment. After this time in the majority of the samples the values appear to stabilise. This indicates that the films grow and form in the first 30 minutes of the experiment. Although it is important to note that these films may be thicker than the penetration depth of the neutrons therefore structural formation may still be occurring in the films, however not in the region of study.

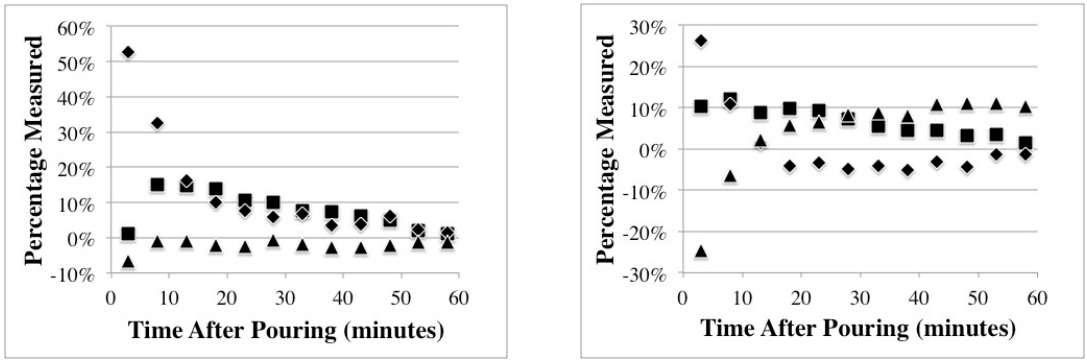

Figure 4-12. Encapsulation of additives into DDAB:20C_{16}TAB/SPEI films. Cyclohexane, left, and cyclohexanol, right, added at 20% (diamond), 30% (squares), and 40% (triangles).

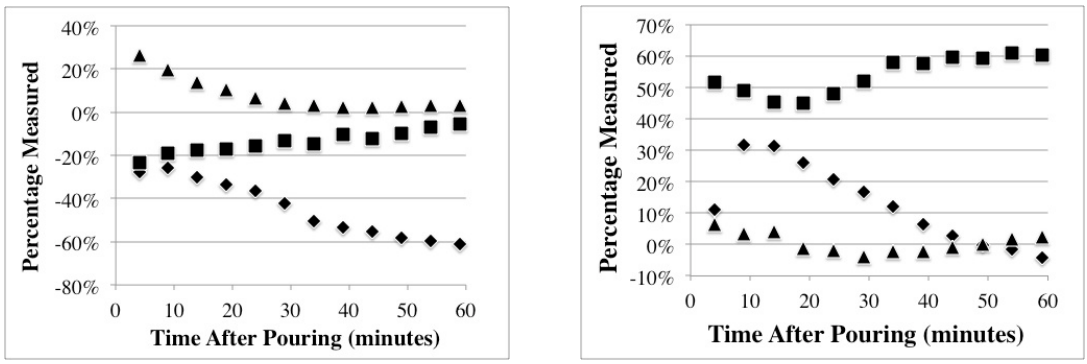

Figure 4-13. Encapsulation of additives into DDAB:2C_{16}TAB/SPEI films. Cyclohexane, left, and cyclohexanol, right, added at 20% (diamond), 30% (squares), and 40% (triangles).

Given these films appear to stabilise after 30 minutes it is then possible to study the encapsulation of additive into the films once the films have stabilised. To do this the final five points of the points of each plot in Figure 4-12 and Figure 4-13 are averaged together to give a value for encapsulation within the film and a measure of stability from the uncertainty in the value, these values are given in Table 4-7. Over these five points the trend in the plots sometimes has a positive gradient and sometimes a negative gradient. The reason for this is unclear however it is probably related to fluctuations caused by evaporation of additive from the sample, this may vary between the hydrogenated and deuterated samples as the ambient temperature and humidity were not controlled during the experiment.

	Cyclohexane					
	20%		30%		40%	
DDAB:20C_{16}TAB	3%	±3%	4%	±3%	-2%	±1%
DDAB:2C_{16}TAB	-58%	±4%	-9%	±4%	3%	±1%

	Cyclohexanol					
	20%		30%		40%	
DDAB:20C_{16}TAB	-3%	±2%	3%	±2%	10%	±2%
DDAB:2C_{16}TAB	1%	±6%	60%	±2%	0%	±3%

Table 4-7. Averaged final percentage measured in different surfactant/SPEI films. Negative encapsulation is reported from films where the deuterated peaks are more intense than the hydrogenated peaks.

These results show no resemblance to the expected amount of additive added to the samples at the start of the experiment. To confirm these results, repeats of the DDAB:2C_{16}TAB samples with 30% cyclohexane and 30% cyclohexanol were performed and the results were found to be within 5% of the values reported in Table 4-7. The physical manifestation of these results is a difference in peak intensity between the hydrogenated and deuterated samples reflectivity patterns. The more similar the peaks in the corresponding patterns are the closer the encapsulation is to zero. From this if the peak from the hydrogenated pattern is less intense than that of the deuterated pattern then the result appears as a negative encapsulation.

There are two explanations for the variation of the results in Table 4-7 and the fact that some values are positive and some are negative. The first explanation is that due to ambient conditions at the different times of the experiments the additives could have evaporated at different rates. If the deuterated additive was to fully evaporate but the hydrogenated additive did not evaporate at all then a negative value for encapsulation would be calculated. The second explanation is that the corresponding films have either different numbers of layers or different amount of roughness between the layers. As stated previously when discussing the Motofit model a difference in either the roughness or the number of layers will have a large impact on the calculated encapsulation. Both explanations probably play a role in the results in Table 4-7; the fact that the repeat samples were within 5% of the original samples, particularly for the DDAB:2C_{16}TAB sample with 30% cyclohexanol, suggests the variation in number of layers or roughness is reproducible, while the slight variation, of less than 5%, between the repeats is likely due to variation caused by the ambient conditions.

4.1.2.3 CTEAB and DDAB films with cyclohexane and cyclohexanol

As stated previously the CTEAB and DDAB films with additive encapsulated were studied separately from the DDAB:C_{16}TAB mixed surfactant systems. The CTEAB and DDAB experiments were performed on the SURF instrument at ISIS, instead of on FIGARO at the ILL. This means that the time resolution for these experiments was much lower than for the mixed surfactant experiments, the time resolution on SURF is 15 minutes while it is 5 minutes on FIGARO.

In the mixed surfactant films and in the DDAB films the structure seen in the reflectivity patterns has been purely from one or two peaks that indicate a repeating layered structure. The CTEAB structure however has been seen to be more complicated. As shown in Figure 3-4 as the film grows a triplet of peaks is visible that grows and then shrinks over the course of the experiment until a single peak is left. When comparing films with hydrogenated and deuterated additive it is possible to see from the relative intensities of the peaks in the triplet that the patterns do not represent the same stages of film growth. This means that determining a value for encapsulation is not possible at these stages. Where determination of a value for encapsulation of additive into the film is possible the results are shown in Table 4-8.

Run Number	Cyclohexane			Cyclohexanol		
	20%	30%	40%	20%	30%	40%
1	-	16%	15%	-1%	-	-
2	-	-	7%	-	-	-2%
3	-	-	4%	-	-	-
4	-	32%	0%	-	-	-
5	17%	54%	17%	-13%	11%	-

Table 4-8. Encapsulation into CTEAB/SPEI films. Blank spaces show where data could not be collected as described in the text due to different structures in the corresponding patterns. Runs lasted 15 minutes each with the first run starting between 6 and 9 minutes after pouring the solution.

As the DDAB patterns only contain one or two peaks, indicating a multilayer structured film, there were no problems similar to those seen with the CTEAB films. An example of the patterns produced during a single experiment is shown in Figure 4-14 and the results are shown in Table 4-9.

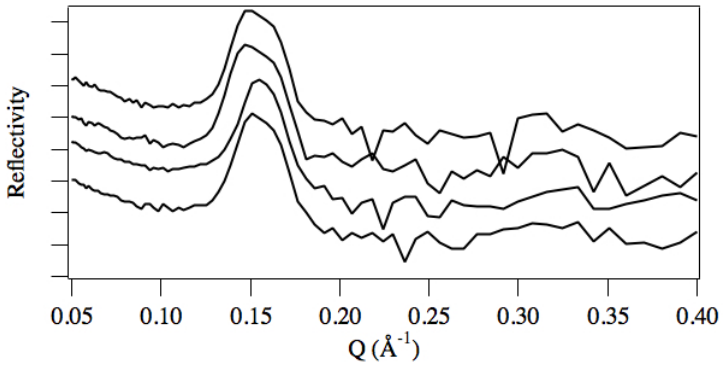

Figure 4-14. Four 15-minute patterns collected over the course of a single experiment to study the encapsulation of additive into the films. The sample pictured is DDAB and SPEI with 30% hydrogenated cyclohexanol.

Run Number	Cyclohexane			Cyclohexanol		
	20%	30%	40%	20%	30%	40%
1	-2%	0%	5%	39%	3%	12%
2	20%	-5%	5%	42%	5%	8%
3	1%		2%	36%	6%	15%
4	-19%	11%	3%	34%	8%	16%

Table 4-9. Encapsulation in DDAB/SPEI films. Runs lasted 15 minutes each with the first run starting between 6 and 9 minutes after pouring the solution.

Both the CTEAB results in Table 4-8 and the DDAB results in Table 4-9 show similar features to the DDAB:C_{16}TAB mixed surfactant systems. In all cases there is structural change occurring in the early part of the experiment, in the CTEAB samples this appears to occur over a period of one hour. With the lower time resolution it is hard to say exactly how long the DDAB films form however in all the cyclohexanol samples the final two points are within 2% and therefore are probably stable. This agrees with the mixed surfactant samples suggesting the films form over the first 30 minutes of the experiment.

As with the mixed surfactant films the actual values calculated for encapsulation bear little resemblance to the expected encapsulation values. Again this is most likely due to the difference in number of layers in the film and the roughness between the films. This is more likely due to the CTEAB sample, which undergoes a re-arrangement during the film formation process, which could lead to variation that is not accounted for in the analysis presented here. Unfortunately there was no time to perform repeats therefore it is unclear whether the results for these films are as reproducible as the results in for the mixed surfactant films.

4.1.3 Structure of surfactant films with encapsulated additives.

As well as performing reflectivity to study the encapsulation of additives into the films, x-ray reflectivity and GIXD were also used to study the effect of the additives on the film structure. Due to limited time to perform this experiment the DDAB:20C_{16}TAB films were not studied as they had previously been seen to be very similar to the DDAB:2C_{16}TAB films. To study whether the additive was able to assist ordering of the mesostructure in the films, and whether this was enough to form ordered structures when LPEI was used as the polymer, all three surfactant solutions were studied with both SPEI and LPEI. To get a more detailed understanding of the effect of different amounts of additive the CTEAB films with both LPEI and SPEI and the DDAB films with SPEI were studied with both 20% and 30% additive, the DDAB:2C_{16}TAB films however were just studied with 30% additive. As discussed above the additives used were cyclohexane and cyclohexanol.

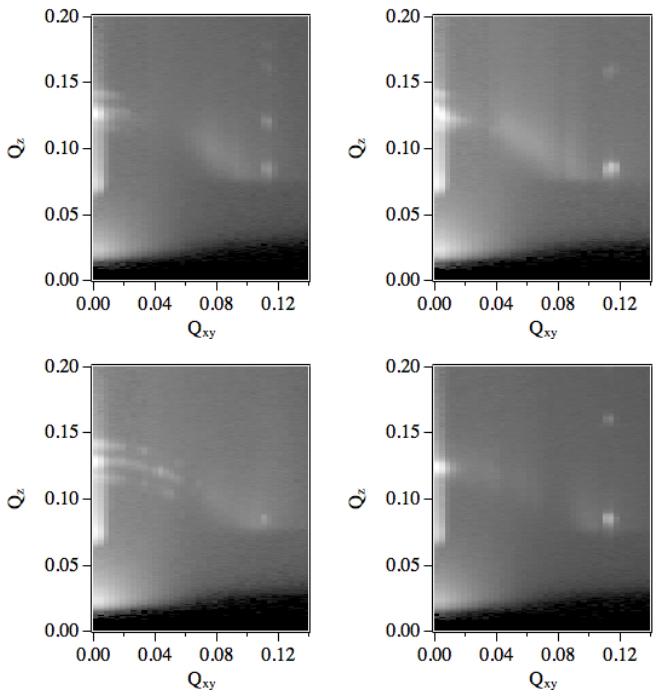

Figure 4-15. CTEAB/SPEI films with 20% (left) and 30% (right) cyclohexane (top) and cyclohexanol (bottom).

As expected and as seen previously[66] the use of LPEI in the films produced structures that showed just one peak in the reflectivity and one ring in the GIXD patterns. This suggests that micelles in the LPEI films are not able to rearrange into an ordered phase at the interface and the addition of additive has no affect on this. In the CTEAB films, where both 20% and 30% additive were used, no difference was seen between the two different amounts of additive.

Variation was seen however between the different additives and different amount of additives in the CTEAB films using SPEI as the polymer. The GIXD patterns of these films are shown in Figure 4-15. The patterns show that the most similar structures are from 30% cyclohexane and 30% cyclohexanol. Although both patterns resemble a 2D hexagonal pattern the positions of the spots indicate that this is not the case, therefore the pattern must be from a cubic structure. Unfortunately the limited number of spots visible in the patterns means that it is impossible to determine which cubic pattern. The triplet of peaks seen in the 20% cyclohexane and cyclohexanol patterns at Q_{xy}=0 are in a similar position to those seen in the CTEAB/SPEI film with no additive. However these peaks do not show the same spacing as the previous film suggesting that although they are reflections from a cubic structure it is either a different cubic structure or different reflections from the same cubic structure due to a change in the orientation of the cubic phase relative to the interface. Using the same $Pn\bar{3}m$ structure, but changing the reflections, would allow these reflections to line up with the 220, 310 and 222 reflections with a unit cell size of 155Å instead of the 175Å unit cell seen in the films with no additive. This difference is surprising as it is expected that if additive is present in the micelles then they are more likely to swell rather than shrink. However without definitive determination of structure it is impossible to properly compare the two films except to say that the presence of additive has some effect that leads to different reflections being visible in the GIXD patterns.

The DDAB:2C_{16}TAB films have not been shown here however they are exactly the same as the films seen in the absence of additive. Multiple spots are seen at Q_{xy}=0 and at Q_{xy}=0.115 which can be indexed to a 2D hexagonal pattern. Even the Q position of the first peak is in exactly the same position suggesting the additive does not alter the film or micelle structure, confirming what has been seen previously.[68]

The DDAB SPEI films with hydrophobes are also considerably different than the films in the absence of additive. With no additive present both the GIXD and reflectivity patterns showed two broad peaks which were indexed to a highly polydisperse lamellar. The GIXD patterns of the DDAB films with additive show that instead of a single broad peak there are two peaks with similar Q positions. This is best seen in the reflectivity curves, an example of which is shown in Figure 4-16. In this pattern it is clear to see that in both positions, where previously only one peak was seen, there are two maxima with a slight minima in between. This suggests that there are two lamellar phases present, probably as separate islands, on the surface of the solution with different d spacing. It is possible that this is also true in the DDAB/SPEI films with no additive as the peaks seen in Figure 4-16 would fit within the peaks seen in the previous reflectivity pattern. Given that no other peaks are

present in either the GIXD or the reflectivity curves, it is hard to say whether the peaks are from lamellar multilayer systems with different d-spacings or from a cubic structure. This structure is the same for all the DDAB/SPEI films with additive and the peak positions do not change between them. One thing that can be said about these films is that the addition of additive helps the ordering of the film since the observed peaks are sharper than without the additive, although it is unclear how this happens or what the resulting structure is.

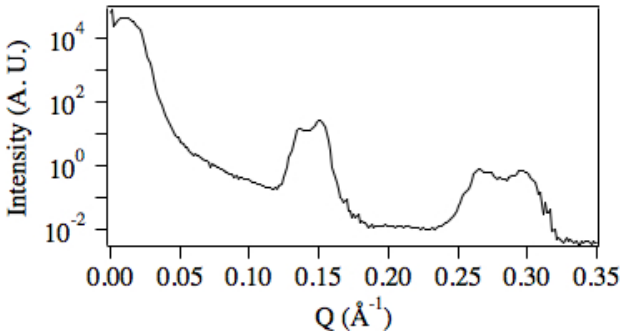

Figure 4-16. X-ray reflectivity pattern from a DDAB/SPEI film with 20% cyclohexane.

4.2 Encapsulation and Release of Nile Red

As mentioned previously, as well as studying the encapsulation of cyclohexane and cyclohexanol, as had been done previously,[68] in this study it was decided to also use the dye Nile red to study encapsulation. Nile red is commonly used in systems with amphiphilic species, such as surfactants and lipids.[121, 125] Usually it is used because it is very sensitive to the hydrophobic environment it is in, allowing differentiation between amphiphilic species forming differently hydrated locations within a single solution.[126, 127] In this study the main role of Nile red is as a fluorescent marker. Due to its fluorescent properties and hydrophobic nature it is a perfect molecule for encapsulation, as it should partition into the micelle core, and then during subsequent release studies, the release can be monitored by fluorescence spectroscopy. It is also similar in size to steroids, which are a common class of drug molecules therefore can simulate the encapsulation and release potential of these films as a drug delivery device for small organic molecules.

4.2.1 Encapsulation of Nile Red in surfactant solutions

The encapsulation of Nile red is slightly harder to study than cyclohexane or cyclohexanol because it is a solid instead of a liquid and also insoluble in water. Due to this the first step is to dissolve the Nile red in a less polar solvent so it can be

added to the surfactant solution. Adding solid Nile red to the surfactant solution was tested but very little encapsulation occurred, as being determined by a change in colour of the solution. Therefore the solvent chosen to dissolve the Nile red was acetone. Acetone is very suited to this task because Nile red is highly soluble in it. Furthermore, acetone is very volatile meaning if the sample is left open to the atmosphere the acetone should evaporate out of the solution. Finally, acetone is miscible in water therefore should not be encapsulated into the micelle core with the Nile red.

Due to time constraints on the SANS experiments the Nile red samples were run at two separate times. During the first experiment the CTEAB and DDAB samples were measured both in the presence and absence of polymer. A stock Nile red solution was prepared to give each solution 0.1M Nile red, however the intense dark colour of the Nile red solution hid the fact that the solid had not completely dissolved. On the addition of the stock solution to the surfactant solutions a small amount of solid Nile red immediately settled to the bottom of the sample. This means the exact amount of Nile red in each sample is unknown however the samples were strongly coloured with different colours suggesting the Nile red was encapsulated within the various surfactant mesostructures. This difference in colour has previously been reported as a way to study structural changes in aqueous surfactant solutions.[126] Nile red is known to sit in the head group region of surfactant micelles and hydrogen bond with the water molecules. The change in the micelle structure alters the way the Nile red is able to pack in the micelles and its ability to interact with the water in the head group region, therefore altering the wavelength and intensity of the absorbance.

As deuterated Nile red was not available, the study of Nile red encapsulation was performed with deuterated surfactants. The solutions were prepared, as for the cyclohexane and cyclohexanol samples with the surfactant being mixed with the polymer and the Nile red being added afterwards, at a 0.1M final concentration. However when adding the Nile red instead of immediately sealing the sample vials, the samples were gently agitated to allow mixing then the lids were replaced. No further steps were taken to seal the vials, therefore allowing some of the acetone to evaporate. Before the measurements were taken, the samples were agitated every few hours to make sure they were well mixed and homogeneous with no precipitate. The samples were measured in batches, all being held in the sample rack at 28°C.

During the course of the batch of experiments the Nile red samples phase separated. This phase separation is shown in Figure 4-17 for samples of deuterated DDAB with Nile red in the absence and presence of PEI, as described by the caption. These

samples were part of a batch of 6 samples that ran for four and a half hours. As can be seen, particularly in the sample with LPEI, there is a strong band of dark colour at the top of the solution. A darker band is also slightly visible in the SPEI sample but hardly seen in the sample without polymer. If the phase separation occurred before the measurement was taken then this would lead to a large deficiency in the amount of measured Nile red in solution. This phase separation is of interest because it appears to be an area of higher concentration which may be the precursor to film formation. The reason film formation would not occur in the vial is because the vial is sealed therefore there is no evaporation.

If this phase separation is an indicator of film formation then it may also be occurring the in the samples containing cyclohexane and cyclohexanol, discussed above. It is hard to tell if this separation always occurs in these sample, as in most cases the samples are colourless therefore this behaviour cannot be seen. However if this phase separation is occurring then it may explain why there is such a low concentration of cyclohexane and cyclohexanol detected in the SANS measurements. A potential experiment to run would be to separate the surface layer of a surfactant/LPEI/cyclohexane sample from the bulk and then analyse both samples using GC to determine if there is more cyclohexane at the interface than in the bulk solution. Given the very small amount of solution in the phase rich region, this experiment would be very hard to perform. The phase separation may also give clues as to why film formation occurs at the solution surface, since it provides a more concentrated phase at the interface, which can more easily form the solid film after evaporation.

Although this figure only shows the phase separation in the deuterated DDAB samples the same separation was reported for the hydrogenated sample and both the hydrogenated and the deuterated CTEAB samples but was not observed for DDAB:C_{16}TAB mixtures.

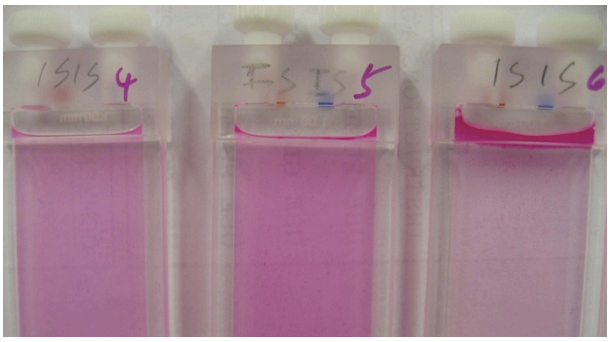

Figure 4-17. Phase separation in deuterated DDAB samples with Nile red and, from left to right, no polymer, SPEI, and LPEI. The phase separation occurred over four and a half hours after transferring the sample as homogeneous solutions from vials to the measurement cells.

The encapsulation results for the solutions of CTEAB and DDAB with 0.1M Nile Red added to the solution are shown in Table 4-10. As seen with the addition of cyclohexane and cyclohexanol, the addition of an additive has very little effect on the structure of the micelle. It is worth noting that the sample of DDAB with no polymer shows a negative value for encapsulation of Nile Red. The negative value is created because the model fits a negative percentage caused by the deuterated pattern being more intense than the hydrogenated pattern. As the Nile red SLD is significantly different from the hydrogenated tails of the surfactant, $1.81 \times 10^{-6} Å^{-2}$ instead of $-0.35 \times 10^{-6} Å^{-2}$, a mismatch in the amounts of Nile red in the hydrogenated and deuterated samples may cause this effect. The CTEAB solution with LPEI has been omitted from this table because the hydrogenated CTEAB and the deuterated CTEAB gave very different SANS patterns indicating different structures. Given the other experiments with deuterated CTEAB did not show the same differences this is probably an isolated anomaly.

		R(a) (Å)	R(b) (Å)	Concentration (mM)	
CTEAB	No PEI	30	22	3.7	
	SPEI	29	21	4.9	
		Bilayer Thickness (Å)	Number of Layers	Layer Spacing	Concentration (mM)
DDAB	No PEI	26	N/A	N/A	-0.3
	SPEI	20	1.57	160	11.1
	LPEI	20	1.27	262	13.0

Table 4-10. Encapsulation of Nile red in CTEAB and DDAB films in the presence and absence of polymer. Errors in dimensions are ±2Å. Error in number of layers is 0.05. Error in concentrations is ±5% of the reported value.

As stated previously due to time constraints the DDAB and CTEAB experiments were performed at different times than the DDAB:$2C_{16}$TAB and DDAB:$20C_{16}$TAB

experiments. Interestingly in these samples there was no phase separation reported for the solutions. It is unclear why this is, however it could suggest that these solutions are less surface active than the DDAB or CTEAB sample.

Two attempts have been made to determine the concentration of Nile red in the solutions of DDAB:2C_{16}TAB and DDAB:20C_{16}TAB. In the first instance no deuterated surfactant was available, therefore the second contrast was a solution contrast of 70% D_2O and 30% H_2O. Although two separate SANS patterns are produced the amount of Nile red in the micelles is so small that the error in determining the SLD of the total micelle is quite large. On top of this, the error in measuring out a mixture of H_2O and D_2O for the solvent adds another discrepancy into possible error. Due to this the value obtained when fitting produced results ranging from -2mM to 6mM with no obvious trend or reason.

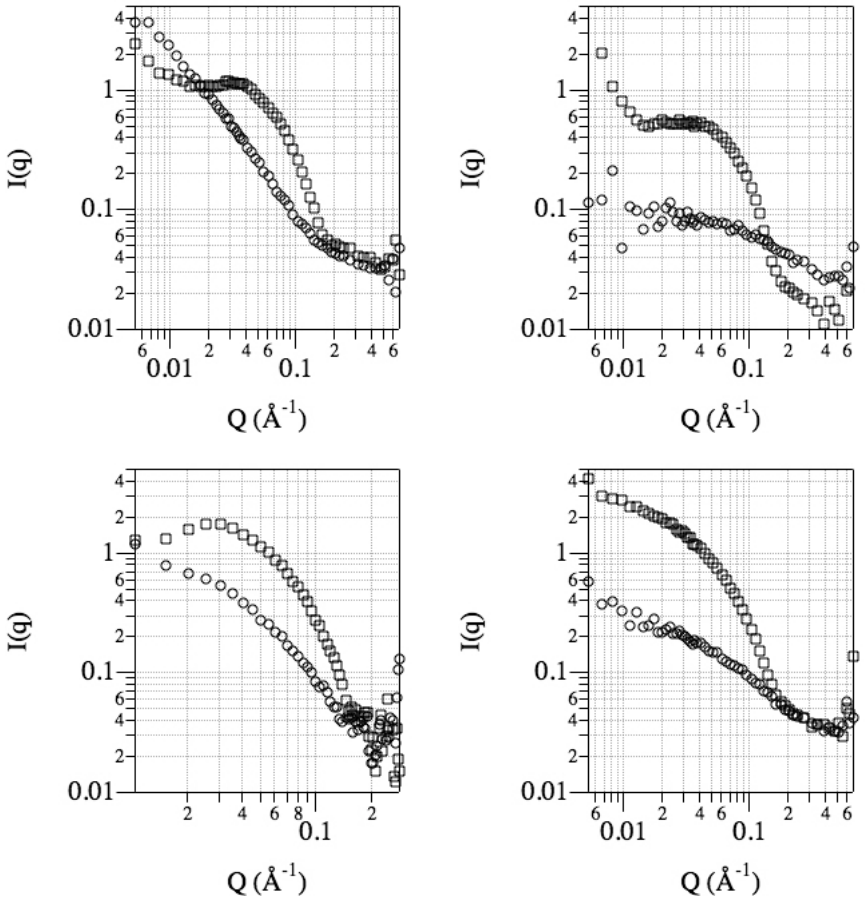

Figure 4-18. SANS patterns of DDAB:20C_{16}TAB (top) and DDAB:2C_{16}TAB (bottom) with either LPEI (left) or SPEI (right). Squares indicate fully hydrogenated samples in D_2O, circles indicate sample with deuterated C_{16}TAB. Error bars have been omitted because they are smaller than the markers.

As this had been unsuccessful the experiment was repeated with the use of deuterated C_{16}TAB to provide a second contrast, however this was also unsuccessful.

In these samples the fitting of the hydrogenated sample was significantly different from the fitting of the deuterated sample. The SANS patterns from these samples are shown in Figure 4-18 and the fitting results are summarised in Table 4-11.

Hydrogenated Sample			
		R(a) (Å)	R(b) (Å)
DDAB:20C_{16}TAB	SPEI	97	19
	LPEI	48	22
DDAB:2C_{16}TAB	SPEI	33	21
	LPEI	43	20
Deuterated Sample			
DDAB:20C_{16}TAB	SPEI	26	11
	LPEI	10427	23
DDAB:2C_{16}TAB	SPEI	63	9
	LPEI	107	20

Table 4-11. Fitting results of separate hydrogenated and deuterated samples containing Nile red. Errors in micelle dimensions are as ±2Å except when the dimensions are greater than 50Å when the error is 10% of the reported.

There are two explanations for these results. The first is the possibility of intra-micellar phase separation of surfactants, similar to that reported by Zemb et al.[128] In this case the DDAB and C_{16}TAB would be mixed throughout the main part of the surfactant micelle, however at the ends where the curvature is high there will be a predominantly C_{16}TAB region. When both surfactants are hydrogenated the structure of the micelle can be seen as an ellipse, however when deuterated C_{16}TAB is used the scattering will come from the DDAB only which reside in the areas of least curvature, therefore the scattering appears to be more elongated. This is supported by the relative elongation between the hydrogenated samples and the deuterated samples where with more DDAB the areas of high curvature will be more likely to contain DDAB. The other explanation for these results is that there is an impurity in the deuterated C_{16}TAB used for these experiments. As the C_{16}TAB is purchased the purity is unknown. It should be possible to purify it prior to the experiment where it will be used however it is often delivered very close to the date of the experiment meaning there is not enough time to test it.

Regardless of the difficulties that have been encountered with the DDAB:2C_{16}TAB and DDAB:20C_{16}TAB solutions it has been clear throughout this experiment that encapsulation of Nile red is possible in these surfactant solutions. This can been seen clearly by eye due to their very strong colour. In almost all cases this encapsulation can be detected by SANS and the calculated values of the encapsulation are in the same order of magnitude as the solutions ability to encapsulate cyclohexane and

cyclohexanol. As with the solutions with cyclohexane and cyclohexanol once the ability of the solutions to encapsulate the Nile red has been studied then it is important to confirm that this Nile red can be incorporated into the polymer/surfactant films.

Possibly the most important finding is the phase separation in small quantities from the solution to the interface during the course of a series of SANS runs. This is shown very clearly in Figure 4-17 and is important because if this phenomenon is occurring in the cyclohexane and cyclohexanol samples, where there is no strong colour to make this separation obvious, then it makes sense of why so little of any type of additive is measured as being encapsulated.

4.2.2 Encapsulation of Nile red in surfactant/polymer films

As with the SANS studies, deuterated Nile red was unavailable therefore deuterated surfactant was used for studies of encapsulation using neutron reflectivity. For the single surfactant systems the deuterated surfactant was used and for the mixed surfactant systems deuterated C_{16}TAB was used. Both SPEI and LPEI samples were prepared however the LPEI sample did not show enough ordering so no analysis was performed. As with the surfactant films with cyclohexane and cyclohexanol a model was used to determine the correction factor for determining the real amount of Nile red in the films.

The CTEAB and DDAB films were both measured at the same time as the respective cyclohexane and cyclohexanol films and as such the measurements were performed on the SURF instrument. As with the previous results the CTEAB was affected by a highly dynamic structure meaning only one plot could be used to determine a percentage and this gave 0% Nile red encapsulated.

The DDAB, DDAB:20C_{16}TAB, and the DDAB:2C_{16}TAB films however were not affected by this dynamic structure as much as the CTEAB, therefore percentages of Nile red encapsulated into these films could be determined. The results are shown in Table 4-12. In these results it is important to note that because the DDAB film was recorded on SURF it has 15-minute time resolution while the surfactant mixtures were performed on FIGARO giving 5-minute time resolution.

Run Time (minutes)	DDAB:20C_{16}TAB	DDAB:2C_{16}TAB	DDAB
5	20%	1%	
10	20%	-4%	
15	19%	-1%	59%
20	20%	-2%	
25	20%	-3%	
30	22%	-8%	63%
35	22%	-7%	
40	20%	-5%	
45	21%	-4%	66%
50	21%	-3%	
55	21%	-2%	
60			58%

Table 4-12. Encapsulation of Nile red into surfactant/SPEI films

Again the trend of the results show that however much Nile red is in the film it is a constant amount over the course of the experiment. In these experiments the expected concentration of Nile red is 1mM, which would give roughly a 10% measured percentage. The percentages measured here give a 2.1mM Nile red concentration for DDAB:20C_{16}TAB and a 12.9mM concentration for the DDAB. These concentrations are based on an even distribution of Nile red in all surfactant micelles in a 0.01M surfactant solution. The DDAB:2C_{16}TAB is not calculated because the percentage values are below 0%. These values for concentration are unexpectedly high because the initial solutions contained only 1mM of Nile red. This suggests the concentration is artificially high at the air/solution interface, which would explain the low values seen in the SANS results and confirm what was seen in Figure 4-17. However as stated in the samples with cyclohexane and cyclohexanol, the observed variation in Nile Red concentration may actually be a result of variation in film formation leading to the hydrogenated and deuterated films having either different number of layers or different roughness between layers.

4.2.3 Release of Nile Red from Surfactant/Polymer Films

The release studies were performed with Nile red as the additive. As with the previous film studies, the concentration of Nile red was 1mM. To enable the films to be removed from the surface of the surfactant solution a cross linker is used to strengthen the films making them strong enough to support their own weight. To maximise the amount of film being removed from the surface, the polymer used was LPEI. The cross linker used is ethylene glycol diglycidyl ether (EGDGE). To determine if the addition of cross linker had any effect on the release of Nile red three concentrations of cross linker were tested, 0.01M, 0.05M and 0.1M. Although

films containing EGDGE were not studied in this report they have previously been studied and, although some changes were seen, these were considered not significant.[67]

After films had been grown they were removed from the solution and allowed to dry before being placed in 20ml of water. The weights of the dried films are given in Table 4-13. The concentration of Nile red released was determined by removing a 1mL aliquot from a sample at specific time intervals, with the same volume of pure water being added so that the total volume was constant. Chloroform was added to the aliquot to dissolve the Nile red from the aqueous solution then the chloroform solution could be studied with fluorescence spectroscopy. Chloroform was used as the solvent as Nile red has a stronger emission spectra in chloroform than a number of other common solvents.[105]

EGDGE Concentration (M)	CTEAB	DDAB:20C_{16}TAB	DDAB:2C_{16}TAB	DDAB
0.01	0.0132	0.0126	0.016	0.0259
0.05	0.0146	0.0171	0.0214	0.0273
0.1	0.0187	0.0189	0.024	a

Table 4-13. Dry mass, in grams, of films formed from different surfactants with different amounts of cross-linker. (a) Due to damage to the film when removing it from the solution no data was able to be collected. Uncertainty in these values is ±0.0005g.

Initially a calibration curve was created from solutions of known concentration of Nile red in chloroform. The emission spectra of the samples were then measured and the intensity of the peak was compared to the calibration curve to determine the concentration of Nile red in the solution. Although the samples were of different colour, by dissolving the samples in chloroform the wavelength of maximum emission was the same in all samples. The concentration of Nile red was then converted to a mass and normalised to the mass of the dried film. The release profiles for the different films are shown in Figure 4-19.

The first thing to note with this data is the similarity in the majority of the patterns showing an initial fast release over the first 200 to 300 minutes, which then levels off to a plateau after around 300-400 minutes. These timings appear to vary randomly across all samples suggesting that rate of release is not dependant on the structure of the films, however this is possibly in part due to the limited time resolution of these studies. Once the release has reached the plateau, the amount released is relatively stable over the course of 5 days. Also apparent from comparison of all the data sets is that the more elongated the structure the more Nile red is released. Looking at the final three points of all the curves shows that the lowest releasing film is that of CTEAB while the highest is either DDAB:2C_{16}TAB or DDAB. The final important

comparison of all the plots is the fact that the increase in cross-linker concentration limits the release of Nile red from the film.

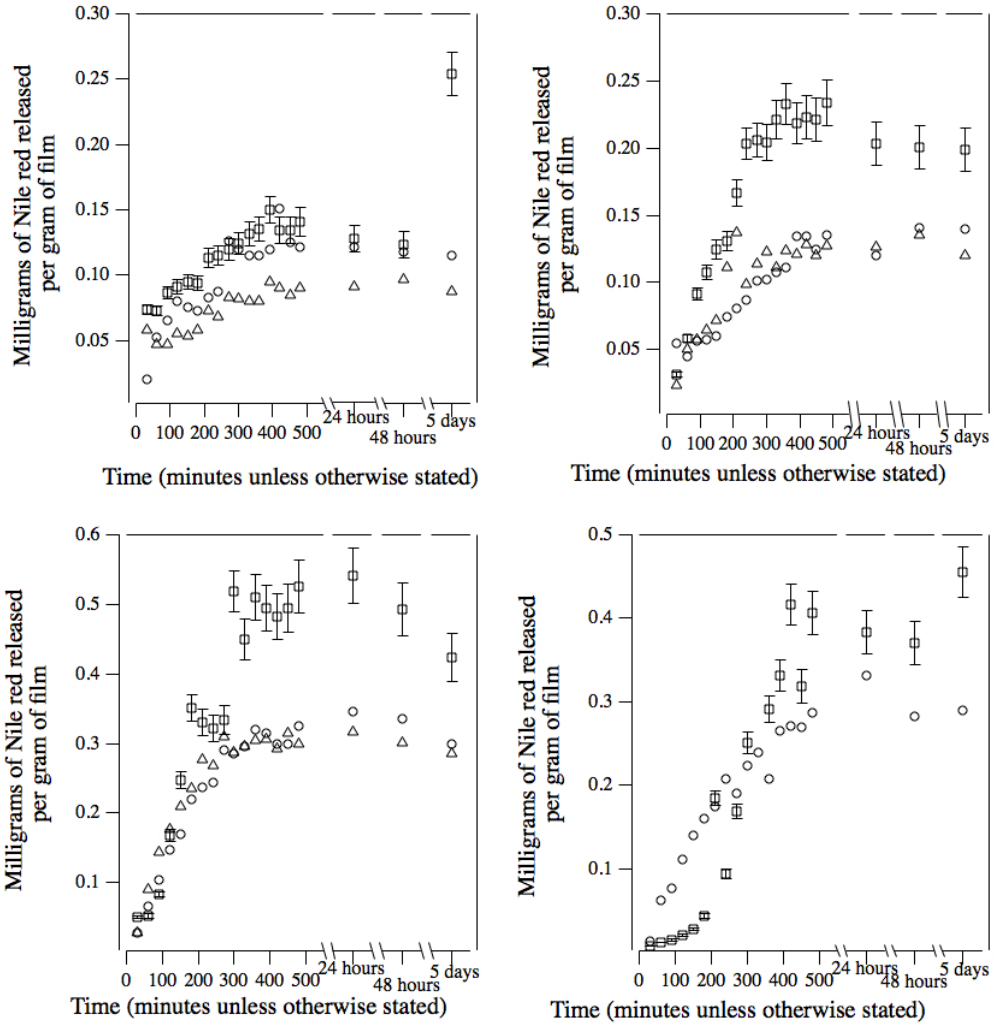

Figure 4-19. Release profiles of Nile red from different surfactant/LPEI films with varying amounts of cross-linker, EGDGE, added. Plots are, top, CTEAB (left) and DDAB:20C_{16}TAB (right), and bottom, DDAB:2C_{16}TAB (left) and DDAB (right). Squares indicate 0.01M cross linker, circles indicate 0.05M cross linker and triangle indicate 0.1M cross linker. Error bars are only shown on the 0.01M samples to improve the clarity of the plots.

Of the different data sets, only one stands out as showing a different release pattern and this is the sample for DDAB with 0.01M Nile red. It shows a very clear different trend to the rest of the sample including the sample of DDAB with 0.05M Nile red. As these two samples are different it cannot be confirmed that this is due to the surfactant structure, therefore without a repeat of these samples it is unclear what is causing this.

After the 5-day aliquot was removed from the sample chloroform was added to the solution with the film to dissolve all the Nile red left in solution and in the film. This

provides information about the total encapsulation of Nile red into the film. Figure 4-20 shows these results along with the grams of Nile red released from the film, as determined by an average between 360 minutes and 480 minutes, and the percentage of Nile red released from the film into solution.

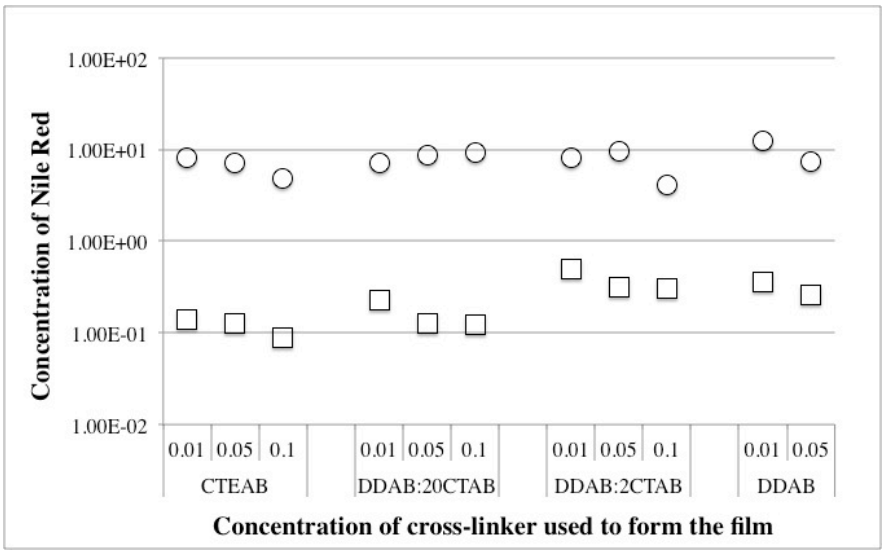

Figure 4-20. Milligrams of Nile Red released from the film compared to the total amount in the film. Circles indicate the total milligrams of Nile Red in the film. Squares indicate the amount of Nile red released from the films as determined by an average between 360 and 480 minutes. Uncertainties are the same size as the markers.

The total amount of Nile red per gram of film varies with the concentration of cross-linker, with an increase in cross-linker leading to a decrease in the amount of Nile red encapsulated. There also appears to be a slight correlation with the amount of Nile Red released from the films as well with all films showing less release with more cross-linker than with the least cross-linker. The total amount of Nile red released from the films however is very small. The DDAB:2C_{16}TAB with 0.1M EGDGE has the highest release in comparison to the total amount encapsulated yet this leads to only 7% of the total Nile red in the film being released.

A summary of this data shows that the CTEAB encapsulates the lowest amount of Nile red and also releases the lowest. The next lowest is the DDAB:20C_{16}TAB, which encapsulates slightly more than the CTEAB but releases roughly the same amount in percentage terms. The DDAB:2C_{16}TAB encapsulates slightly more Nile red than the DDAB:20C_{16}TAB however on average it releases three times as much in percentage terms. The DDAB films encapsulate the most Nile red per gram of film, on average, however they release the same amount of Nile red as the DDAB:2C_{16}TAB in real terms, meaning that in percentage terms they do not release as much Nile red. The encapsulation results can be explained by an increase in size of the micelles and therefore an increase in hydrophobic area for the Nile red to be

encapsulated into. Given the large size of the Nile red molecule it is unsurprising that it needs a large micelle to be able to be encapsulated. The release results are also probably due to the structure with the release being related to effective surface area of the film. If the solvent is in contact with a long rod like micelle at the surface of the film and the rod is buried in the film then the rod can act as a conduit for the release of the Nile red in the centre of the film. If the micelles are more spherical then they are less able to penetrate into the film structure.

It is possible to use the total mass of Nile red in these films to calculate the concentration assuming all the Nile red in the starting solution was incorporated into the film; this data is shown in Table 4-14. Even the highest concentration of Nile red in a film, DDAB with 0.01M EGDGE, at 0.05mM is much lower than the 12.9mM calculated using neutron reflectivity. It is possible that this is caused by the addition of the cross linker to the system, however this dramatic an effect is unlikely. Therefore it is more likely that the use of neutron reflectometry for determining the concentration of Nile red in the films is a flawed technique. A potential alternative may be the use of fluorescence in conjunction with BAM to measure the how the fluorescence of the Nile red in the film changes as a function of film thickness and therefore Nile red concentration.[129]

Concentration of EGDGE (mM)	CTEAB	DDAB:20C16TAB	DDAB:2C16TAB	DDAB
0.01	0.0168	0.0139	0.0203	0.0500
0.05	0.0164	0.0231	0.0317	0.0319
0.1	0.0140	0.0274	0.0152	

Table 4-14. Concentration (mM) of Nile red in the film.

4.3 Conclusions and discussion

In chapter 3 it was shown that it was possible to control the structure of the films by rational selection of surfactants, therefore the next step was to build on this. One area that had been studied previously was the effect of adding sparingly soluble species to the micelles.[68] Although this study was attempting to control the film structure by swelling the micelles it also showed that it was possible to encapsulate these species within the film structure. This study then led to the possibility of using these films as a storage and release device.

Therefore the general aim of this study was to determine whether it is possible to encapsulate sparingly soluble species within the surfactant micelles. Then building on this if the additives were in the surfactant micelles could these micelles be

incorporated into the films, creating films with additive encapsulated. Finally taking this study to the next step, whether the additive could be released from the films. Over arching this study, and relating it to the work in chapter 3, was the comparison within the results to see whether the structure of the surfactant micelles has any effect.

With the results discussed in this chapter, it can be concluded that cyclohexane and cyclohexanol can be encapsulated into surfactant micelles, although in relatively small quantities. It is then possible to incorporate these micelles into films to give additive loaded films, however the loading of the films is hard to determine using neutron reflectometry. As well as studying encapsulation with cyclohexane and cyclohexanol in this study the fluorescent dye Nile red was also used. From the Nile red results it can be concluded that, as with the cyclohexane and cyclohexanol results, it is possible to encapsulate Nile red into the surfactant micelles and into the films. This is easy to see with Nile red due to its very strong red colouring. The total amount of Nile red encapsulated in the film was then studied using fluorescence spectroscopy after dissolving the film up in chloroform. This technique was also used to show that it is possible to release the Nile red over time from the film into an aqueous environment.

The starting point for this study was to build upon the previous work done by O'Driscoll et al.[68] However where O'Driscoll et al concentrated on the swelling of the micelles by the different species, here it was decided to expand that study to concentrate more on the encapsulation of the species, with the main driving force being the potential of these films to encapsulate and release different species. To keep continuity and the ability to compare with the previously studied systems, cyclohexane and cyclohexanol continued to be used as additives. A completely new set of experiments was also performed with the dye Nile red, which is commonly used in amphiphilic systems and is highly fluorescent so is a useful substance to use to study release from the systems.[105, 125, 126]

After studying the surfactant solutions in the presence and absence of polymer, in solutions and as films, as described in chapter 3, the next step was to use these surfactant systems to study the encapsulation and release of the additives. For clarity the research was spit into two sections, first the cyclohexane and cyclohexanol samples and second the Nile red samples. Throughout these experiments, due to time constraint of having so many samples to be run on neutron and x-ray instruments, the emphasis has been placed on the solutions with no polymer and with SPEI while the films have concentrated on SPEI as the polymer. The LPEI samples are still of interest due to their greater thickness than the SPEI films, however the film structure

was shown in chapter 3 and previously by O'Driscoll et al[66] to be less well ordered and it is the highly ordered nature of these films that mark them apart from other thin films.[7, 38]

As continuity with previously reported results was important, the set up of the experiments was very similar to O'Driscoll's work.[68] Due to this the additives were added to create a theoretical loading of the micelles as a percentage of the methylene groups in the core belonging to the additive and to the surfactant. A benefit of this was that the fitting of the actual percentage in the samples was very simple using SANS and varying the SLD of the additive by using hydrogenated and deuterated additive.

As had been seen by O'Driscoll in the previous work[68], the encapsulation of cyclohexane and cyclohexanol to the solutions did not appear to change the shape of the micelles, except in the case of DDAB:$2C_{16}$TAB. However this was only in the surfactant solution in the absence of polymer as the solution with polymer was very similar to the solution results when no additive was encapsulated. Also agreeing with the previous work the amount of additive actually measured in the micelles was much lower than had been expected. However the quantities are in line with other reported loadings in micellar systems which are between 0 and 25%.[62]

This study then moved on to looking at the encapsulation in the films. The data was collected without any problems however the analysis of the data proved to be very difficult. The reflectivity analysis program, Motofit,[93] was used to simulate the expected reflectivity patterns from a range of films while varying different parameters. From these simulations it was found that as long as the hydrogenated and deuterated films were the same then it was possible to calculate a value for the percentage of additive in the film. However in the real systems it became clear that the films did not have exactly the same composition and as therefore the results appeared to be scattered with very little trend. Fortunately some experiments were performed on the FIGARO instrument at the ILL, which allows a much better time resolution, 5-minutes instead of 15. These FIGARO data also showed apparently random percentages, however these were stable within each individual experiment. Although these results did not give a clear amount of additive in the solution the comparison of the hydrogenated and deuterated films appeared to give an insight into the rate of film formation that had previously not been seen. This variation showed that although there was structure at the interface from the beginning of the experiment it wasn't until between 20 and 30 minutes that this structure stopped developing.

As well as studying the encapsulation of the additives in the films, the structure of the films was also studied with quite vaired results. The DDAB:2C_{16}TAB film did not appear to change at all. As this structure has always been similar to the DDAB:20C_{16}TAB film structure and, although this sample was not studied, it is likely that similar patterns would have been measured. The CTEAB film on the other hand showed a variation in the peaks seen in off-specular region of the GIXD pattern. These peaks do not conclusively indicate a structure however it is possible that the peaks are from different reflections in a very similar structure to that seen in the absence of additive. The DDAB sample is the most interesting though. In the absence of additive the pattern shows two broad rings that can be indexed to a polydisperse lamellar. In the presence of additive however the structure appears to have split the two lamellar peaks to four peaks, which can be indexed to two separate lamellar phases. This is interesting because the peaks are almost close enough together to fit within a single peak. This means that it is possible that the structure seen in the absence of additive has the same four peaks but not well defined enough to be separate at the resolution used in that experiment.

As stated earlier the Nile red results were kept separate for clarity. As Nile red is a more complex molecule than cyclohexane and cyclohexanol it is not available in deuterated form therefore deuterated surfactants were used instead. Also because it is a more complex molecule instead of adding it to the solution as a percentage, as had been done with the other additives, it was added at a particular concentration instead. Initially the concentration used was 0.1M and the first set of experiments was performed with CTEAB and DDAB. As with the previous samples here there was very little effect on the shape of the micelles and the amount of encapsulated material was fairly good with values of up to 10mM being seen. However, a lower concentration was used in subsequent experiments due to the presence of precipitated Nile red in these solutions meaning the actual concentration of Nile red as unknown.

The most interesting part of this experiment however was not the encapsulation of Nile red but the obvious phase separation that occurred in all the samples, to varying degrees. The most obvious set of samples to phase separate was the DDAB samples with polymer, as is shown in Figure 4-17. This phase separation is of interest because it is only visible due to the colour of the Nile red, although a similar separation is possibly occurring in the samples with the other additives. This seperation may explain the low encapsulation amounts measured in the other surfactant samples. A potential experiment to test whether this result is also seen in other systems would be to separate the surface part of a solution of surfactant/polymer and cyclohexane from the bulk solution and use GC to determine

if there was a difference in the concentration of cyclohexane at the surface compared to the bulk solution. The DDAB:2C_{16}TAB and DDAB:20C_{16}TAB samples were also studied using SANS, however the two different contrast experiments performed gave either too low contrast or different structures between contrasts meaning the amount of encapsulated Nile red could not be determined. The explanation for the different structures is either impurities in the deuterated C_{16}TAB used for the experiment or intra-micellar phase separation of surfactants leading to only C_{16}TAB being present in the high curvature regions of the micelle, as described by Zemb et al.[128]

The encapsulation of Nile red into these films was also studied. However as with the cyclohexane and cyclohexanol loaded films, the use of neutron reflectometry was hampered by differences between the hydrogenated and deuterated samples meaning the results appear random. However the total encapsulation of the Nile red was possible to determine using fluorescence spectroscopy after dissolving the film in acetone. These results compare well with the previous solution results suggesting that more elongated the surfactant micelles results in better loading.

Finally, the ability to release the additive from the sample was studied. As cyclohexane and cyclohexanol are both volatile and the films required drying before the release studies, all of the release studies were performed with Nile red. The release studies were performed by submerging the films in water and removing an aliquot at defined time intervals over the course of the experiment. The release profiles collected for the different surfactant solutions showed similar well defined release profiles although very limited total release from the films. As with the total encapsulation, there was also a slight trend in the release dependant on the structure of the micelles. The more elongated the micelles the more Nile red was released. This trend is slightly bucked by the DDAB, which has a slightly lower release than the DDAB:2C_{16}TAB, however this may be due to the ordering within the film as the DDAB:2C_{16}TAB films appeared more ordered than the DDAB films.

5 Cat-anionic Surfactant Solutions

5.1 Aims of studying cat-anionic surfactant systems

As mentioned previously, the cationic surfactant system and the cat-anionic surfactant system are effectively two sub-projects in the study of nanostructured hydrogel films. While a fair amount is known about the cationic system[59, 66-68], relatively little work has been done on the cat-anionic system.[71]

Although the cationic system has had more study it has had one major disadvantage, which is that films have only ever been formed with polyethylene imine (PEI) as the polymer. However the cat-anionic surfactant system was reported to form films with polyacrylamide (PAAm) and PEI. Therefore as well as studying the cationic surfactant system, as discussed in chapters 3 and 4, it is also of great importance to study the cat-anionic surfactant system, here and in chapter 6.

The main aim for the study of the cat-anionic surfactant system is to study the role of the surfactant and of the polymer on film formation. In the cationic surfactant system, the surfactant had the role of a templating agent while the polymer had the role of the binding matrix around the surfactant. Therefore the primary question is, does this hold true in the cat-anionic system? Given that different polymers can be used to form films with the cat-anionic surfactant system, the effect of different polymers on the films will be studied. Also, as seen in chapter 3, using a mixed surfactant system can lead to variations in the solution, and film, structure therefore this will also be studied.

5.2 Cat-anionic surfactant solutions

Although both C_{16}TAB and SDS are highly used surfactants in research, their mixtures have not been as heavily studied. For instance, it is much more common for SDS to be studied with dodecyltrimethylammonium bromide (DTAB) due to their comparable tail lengths.[130-132] Four studies that have focused on the mixtures of C_{16}TAB and SDS are by Andreozzi et al,[133] Tomašić et al,[134] Letiza et al,[135] and Tah et al.[136] Of these studies, Tomašić et al report the solution interactions in both the cationic rich and the anionic rich parts of the phase diagram, however only in enough detail to show where on the phase diagram precipitation occurs and where formation of mixed micelles occur. Tah et al also report the mixtures of C_{16}TAB:SDS in both the cationic and anionic rich parts of the phase diagram however this report is

confined to the surface of solutions. The structure of these micelles and aggregates has been suggested as large vesicles however this is not confirmed. Andreozzi reports only results in the anionic part of the phase diagram but shows that vesicles are present using a combination of dynamic light scattering, transmission electron microscopy and SAXS.

Given these films have previously only been seen in the cationic rich part of the phase diagram, the results from Andreozzi are not directly relevant, however they give indications of the likely structures as the phase diagrams are similar on either side of the equimolar line. Letiza et al[135] is an extension of the work performed by Anreozzi et al and is more concerned with the interactions of the vesicles with proteins. However Letiza et al also give a partial phase diagram for the both sides of the equi-molar line. This partial phase diagram, shown in Figure 5-1, is given only at lower concentrations than are used in this thesis, however an extrapolation of the phase diagram would suggest that the studies reported in this thesis are well within the multiphase region of the cationic rich side of the phase diagram. This work by Letiza et al combined with the results from Tomašić et al also suggests that the 60:40 ratio of C_{16}TAB to SDS, used in this study, is just only outside the precipitation region.

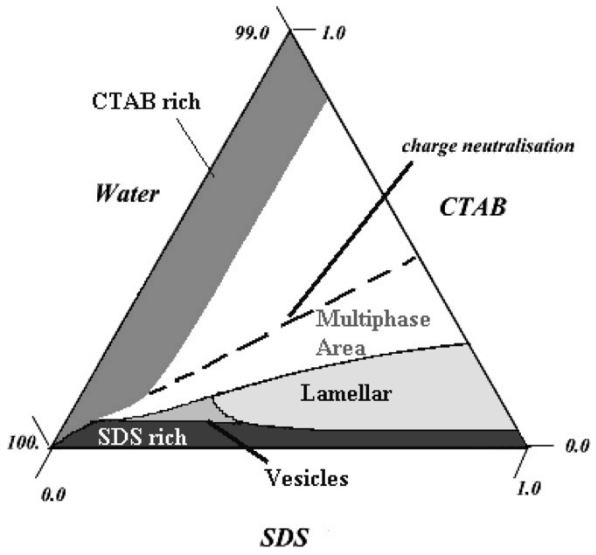

Figure 5-1. Partial phase diagram of C_{16}TAB:SDS in water at 25°C. 1. C. Letizia, P. Andreozzi, A. Scipioni, C. La Mesa, A. Bonincontro, and E. Spigone, J Phys Chem B, 2007, 111, 898–908. Copyright 2011 American Chemical Society.[135]

Bergstrom et al report the phase diagram for DTAB with SDS[112] while O'Connor et. al. report the phase diagram for C_{16}TAB with sodium octyl sulphate (SOS).[137] In both cases, in the region of 60 mol% cationic and 40 mol% anionic surfactant, the ratio most studied for film formation in our systems, either vesicles or lamellae are reported, dependent on the concentration of surfactant. As can be seen from these

phase diagrams and as reported by Yuet et al.[138] systems with asymmetric surfactant tails give enlarged vesicle regions in comparison to symmetric tailed systems. Given this, and the fact that the C_{16}TAB/SDS system reported by Andreozzi et. al.[133] shows vesicles, it is likely that the C_{16}TAB/SDS films reported by O'Driscoll et. al.[71] were formed from an interaction of the polymer with large multi-lamellar vesicles with a slight positive charge. A paper by Wolff et al suggests that this is a not unusual for C_{16}TAB,[139] since on the addition of the additives the aggregation number of C_{16}TAB is dramatically increased and large aggregates can be seen in electron micrographs.

Although the main focus of the studies discussed above is the structure of the aggregates made from these mixed surfactant systems, it is also important to consider the effect of mixing on the physical properties. An interesting study into a range of solution properties was performed by Patist et al.[140] This study suggests that that a 3:1 ratio of cetylpyridinium bromide to SDS appears to be an important ratio of surfactants for a number of the physical properties, such as the surface tension, the surface viscosity and the rate of evaporation. This has been attributed to the ability of the solution to form a stable hexagonal array of micelles. With this in mind it is therefore possible that there is also a preferential ratio of C_{16}TAB to SDS and that this may lead to enhancement of the film properties.

5.3 Solutions without polymer

As the original films were reported from a 60:40 mole ratio C_{16}TAB:SDS solution, it was decided that this should be the starting point to further study of these solutions. More specifically, an understanding was needed of the structures formed in the 60:40 mole ratio of C_{16}TAB and SDS solutions and how these structures are affected by the addition of polymer. The effect on the surfactant structure of the polymer is particularly interesting because, as well as forming films with multiple different polymers, the structure of the films has also been seen to be different depending on the polymer used.[102] This data will also be discussed in more detail in chapter 6.

5.3.1 6C_{16}TAB:4SDS in D_2O

The initial investigations into these solutions were performed using SANS on LOQ. Figure 5-2 shows the scattering patterns from a 0.01M 6C_{16}TAB:4SDS surfactant solution in D_2O using deuterated C_{16}TAB to give a second contrast. Also shown are lines of best fit from mathematical models. The models used for the two plots however are different. In the fully hydrogenated system the model is for a uniform

ellipse and has the structure of a cylinder. The system with deuterated C_{16}TAB is fitted with a model for a dilute lamellar phase.

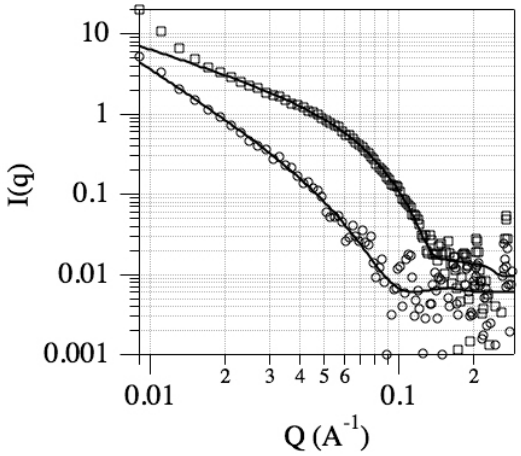

Figure 5-2. 0.01M 6C_{16}TAB:4SDS solution with no polymer. Squares are from the sample with hydrogenated C_{16}TAB, Circles are from the sample with deuterated C_{16}TAB. Best-fit lines are from models for a uniform ellipse and a dilute lamellar phase respectively.

Given these two drastically different structures and the up turn of the fully hydrogenated data in the low Q region, it was decided that SANS data alone would not give enough detail fully understand the C_{16}TAB:SDS structures in solution. This was not surprising given the size of the structures seen in previously reported papers is around 300nm, as discussed above.[133]

From this, it was decided to use a SANS instrument with a larger Q range and couple this with USANS data to pick up the maximum extent of the surfactant aggregates. Although Andreozzi et. al. only report structures up to 700Å which would be visible in a SANS instrument, USANS was also used because previous work within the group had shown aggregates larger than 1μm in scanning electron microscopy images, Figure 5-3. Another motivation for the experiments reported below was to determine whether or not these aggregates were real or an artefact of the sample preparation process.

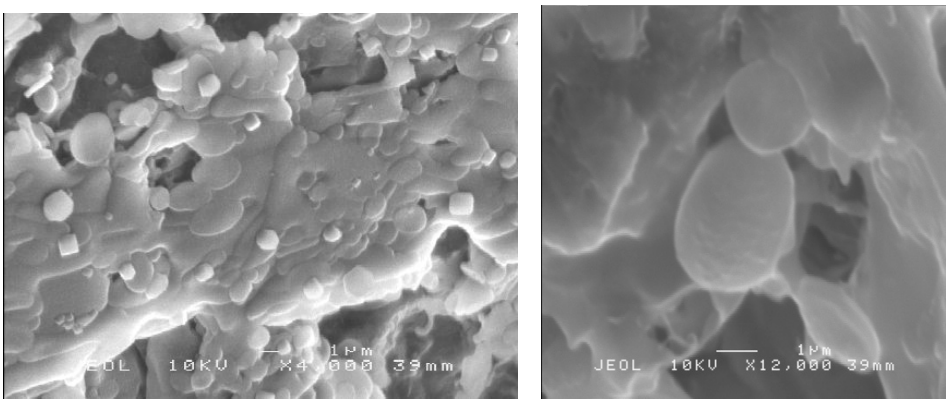

Figure 5-3. Scanning electron microscopy images of a freeze-fractured solution of 0.05M $6C_{16}$TAB:4SDS with no polymer (left) and PAAm (right). Data collected by BMD O'Driscoll, 2008, unpublished.

Analysis of the aggregates visible in the left plot in Figure 5-3 gives an average radius of 0.75μm with a standard deviation of 0.25μm. Analysis of the ellipses shows that as they become smaller they tend to be more circular than ellipsoidal. The plot in Figure 5-3 right is interesting because as well as showing an ellipse looking relatively circular it is also possible to see a profile view of the ellipse suggesting the ellipse is only 0.3μm thick. Although no comparison is available for the thickness of the vesicles reported by Andreozzi et al.[133] the diameters of the largest vesicles reported are only half the size of the aggregates seen in these SEM images. Given Andreozzi et al are working at a much lower surfactant concentration it is likely this is the reason for the lack of very large aggregates in their work. However the structures are similar therefore it is probable that similar vesicles are created in the solutions in the study reported in this thesis.

The decision to use USANS was well justified as can be seen in Figure 5-4, which shows the combined SANS and USANS data for a solution of 0.05M $6C_{16}$TAB:4SDS with no polymer in D_2O, using either hydrogenated C_{16}TAB or deuterated C_{16}TAB. In this figure the USANS data has been desmeared to show the full Q range in what appears to be a single curve. The fact that the plots line up shows that the samples are stable, as the SANS experiment was performed prior to the USANS experiment but the samples were the same. Between the experiments the samples were kept on a bench top under ambient conditions in sealed containers to minimise hydrogen exchange with the air.

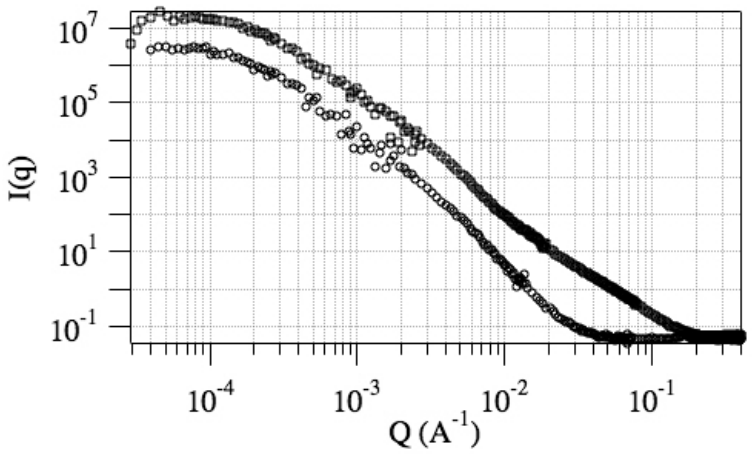

Figure 5-4. 0.05M 6CTAB:4SDS in D_2O with no polymer present. The plots with squares have hydrogenated C_{16}TAB. The plots with circles have deuterated C_{16}TAB. Error bars are not included because they are smaller than the markers.

Although the desmeared data produces a contiguous plot that is simpler to visualise than smeared data, the desmearing process can introduce errors and artefacts into the data. Therefore when the data is compared to a mathematical model the raw data is used and the model is smeared. The fitted data is shown in Figure 5-5. No single model was able to accurately describe the complete scattering curve therefore the scattering from two models was summed together. The models that are used to describe the data are for a uniform ellipse[111] and a non-interacting lamellar phase.[113]

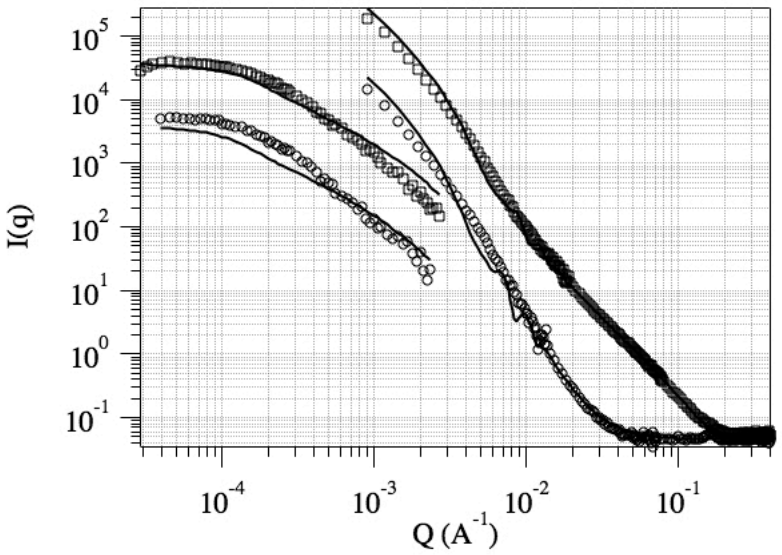

Figure 5-5. 0.05M 6CTAB:4SDS in D_2O with no polymer. The plots with squares have hydrogenated C_{16}TAB. The plots with circles have deuterated C_{16}TAB. The lines are a simultaneous fit to the model described in the text. Error bars are not included because they are smaller than the markers and to simplify the plot.

In the hydrogenated data a transition can be seen at around Q = 10^{-2} Å^{-1} and in the fitting this relates to the point where the main influence of the fitting is from the uniform ellipse model, to the left, and the lamellar model, to the right. This point is also very close to the low Q limit on the LOQ instrument. In fitting this data the parameters held constant were the SLD of the hydrogenated surfactant, -3.53x10^{-7} Å^{-2}, and the SLD of the solvent, 6.37x10^{-6}Å^{-2}. In addition the background level was held constant, while all the other parameters were fitted. These results are given in Table 5-1.

		Contrast 1	
		Fit Results	Uncertainty
Ellipse	R(a) (Å)	670	±50
	R(b) (Å)	15300	±2000
Lamellar	Thickness (Å)	25	±2
	Polydispersity	0.30	±0.01
		Contrast 2	
Ellipse	R(a) (Å)	810	±50
	R(b) (Å)	19600	±2000
Surfactant Ratio		C_{16}TAB	SDS
	Ellipse	69%	31%
	Lamellae	87%	13%

Table 5-1. Fitting results for global fitting SANS and USANS data of two contrast of 0.05M 6C_{16}TAB:4SDS in D_2O. Uncertainty in the surfactant ratios are ±5%

These results show that the aggregates in C_{16}TAB:SDS solutions are very large. These values are radii, therefore the full aggregate length will be between 3 and 4μm. This value is slightly larger, but of the same order of magnitude, as the disk shaped aggregates seen in Figure 5-3. Usually in fitting, the second contrast is assumed to have the same structure as the first contrast as any isotopic variation should be within instrumental resolution. In this fitting however it was clear that the aggregate size in the second contrast was much larger than in the first contrast therefore the aggregate dimensions were not globally fitted. A 10% variation in molecular volume between a hydrogenated surfactant and deuterated surfactant in a 30Å micelle would lead to ±3Å error, in a 15,000Å aggregate this would be ±1,500Å therefore much more obvious.

The only other parameters not to be globally fitted between the hydrogenated and deuterated plots were the SLDs for the aggregates. Fitting these values showed that there is different mixing occurring in the two models. These values are fitted using the surfactant tail SLDs, as it is assumed that penetration of the solvent will affect the scattering of the head group of the scattering body, although the use of the full surfactant SLDs gave values within 2% of those reported above. These values are

interesting because they are very different from the 60%:40% molar mixture used to make the solutions. This will be further discussed in comparison with other results below.

5.3.2 $7C_{16}TAB:3SDS$ in D_2O

The molar ratio of 70% $C_{16}TAB$ and 30% SDS is significant because, although O'Driscoll et al[71] focused on a 6:4 molar ratio, further work within the group has shown that a 70:30 ratio is more stable as a solution over a long period of time and less likely to phase separate upon mixing with polymer. Due to this, at the same time as performing SANS and USANS measurements on 6:4 ratio mixtures of $C_{16}TAB$ and SDS 7:3 ratio mixtures were also studied. Fitting of the $7C_{16}TAB:3SDS$ solution with no polymer in D_2O is shown in Figure 5-6.

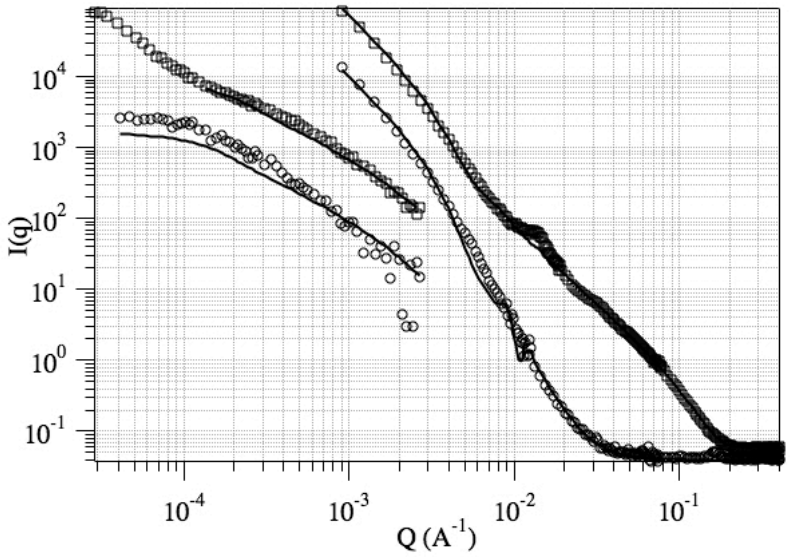

Figure 5-6. 0.05M 7CTAB:3SDS in D_2O with no polymer. The plots with squares have hydrogenated $C_{16}TAB$. The plots with circles have deuterated $C_{16}TAB$. Error bars are not included because they are smaller than the markers.

The same summed model used to fit the 6:4 ratio was used to fit the 7:3 ratio as the plots are very similar. Two major differences in the shapes of the plots are in the fully hydrogenated surfactant sample where below $Q = 1\times10^{-4}$ Å^{-1} the data shows an increase in scattering instead of the flattening out as seen in the pattern observed in Figure 5-5. As it is not clear what this increase in intensity is related to and, as it is not seen in the deuterated pattern, the fitting was not performed in this region of this plot. The second difference between the plots is between $Q = 1\times10^{-2}$ Å^{-1} and 2×10^{-2} Å^{-1} in the hydrogenated pattern where there appears to be a wide ripple in the data. It is likely that this is due to the interaction between the lamellar layers imposing a

correlation distance between layers, which is reflected by this feature in the data, however it is not strong enough to be fitted in this case. Apart from these differences the data and the fitting was very similar for both ratios of C_{16}TAB:SDS.

Contrast 1			
Ellipse	R(a) (Å)	640	±50Å
	R(b) (Å)	11300	±2000Å
Lamellar	Bilayer Thickness (Å)	28	±2Å
	Bilayer Polydispersity	0.02	±0.04
Contrast 2			
Ellipse	R(b) (Å)	15300	±2000Å
Surfactant Ratio		C_{16}TAB	SDS
	Ellipse	58%	42%
	Lamellar	97%	3%

Table 5-2. Fitting results for global fitting SANS and USANS data of two contrast of 0.05M 7C_{16}TAB:3SDS in D_2O. Uncertainty in the surfactant ratios are ±5%.

The results here show that the same isotopic variation occurs in both the 6:4 ratio and the 7:3 ratio with the deuterated contrast aggregate being roughly 4000Å larger than the hydrogenated contrast aggregate. However the 7:3 ratio aggregates are smaller than the 6:4 ratio aggregates. The bilayer thickness however is hardly changed, suggesting the internal structure of both aggregates is the same, which would be expected as the chemical components are not changing much.

Surprisingly, an area of fitting which is very different for the two ratios of C_{16}TAB to SDS is the ratio of C_{16}TAB to SDS as determined by the SLDs. In the 6:4 ratio the SLDs suggested the ellipse had a 7:3 ratio of C_{16}TAB to SDS while the lamellar had a ratio of 85:25. In the 7:3 molar ratio solutions the ellipse appears to have a 6:4 ratio of C_{16}TAB to SDS while the lamellar has a ratio of 95:25. It is not clear why this is but it is confirmed in both the USANS and SANS data. It is therefore possible that these structures are not equilibrium structure, as expected, and instead are kinetic structures that are formed as the two surfactants are mixed together. This may be due to the increase in viscosity on the mixing of the two surfactants and the polymer and the variation seen in these results may be due to the time the surfactants have to equilibrate before mixing the polymer. A large increase in viscosity has previously been reported in similar systems.[137] The change of surfactant ratios within a surfactant micelle however has not been seen, although this could be related to the surfactant being distributed to optimise a particular parameter. Patist et al reported the enhancement of physical parameters such as the surface tension and surface viscosity at particular ratios of SDS and cetylpyridinium chloride[140].

From handling these solutions, but without any supporting evidence, the $6C_{16}$TAB:4SDS solutions appear to start out less viscous but become more viscous over time. The $7C_{16}$TAB:3SDS samples however start off more viscous than the $6C_{16}$TAB:4SDS samples but do not appear to change viscosity much over time. Therefore if a structure is being frozen into place before equilibrium is reached, then it is likely that the $6C_{16}$TAB:4SDS structure would be closer to the equilibrium structure suggesting there should be an even distribution of C_{16}TAB to SDS throughout both structures.

5.3.3 Surfactant solutions mixed at 70°C

To try and address any inconsistencies in mixing, it had been seen that mixing solutions at higher temperatures produced solutions that were more homogeneous and less likely to phase separate over time. The original experiments were performed by mixing solutions at 30°C, above the Kraft point of C_{16}TAB, and then storing the solutions at room temperature, usually between 20°C and 25°C depending on where the experiment was being performed. To test what affect a variation in mixing would have on the solutions, the experiments discussed above were duplicated but the mixing and storage was performed at 70°C while the measurements were made on solutions rapidly cooled to 25°C. Visually the samples appeared more homogeneous, as shown in Figure 5-7, and, as expected, were less likely to phase separate than the samples prepared at room temperature. They also appeared a lot less viscous when being transferred from the storage vial to the experimental sample holder. This possibly suggests that the aggregates are either smaller or more mobile in these solutions as has been seen previously.[141]

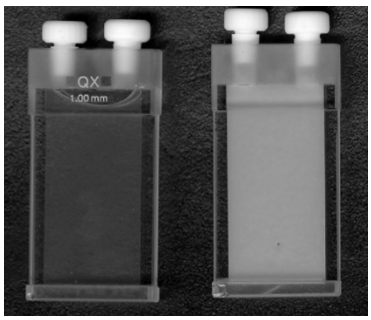

Figure 5-7. 0.05M $6C_{16}$TAB:4SDS samples without polymer prepared at 70°C (right) and at 30°C (left).

However there were some problems with the data collected. The main problem was that the SANS and USANS data did not line up after desmearing. This means that the data collected in the USANS samples is different from the data collected in the SANS samples. Given the length of time it takes to perform a USANS experiment

and the fact that the samples were prepared early on during the experiment it is possible that during storage at 70°C one or both of the surfactants had decomposed, therefore significantly altering the chemical makeup of the sample. SDS is well known to be unstable at higher temperatures[142] although the degradation proceeds faster at basic or acidic pH, while the samples here were at pH 7. The samples were prepared in 3ml vials at the beginning of the experiment, allowing aliquots of 1.5ml to be taken for either SANS or USANS experiment when needed. As long as the samples had reached equilibrium by the time the SANS aliquot was removed from the sample, the USANS aliquot, which was taken between 2 and 5 days later, should be identical. The second problem was that there is a significant different between the hydrogenated and deuterated SANS patterns. The hydrogenated patterns line up almost perfectly with the SANS patterns collected for the room temperature data while the deuterated patterns are very different. The hydrogenated and deuterated patterns for both the room temperature samples and the 70°C samples are shown in Figure 5-8.

0.05M $6C_{16}$TAB:4SDS D_2O
Contrast 1

Ellipse	R(a) (Å)	358	±50
	R(b) (Å)	7020	±500
Lamellar	Bilayer Thickness (Å)	26	±2
	Bilayer Polydispersity	0.2	±0.05

Surfactant Ratio	Ellipse	94%	6%
	Lamellae	52%	48%

0.05M $7C_{16}$TAB:3SDS D_2O
Contrast 1

Large Ellipse	R(a) (Å)	502	±50
	R(b) (Å)	9183	±500
Small Ellipse	R(a) (Å)	27	±2
	R(b) (Å)	0.25	±0.01

Surfactant Ratio	Ellipse	78%	22%
	Lamellae	78%	22%

Table 5-3. Fitting results for surfactant solutions mixed at 70°C

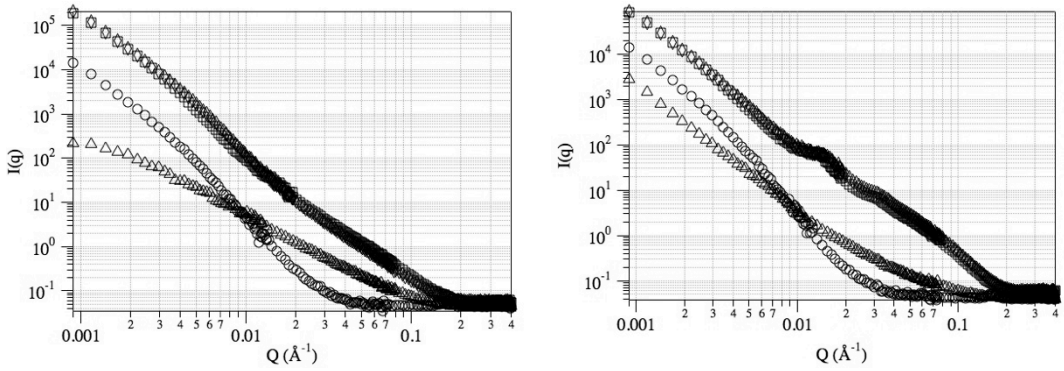

Figure 5-8. 0.05M 6C_{16}TAB:4SDS in D_2O (left) and 0.05M 7C_{16}TAB:3SDS in D_2O (right). Plots are hydrogenated surfactant prepared at room temperature (squares), hydrogenated surfactant prepared at 70°C (diamonds), deuterated C_{16}TAB prepared at room temperature (circles) and deuterated C_{16}TAB prepared at 70°C (triangles).

As mentioned previously the hydrogenated plot gives the same structure regardless of preparation temperature, suggesting that in that case the sample is still composed of ellipses and lamellar sheets. If this is still the case then the ratios of C_{16}TAB to SDS in the different aggregates must be altered from the room temperature sample to the 70°C samples to allow the same models to fit to the deuterated data. Both plots were fitted with the summed ellipse lamellar model and the results are given in Table 5-3.

What these results show is that the temperature has a slight effect on the surfactant solutions causing the aggregates to be smaller, which is to be expected given the difference in opacity seen in Figure 5-7. The distribution of C_{16}TAB to SDS is altered much more significantly, as suggested above, however this alteration is very different for the two solutions. In the 6C_{16}TAB:4SDS sample, the ratios have become more different from each other with practically all of the SDS being redistributed to the lamellae leaving very little in the ellipse. This result means that the lamellar is almost equi-molar C_{16}TAB to SDS, which might be expected if charge compensation was the driving force. The 7C_{16}TAB:3SDS sample however has become more evenly distributed with more aggregates showing a roughly 80:20 ratio of C_{16}TAB to SDS. Given these numbers however there is then a missing component of SDS. As these solutions are opaque it is possible that a small amount of precipitation occurred which was not noticed. This ratio of 78% C_{16}TAB to 22% SDS is particularly interesting given the results reported by Patist et al who report an enhancement of the physical properties of a mixed surfactant system at mixing ratios of 1:3, 1:1, and 3:1.[140] Patist et al however report the system of cetylpyridinium bromide with SDS, which although similar in molecular structure to C_{16}TAB:SDS, is still very different due to the pyridinium head group.

5.3.4 Comparison of data from different instruments

Once the aggregate structure had been fitted using SANS and USANS data it was possible to return to the original studies of C_{16}TAB and SDS and compare the patterns from different instruments. Figure 5-9 shows the patterns of 0.05M 6C_{16}TAB:4SDS in D_2O collected separately on NG7 at the NCNR and on D11 at the ILL. From this data it can be seen that the scattering is fairly reproducible, although there is variation between the two plots. However there is one major difference between the plots and that is a diffraction peak visible in the data collected at the ILL.

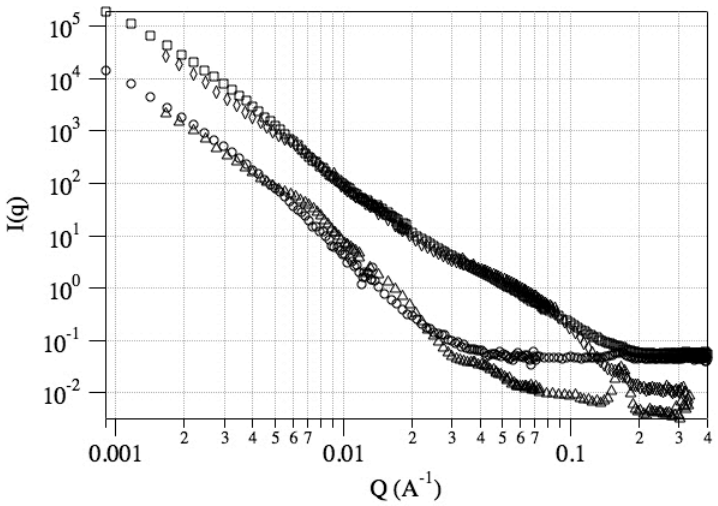

Figure 5-9. 0.05M 6C_{16}TAB:4SDS in D_2O. Hydrogenated (squares) and deuterated (circles) samples collected on NG7, and hydrogenated (diamonds) and deuterated (triangles) samples collected on D11.

This diffraction peak is of interest as it is an indicator of highly ordered repetitive structure. The likely explanation of this is precipitation of some of the surfactant. This explanation would fit well with the ratios of C_{16}TAB:SDS as the ratios from the fitting would lead to unaccounted for SDS, the excess SDS could then be accounted for by precipitation of a close to equi-molar mixture of C_{16}TAB:SDS, which has previously been seen to precipitate.[134]

The second explanation for the structures is that they are the same structure, which would be a flattened oblate bilayer vesicle. For this structure to work the vesicle must be so large that the flattened regions are able to act as lamellar bilayers. The ellipse structure is then explained by the curved edges of the bilayer. However this is hard to explain due to the different ratios of C_{16}TAB:SDS with a single structure. Although due to the different packing parameters of the C_{16}TAB and SDS, it is possible that the SDS, with the larger head group, aggregates on the outer edge of the vesicle, increasing the curvature, while the C_{16}TAB is on the inside edge of the

vesicle reducing the curvature. This would then lead to a mis-match in surfactant ratios in the curved region of the structure and the flat region of the structure. A similar separation of surfactants has previously been reported by Zemb et al. to create a higher curvature for a nanodiscs.[128]

5.4 Solutions with Polymer

Although the structure of the surfactant solutions in the absence of polymer is interesting, of more interest for the understanding of film formation is the effect of the addition of polymer on the solutions. The main polymer used was PEI and, as with the previous studies, two molecular weights were used, 750,000 (LPEI) and 2,000 (SPEI). Along with PEI, polyacrylamide (PAAm), 10,000, was used as this was the polymer first reported to form films with C_{16}TAB:SDS. Finally two molecular weights of polyethylene oxide were used, 100,000 (LPEO) and 10,000 (SPEO). Although PEI and PAAm are used because they were the first polymers to be reported to form films, the use of PEO may be of more interest for potential applications because of its greater biocompatibility. Due to the potentially large number of samples, the polymer concentration was fixed at 1weight%. This data was collected on NG7 and BT5 at the NCNR therefore the full Q range could be fitted.

Although no studies of C_{16}TAB:SDS aggregates in the presence of polymer have been reported, there are reports of work on the effect of polymers on cat-anionic vesicles formed with SDS and DDAB.[143, 144] These reports suggest that the addition of polymer creates a region where the interaction of the cat-anionic aggregate with the polymer can lead to precipitation, although at other concentrations there is very little change to the solution. Interestingly, in these systems when the concentration of the polymer is high enough to neutralise any charge on the aggregates then, instead of precipitation, it is found that a gel is created.

5.4.1 0.05M 6C_{16}TAB:4SDS with Polymer in D_2O mixed at room temperature

The fitting results for 0.05M 6C_{16}TAB:4SDS with different polymer in D2O mixed at room temperature is shown in Table 5-4, the graphs of these fits are shown in Figure 5-10. What the fitting shows is that SPEI and SPEO act in a similar fashion with the large aggregate size being roughly the same and expanding the same amount when using deuterated C_{16}TAB, although this increase in size is much larger than had been seen in the systems with no polymer. Interestingly the aggregate size in the fully hydrogenated system with polymer stays similar to the aggregate size with no polymer present. However due to the different interactions with the polymer

and the surfactant the distribution of SDS is different. In both samples the ellipsoidal aggregate has 72% C_{16}TAB and 28% SDS, however the lamellar aggregates with SPEI have more C_{16}TAB at 79% instead of the SPEO at 70%.

The change from SPEI to LPEI has two effects on the aggregates; firstly the LPEI leads to formation of larger aggregates. The second effect is that the distribution of C_{16}TAB to SDS, although being the same in the ellipse at 70% C_{16}TAB and 30% SDS for both samples the addition of LPEI, leads to more SDS in the lamellae to give 60% C_{16}TAB and 40% SDS. As well as the change in the molecular weight between the two polymers there is also a difference in molecular structure with the SPEI being composed of short branches on a relatively short back bone while the LPEI is a hyperbranched polymer with undefined branch lengths and branches off branches. Due to this, it is possible that there is an effect from the molecular weight of the LPEI for example it can interact with more micelles leading to larger aggregates. However it is also possible that the molecular structure of the polymer also plays a role with the SPEI being able to interact better with the molecules within the aggregates because it is less sterically hindered.

		No Polymer Contrast 1		SPEI Contrast 1		LPEI Contrast 1		SPEO Contrast 1		PAAm Contrast 1	
Ellipse	R(a) (Å)	670		570		810		640		1120	
	R(b) (Å)	15300		13500		15100		13700		17100	
Lamella	Thickness (Å)	25		20		24		23		20	
	Polydispersity	0.30		0.49		0.30		0.20		0.80	
		No Polymer Contrast 2		SPEI Contrast 2		LPEI Contrast 2		SPEO Contrast 2		PAAm Contrast 2	
Ellipse	R(a) (Å)	810		1260		1650		930		1790	
	R(b) (Å)	19600		24600		28100		21000		31300	
		C_{16}TAB	SDS	C_{16}TAB	SDS	C_{16}TAB	SDS	C_{16}TAB	SDS	C_{16}TAB	SDS
Surfactant	Ellipse	69%	31%	72%	28%	71%	29%	72%	28%	68%	32%
Ratio	Lamella	87%	13%	79%	21%	63%	37%	70%	30%	83%	17%

Table 5-4. Fitting results from simultaneous fitting of two contrasts of SANS and USANS data for 0.05M 6C_{16}TAB:4SDS with different polymers. Contrast 1 is hydrogenated surfactant in D_2O, contrast 2 is deuterated C_{16}TAB and hydrogenated SDS in D_2O. Errors in ellipse R(a) values are ±50Å, R(b) values are ±2000Å. Errors in lamella thicknesses are ±2Å, polydispersity values 0.05.

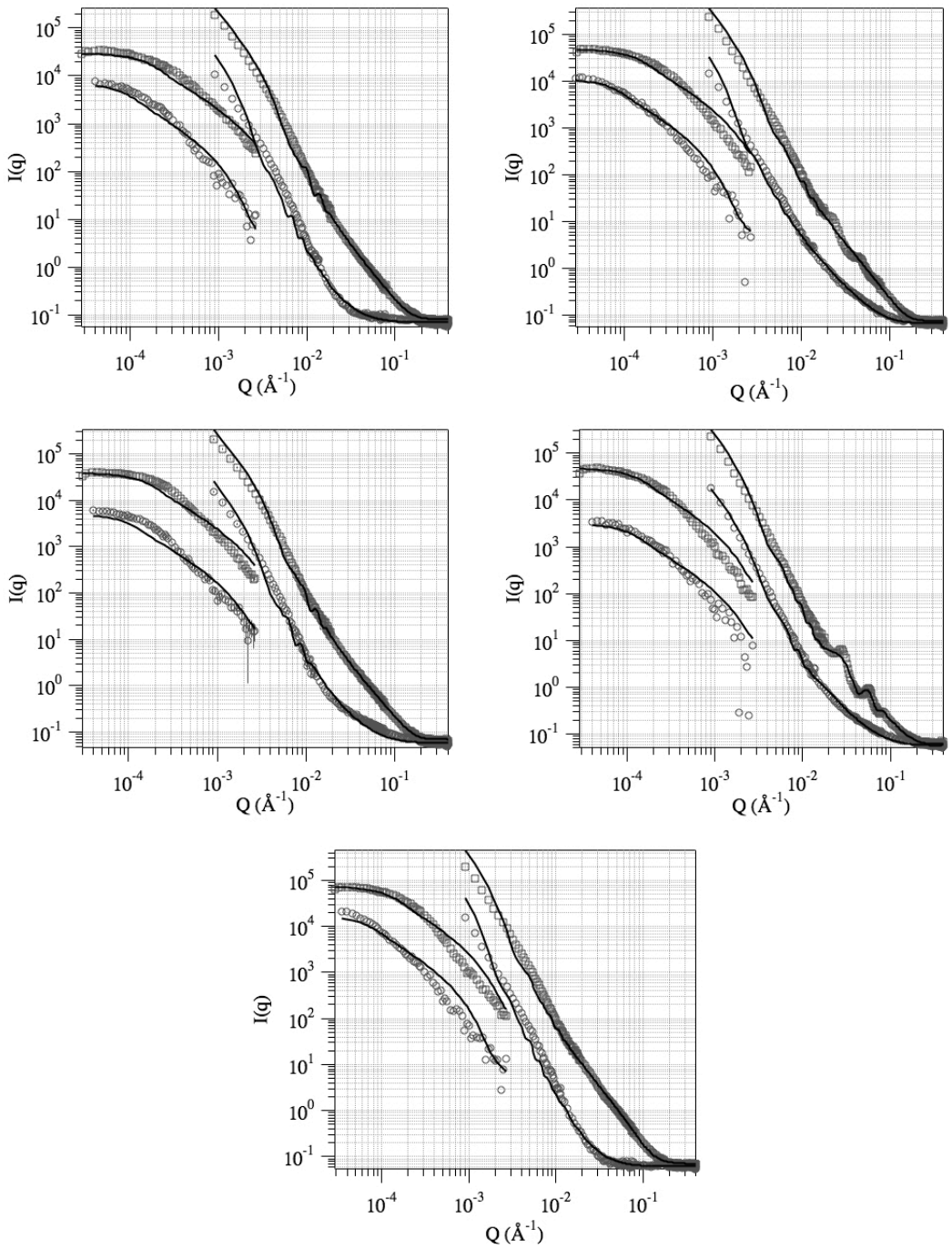

Figure 5-10. Simultaneous SANS and USANS fitting of 0.05M 6C_{16}TAB:4SDS with SPEI (top left), LPEI (top right), SPEO (middle left), LPEO (middle right), and PAAm bottom. Squares represent hydrogenated samples, circles represent deuterated samples, and lines are best fits through the data points.

The largest aggregates are seen in the PAAm sample even though the molecular weight of this polymer is a lot lower than the LPEI molecular weight. O'Driscoll et al[71] suggested that due to the lack of change in the diffraction peaks in the reflectivity pattern seen upon the addition of PAAm to the system this meant that the PAAm did not interact with the surfactant very strongly. It is unclear whether this is supported by the SANS or USANS data. The aggregate size changes although this

could be due to swelling. Although the size of the aggregates has changed the distribution of C_{16}TAB and SDS remains the same as in the sample with no polymer, 70% C_{16}TAB in the ellipse and 80% C_{16}TAB in the lamellar.

One sample that has been omitted from the table above is the sample with LPEO. The reason for this is because the structure of the aggregates is significantly different from the other samples. This meant the model fitted to the data had to be changed, therefore instead of using an ellipse and a dilute lamellar phase the LPEO sample shows ripples indicating interacting lamellar sheets. Therefore the model used was of a summed model of an ellipse[111] and a lamellar paracrystal.[112] The data with fitted model can be seen in Figure 5-10 (middle right) and the fitted parameters are shown in Table 5-5.

Contrast 1			
Ellipse	R(a) (Å)	950	±50
	R(b) (Å)	16400	±2000
Lamellar	Thickness (Å)	20	±2
	Number of Layers	1.61	±0.01
	Layer Spacing (Å)	223	±5
	Polydispersity	0.07	±0.02
Contrast 2			
Ellipse	R(a) (Å)	930	±50
	R(b) (Å)	19400	±2000
Lamellar	Number of Layers	1.93	±0.15
	Polydispersity	0.55	±0.03
		C_{16}TAB	SDS
Surfactant Ratio	Ellipse	73%	27%
	Lamellar	60%	40%

Table 5-5. Fitting results for 0.05M 6C_{16}TAB:4SDS with LPEO in D_2O.

This data shows a lot of similarities with the data discussed above. If the fully hydrogenated systems are compared then, as discussed previously, the increase in molecular weight leads to an increase in aggregate size. This increase in size from the hydrogenated system to the deuterated system is much smaller than in the other polymer samples and is more comparable to the samples with no polymer. This means that of the deuterated aggregates in the study these are the smallest.

Another similarity with the LPEI sample is the ratio of C_{16}TAB to SDS in the different aggregates with the ellipse having 70% C_{16}TAB and the lamellae having 60% C_{16}TAB. Although the lamellae ratios vary across the systems with no obvious reason the ellipse ratios are very consistent at 70:30 which makes it surprising that the 0.05M 7C_{16}TAB:3SDS with no polymer sample showed 60% C_{16}TAB.

5.4.2 0.05M 7C_{16}TAB:3SDS with polymer in D_2O mixed at room temperature.

As mentioned previously, although the majority of previous results have been collected using the 6C_{16}TAB:4SDS it has been seen during this research that the 7C_{16}TAB:3SDS system is more stable over time. It also appears, given the results above, that the 7C_{16}TAB:3SDS solution is actually closer to the natural mixing ratio of C_{16}TAB with SDS, therefore it is important to understand the polymer interactions at this surfactant ratio as well. The same conditions, as described in the 6C_{16}TAB:4SDS with polymer section, were used and the same polymers were tested. The results are shown in Table 5-6.

Due to timing the SPEI and LPEI USANS samples were collected during a different experiments than the rest of the samples and only fully hydrogenated samples were measured. In the SANS measurements of the same samples two contrasts were still collected, the first using hydrogenated surfactant in D_2O and the second using deuterated C_{16}TAB and hydrogenated SDS in D_2O. In the rest of the samples two contrasts of both USANS and SANS data was collected.

In general there are lots of similarities between aggregates in the 7:3 ratio and the 6:4 ratio. The biggest difference is between the LPEI samples where in the 7:3 ratio the model is a summed ellipse and lamellar paracrystal while in the 6:4 ratio the model is a summed ellipse and dilute lamellar. In this sample to fit the ripples associated with the interacting bilayers, both the number of layers and the polydispersity of the layers have an influence on the broadness and height of the ripples. Variation of these parameters during fitting has shown that the effect of changing one parameter can be reduced by the other parameter. To overcome this issue, the polydispersity was held at 0.1 to allow comparison between the two samples. It is worth noting that the same problem was not experienced with fitting of the 0.05M 6C_{16}TAB:4SDS LPEO sample.

		No Polymer Contrast 1		SPEI Contrast 1		LPEI Contrast 1		SPEO Contrast 1		LPEO Contrast 1		PAAm Contrast 1	
Ellipse	R(a) (Å)	640		590		730		660		1300		770	
	R(b) (Å)	11300		7100		13800		13400		17900		18500	
Lamella	Thickness (Å)	28		26		27		22		26		25	
	Number of Layers	a		a		2.64		a		2.55		a	
	Layer Spacing	a		a		274		a		257		a	
	Polydispersity	0.02		0.20		0.10		0.31		0.10		0.39	
		No Polymer Contrast 2		SPEI Contrast 2		LPEI Contrast 2		SPEO Contrast 2		SPEO Contrast 2		PAAm Contrast 2	
Ellipse	R(a) (Å)	b		b		b		900		b		1020	
	R(b) (Å)	15300		b		b		21100		b		19500	
Lamella	Polydispersity	b		b		0.58		b		0.03		b	
		C_{16}TAB	SDS	C_{16}TAB	SDS	C_{16}TAB	SDS	C_{16}TAB	SDS	C_{16}TAB	SDS	C_{16}TAB	SDS
Surfactant Ratio	Ellipse	58%	42%	73%	27%	73%	27%	70%	30%	74%	26%	69%	31%
	Lamella	97%	3%	89%	11%	74%	26%	76%	24%	72%	28%	75%	25%

Table 5-6. Fitting results from simultaneous fitting of two contrasts of SANS and USANS data for 0.05M 7C_{16}TAB:3SDS with different polymers. Contrast 1 is hydrogenated surfactant in D_2O, contrast 2 is deuterated C_{16}TAB and hydrogenated SDS in D_2O. (a) The model used to fit this sample did not require this parameter. (b) The parameter was linked to the contrast 1 parameter during fitting. Errors in ellipse R(a) values are ±50Å, R(b) values are ±2000Å. Errors in lamella thicknesses are ±2Å, number of layer ±0.01, layer spacing ±5Å, polydispersity values 0.05.

Apart this difference the fitting is very similar to the 0.05M 6C_{16}TAB:4SDS with polymer fitting. The aggregate dimensions are fairly similar, particularly for the ellipse dimensions, the exception to this being the R(b) for the SPEI sample being a lot smaller than expected. There is a small amount of variation in the bilayer thickness in the lamellae however this is probably due to difficulties fitting this value accurately given the shape of the curves. The distribution of C_{16}TAB to SDS is also fairly similar with all the ellipse models showing a 7:3 ratio of C_{16}TAB to SDS. There is more variation in the lamellar phase molar ratios, however, with the two high molecular weight polymers showing a 7:3 ratio instead of a 6:4 ratio. At the same time the SPEI sample lamellar phase shows a ratio of 9:1 that is even more extreme than 8:2 seen in the 6C_{16}TAB:4SDS sample with this polymer.

5.4.3 Solutions with polymer mixed at high temperature.

As with the surfactant solutions without polymer, it was decided to study the surfactant solutions with polymer when mixed at high temperature help the solutions to mix. Again 70°C was the higher temperature used and, as mentioned previously, the samples appeared visually more homogeneous and were less viscous when being transferred between the storage vial and the experimental sample holder. In all the samples where USANS data was recorded this did not line up with the SANS data therefore all the data has been fitted with just the SANS data. The 0.05M 6:C_{16}TAB:4SDS data with the different polymers is shown in Table 5-8.

Omitted from these results are the results for 0.05M 6C_{16}TAB:4SDS with PAAm. This is because the data could not be fitted with a summed ellipse and lamellar model and without the USANS data it is not possible to confidently determine what model should be used. The rest of the samples have been fitted with the summed ellipse dilute lamellar model, as in the samples mixed at room temperature, with the exception of LPEO, which again is fitted with the summed ellipse and lamellar paracrystal model.

Interestingly in these results the SPEI and SPEO samples show a decrease in aggregate size, similar to the decrease seen for the surfactant solutions without polymer. The LPEI and LPEO samples on the other hand do not show any decrease in aggregate size suggesting the high molecular weight polymer helps stabilise the large aggregates.

The ratios of C_{16}TAB to SDS in the aggregates are also affected by the temperature for all the samples, except the LPEI sample, which behaves in the same manner as the 6C_{16}TAB:4SDS sample without polymer. This is particularly true in the molar ratios in the ellipse, which are all around 95:5. The lamellar phase ratios are not as

extreme as the sample with no polymer however in the presence of polymer the ratio is consistently 65:35. The 6C_{16}TAB:4SDS sample with LPEI is very different because the ellipse appears to have an excess of SDS, this could indicate that there was a problem with one of these samples, similar to that seen in the USANS data in which the sample was decomposing. The continuity of the ratios of C_{16}TAB to SDS in these samples is highly interesting given that the samples were prepared from separate stock solutions of C_{16}TAB, SDS and polymer, which were mixed together at the same time. This therefore indicates that the ratio of C16TAB:SDS within the different structures is a fundamental property of the surfactant solution regardless of the polymer added.

	SPEI Contrast 1		
Ellipse	R(a) (Å)	1000	±50
	R(b) (Å)	20400	±2000
Lamellar	Thickness (Å)	27	±2
	Number of Layers	1.46	±0.01
	Layer Spacing (Å)	353	±5
	Polydispersity	0.16	±0.05
	SPEI Contrast 2		
Lamellar	Polydispersity	0.41	±0.05
Surfactant Ratio		C_{16}TAB	SDS
	Ellipse	95%	5%
	Lamellar	80%	20%
	SPEO Contrast 1		
Ellipse	R(a) (Å)	1000	±50
	R(b) (Å)	23400	±2000
Lamellar	Thickness (Å)	29	±2
	Number of Layers	1.23	±0.01
	Layer Spacing (Å)	378	±5
	Polydispersity	0.14	±0.05
	SPEO Contrast 1		
Lamellar	Polydispersity	0.52	±0.05
Surfactant Ratio		C_{16}TAB	SDS
	Ellipse	95%	5%
	Lamellar	73%	27%

Table 5-7. Fitting of 0.05M 7C_{16}TAB:3SDS with polymers mixed at 70°C

		No Polymer Contrast 1	SPEI Contrast 1	LPEI Contrast 1	SPEO Contrast 1	LPEO Contrast 1
Ellipse	R(a) (Å)	360	500	620	440	770
	R(b) (Å)	7020	9400	14500	8400	17200
Lamella	Thickness (Å)	26	30	43	30	31
	Number of Layers	a	a	a	a	2.34
	Layer Spacing	a	a	a	a	230
	Polydispersity	0.20	0.20	0.17	0.20	0.14

		No Polymer Contrast 2		SPEI Contrast 2		LPEI Contrast 2		SPEO Contrast 2		SPEO Contrast 2	
Lamella	Polydispersity	b		b		0.00		b		b	
		C_{16}TAB	SDS	C_{16}TAB	SDS	C_{16}TAB	SDS	C_{16}TAB	SDS	C_{16}TAB	SDS
Surfactant	Ellipse	94%	6%	95%	5%	39%	61%	92%	8%	95%	5%
Ratio	Lamella	52%	48%	68%	32%	79%	21%	65%	35%	67%	33%

Table 5-7. Fitting results from simultaneous fitting of two contrasts of SANS and USANS data for 0.05M 6C_{16}TAB:4SDS with different polymers mixed at 70°C. Contrast 1 is hydrogenated surfactant in D_2O, contrast 2 is deuterated C_{16}TAB and hydrogenated SDS in D_2O. (a) The model used to fit this sample did not require this parameter. (b) The parameter was linked to the contrast 1 parameter during fitting. Errors in ellipse R(a) values are ±50Å, R(b) values are ±2000Å. Errors in lamella thicknesses are ±2Å, number of layer ±0.01, layer spacing ±5Å, polydispersity values 0.05.

Samples were also measured for the $7C_{16}$TAB:3SDS solutions with polymer mixed at 70°C. A single model could not be found to fit both contrasts in the LPEI and LPEO data therefore it has so far not been possible to draw conclusions from these samples. The SPEI and SPEO samples however could still be fitted with a summed model however these samples showed ripples that required the lamellar paracrystal model instead of the dilute lamellar model. The results for this fitting are shown in Table 5-7.

As with the $6C_{16}$TAB:4SDS samples with polymer mixed at high temperature the distribution of C_{16}TAB and SDS in the samples is very different depending on the aggregate. The value of 95:5 appears to be very repetitive and corresponds to an aggregate SLD, which is equal to that of the solvent used in the fitting. This therefore suggests that the large aggregates seen in these samples are either contrast matched out perfectly in the d-C_{16}TAB samples or there is an isotopic effect under heating meaning there are no large aggregates in the deuterated samples. This means determination of the ellipsoidal aggregate size is only possible with a small amount of the hydrogenated data. This coupled with the lack of USANS data means that these values are possibly anomalous and therefore would require a repeat to confirm the structure.

5.5 Comparison of data with other techniques

One disadvantage of USANS is that there are very few instruments around the world. As there are none in the UK this means that performing USANS experiments is difficult due to the cost associated with sending experimenters to facilities outside Europe. However with the recent development of Target Station 2 at the ISIS Pulsed Neutron and Muon Source in Chiltern, UK an alternative to USANS is now available in the form of Spin-Echo Small Angle Neutron Scattering (SESANS) as one of the possible variations of the OFFSPEC instrument.

As described in chapter 2, USANS and SESANS are able to give similar information about the sample. An advantage of these differences is that SESANS experiments are faster than USANS experiments meaning more samples can be run over a shorter amount of time. The disadvantage, however, is that because SESANS is still a relatively new technique with a limited user community, analysis tools are still to be really developed meaning complex structures are hard to analyse.

The simplest model, in most cases, to fit is that of a sample of discrete sized non-interacting hard spheres. The mathematical function to fit this model has been

determined by Andersson et. al.[92] and had previously been converted to a fit function for use with IgorPro within the group. Figure 5-11 shows the SESANS pattern collected on OFFSPEC for 0.05M $7C_{16}$TAB:3SDS with no polymer. The dashed line on this plot shows the best fit obtained when using the sphere model discussed above. It can be seen that although the sphere model approximates the fit, it is too steep at low spin echo length indicating that the sample is not composed of spheres.

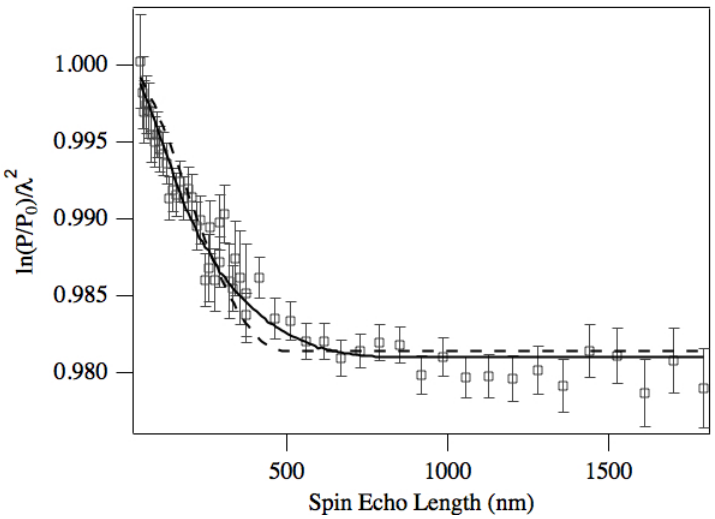

Figure 5-11. SESANS of 0.05M $7C_{16}$TAB:3SDS with no polymer. Full line shows best manual fit of an ellipsoid, dashed line is best computer fit of a spherical model.

As the sphere model did not fit the data and after analysis of the USANS data it was obvious that the aggregate structure in the solution was different, probably ellipsoidal, therefore a different fit function was needed. With the help of the instrument scientists on OFFSPEC the mathematical function for the depolarisation of a neutron beam due to ellipsoidal aggregates[92] was converted into a fit function for use with IgorPro, more detail given in appendix 4. Due to lack of experience writing C code and working with IgorPro XOP's, use of the function in conjunction with the fitting approach taken by Igor Pro does not fully work therefore instead of allowing the fit to be performed by the program, only a manual fit is currently possible. It is possible to see from Figure 5-11, where the full line is the calculated ellipsoidal fit, that even a manual fit of the data using this fit function is able to give a better approximation to the data than was possible with the model for a sphere, particularly at low spin echo length.

All the SESANS data was fitted manually to the ellipse model and the results are given in Table 5-9. The parameters in the fitting model are the scale, the radius of the axis of rotation, the ellipticity of the ellipse and the SLD contrast. As with the SANS and USANS fitting, the SLD contrast and the scale have similar effects on the model therefore the SLD contrast was held at 6.73×10^{-6} Å^{-2} with any error in this

value being corrected for by the scale. As well as fitting the scale, the radius of the axis of rotation and the ellipticity of the ellipse were also fitted. Between these two parameters the ellipse dimensions are determined, with an ellipticity of greater than one indicating an oblate ellipse and an ellipticity of less than one indicating a prolate ellipse. The fit for 0.05M $7C_{16}$TAB:3SDS with no polymer is shown in Figure 5-11, the other fits are shown in Figure 5-12.

It should be noted that the instrument could be set up to measure different spin echo lengths. As the range of spin echo length needed was unknown at the beginning of the experiment, two separate patterns were needed to measure the full spin echo length pictured in Figure 5-11 and Figure 5-12. The variation is in the angle of the magnetic field, known as the pole shoe angle, was either 55° or 85°. The difference between the two setups is shown in Figure 5-13.

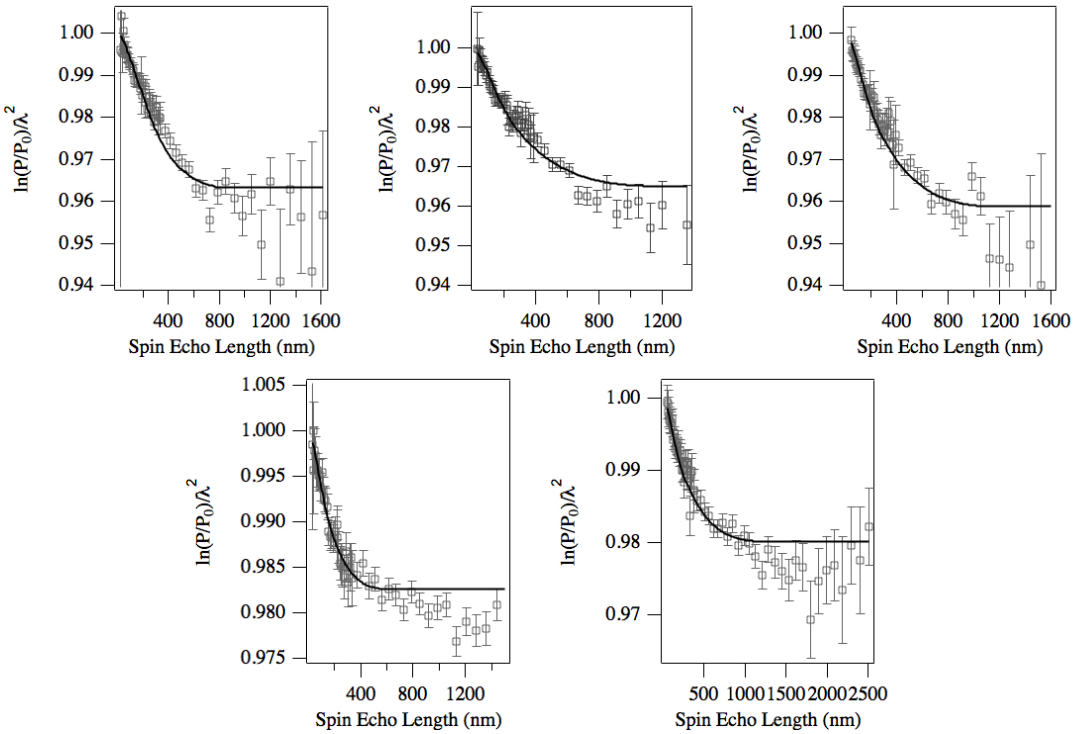

Figure 5-12. Fitting of SESANS data. Top line 0.05M $6C_{16}$TAB:4SDS with, left to right, no polymer, SPEI and LPEI. Bottom-line 0.05M $7C_{16}$TAB:3SDS with SPEI (left) and LPEI (right). Solid lines represent lines of best through the data.

0.05M $6C_{16}$TAB:4SDS			
	No Polymer	SPEI	LPEI
R(a) (Å)	1500	1050	1050
Ellipticity	3.2	6	6
Calculated R(b) (Å)	4800	6300	6300

0.05M $7C_{16}$TAB:3SDS			
R(a) (Å)	1000	700	1000
Ellipticity	4.5	4.5	6.5
Calculated R(b) (Å)	4500	3150	6500

Table 5-9. Fitting results from 0.05M surfactant solutions with and without polymer collected on OFFSPEC. Calculated R(b) values are for easy comparison to USANS fitting results. Error in R(a) is ±300Å, error in ellipticity is ±0.5.

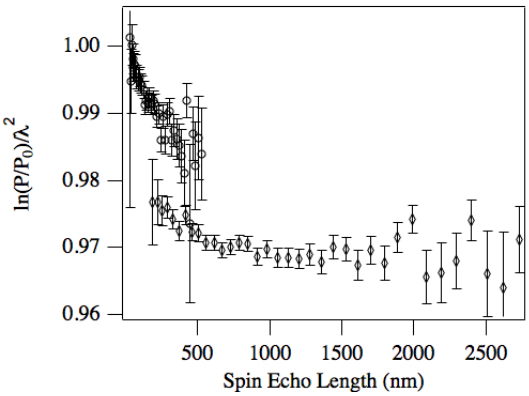

Figure 5-13. SESANS of 0.05M $7C_{16}$TAB:3SDS. Circles indicate the sample was collected with a pole shoe angle of 85°. Diamonds indicate the sample was collected with a pole shoe angle of 55° and has been offset for clarity.

Manual fitting of multiple parameters in a recursive fashion, similar to that of a computer program, is much slower and far less accurate than a computer in determining the best fit of a line through the data points. Therefore the uncertainty associated in fitting this data is much higher than the SANS and USANS data fitting, however it is still possible to see trends in the data. The main point to notice is that in all cases the ellipticity is greater than one confirming the results seen previously that these aggregates are oblate in structure. The spin echo lengths studied here are high enough that there is no affect from the lamellar structure, however the ellipticity in all cases is much lower than seen in the USANS data. With the ellipticity being lower the calculated R(b) values are also lower. Even if the ellipticity values were increased, this would lead to a reduction in R(a) value rather than an increase in R(b) because the point at which the gradient of the slope becomes 0 is indicative of the size of the aggregates and this can clearly be seen to be lower than 10,000Å. The calculated R(b) values however are also determined in part by the R(a) values which, in contrast to the R(b) and ellipticity values, are slightly larger than those determined

by USANS fitting. Although these R(a) values are larger than in the USANS fitting they are of the same order of magnitude. Although few studies have been performed using SESANS a comparison of SESANS and USANS on the same system has been performed by van Heijkamp et al and shown that the results are comparable.[145] Given the manual nature of the fitting it is possible that the difference in aggregate size is due to error in fitting rather than a real feature of the data.

Comparing the general results from the SESANS data with the USANS and SANS data collected at NIST and the ILL, discussed earlier, it is important to note that the general conclusion from all instruments is that the structures are large ellipses. These results are similar enough to the results collected previously to say that when a more robust analysis package for SESANS data is created that SESANS will provide a useful tool for UK based researchers studying aggregates larger than can be studied on SANS instruments.

5.6 Low Concentration Surfactant Solutions

Due to the high viscosity of the surfactant solutions studied above it was decided to perform some experiments at a lower total surfactant concentration. This would then give some comparison with the results already in the literature.[133-135] It was hoped that the lower viscosity of the solution would allow the structures to reach a reproducible equilibrium. Due to time constraints, and as these experiments had secondary importance to those discussed above, only SANS experiments were performed on these solutions.

The solutions studied were all using the surfactant ratio of $6C_{16}$TAB:4SDS and were at a total surfactant concentration of 0.01M. The polymers used in this study were SPEI, LPEI and PAAm at a concentration of 1wt%. At the same time experiments were performed with a total surfactant concentration of 1mM with no polymer and with PAAm but these samples have so far not been able to be fitted, because a model has not been found, so will not be discussed here.

The models used to fit the data vary between the different samples measured. The SPEI and PAAm sample can both be fitted with the same summed ellipse and lamellar sheet model that has been widely used above. The sample with no polymer however requires a model that is a summation of two different ellipses, as the scattering gives a curved pattern in the region between $Q = 0.03Å^{-1}$ and $Q = 0.2Å^{-1}$. Finally the LPEI sample is very different from previous samples in the Q range from $0.001Å^{-1}$ to $0.01Å^{-1}$ and this area cannot be fitted, however the rest of the data fits well to a lamellar paracrystal model. Examples of three different fitting models compared to the real data are shown in Figure 5-14 with fitting results given in

Table 5-10.

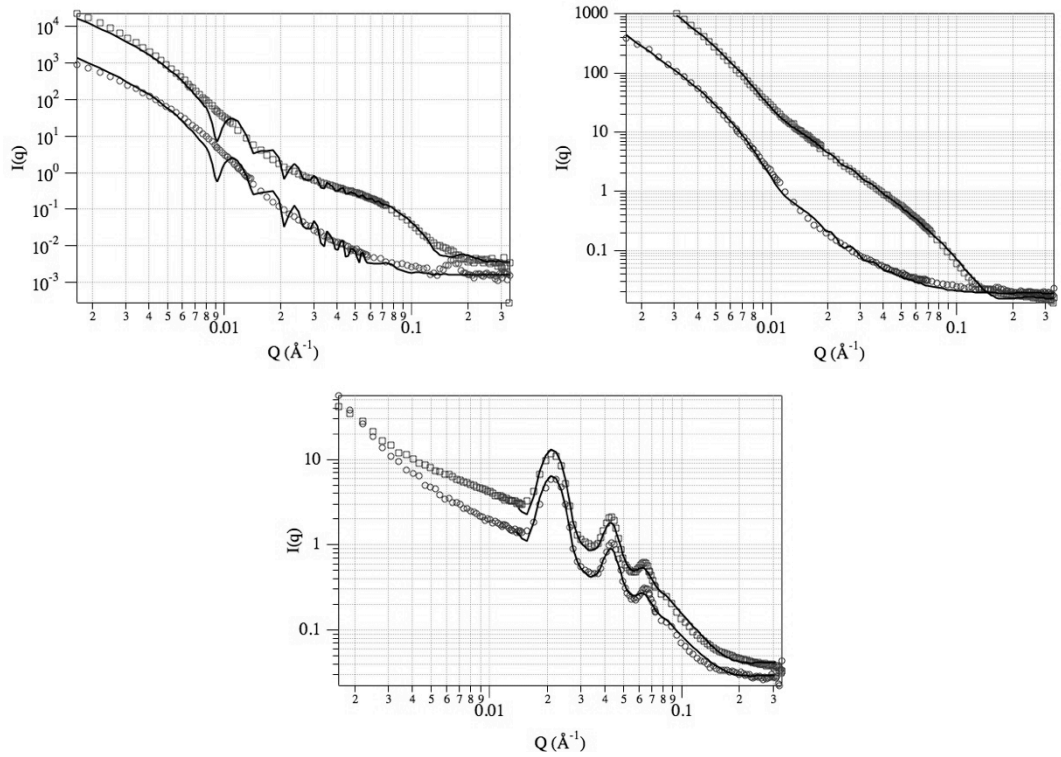

Figure 5-14. 0.01M 6C_{16}TAB:4SDS with no polymer (top left), PAAm (top right), and LPEI (bottom). Squares represent hydrogenated surfactant samples, circles represent samples with deuterated C_{16}TAB. Lines represent lines of best fit for the models discussed in the text.

The sample with no polymer has a large ellipse, which is very similar to the results discussed previously. However, as mentioned above, instead of using an ellipse/lamellar model, the model was two different ellipses with the smaller ellipse appearing to be almost spherical. This is also supported by the ratios of C_{16}TAB to SDS in the different structures as the large structure is has a ratio 68:32, similar to the results seen previously, but the small structure has a ratio of 89:11, which means the small structure will be similar to a C_{16}TAB micelle.

		No Polymer		SPEI		LPEI		PAAm	
Large Ellipse	R(a) (Å)	420		310		a		310	
	R(b) (Å)	13500		6300		a		6000	
Small Ellipse / Lamella	R(a) (Å)	25		a		a		a	
	R(B) (Å)	33		a		a		a	
	Thickness (Å)	a		30		27		35	
	Number of Layers	a		a		3.61		a	
	Layer Spacing	a		a		285		a	
	Polydispersity	a		0.10		0.11		0	
		C_{16}TAB	SDS	C_{16}TAB	SDS	C_{16}TAB	SDS	C_{16}TAB	SDS
Surfactant Ratio	Large Ellipse	68%	32%	73%	27%	a	a	61%	39%
	Small Ellipse / Lamella	89%	11%	76%	24%	29%	71%	79%	21%

Table 5-10. Fitting results from simultaneous fitting of two contrasts of SANS data for 0.01M 6C_{16}TAB:4SDS with different polymers. Contrast 1 is hydrogenated surfactant in D_2O, contrast 2 is deuterated C_{16}TAB and hydrogenated SDS in D_2O. (a) The model used to fit this sample did not require this parameter. Errors in large ellipse R(a) values are ±50Å, R(b) values are ±2000Å. Errors in small ellipse R(a) and R(b) values are ±2Å. Errors in lamella thicknesses are ±2Å, number of layer ±0.01, layer spacing ±5Å, polydispersity values 0.05.

The samples with SPEI and PAAm are much more similar to the other samples discussed in this chapter and have been fitted to the same summed ellipse and lamellar model. The ellipse dimensions are significantly lower than have been seen previously although this is not surprising given the lower concentration of surfactant. The ratios of C_{16}TAB to SDS are also similar to those seen in the higher concentration samples although the 6:4 in the PAAm ellipse is slightly different from the 7:3 seen previously.

As mentioned previously the most different sample is that of 0.01M 6C_{16}TAB:4SDS with LPEI. This sample fits very well to a lamellar paracrystal above Q = 0.01Å^{-1}, as can be seen in Figure 5-14, however below Q = 0.01Å^{-1} the model does not work. So far no models have been found that accurately represent this fitting and without the USANS data, which provided the important extra detail previously, it is unclear what the larger structure of this sample is.

5.7 Addition of additives to surfactant solutions.

A further study performed with this system was to test the ability of these surfactant aggregates to encapsulate other species. This study had two purposes, firstly to link in with the study discussed in chapter 4 and provide some extra continuity in this project. The second purpose was to scale up the encapsulation of the different additives because films made with C_{16}TAB:SDS have been seen to be much thicker and more robust than the cationic surfactant films.[71]

Given these films have been seen to form with a wide range of polymers and variation in aggregate charge it appears that they may be less sensitive to change than the cationic surfactant films. The potential use of cat-anionic vesicles for pharmaceutical uses has already been established.[119] If these films are less sensitive to change then it is possible that they will also form with slightly varied surfactants such as hexadecyltrimethylammonium tosylate with sodium dodecylbenzenesulfonate, which have previously been shown efficient long-term storage devices for dyes.[146]

This study was performed using both hydrogenated and deuterated cyclohexane and cyclohexanol in fully hydrogenated surfactant solutions, as in chapter 4. The solutions studied were both 6:4 and 7:3 C_{16}TAB:SDS with no polymer, SPEI or LPEI. The total surfactant concentration used was 0.05M and the polymer concentration was 1wt%, these values are in line with the other results in this chapter but different from chapter 4. However, as in chapter 4, the additive was added to give 30vol% in the surfactant micelle. As stated in chapter 4, this value is used so

results are comparable to previously published work however this value can also be thought of as 53mol%.

This data was collected on the LOQ instrument at ISIS giving a Q range of 0.007Å^{-1} to 0.3Å^{-1}, which is much smaller than the Q ranges fitted previously. Due to this it is not possible to fit the larger aggregates limiting the Q range that can be fitted in the majority of samples to between Q = 0.02Å^{-1} and Q = 0.3Å^{-1}. Figure 5-15 shows the fitting of a lamellar model to 0.05M 6C$_{16}$TAB:4SDS with no polymer and with cyclohexanol. The models used to fit the data are either the dilute lamellar[113] or the lamellar paracrystal.[112] The model used to fit the data is given along with the percentage encapsulation as determined by fitting in Table 5-11.

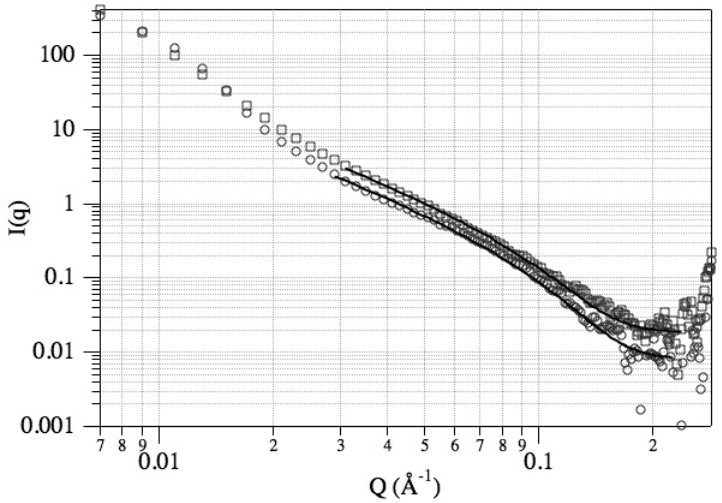

Figure 5-15. 0.05M 6C$_{16}$TAB:4SDS with no polymer and added cyclohexanol. Squares indicate the sample with hydrogenated cyclohexanol, circles the deuterated cyclohexanol. Line is of best fit for a dilute lamellar model.

	6CTAB:4SDS		7CTAB:3SDS	
	Cyclohexane	Cyclohexanol	Cyclohexane	Cyclohexanol
No Polymer	2%[c]	16%[c]	8%[d]	4%[c]
SPEI	a	5%[c]	4%[d]	a
LPEI	7%[d]	9%[c]	-6%[b,d]	-6%[b,d]

Table 5-11. Fitting results for the percentage encapsulated in different surfactant/polymer solutions with different additive. (a) sample could not be fitted, (b) deuterated sample scatter more than hydrogenated sample, (c) sample fitted with a dilute lamellar model, (d) sample fitted with a lamellar paracrystal model.

This data shows encapsulation amounts similar to those seen in in cationic surfactant solutions. This is unsurprising because the micelle core is a mixture of 16 carbon atom chains and 12 carbon atom chains in both cases. As so few samples were

tested, it is difficult to draw conclusions. This is made even harder due to the two samples that could not be fitted. In these samples there was a significant structural change between the hydrogenated sample and the deuterated sample meaning one model could not fit both patterns. In general, the fact that these solutions are able to encapsulate different species is a good sign for potential future uses of films prepared using surfactant mixtures.

5.8 Conclusion and discussion

As mentioned previously relatively little work has been performed on the cat-anionic surfactant system for film formation. Therefore one of the aims of this thesis was to expand the current knowledge about this system in an effort to further understand the formation of these surfactant/polymer films. As with the results in chapters 3 and 4, the study was performed in two steps, the first being studying the solutions that make the films and the second step was studying the films themselves. Due to the number of experiments performed and the complexity of the system the aim of this chapter was to study the solutions. More specifically than this, the aim was to study the effect of different ratios of C_{16}TAB to SDS on the solutions and also study the effect of different polymers on the solutions.

The overall results from this chapter show that the solutions of C_{16}TAB:SDS with and without polymer are more understood than they were previously. Previously there was no knowledge of the structures in the solution and now there is an understanding, although precise determination of solution structures is not possible due to the complexity of the structures in solution. Variation in surfactant ratio appears not to have a major role on the structures in solution, which is probably due to non-equilibrium structures caused by the high viscosity of the surfactant solutions. Variation in structures due to the effect of different polymers however does appear to occur which may impact the structures of the films, to be discussed in chapter 6.

The starting point for this study was the work performed by O'Driscoll et al.[71] However in this previous work the main emphasis was on the films created by these mixtures and not on the solutions themselves. One piece of work that was not published was the structures of aggregates seen in solution using cryo-SEM. It was these images, along with the obvious opaque nature of the solutions, which first suggested that these solutions were made up of larger aggregates.

Other previous work in this area has been limited so far, with the majority of the work being performed on symmetrically tailed surfactants. However the few studies

into C_{16}TAB:SDS solutions that have been published show that large mixed vesicles are formed close to the equi-molar line in the phase diagrams with more single surfactant rich aggregates being formed the further from the equi-molar line the study was performed.[133-135]

Given the lack of any previous research at this particular concentration and surfactant ratio the obvious starting point was therefore the structure of the mixed surfactant solution with no polymer. It was decided that a ratio of 60:40 C_{16}TAB:SDS should be used as this was the original surfactant ratio and allowed comparison of data. The original choice had been made due to visual observations in which it was decided that the 60:40 ratio provided slightly thicker films at a slightly higher rate than other ratios. However during the course of this thesis these observations have been bought into question. The more experiments that were performed, it became clear that there was very little difference, visually, to the film made from 60:40 and 70:30. However 70:30 surfactant mixtures were easier to handle because the viscosity did not increase in the same way that it did in the 60:40 ratio sample, and usefully there was less likelihood of phase separation in the 70:30 samples than the 60:40 samples. For this reason, as well as studying 60:40 ratios of C_{16}TAB:SDS it was decided that 70:30 ratios should also be studied.

The initial experiments were performed on LOQ at ISIS however it was not possible to fit the full data set with a single model. With this result it was decided that a larger Q range was needed therefore SANS and USANS were performed at the NIST Centre for Neutron Research. These results showed that the scattering could be thought of in two separate areas. At low Q the scattering was of a very large ellipsoid, while at high Q the structure was more of a lamella. In both the 60:40 and the 70:30 ratio solutions the lamella results are quite consistent, in the ellipse however there is some variation with the size of the ellipse in the 60:40 sample being slightly larger than the 70:30 sample. This difference in size of the aggregates may explain some of the lack of viscosity in these samples.

Two potential structures have been suggested for these structures. The first is a mixed structure of large uni- and multi- lamellar vesicles along with a separate lamellar phase, with the different phases being made up of different ratios of C_{16}TAB:SDS. The second structure is a large flattened bilayer vesicle where on short length scales in the flattened region the scattering approximates a lamella bilayer, where as at long length scales the full, flattened ellipsoid structure can be seen. The difference in ratios of C_{16}TAB to SDS in this single structure is then explained by rearrangement of the surfactants to create the curved edges.[128]

This second structure would partially agree with previously reported data,[133-135, 139] including the unpublished SEM images collected by O'Driscoll. In these reports the structure is generally considered to be a vesicle, however it is never clearly stated whether this should be a multi-lamella vesicle or just a bilayer vesicle. This would therefore agree with the data reported here, except for the fact that the vesicle is compressed. This however may be due to the high concentration used in this report. Another reported conclusion from the previous data that is fairly consistent is the size of the aggregates at around 700nm at the largest.[133] This value again is probably an effect of the lower concentration of the previous studies in comparison to the one performed in this thesis.

As well as deciding to study the surfactant solutions at a ratio of 70:30, it was also decided to study the same solutions but under different preparation techniques. As mentioned previously the 60:40 ratio of surfactants leads to a large increase in viscosity after the solution has been mixed. This same increase in viscosity is not seen in the 70:30 ratio of surfactants however the viscosity of the 70:30 ratio surfactant solution is still relatively high. To combat any effects caused by the viscosity, it was decided that an increase in temperature should make the surfactant more soluble and therefore the aggregates smaller and that should reduce the viscosity. The temperature chosen for these samples was 70°C and as expected the increase in temperature made the surfactant aggregates smaller and the solutions appeared to be much less viscous. However it must be noted that the instruments were temperature controlled to 28°C therefore it is likely that the aggregates shape would be affected by the cooling during the measurement.

Interestingly studying the relative ratios of C_{16}TAB:SDS in the different parts of the structure shows that as well as creating smaller aggregates, the solutions prepared at 70°C have a more homogeneous mix of C_{16}TAB:SDS in the two structures within the solution, where as the samples prepared at room temperature showed a large variation in ratios of C_{16}TAB:SDS. This result leads to the conclusion that the aggregates in the room temperature sample are kinetic structures frozen into place during the mixing of the two surfactants. The lower viscosity and the more soluble nature of the surfactants in the higher temperature sample are then more likely to form equilibrium structures. Interestingly this ratio of C_{16}TAB to SDS starts to approximate a mixture of 3:1 C_{16}TAB:SDS that has been previously seen, in a different system, to be important for the solution properties.

After concentrating on the ratio of C_{16}TAB to SDS in the solutions the next step was to study the effect of the addition of polymer to these solutions. The polymers used were a high and a low molecular weight of PEI and PEO, referred to as LPEI, SPEI,

LPEO and SPEO respectively and a single molecular weight of PAAm, which is similar to the molecular weights of the other low molecular weight polymers. Of these samples, when mixed with a 60:40 ratio of C_{16}TAB:SDS they can all be fitted with the same uniform ellipse and dilute lamella model, except the LPEO sample. In the LPEO sample ripples are seen in the SANS plot of the data suggesting an interaction between the lamella bilayers therefore the model was amended slightly to use the lamella paracrystal model.

When the polymers were mixed with the 70:30 ratio surfactant solution the low molecular weight polymers were still able to be fitted with the ellipse and dilute lamella model, the LPEO and the LPEI samples however needed the lamellar paracrystal again. The explanation for this is probably due to the higher molecular weight polymers interacting with more bilayer and bringing them closer together. Why the LPEI does not need the lamella paracrystal model when mixed with the 60:40 ratio solution is unclear however it may be an indicator of a stronger interaction between the surfactant aggregates and PEO.

The lamella thicknesses in all samples are very similar, once again suggesting this is a fundamental property of these surfactant solutions. The aggregate sizes with SPEI and SPEO are both very similar with both surfactant mixtures and these results are also similar to the results with no polymer. There may be a slight tendency for the SPEI sample to have slightly smaller aggregates however the results are within error so this cannot be confirmed. The LPEI and LPEO samples in both cases also show very similar results with all aggregate sizes being slightly larger than the aggregates with no polymer. Given the increased interaction if the ellipse was a bilayer vesicle this would lead to smaller aggregates. However as the aggregates are larger, the ellipses are either made up of a number of lamellar bilayers or the addition of the polymer allows the vesicles to undergo a structural rearrangement to form multi-layer vesicles. Interestingly the number of interacting bilayers causing the ripples in the 60:40 LPEO sample is relatively low, at 1.67, while with the 70:30 ratio both the LPEO and LPEI samples have around 2.5 interacting bilayers. This suggests that actually the LPEO and LPEI interact with the aggregates in a similar manner. A closer look at the patterns in Figure 5-10 shows that the LPEI sample does have ripples, however they are not quite strong enough for the lamellar paracrystal model to fit.

The other polymer studied was the PAAm. This gave very interesting results as it had been suggested that there was very little interaction between this polymer and the surfactant, given the lack of effect the polymer had on the film structure as reported by O'Driscoll et al.[71] However the aggregates seen in the presence of

PAAm are the largest reported. A possible explanation for this is that the polymer is able to get inside the vesicle but as there is no interaction therefore the vesicle is swollen. It is probably not a change to multi-lamella vesicles as seen in the LPEO and LPEI case because there is not interaction of bilayers.

If this explanation for the PAAm sample is correct then the trend in the results could be described as follows. The PAAm has no interaction with the aggregate so causes the vesicles to swell. With no evidence of interaction of the bilayers it is unlikely to be a multi-lamella vesicle. The SPEO and SPEI also show no interaction of bilayers so are also probably bilayer vesicles however there is probably some charge screening allowing the vesicles to collapse slightly to an equilibrium size similar to that seen in the no polymer samples. The most interaction is seen in the LPEO and LPEI samples where the interacting bilayers and the increased size of the micelles probably indicates good change screening in the aggregates allowing them to become multi-lamellar vesicles.

On heating these solutions to try and allow them to come to equilibrium, an error was encountered with the deuterated samples. The deuterated USANS data did not line up with the SANS data. This suggests that one of the surfactants has decomposed at the high temperature. The main difference seen in the patterns is in the deuterated data therefore this suggests it is the C_{16}TAB that has decomposed. However it is more likely that it is the SDS that has decomposed, as it is known to be unstable at high temperature.[142] The reason it decomposes more with the deuterated C_{16}TAB is that problems have been found with impurities in some batches of C_{16}TAB from one of the suppliers, which are usually delivered with little time to purify them. One possible impurity in the C_{16}TAB synthesis is trimethylamine, which would make the solutions highly alkali, which would increase the decomposition of the SDS.

The results were fitted, without the use of the USANS data, and the results for the 60:40 ratio samples show an overall decrease in aggregate size, as was reported for the surfactant only system which was measured with two complete contrasts. The difference in the different polymers is the same as described above for the room temperature samples.

The 70:30 ratio samples however were very different. The LPEI, LPEO and PAAm could not be fitted and the SPEO and SPEI samples showed interacting bilayers and vesicles much larger than anything else so far reported. The vesicles studied here had ellipse dimensions of twice the size of the ellipses in the system with no polymer. This suggests that the SPEI and SPEO at higher temperatures cause a structural

rearrangement to multi-lamellar vesicles however the polymer is not large enough to screen the charge as effectively as the high molecular weight polymer could be expected to therefore the overall increase in aggregate size is quite dramatic.

As well as studying these samples with SANS and USANS, it was decided to test out the new technique of SESANS. Only a small number of samples were studied as it was not clear what results could be expected from the samples. The fitting was problematic due to a lack of previously written fit functions however with the help of the instrument scientists at ISIS a fit function was created for use in IgorPro and the data was able to be fitted. Although we expected the sample to show ellipsoidal structure, the first fit was performed to a sphere and it was clear that this fit did not work. However the use of the ellipsoidal model was able to fit to the data relatively well, even though a manual fit was necessary. What was found was the structures were slightly small, but very similar in shape to the previously studied samples. This means that with some more refinement and time taken by a number of researchers to properly develop the fitting functions for SESANS it is possible that SESANS will become a highly affective alternative to USANS which is currently unavailable in the UK.

The final two sets of results were small studies, firstly on the use of lower concentration surfactants, and secondly on the ability of these solutions to encapsulate different species. The low concentration samples did not show any trends, this is possibly due to the lack of USANS data meaning it is hard to fully characterise the system. However there appear to be similar structures indicating there is potential for these solutions to form similar films and with the lower viscosity of the solutions, the solutions will be easier to work with.

The addition of additive to the sample was to try and bridge some of the work described in chapter 4 with this work. This was a fairly limited study just performed on LOQ. Due to this, the full data set could not be fitted and therefore the results don't necessarily represent the complete encapsulation. However the results do compare fairly well to the results discussed in chapter 4 and the values are in the same region as has previously been reported.[119]

Looking at the results overall, the conclusions that can be drawn are that the interaction of C_{16}TAB with SDS in the cationic rich part of the phase diagram leads to very large aggregate structures which appear to be bilayer vesicles. This is comparable to previously reported results.[133-135, 139] The addition of polymer appears to suggest that the most important feature of the polymer is the molecular weight. This is from the fact that the LPEI and LPEO behave similarly and the SPEI and

SPEO behave similarly. The results from the PAAm are slightly contradictory as it has a similar molecular weight to the SPEI and SPEO. Therefore this may be explained by the ability of the polymer to interact with the aggregate and that polyacrylamide is less able to interact with the aggregate than the SPEI and SPEO. If this interaction could be understood then it would probably help expand the possible polymer/surfactant combination that could be used to form films.

From these results it would be useful to know a number of things, firstly how reproducible the experiment is. Due to time constraints no repeat experiments were performed at the same time. Secondly, how do the samples change over time? Given some samples were prepared for a SANS experiment followed by a USANS experiment it is possible that the USANS sample has a different structure from the SANS sample as they were not run at exactly the same time. Although these experiments should be performed at the same facility it would be useful to know in more detail how reproducible these experiments are at different facilities. These results show differences between the same samples at different facilities, however it is unknown whether these differences are caused by inconsistencies in the mixing method, the temperature of surfactants and polymers before mixing, or other more difficult to control factors such as impurities in the solvent or ambient humidity where the samples are stored.

Finally it is worth saying that with the cost and time requirements making USANS experiments prohibitive the availability of SESANS as an alternative will be very useful for future work. However before this can really happen analysis or modelling tools will probably need to be available so new users can confidently compare data from SANS and SESANS experiments.

6 Cat-anionic Surfactant Films

In chapter 5 the use of the cat-anionic surfactant system for forming films was discussed. It was mentioned that these films have the advantage over the cationic surfactant film as they can be formed with a range of different polymers. As little research had previously been performed on these films, it was decided to start by examining the solutions. The results, discussed in chapter 5, show that the solutions are made up of large aggregates made up of a mixture of C_{16}TAB and SDS. Control over these aggregates cannot be obtained by changing the ratio of C_{16}TAB to SDS, however the addition of different polymers did show a change in the solution structure suggesting that the surfactant polymer interactions are important for these mixtures.

Following on from chapter 5, the aim was to take the solutions discussed in chapter 5 and study the films that are made at the interface. Once again particular note was placed on two areas, the first was the effect of changing the ratio of C_{16}TAB to SDS and the second was the effect of different polymers. The aim of using different polymers is to make these films more biocompatible and therefore increase the potential applications, such as drug delivery devices in bandages.[119, 146] It is hoped that by understanding how the films form and how the structures in the films relate to the surfactant phase in the bulk solution that it will then be possible to control the film formation. The most useful form of film control would be structural control to enhance applications such as absorption, encapsulation and release of different species.

The main polymers studied were the same polymers studied in Chapter 5, which are the two molecular weights of PEI (2,000Da SPEI, and 750,000Da LPEI), as these are the standard polymers used through out this thesis and in previous work within the group[59, 66-68]. In addition, two molecular weights of PEO (10,000Da SPEO, and 100,000Da LPEO) are studied, as this is a biocompatible polymer that can be purchased in two molecular weights to test the effect of molecular weight as a comparison to the two molecular weights of PEI. Both these polymers can then be compared to the previously reported PAAm (10,000Da).[71, 102]

The downside to studying commercial polymers is that you are limited to the molecular weights of polymer that are available and you are often not certain of the physical nature of the polymer. This is particularly true of the two molecular weights of PEI being used as, although the nominal molecular weight is known, there is very little information available as to the extent of branching or polydispersity, see appendix 1 for more details. To help clarify if there is an effect caused either by the

molecular weight or the extent of branching of the polymers on the films, like the change in structure of the solutions seen with LPEI and LPEO in Chapter 5, a postdoctoral researcher was employed as part of the wider research project into these films. The initial aim for the postdoctoral researcher was to synthesise a range of molecular weights of linear PEI to get a more accurate understanding of the effect of molecular weight of these polymers on film formation and whether the polymer branching was required for film formation. Following this, the aim was to create branched PEI with varying molecular weights and degree of branching to study the effect of different degrees branching of the polymers on the films. Although the postdoctoral researcher did all the polymer synthesis, the film formation studies and analysis of the resultant structures were performed jointly by the postdoctoral researcher and the candidate, with the candidate being responsible for structure determination and comparisons with studies of the commercial polymers.

The initial study of these films, reported in the literature by O'Driscoll et al, [71] used a mixture of 6:4 C_{16}TAB to SDS and used the polymer polyacrylamide (PAAm). This study focused on whether films could be formed from with varying ratios of C_{16}TAB:SDS. It was found that a ratio as cationic rich as 97:3 was able to form films with PAAm, although they were thin and took a very long time to form, ~48 hours. The rate of film formation increased as the ratio of C_{16}TAB:SDS was altered to 60:40 where film formation took ~10 hours. Visually, however, the films were very similar at ratios between 80:20 and 60:40 The film structure of the 60:40 film with PAAm was determined using grazing incidence x-ray diffraction (GIXD) and a series of rings was seen corresponding to a well ordered lamellar phase. Interestingly this lamellar phase was exactly the same as the concentrated surface layer that was measure from a 60:40 C_{16}TAB:SDS solution measured without polymer. The difference between the two, however, is that the film can be removed from the surface where as the solution without polymer appears to form a highly concentrated surface layer that has long range order but no structure to hold it together like a film.

This result was attributed to the fact that there was very little interaction between C_{16}TAB:SDS aggregates and the PAAm. This meant that the PAAm was acting just as a supporting matrix holding the aggregates together. This idea was then taken forward and a study was performed looking at the effect of changing the surfactant tail.[102] By changing the cationic surfactant from C_{16}TAB to C_{14}TAB and C_{12}TAB a reduction in film structure was seen. This was very similar to the effect on C_nTAB-PEI films previously reported by O'Driscoll et al.[66] As well as a decrease in ordering, as seen by the loss of all but the first diffraction peak, there is also movement in the diffraction peak position indicating a shrinking of the structure. This shrinking corresponds well to the expected alteration of micelle size due to the

decrease in average tail length caused by changing C_{16}TAB to either C_{14}TAB or C_{12}TAB.

Outside of the work by O'Driscoll et al there are two papers currently in the literature that deal with mixtures of C_{16}TAB with SDS and report studies at the interface. These papers are by Tomašić et al[134] and by Tah et al.[136] In the study by Tomašić et al the surface related properties that are reported include the surface mole fraction of SDS in the monolayer formed at the surface. This value is reported to be 0.48 over a wide range of bulk mixing ratios. This is supported by similar research where cat-anionic monolayers at the air-solution interface preferentially form as equi-molar layers over a wide range of bulk mixing ratios.[147] Interestingly, although Tomašić et al report their work up to 0.01M, they do not report the appearance of a concentrated phase at the solution interface. Given there is no polymer in the system they are studying this is not necessarily surprising as the surfactant only layer is very difficult to spot with the naked eye. The ternary phase diagram for C_{16}TAB:SDS at lower concentrations than studied in this thesis is shown in Figure 5-1.

In the study by Tah et al, the emphasis was on studying the surface aggregation at various ratios of C_{16}TAB to SDS. This study differs from Tomašić et al as the aggregation of C_{16}TAB to SDS at the interface is inline with the mixing ratio rather than an equi-molar ratio. The work by Tah is also of interest to this study as they report large aggregates formed as Langmuir-Blodgett films (LB) on glass cover slips using a mixture of 65:35 C_{16}TAB:SDS. Atomic force microscopy of these LB films gives aggregates of roughly 2μm, which is similar to the size of the aggregates reported in the C_{16}TAB:SDS solutions in chapter 5. The visibility of these aggregates so clearly is probably due to the low concentrations, less than 1mM for each surfactant, meaning that the vesicles are well dispersed instead of forming a contiguous film.

6.1 Air/Liquid Films

6.1.1 Commercial Polymers

As stated above the commercial polymers studied were two molecular weights of PEI, two molecular weights of PEO and one molecular weight of PAAm. They were studied with varying ratios of C_{16}TAB:SDS from 6:4 to 9:1. Some of these results have previously been published by the candidate,[102] however the discussion here is based on the published data as well as newly collected data and understanding of the system.

6.1.1.1 PEI

When studying the cationic surfactant films it was found that the initial film formation occurred very quickly therefore the film formation processes could never be studied. However the films formed with C_{16}TAB:SDS had previously been seen to form much more slowly, therefore structure formation in these films was studied using the time resolved off-specular x-ray reflection technique discussed in chapter 2.

Due to the experimental setup, the measurement is not started immediately after pouring and in this sample there are no measurements for the first 10 minutes. In the sample of 6C_{16}TAB:4SDS with SPEI once the experiment is started a strong narrow peak is visible at Q = 0.17Å^{-1}. This peak does not change over the course of the experiment therefore suggesting that the structure at the interface forms within the first ten minutes of the experiment, although the solid film is not visible at this time.

In all the time resolved, off-specular reflection measurements from ID10B the specular reflection peak should be at 0.18Å^{-1}, however in all cases it is not visible due to either surface roughness or the high intensity of the scattered peak that has already formed. Given there is no Yoneda wing, which is usually an indication of surface roughness, it is likely that the intensity from the scattering is too strong and therefore hides the smaller peaks.

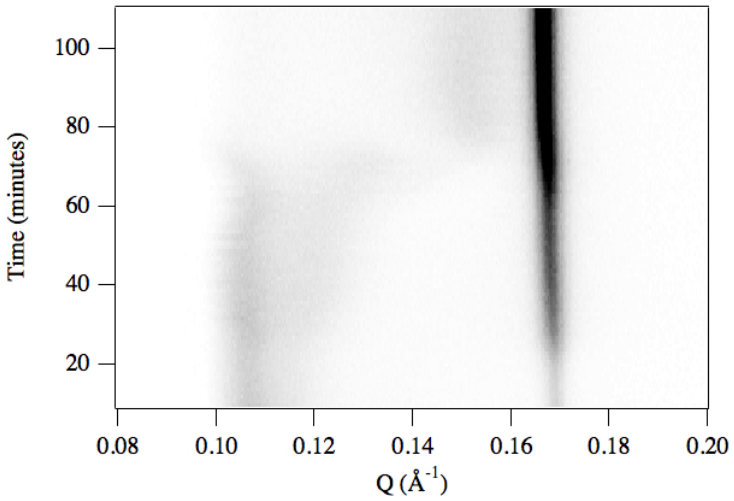

Figure 6-1. Time resolved off-specular scattering from 6C_{16}TAB:4SDS with LPEI.

Although the sample of 6C_{16}TAB:4SDS with SPEI showed no change over the course of the experiment, the sample of 6C_{16}TAB:4SDS with LPEI did show some structural change and this is shown in Figure 6-1. As in the SPEI sample, the measurement was started 10 minutes after pouring the solution, however in the LPEI

sample it is possible to see that there is some structure formation, indicated by a weak peak at 0.106Å^{-1}, although this becomes weaker over the first 60 minutes of the experiment. During this 60 minutes, as well as the 0.106Å^{-1} peak becoming weaker, a peak at 0.170Å^{-1} grows in to become very intense and sharp.

The 9C_{16}TAB:1SDS samples act very differently to the 6C_{16}TAB:4SDS. The SPEI sample in Figure 6-2 (top) shows sharp peaks as seen in the 6:4 samples, however the main peak position is very different. Along with the main peak visible at 0.130Å^{-1} there are three weak peaks at 0.108Å^{-1}, ~0.15Å^{-1}, and 0.198Å^{-1} which indicates the growth of a cubic structure. The growth of this structure appears to be quite slow with stable features only appearing after 30 minutes from pouring the sample. Interestingly, the peak that ends up around 0.15Å^{-1} starts closer to 0.14Å^{-1} suggesting a restructuring during the first 30 minutes. The stabilisation of this peak position is also around the same time that the peaks at 0.108Å^{-1} and 0.198Å^{-1} become sharper, possibly indicating the stabilisation and growth of the final structure at this time.

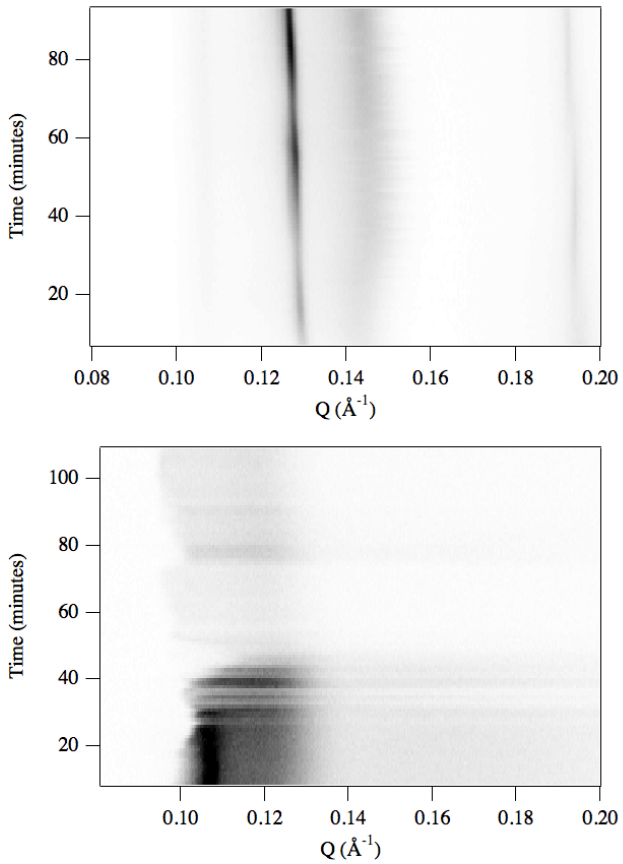

Figure 6-2. 0.05M 9C_{16}TAB:1SDS with SPEI (top) and LPEI (bottom)

The 9C_{16}TAB:1SDS sample with LPEI however shows very little structure. A broad peak is visible, with an initial maximum around 0.108Å^{-1}, which becomes less intense after 40 minutes. Although the peak becomes less intense it is still visible,

however the position of the maxima changes to around 0.12Å^{-1}. These samples suggest that there are two different structures being formed in the LPEI films. The first structure is the kinetically favoured structure, which rearranges over time to the thermodynamically favoured structure. The reason the two structures are seen in the LPEI films and not in the SPEI films is that the LPEI has a much higher molecular weight and has a much more extended branched structure, meaning that it diffuses in solution much more slowly than the SPEI so it takes longer to reach the final structure.

The 9C_{16}TAB:1SDS SPEI sample shows the slow formation of structure over the course of the experiment with no structural rearrangement. This suggests that there is only one structure formed which is probably due to the higher mobility of the SPEI in the solution allowing it to reach the thermodynamically favoured structure as it starts to form. Also visible in the 9C_{16}TAB:1SDS sample is the gradual increase in intensity over the course of the experiment. As the intensity of the peak is related to the number of layers and the degree of ordering this increase in intensity is related to the growth of the film suggesting the film formation was slower in the 9C_{16}TAB:1SDS sample than in the 6C_{16}TAB:4SDS regardless of the polymer. This therefore suggests a weaker interaction between the 9C_{16}TAB:1SDS surfactant mixture and the PEI than the 6C_{16}TAB:4SDS surfactant mixture and the PEI. This is also supported in the previously studied work where O'Driscoll et. al.[71] report, using PAAm as the polymer, as the ratio of SDS to C_{16}TAB increases the visual speed of formation decreases from ~2days for 97C_{16}TAB:3SDS to ~10 hours for 6C_{16}TAB:4SDS.

Taking this information regarding film formation speeds decreasing with increase of the proportion of C_{16}TAB, it could be concluded that film formation with just C_{16}TAB and polymer would take a very long time, and in some cases no film would form at all. It is fair to say this could be what is happening with other polymers except with PEI where the film formation with cationic surfactants is very rapid, as seen in chapter 3 and chapter 4.[71] This suggests that although the same result occurs, with films being formed from PEI with both the cationic and cat-anionic surfactant system, the mechanisms of formation for the different system films are different.

It is also possible to study the structural formation of the films using neutrons on the SURF instrument. With the flux available on SURF, and due to its setup as a time of flight instrument, it is possible to collect a full reflectivity pattern in 15 minutes. Due to this, patterns were collected in a 15-minute loop giving some indication of structural change over the course of the experiment, although not as detailed as in the

x-ray data. The neutron data shows very different structural information to the x-ray data and is shown in Figure 6-3.

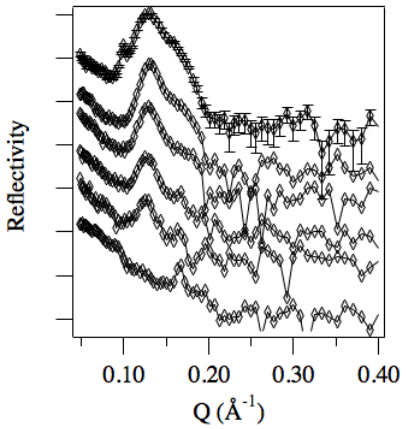

Figure 6-3. 0.05M 6C_{16}TAB:4SDS with SPEI in D_2O. Pattern collection started, from top to bottom, 5, 20, 35, 50, 65 and 160 minutes after pouring the solution. Error bars only shown on top graph for clarity. Lines between points are to help identify plots and do not indicate measured values.

It is clearly visible in this data that the major peak is at Q = 0.129Å^{-1} which gradually decreases in intensity over time. This gradual decrease in intensity is coupled with a shoulder peak becoming more obvious until it becomes a peak at Q = 0.165Å^{-1}. After the structure appeared to stabilise the sample was left on the beam line, but to one side, allowing the film structure to finalise before a final reflectivity pattern was collected to confirm the stable structure of the film. This final pattern is the bottom pattern in Figure 6-3 and shows the peak at Q = 0.129Å^{-1} has completely disappeared and the only peak left is a very weak peak at Q = 0.167Å^{-1}. This final peak at Q = 0.167Å^{-1} corresponds relatively well to the single peak in the x-ray data of the same surfactant/polymer mixture.

One of the main reasons to use neutrons is usually to utilise the contrast variation to help with structural determination. Figure 6-3 shows only the data from the fully hydrogenated C_{16}TAB and SDS sample while the pattern for an equivalent system, using tail deuterated C_{16}TAB, is shown in Figure 6-4. Here the peak at Q = 0.129Å^{-1} is still visible, as in Figure 6-3, for the first few runs but it does loose intensity. Also, similar to Figure 6-3, a peak is left visible at Q = 0.167Å^{-1} however this is much smaller and is therefore within error and therefore might only be noise in the pattern. In general, the use of contrast variation in this system just decreases the overall intensity. No peaks are obviously different from the fully hydrogenated system, which means these patterns don't really help with structural determination.

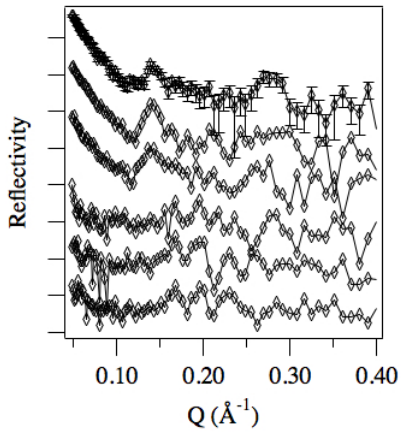

Figure 6-4. 0.05M $6C_{16}$TAB:4SDS with SPEI in D_2O. Pattern collection started, from top to bottom, 5, 20, 35, 50, 65 and 80 minutes after pouring the solution. Error bars only shown on top graph for clarity. Lines between points are to help identify plots and do not indicate measured values.

Interestingly, in the neutron data there is indication of growth of structure in the $6C_{16}$TAB:4SDS with SPEI sample where there was only fixed structure in the x-ray data. There are a number of possible reasons for this. The first is a chemical reason caused by using D_2O instead of H_2O in the neutron experiment. As it appears that evaporation is very important for film formation, the stronger hydrogen bonding in D_2O may be enough to alter the evaporation leading to a change in the film formation speed. There are also a number of experimental factors that also might be responsible. Firstly both samples were placed on warm plates to keep the surfactants in solution. The temperature of water baths connected to these plates was set to 28°C however variations in heat transfer, potentially caused by the ID10B troughs being thinner than the ISIS troughs or by the fact that the ISIS troughs are warmed from three sides rather than just underneath, may affect the evaporation rate of the solution. A second experimental difference that may cause this effect is the shape of the container holding the sample. At the ESRF it is completely open allowing movement of air around the surface of the solution, while at ISIS the sample holder is designed to have a lid and therefore the sides of a box create an enclosed space only open to the top of the sample potentially limiting movement of water vapour from the surface of the sample.

Although these experimental factors are plausible, it is potentially more likely that a difference in ambient temperature and humidity is responsible for the difference in rate of evaporation and therefore film formation structure. The ESRF experiment was performed in July 2008 and the temperature in the experimental hutch over the course of the experiments was 22.3 ±0.5°C and the relative humidity was 49 ±4%. The temperature and humidity were not recorded on the SURF experiment however the weather data for the experiment gives an average temperature of 8°C and an average humidity of 80%. This therefore suggests that with faster evaporation the

movement of liquid at the interface is rapid therefore hindering structural formation. This result contradicts the previous understanding of these films as it was previously thought that the higher the rate of evaporation the more material would be taken to the surface to allow film formation. However it agrees with the phase separation seen with Nile red in chapter 4. It is therefore possible that the film formation for the best ordered films is a combination of having evaporation that is fast enough to bringing material to the interface although slow enough to allow the structure to organise before the film solidifies.

To really understand the formation mechanisms of these films the intermediate and final structures need to be identified to give a picture of the full film formation process. Unfortunately the intermediate structures have so far been too short lived and not well ordered enough for structure determination. Final structure determination is also slightly hindered as can be seen in Figure 6-3 where the final structure in the neutron data shows limited structure. The use of x-ray reflectivity and grazing incidence x-ray diffraction (GIXD) however give good results therefore it is these experiments that are the main results used for structural determination of these films.

In the 0.05M $6C_{16}$TAB:4SDS with either SPEI or LPEI it appears that regardless of the film formation mechanism the final structure is very similar in both samples. This is shown in Figure 6-5 where the two specular reflectivity patterns are compared. Also shown in Figure 6-5 are lines indicating where peaks have been reported for the lamellar phase seen in the initial studies of 0.05M $6C_{16}$TAB:4SDS with PAAm.[71]

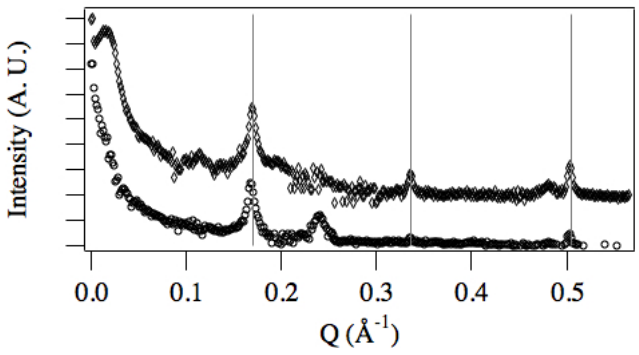

Figure 6-5. 0.05M $6C_{16}$TAB:4SDS with SPEI (top) and LPEI (bottom). Grey vertical lines are guides for the eye showing previously reported peak positions.[71] Error bars have been omitted because they are smaller or of the same order of magnitude as the markers. Plots have been offset for clarity.

The peaks at 0.168Å^{-1} and 0.503Å^{-1} are clear in both patterns and are the n and 3n peaks of a regular repeating layered structure. The Q position of the 2n peak is

0.336Å^{-1}, which is the middle peak indicated by the grey vertical lines. This 0.336Å^{-1} peak is more visible in the SPEI sample however all peaks are more intense in the SPEI sample and the corresponding peak can be seen by close examination of the LPEI data. If these three peaks were alone then this would probably indicate a lamellar structure, however there are also peaks visible at 0.481Å^{-1} in the SPEI sample and 0.240Å^{-1} in the LPEI sample. As with the 0.336Å^{-1}, the 0.481Å^{-1} peak is also visible, by close inspection, in the LPEI data. However, for an unknown reason the 0.240Å^{-1} peak is not visible in the SPEI sample although this may be due to an increased level of noise in this area.

Initially it was unclear whether there were two independent lamellar structures or a single cubic structure with two strong sets of reflections. The two sets of peaks are related by a squared relationship therefore it is most likely that the two sets of peaks are part of the same cubic structure where two sets of reflections are much stronger than any other reflections, possibly due to the structure being in a favoured orientation relative to the surface. To help clarify the structure, GIXD was performed, as it can show any off specular detail related to the in-plane structure and has been seen to give more information than reflectivity alone. The two GIXD patterns are shown in Figure 6-6.

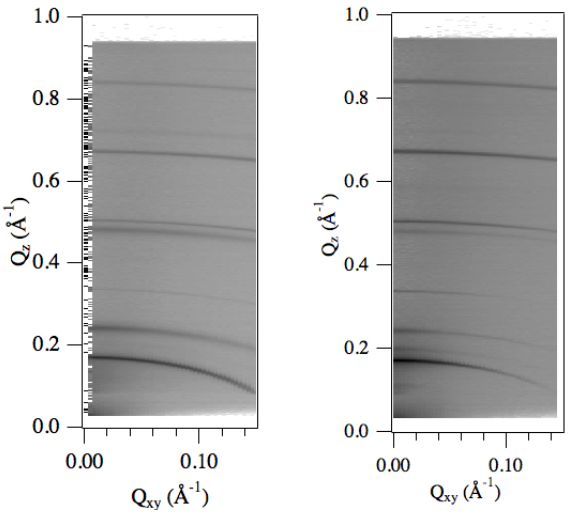

Figure 6-6. GIXD patterns of 0.05M $6C_{16}$TAB:4SDS with LPEI (left) and SPEI (right). The incidence angle for the experiment was 1.12° (left) and 1.19° (right)

These patterns appear very similar with both showing a number of rings. The intensity of the peaks in the right pattern are higher due to the higher incidence angle, which is able to penetrate into the solution more deeply and therefore scattering from more repeat units. This indicates that the structure is a powder structure rather than a single discrete crystallite. The position of the rings are Q_z = 0.169, 0.239, 0.334, 0.481, 0.501, 0.669, and 0.839Å^{-1}. The Q range of the

reflectivity patterns did not extend far enough to pick up the 0.669 and 0.839Å^{-1} peaks although these are just extensions of the previously seen structure. For a more detailed study of the exact peak positions, a line profile is taken from the SPEI sample at $Q_{xy} = 0$, which should be similar to the reflectivity pattern, this line profile is shown in Figure 6-7. The peak at $Q_{xy} = 0.169$Å^{-1} is particularly intense however as this is also the position of the specular reflection peak.

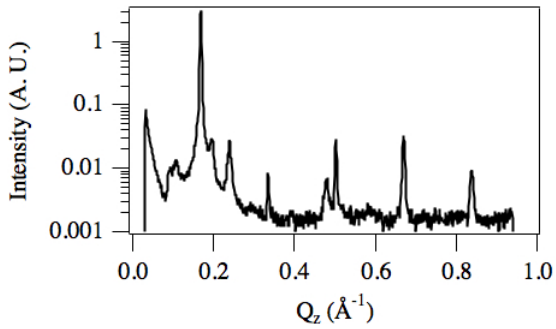

Figure 6-7. Line profile from a GIXD pattern at $Q_{xy} = 0$Å^{-1} and incident angle of 1.19°. The sample was 0.05M $6C_{16}$TAB:4SDS 1wt% SPEI.

From Figure 6-7 it is clear to see that the peaks are much more intense in the GIXD pattern than in the previous reflectivity pattern and that they are also much sharper. The sharpness of the peaks suggests that the structure, although a powder pattern, is well ordered. Unfortunately, although the GIXD pattern shows more peaks there is only one peak that is not part of the previously assigned series, this peak is at Q = 0.195Å^{-1}. This extra peak is not part of a lamellar phase or a 2D hexagonal, given it position relative to the peak at Q = 0.169Å^{-1}. Therefore it must be from a cubic pattern, which supports the idea that there is an unknown cubic pattern with two series of very strong reflections that effectively hide all other reflections. This extra peak is only visible in the SPEI pattern and not in the LPEI pattern although given the rest of the peaks are visible in both GIXD patterns it is likely this is just hidden due to less ordering in the LPEI samples.

In the publication relating to this data[102] the structure assigned to this pattern was a mixture of an $Ia\bar{3}d$ cubic structure and a lamellar phase. This has been a point of contention within the group as the peak at Q = 0.195Å^{-1} is the only peak that indicates a cubic pattern. To try and get a better understanding of the structures and what the peaks relate to, a small project was undertaken by an undergraduate to study the effect of changing the surfactant tail lengths with the films. The surfactants were C_nTABs with tail lengths of 14, 16 and 18 carbons and sodium alkyl sulfates (SC_mS) with tail lengths of 12, 14 and 16 carbons. Film formation was performed as in all previous studies however after formation the films were removed from the surface of the solution and allowed to dry. Due to the greater thickness of the LPEI

films over the SPEI films the predominant polymer in study was LPEI as they were easier to remove from the surface and be thick enough to give good scattering patterns. After the films had been dried they were gently broken up and the powders were studied using small angle X-ray scattering in transmission on the Anton Parr SAXSess available within the University of Bath.

Although LPEI was the main polymer used, a small number of SPEI films were made to confirm that the film structure was the same in both the LPEI and SPEI films and this was found to be the case. Along with this a 0.05M $6C_{16}$TAB:4SDS SPEI film was tested to confirm that the dried film structure is the same as the structure in the film left on the air/solution interface. There is only one peak in the dried film however it is at Q = 0.168Å^{-1} which is in good agreement with the GIXD pattern from the film at the air/solution interface. An example of the patterns collected on the SAXS is shown in Figure 6-8 and the other data is shown in Table 6-1.

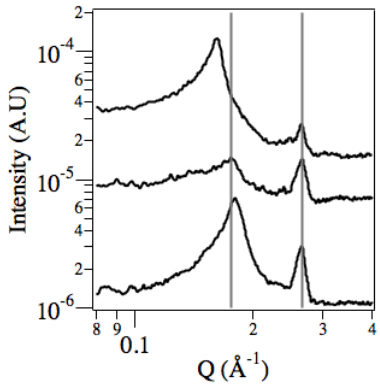

Figure 6-8. 0.05M $6C_n$TAB:4SC_mS with LPEI patterns collected on the SAXS. Samples are n=14 and m= 16(top), 14(middle) and 12(bottom). Grey vertical lines are guides for the eye indicating peaks from the n=14 m=14 sample.

C_nTAB	SC_mS	Peak Positions	
n	m	1st Peak (Å^{-1})	2nd Peak (Å^{-1})
18	16	1.45	2.25
18	14	1.51	2.19
16	16	1.56	2.43
16	14	1.62	2.44
16	12	1.69[a]	2.39[a]
14	16	1.62	2.64
14	14	1.75	2.66
14	12	1.80	2.65

Table 6-1. Peak positions from $6C_n$TAB:4SC_mS LPEI films collected on the SAXS. (a) sample from $6C_{16}$TAB:4SDS collected at the air solution interface using GIXD. Error in peak positions is 0.05Å^{-1}

What these results show is that changing the tail length of C_nTAB surfactant changes the position of both peaks in the scattering pattern, however changing the tail length of the SC_mS surfactant only changes the position of the 1st peak. There are two obvious explanations of this; the first is that they are two completely different structures, one made up of C_nTAB and SC_mS while the other is just C_nTAB. The second explanation is that both peaks are from the same structure and there are parts of the surfactant aggregates that are purely C_nTAB due to more favourable packing. The solution structures of the surfactants are too complex to be able to say for certainty whether there is one structure or two. The first explanation is the more obvious however the fact that the ratio of the second and first peaks in the GIXD pattern of $6C_{16}TAB$:4SDS is the square root of two is such a good indicator of a cubic pattern that it is difficult to completely discount the two sets of reflections coming from the same structure. The ratio of the peak positions for the other samples, from Table 6-1, do not indicate the structures are linked therefore it is possible that the $C_{16}TAB$:4SDS sample peaks are only linked by coincidence.

Although the $6C_{16}TAB$:4SDS samples are the most discussed, as with the time resolved data $9C_{16}TAB$:1SDS surfactant mixtures were also used to form films. An intermediate surfactant mixture of $7.5C_{16}TAB$:2.5SDS was also used although due to time constraints only reflectivity and GIXD were performed with no time resolved studies. As with the $6C_{16}TAB$:4SDS samples, the GIXD patterns were more informative showing a series of rings in all structures therefore only line slices of the GIXD patterns have been shown here, Figure 6-9

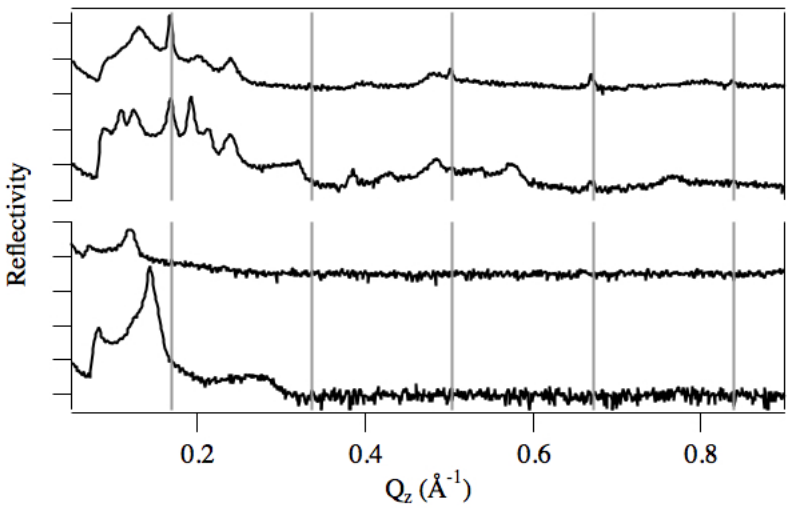

Figure 6-9. Line profiles at $Q_{xy} = 0$ from GIXD patterns of, from top to bottom, 0.05M $7.5C_{16}TAB$:2.5SDS with LPEI, 0.05M $7.5C_{16}TAB$:2.5SDS with SPEI, 0.05M $9C_{16}TAB$:1SDS with LPEI, and 0.05M $9C_{16}TAB$:1SDS with SPEI. Grey vertical lines show the $0.17Å^{-1}$ lamellar series seen in PAAm films as a guide for the eye. Incident angles are, from top to bottom, 1.19°, 1.19°, 0.85°, and 1.03°

In both the 7:5C_{16}TAB:2.5SDS and 9C_{16}TAB:1SDS samples with LPEI, as in the 6C_{16}TAB:4SDS LPEI sample, the number of visible peaks is greatly reduced from those seen in the samples with SPEI. This continues to support the assumption that the LPEI, due to its size and branched nature, is less able to rearrange and to be accommodated in the space between micelles giving a limit to long-range structural order within the films. The SPEI samples show more structure however the 9:C_{16}TAB:1SDS sample with SPEI only shows two peaks at Q = 0.144Å^{-1} and a broad peak which covers the expected position of the (110) and (200) of the 2D hexagonal phase at ~Q = 0.27Å^{-}1 The calculated unit cell spacing is, however, slightly smaller than that observed for CTAB-SPEI films at similar polymer and surfactant concentrations, which had a unit cell parameter of ~60Å. The difference may be due to the small amount of SDS reducing the charge on the micelles slightly, allowing closer packing of the cylindrical micelles in the case of the cat-anionic surfactant films. Both 0.05M 7.5C_{16}TAB:2.5SDS samples show a range of peaks. The LPEI sample shows peaks at Q = 0.131, 0.167, 0.200, 0.240, 0.481, 0.502, 0.669Å^{-1}. Apart from the peak at Q = 0.131Å^{-1} the rest of the peaks are in good agreement with the 6C_{16}TAB:4SDS SPEI sample although the peaks are a lot less intense. Although the peak positions are very similar they are not exactly the same suggesting a slight change in structure. This structural change has been attributed to a change from the $Ia\bar{3}d$ structure to an $Im\bar{3}m$ structure, which has previously been seen in liquid crystal systems.[148]

The 7.5C_{16}TAB:2.5SDS SPEI film is more complicated however with peaks at Q = 0.109, 0.124, 0.169, 0.193, 0.212, 0.239, 0.320, 0.385, 0.430, 0.485, 0.575, 0.668Å^{-1}. These peaks suggest a series of reflections, some discussed previously, however some only seen in this sample. Garsteki and Holyst determined a model to simulate the intensities of peaks in given cubic structures, this model is discussed in chapter 2.[94, 95] After implementing this model in IgorPro it was possible to test various simulated cubic patterns against the collected data and the best fit came from the Gyroid $Ia\bar{3}d$ structure, Figure 6-10. This is not a perfect fit although it does give a good indication of possible structure. A major problem of performing this type of fit is that as the water evaporates from the surface of the solution, forming a film, the material will dry and the drying can cause shrinking of the structure. As the evaporation occurs from just one side the shrinking will be normal to the surface, which has been seen to cause distortion in the peak position of templated materials.[149, 150] In the previously published paper relating to this work, this distorted $Ia\bar{3}d$ structure was assigned to this pattern and this was the major factor in assigning an $Ia\bar{3}d$ structure to the 6C_{16}TAB:4SDS SPEI sample discussed above.

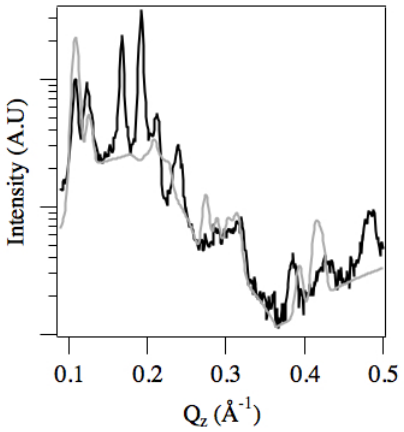

Figure 6-10. Line profile of 0.05M 7.5C_{16}TAB:2.5SDS with SPEI (dark line), t 1.19°, with fit for simulated $Ia\bar{3}d$ structure (grey).

Neutron reflectivity patterns were also taken of different ratios of C_{16}TAB:SDS. These were 7:3, 8:2 and 9:1 however in all cases, like in the 6:4 samples, neither the hydrogenated samples nor deuterated samples showed stable high intensity peaks. In all cases any strong peak seen initially in the structure lost its intensity over ~30-45 minutes leaving an almost flat line in the reflectivity by the end of the experiment. It is possible that due to the complex nature of the film structures that the contrast is not great enough to give strong scattering using neutrons where as it is with x-rays.

6.1.1.2 PEO

The original paper published about the mixed cat-anionic surfactant films used the polymer PAAm. Since then the focus has been on PEI because it is the polymer that forms films with the cationic surfactant and therefore comparisons can be made. Due to this, as with the solution studies mentioned in the chapter 5, although studies have been carried out using different polymers they are much more limited than the studies with PEI. The only other commercial polymer that has really been studied to any extent for film formation is PEO. This is because it represents a more biocompatible alternative to PEI and can be easily purchased in a variety of molecular weights allowing comparison with the effect of molecular weight on the formation of PEI films.

As with the PEI films, the main form of analysis was x-ray reflectivity and GIXD. The data for the 0.05M 6C_{16}TAB:4SDS samples with the two molecular weights of PEO were collected prior to the start of this project by B. M. D. O'Driscoll but was unpublished, these results are shown in Figure 6-11. Before discussing the results it is worth noting that although the two molecular weights of PEO have the acronyms LPEO and SPEO they are not the same molecular weights as the LPEI and SPEI.

SPEO and SPEI have relatively similar molecular weights with SPEI being 2,000Da and SPEO being 10,000Da. LPEO and LPEI however are very different with LPEO being 100,000Da and LPEI being 750,000. Not only are the molecular weights different but the structure of the polymers is different as well. PEO is a linear polymer where as the PEI used in this project is branched, the SPEI however is only slightly branched due to the way it is synthesised. The LPEI is very different than the LPEO however as it is a highly branched polymer

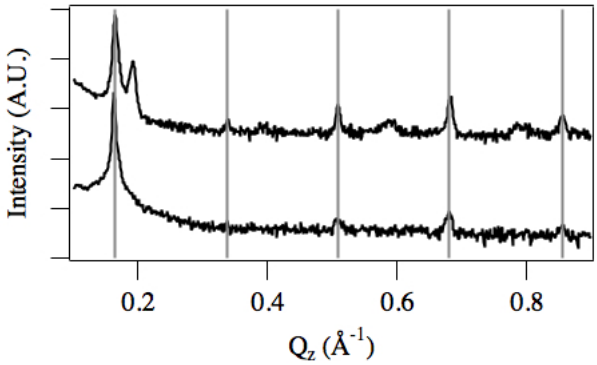

Figure 6-11. Line profiles from GIXD patterns of 0.05M 6C_{16}TAB:4SDS with LPEO (top) and SPEO (bottom). Grey vertical lines show the peak positions of the 0.17Å^{-1} series of peaks seen for PAAm described in the earlier publication.[71] Incident angle is 1.19° in both patterns.

These results show, in contrast to the PEI results, that the film made from LPEO is better structured than the film made with SPEO. This is probably due to the lack of branching and the low molecular weight in the SPEO, while the LPEO, although not branched, is of high enough molecular weight for a single polymer chain to be able to interact with more than one micelle. The peaks seen in both films are part of the 0.17Å^{-1} series of peaks described previously suggesting that regardless of polymer the general structure of all the films is roughly the same. Given there is only one series of reflections in the SPEO sample the structure is most likely a lamellar structure. The extra peaks visible in the LPEO samples are all part of a series of reflections with peak positions at Q = 0.192, 0.392, 0.589, 0.788Å^{-1}. The peak at Q = 0.192Å^{-1} is probably the same reflection seen in SPEI sample however the other peaks in the series were not visible previously.

In the LPEO solutions, discussed in the chapter 5, it was seen that the addition of LPEO increased the interaction between lamellae suggesting the C_{16}TAB:SDS aggregates were packing closer together in solution. If this has followed into the films then the packing during film formation is more ordered which is the reason for seeing the extra peaks that haven't been seen previously. As only two series of reflections are visible it is again almost impossible to determine the film structure

however the $Ia\bar{3}d$ structure is still a possibility and given the similarity to the PEI films it is likely that this is still the structure.

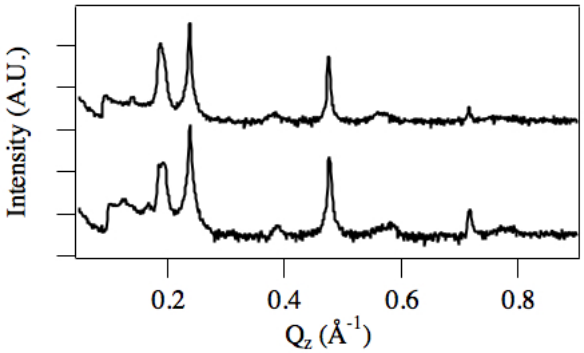

Figure 6-12. Line profiles taken at Q_{xy} = 0 of 0.05M $9C_{16}$TAB:1SDS with LPEO (top) and SPEO (bottom). Incident angle is 1.3° in both patterns.

Figure 6-12 shows the line profile from GIXD patterns of $9C_{16}$TAB:1SDS with LPEO and SPEO and unlike all previously discussed samples they are both very similar. The peaks are part of two series of reflections. The first starts at Q = 0.189Å^{-1} with small peaks at 0.380Å^{-1} and 0.577Å^{-1}. The second set of peaks is at Q = 0.238Å^{-1} with two sharp peaks at higher Q at 0.476Å^{-1} and 0.716Å^{-1}. These two series of reflections are similar to series of reflections seen before however this is probably coincidence and the structure of the films is probably very different to the films from $6C_{16}$TAB:4SDS. As only two series of reflections are visible in the patterns, the exact structural determination is very difficult. If the 0.189Å^{-1} peak is really the 1st peak from the structure then the structure is most likely a $Im\bar{3}m$ cubic phase, the reasoning for this is that the first two peaks would be from the 110 and 111 reflections and no other common cubic pattern shows these two peaks.

6.1.1.3 Other systems.

One other system that is worth mentioning here was $6C_{16}$TAB:4SDS with poly(*N*-isopropyl acrylamide) (PNIPAM). This was a small project performed by an undergraduate to study the possibility of forming films with a responsive polymer that might be used for any potential application. These films will potentially be temperature responsive as PNIPAM is known to change configuration at ~32°C, this has previously been studied to induce swelling and deswelling of a PNIPAM gel.[151]

The molecular weight of the PNIPAM used for this study as 25,000Da. As part of the project was to compare films of PEI and PNIPAM a different molecular weight of PEI was used. The molecular weight of this new PEI was 25,000Da (MPEI) and

had previously been studied with C_{16}TAB films by O'Driscoll et. al. where it was found to behave very similarly to SPEI.[67] Differently to the studies discussed above, the ratio of C_{16}TAB to SDS used was 7:3. This was because the 7:3 ratio has been seen to produce similar surfactant structures and the surfactant mixture was more stable and less likely to phase separate.

Visually the MPEI behaved very similarly to previous reports of LPEI and SPEI with thick rubbery films forming at the air/solution interface. To study these films they were removed from the surface of the solution using plastic mesh and allowed to dry. Interestingly it was reported that although the films were left to dry for a number of days, due to the hydroscopic nature of the PEI they always remained quite flexible and rubbery. This is in contrast to the PNIPAM films, which were also removed from the solution surface using plastic mesh and allowed to dry. The PNIPAM films however, after 12 hours of drying, became very brittle suggested they had dried out much more than the PEI films.

As well as the dried films being much more brittle, the PNIPAM films were visually thinner than the MPEI films grown for the same period of time. It was possible to correlate this with the rate of evaporation with the MPEI films forming from a greater rate of evaporation than the PNIPAM films. The different solutions started with ~20g of solutions, 10ml surfactant and 10ml polymer, and were grown next to each other with their weights being recorded every 10 minutes. After one hour the decrease in weight from the solutions was 0.38g for the MPEI and 0.29g of the PNIPAM. The reason for a higher rate of evaporation is probably the more hydroscopic nature of the MPEI that helps draw water from the bulk solution to the surface of the solution.

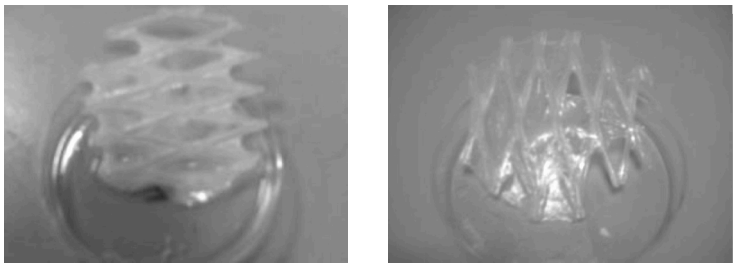

Figure 6-13. Recovered films of 0.05M 7C_{16}TAB:3SDS made with MPEI (left) and PNIPAM (right)

After the recovered films, seen in Figure 6-13, had dried they were gently broken up into powders that were studied with SAXS. In the majority of the films formed, the scattering patterns showed two peaks, similar to those seen in Figure 6-8, and those that didn't show two peaks at least showed one. The main peak that was seen in all of the scattering patterns was ~Q = 0.168Å^{-1}, as seen in previous film structures. The

second peak, when it was seen, was at ~Q = 0.242Å^{-1} that again is in the same position as seen in the previous structures. This therefore supports the previously mentioned theory that the structure of the films is entirely determined by the surfactant aggregates and the polymer only has a role in binding the surfactant aggregates together to form a film.

As well as studying the structure of the films, the potential applications were also studied using the dye Nile red. To perform the release studies, instead of breaking up the dried film for SAXS study, the film was placed in water. Two films were made and studied simultaneously with aliquots of solution being removed every 2 minute. The difference between the studies was the first was performed at room temperature while the second was performed at 40°C. As PNIPAM is known to be more hydrophobic at higher temperatures the film was effectively swollen at room temperature and compressed at 40°C. This resulted in a much slower release of Nile red into the solution at higher temperature. There is still an issue with the amount of encapsulated dye being very small however for an initial experiment the results are promising.

6.1.2 Synthesized Polymers

As discussed previously, cationic films have so far only been found to form with commercial PEI. Although an interaction between the polymer and the surfactant can be inferred from measuring the thickness and ordering from the film, it has been unclear what interactions lead to film formation. One suggestion has been that it is the branching of the polymer that leads to interactions between multiple surfactant micelles, in effect crosslinking the surfactant micelles together. To test this and to help understand the interactions between the polymer and the surfactant a postdoctoral research assistant synthesised a range of different polymers with controlled variations in the polymer architecture. Film formation was then attempted with these polymers jointly between the candidate and the postdoctoral researcher.

Although it was hoped that these polymers would be able to improve the understanding of the interactions of C_{16}TAB with polymer, unfortunately none of the polymers formed films with the C_{16}TAB surfactant alone. The first polymers to be synthesised were a range of linear and branched poly(2-ethyl-2-oxazoline) (PEtOx). The polymers were soluble however there was no sign of film formation with C_{16}TAB. The PEtOx polymers were then hydrolysed to create a range of linear and branched PEI polymers for comparison with the commercial polymers, however these were insoluble at temperatures under 40°C and, although film formation was

attempted at this temperature, no films were seen to form, possibly due to the increased solubility of the surfactant at higher temperatures affecting micelle formation.

The postdoctoral research assistant performed the synthesis of the PEtOx polymers by cationic ring opening polymerisation of 2-ethyl-2oxazoline with methyl-p-toluene sulfonate as the initiator. The polymer was then split into two batches, the first batch was retained for study while the second batch was hydrolysed in concentrated hydrochloric acid for 3 hours to create linear PEI polymers. Details of the polymer synthesis have been reported in Halacheva et al.[152] A list of the polymers synthesised is given in Table 6-2

Polymer Series	Molecular weight	Degree of polymerisation	Abbreviation
PEtOx	1100[a]	11[d]	$(EtOx)_{11}$
	1700[a]	20[d]	$(EtOx)_{20}$
	4700[a]	48[d]	$(EtOx)_{48}$
	6500[a]	65[d]	$(EtOx)_{65}$
	b	96[d]	$(EtOx)_{96}$
PEI	500[c]	11[e]	$(EI)_{11}$
	890[c]	20[e]	$(EI)_{20}$
	2100[c]	48[e]	$(EI)_{48}$
	2870[c]	65[e]	$(EI)_{65}$
	4420[c]	96[e]	$(EI)_{96}$

Table 6-2. Synthesised linear polymers. (a) Calculated from the mass value of the most intense signals from MALDI TOF spectra of the polymers. (b) Not measured. (c) determined from ^{1}H NMR in D_2O at 60 ºC. (d) Determined from ^{1}H NMR in D_2O. (e) Taken from the PEtOx polymer they were synthesised from.

As well as synthesising linear polymers, controlled branched polymers were also synthesised for comparison with the commercial hyperbranched polymer. To synthesise the branched polymers the first step was to graft PEtOx chains onto a PEI backbone. These polymers could then be studied to determine the degree of grafting to ensure branched polymers had been made. The final step was to hydrolyse these polymers to create branched PEI homopolymers. A list of synthesised polymers and their abbreviations is given in Table 6-3.

Synthesised PEI and PEtOx precursors			Grafted PEI-EtOx		Grafted PEI	
Degree of Polymerisation of the LPEI main chain[a]	Degree of Polymerisation of the PEtOx branches[a]	Degree of grafting[a]	M_n[b]	Abbreviation	Theoretical Molecular Weight	Abbreviation
48	48	4%	11,500	$(EI)_{48}$-$(EtOx)_{48}$	6,100	$(EI)_{48}$-$(EI)_{48}$
20	96	40%	76,922	$(EI)_{20}$-$(EtOx)_{96}$	33,914	$(EI)_{20}$-$(EI)_{96}$
65	20	30%	67,750	$(EI)_{65}$-$(EtOx)_{20}$	4,520	$(EI)_{65}$-$(EI)_{20}$
65	65	7%	36,440	$(EI)_{65}$-$(EtOx)_{65}$	16,700	$(EI)_{65}$-$(EI)_{65}$
96	20	7%	17,824	$(EI)_{96}$-$(EtOx)_{20}$	9,980	$(EI)_{96}$-$(EI)_{20}$
96	48	16%	74,660	$(EI)_{96}$-$(EtOx)_{48}$	34,340	$(EI)_{96}$-$(EI)_{48}$

Table 6-3. Synthesised grafted polymers. (a) determined from ^{1}H NMR of the precursors (b) Determined from ^{1}H NMR in D_2O.

Due to the small quantities of polymer synthesised and the range of experiments to be performed, it was decided to use a lower polymer concentration in these experiments than in the commercial polymer experiments, 0.375wt% instead of 1wt%. Also due to the relative solubility of the different polymers, mentioned previously, the linear PEtOx polymers and the graft polymer with (EtOx) chains could be studied in solutions at room temperature. The linear PEI polymers and surprisingly also the $(EI)_x$-$(EI)_y$ had to be dissolved in solutions above 45°C and the film formation studies run at 45°C.

As mentioned previously, no films were seen to form from mixtures of the synthesised polymers and C_{16}TAB, even after 48 hours. As no films were formed from the synthesised PEI it is possible that the high degree of branching is very important for film formation. However due to the high temperatures needed to perform these experiments this conclusion is very tentative. All the polymers did form films with $6C_{16}$TAB:4SDS mixed surfactant solutions. The formation time for the room temperature films was around 6 hours while the 45°C films only took one hour to form. This difference in film formation time for the room temperature films can be attributed to the lower polymer concentration as this is known to cause slower film formation. The fast times for film formation seen in the 45°C films is probably due to an increased rate of evaporation. However visually the films formed from the 45°C solutions were much thinner and more brittle that the films formed at room temperature. The films were removed from the surface and allowed to dry so they could be studied in the SAXS to confirm if structure was present. In all cases a peak at ~Q = 0.17Å^{-1} is observed indicating all the films are structured. A peak at ~Q =

$0.24Å^{-1}$ is also observed indicating the structure of these films is very similar to that seen in the previously discussed commercial polymer films.

More accurate structural information was collected for some of the films using GIXD on ID10B. As with the films studied in the lab, the polymer concentration was 0.375wt%, which is lower than the standard film forming concentration. The films studied were the linear $(EtOx)_{65}$ and $(EtOx)_{96}$ and the branched $(EI)_{96}$-$(EtOx)_{48}$, $(EI)_{65}$-$(EtOx)_{65}$ and $(EI)_{65}$-$(EtOx)_{20}$. The film formation in the linear polymers was so slow that it was decided not to study them with time resolved measurements. The branched polymers however formed faster and therefore were studied with the time resolved measurements, the graphs of these plot are shown in Figure 6-14.

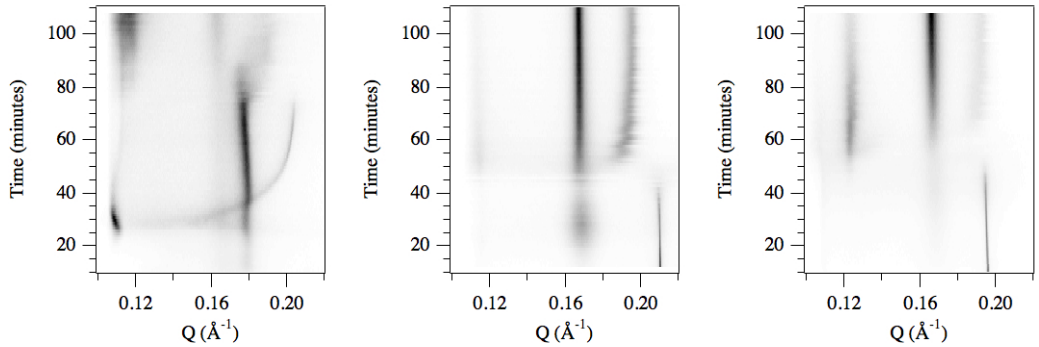

Figure 6-14. Time resolved off-specular reflection from films of 0.05M $6C_{16}$TAB:4SDS with $(EI)_{65}$-$(EtOx)_{20}$ (left), $(EI)_{65}$-$(EtOx)_{65}$ (centre), and $(EI)_{96}$-$(EtOx)_{48}$ (right).

In the $(EI)_{65}$-$(EtOx)_{65}$ and $(EI)_{96}$-$(EtOx)_{48}$ the sharp peak visible at $Q = 0.212Å^{-1}$ and $Q = 0.198Å^{-1}$ respectively is the specular reflection peak for this experiment. The specular reflection would be at $Q = 0.212Å^{-1}$in the $(EI)_{65}$-$(EtOx)_{20}$ sample if a specular peak was seen. What this data shows is that the film formation is much slower than has been seen previously in C_{16}TAB:SDS films. As stated previously this is probably due to the low concentration of the polymer. In all patterns, structural formation can be seen to have started within the first 20 minutes of the experiment, however these peaks are not very sharp. Then after 25 minutes in the $(EI)_{65}$-$(EtOx)_{20}$ film, 45 minutes in the $(EI)_{65}$-$(EtOx)_{65}$ film, and 55 minutes in the $(EI)_{96}$-$(EtOx)_{48}$ film the structure undergoes a re-arrangement.

The structure that undergoes the most rearrangement is the $(EI)_{65}$-$(EtOx)_{20}$ sample, which happens to be the earliest changing film and the lowest molecular weight polymer. The film with the next most rearrangement is the $(EI)_{65}$-$(EtOx)_{65}$ sample, which is the middle changing film and the middle molecular weight. Therefore the least changed film is the slowest film to form and the highest molecular weight. This suggests a direct link to the film formation rate and the molecular weight of the

polymer. This also suggests that the higher molecular weight of the polymer the less the film is able to re arrange. Interestingly, after the structural rearrangement the structures of the films all appear to be very similar, particularly in the highest molecular weight structures where peaks are visible at ~Q = 0.17Å^{-1} and 0.195Å^{-1}. Less intense peaks are also seen around Q = 0.11Å^{-1}. Although interestingly the highest molecular weight film also has a peak at ~Q = 0.13Å^{-1}.

The lowest molecular weight sample is slightly different however. The peak at ~Q = 0.11Å^{-1} is still visible however the main peak is visible at ~Q = 0.18Å^{-1} with a secondary peak for a short time at Q = 0.2Å^{-1}. At around 75 minutes however the Q = 0.2Å^{-1} peak disappears and shortly after the peak at Q = 0.18Å^{-1} appears to split into two peaks around Q = 0.17Å^{-1} and Q = 0.195Å^{-1} suggesting that all three films actually end up with the same structure even if they go through different intermediate stages to get to the end structure. The ability of the structure to go through these intermediate stages appears to be correlated to the molecular weight with the lowest molecular weight being the most able to rearrange.

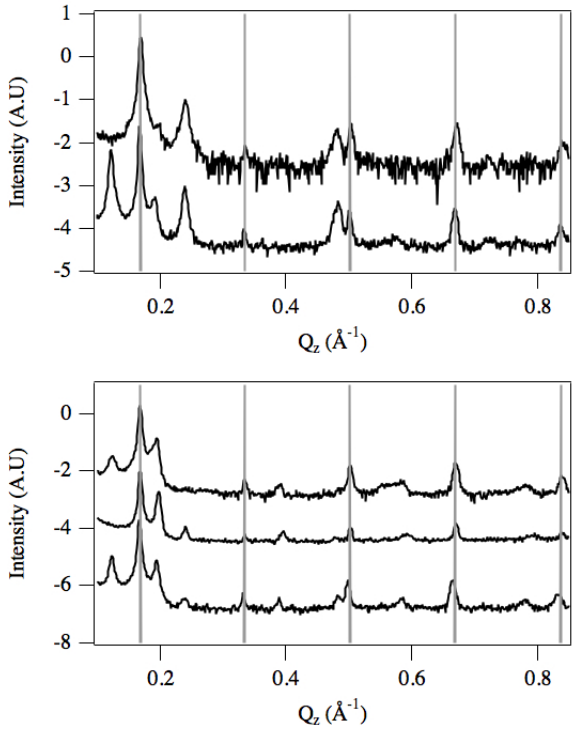

Figure 6-15. Line profiles from GIXD patterns of 0.05M $6C_{16}$TAB:4SDS with synthesised polymers. Top graph shows $(EtOx)_{65}$ (top) and $(EtOx)_{96}$ (bottom). Bottom graph shows $(EI)_{65}$–$(EtOx)_{20}$ (top), $(EI)_{65}$–$(EtOx)_{65}$ (middle), and $(EI)_{96}$–$(EtOx)_{48}$ (bottom).

Although reflectivity patterns were collected for all the samples the GIXD patterns provide the largest Q range and the most intense peaks increasing the chance for structural determination. For ease of study, it is the line profiles that are shown in

Figure 6-15, along with grey vertical lines indicating the Q = 0.17Å^{-1} series of peaks seen in the previous studies as a comparison and guide for the eye.

These results are very similar to the PEO results discussed above, showing a similar number of peaks at similar intensity. This is interesting because the linear PEtOx polymer all have lower molecular weights than the SPEO, this therefore suggests PEtOx has a stronger interaction with the aggregates. As the molecular weight of the polymer appears to help film formation by increasing the number of interactions between the polymer and the aggregates, an increase in the synthesised polymer molecular weight should increase the interaction. With the synthesised branched polymers the molecular weights are all higher than the linear PEtOx polymers, and they are more similar to LPEO molecular weight. However the GIXD patterns show that this produces a pattern indicative of a lower interaction. This difference may be caused by steric hindrance of the branched polymer chains effectively limiting the potential number of interactions between the polymer and the surfactant aggregates.

With these results it is therefore interesting to see whether a reduction in the number of branches in the PEI system would increase the apparent strength of the interaction between the polymer and the aggregates. Unfortunately given the limited amount of time available on ID10B it was decided that it was not possible to run the synthesised PEI polymers at high temperature, although the room temperature samples were run. There were two reasons for this, firstly the time it would take to heat up and cool down the instrument sufficiently to perform the experiments would limit the time to actually perform the experiments. Also the rate of evaporation from the surface of the solution due to the high temperature would mean the amount of bulk solution would be constantly decreasing causing the position of the surface to constantly change. This would make the experiment and the subsequent analysis of the data very difficult.

6.2 Spin/Spray Coated Films

As well as studying the growth films at the air/solution interface, part of this work was to test different methods of film formation. To find different film formation techniques knowledge was taken from the growing area of research into layer-by-layer (LbL) systems, which is commonly used to create multi-layered systems via dip or spin coating or aerosol spraying. A recent review by Argia et al[38] shows the versatility of the LbL techniques.

One apparent downside to the LbL technique is the dimensionality of the multilayers that are produced. Due to the repetitive layering of different components onto the substrate, ordering can be achieved parallel to the substrate but not perpendicular.[46, 153] In the surfactant/polymer films described in this report, the ordering is created in the bulk solution rather than on the substrate therefore it is hoped that despite using techniques such as spray coating to deposit the film on a substrate, the 3-dimensional ordering will still be formed.

The most common LbL technique is dip coating where a substrate is alternately dipped in solutions containing oppositely charged components. This technique is known to be very good at forming multi-layered systems however it is very time and labour intensive. Therefore more recently researchers have instead been turning to spin and spray coating. In the majority of cases the same principle applies in that the different solutions are alternately deposited onto the substrate. The main difference with spin and spray coating is that the deposition is much quicker and the thickness of the layer is more controllable resulting in reduced drying times between deposition steps. It has also been shown to be more reproducible[43] even in systems containing vesicles and other small self assembled molecules.[45]

In the study performed for this thesis, attempts at producing spin-coated membranes using the polymer surfactant film forming solutions have been unsuccessful. This has been due to difficulties in reproducibly creating a first layer on the substrate. The main factors affecting the deposition of a layer in spin coating are the speed of rotation of the substrate and the viscosity of the solutions,[154] or in this case the single solution. The surfactant/polymer solution using a 6:4 ratio of C_{16}TAB:SDS is very viscous at room temperature and therefore the drop does not spread at low substrate rpm as there is not enough force to allow it to spread. However at higher substrate rpm the force is so great that the drop moves in a single direction instead of evenly spreading.

Spray coating on the other hand has been much more successful. The substrate used was either a glass microscope slide or more commonly a 0.5mm thick, 100mm diameter silicon wafer. The advantages of using the silicon wafer is that it is a large flat surface that can be fairly easily cleaned and, being a single crystal with the [100] orientation at the surface, does not interfere with x-ray or neutron measurements.

The films studied in this report using this technique are not standard LbL multilayers. This is because the two components are sprayed together onto the substrate. Therefore as the solution dries a thin film, similar to those discussed earlier, forms on the substrate. Multiple depositions will also probably dissolve the

top layer of the previously deposited layer allowing integration of the new solution with the original layer and therefore continuation of the structure already formed. As the structure can be formed from a single deposition of solution onto the substrate, building up a thick 3-dimensionally ordered structure should therefore be much quicker and easier to create than previous spray coated films. This technique is equivalent to "painting a mesostructured coating" onto a surface.

This study has been based on the previous work with both C_{16}TAB on its own and with mixtures of C_{16}TAB with SDS. As C_{16}TAB is used on its own the polymer used was PEI and to maximise the chance of well ordered structure the low molecular weight PEI was used. Prior to use, the silicon wafers were cleaned with a modified RCA procedure.[155, 156] The spray bottles used were HDPE bottles with a solution atomiser and a hand pump for pressurisation using air (Fisher). Consistency was achieved by keeping the pressure in the bottles at 1atm between deposition steps. Pressurising the bottle was only performed immediately prior to deposition using 20 "pumps" of the hand pump.

Due to the limited nature of this study and the limited amount of time available at large facilities, so far only x-ray measurements have been performed. As with the film studies discussed above the measurements performed were reflectivity and GIXD. Brewster angle microscopy was also used to study the surface of the substrate after film formation to visualise the build up of film on the substrate.

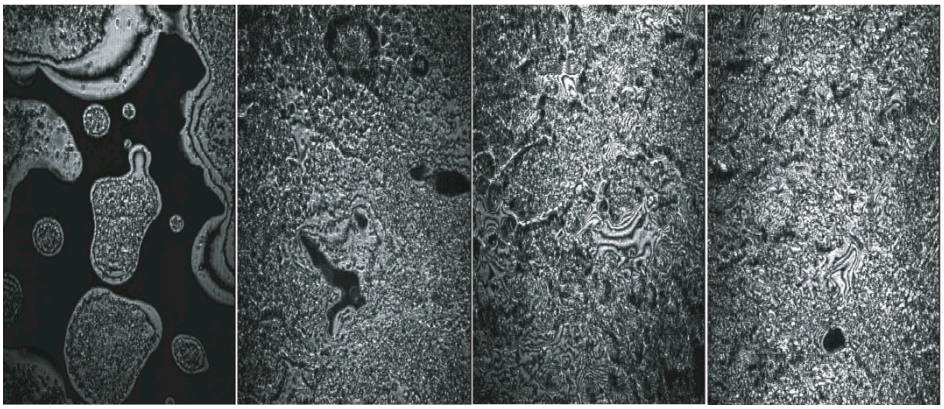

Figure 6-16. Brewster angle microscopy images of a 6C_{16}TAB:4SDS SPEI film on a silicon wafer after increasing applications of solution from left to right, layers 1 to 4. Images are 430μm by 630μm.

The Brewster angle microscope images, Figure 6-16, show initially the solution does not achieve complete coverage of the relatively hydrophobic silicon oxide substrate surface. Even after two deposition steps gaps can still be seen in the film surface. As the number of deposition steps increases the surface of the substrate appears to become smoother. In the following x-ray experiments 10 depositions were

performed therefore the surface of the substrate should have been relatively smooth. Although these images are only showing a small area of the substrate they were chosen as they represent the general surface structure of the substrate.

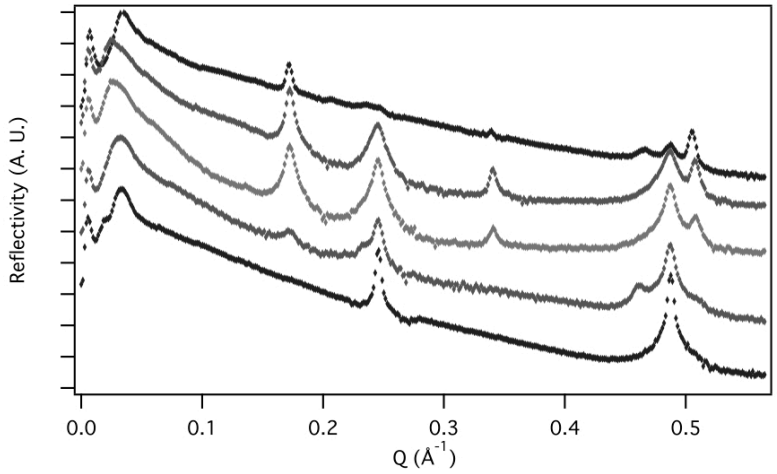

Figure 6-17. Reflectivity patterns of spray coated films of C_{16}TAB:SDS with SPEI. Ratios of C_{16}TAB to SDS are, from top to bottom, 6:4, 7:3, 8:3, 9:1 and pure C_{16}TAB at the bottom. Plots are offset for clarity.

The reflectivity patterns in Figure 6-17 show the spray-coated films are very similar in structure to the films grown at the air/solution interface discussed above. The strongest peaks visible in most patterns are part of either the ~0.17Å^{-1} series or the ~0.24Å^{-1} series. Interestingly in the C_{16}TAB SPEI films, the bottom trace in Figure 6-17, the only peaks visible are from the ~0.24Å^{-1} series. This is interesting as it was this set of peaks that was attributed to purely C_{16}TAB during the study into the effect of changing the tail lengths of the surfactants used, as discussed above for films made with the commercial PEI results.

As the amount of SDS in the mixtures increases, the intensity of the series of peaks at 0.17Å^{-1} increases suggesting these are due to either the SDS on its own or more likely, given the previous results, aggregates formed from a mixture of C_{16}TAB with SDS. The peaks are most intense and sharpest in the films of 7:3 and 8:2 C_{16}TAB:SDS suggesting that these films are able to form ordered films best under these conditions. It has previously been seen that C_{16}TAB SPEI films are very thin compared to the C_{16}TAB:SDS films. Also it is known that at equi-molar C_{16}TAB:SDS the surfactant precipitates. It is therefore expected that the 7:3 solution will give the thickest and most robust films without precipitation of pure surfactant phases occurring. As stated previously, towards the end of the project the standard surfactant solution was changed from the 6:4 ratio to the 7:3 ratio as the 7:3 ratio was less viscous and less prone to precipitate in large aggregates.

As well as the main two series of peaks other peaks are also visible in the 6:4 and 9:1 ratio films. The most obvious of the peaks is at ~Q = 0.46Å^{-1}. This peak also has a potential lower order version which is most obvious as a shoulder on the Q = 0.24Å^{-1} in the 9:1 ratio film although also visible under close inspection of the 6:4 ratio film. It is these two peaks that indicate that the structure of these films is more complex than two separate lamellar phases, however the lack of peaks to define the structure makes this difficult. This lack of other peaks in the scattering pattern may be due to the orientation of the samples, being in thin film form, which has been shown to cause absences of expected peaks and inclusion of unexpected peaks in samples with known structure.[99]

The same set of experiments was also performed without the addition of polymer to the system. Although it is known that C_{16}TAB:SDS does not form films on its own it was previously shown[71] that the interface structure of 6C_{16}TAB:4SDS with no polymer was the same as on the addition of PAAm. An advantage of spray coating is that the surfactant mixtures can be layered on a substrate and are held together by the lack of water instead of needing a polymer to bind them together. These films would not be able to be removed from the substrate as the films with polymer should but they can show the effect of the polymer on the film structures.

These samples without polymer were performed on a separate experiment to the sample with polymer due to timing issues. The instrumental setup for this second experiment used 20keV x-rays instead of the standard 8keV, due to this the reflectivity results were of very poor quality and do not show any structure. It is assumed this is a result of incorrect instrumental setup rather than there being a problem with the sample is because the GIXD patterns are very similar in both experiments. A comparison of the GIXD patterns is shown in Figure 6-18.

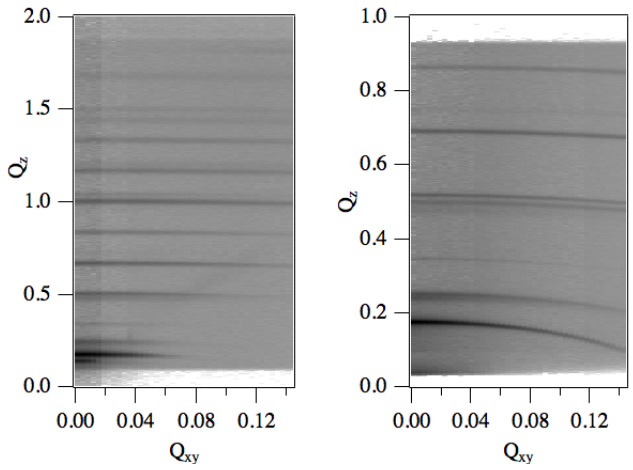

Figure 6-18. GIXD patterns of 6C_{16}TAB:4SDS without (left) and with (right) SPEI.

The main difference that is immediately obvious is the fact that with 20keV x-rays the wavelength is less than half that of 8keV x-rays. This means that for a fixed angle range, such as the linear detector at a set distance, the measurable Q range is more than doubled although the pixel size is the same so the resolution is lower making peaks positions close together harder to resolve. Apart from this, the patterns are very similar with both showing rings and the rings visible in both plots being in very similar positions. As shown previously the easiest way of comparing peak positions from GIXD patterns is by taking a line profile at $Q_{xy} = 0$, these patterns are shown in Figure 6-19.

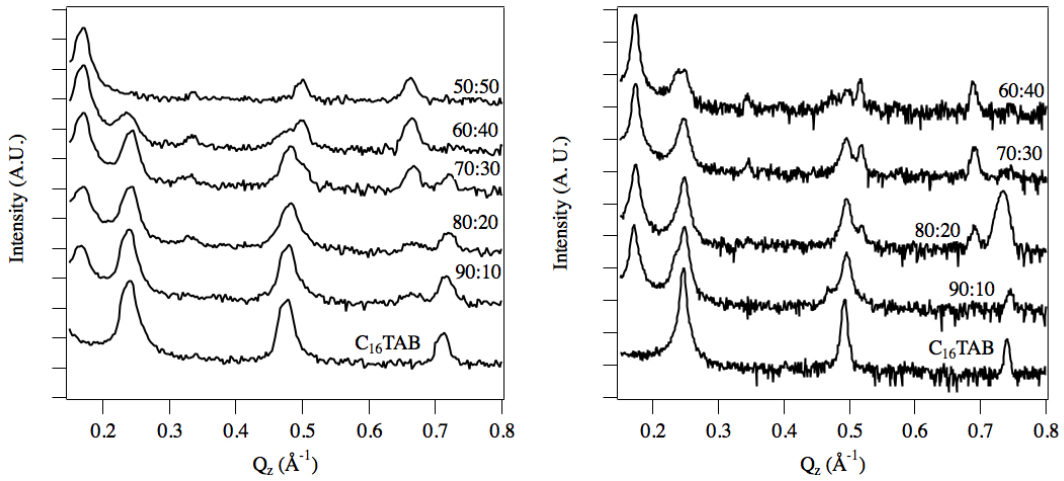

Figure 6-19. Line profiles at $Q_{xy} = 0$ for C_{16}TAB:SDS without (left) and with (right) SPEI. Ratios of C_{16}TAB:SDS are included on the plots for clarity. No 50:50 line profile was collected with SPEI. Lines are offset for clarity. Incident angles were 0.34° with polymer and 1.22° with polymer. The difference is due to a difference in energy of the incoming radiation.

There are minor differences between the peak positions in the two sets of profiles. This is because the profiles have not been corrected for collecting spherical scattering on a linear detector. Another difference between the two sets of patterns is that the resolution is much greater for films with SPEI, this is due to the difference in x-ray energy.

As discussed for the reflectivity patterns, in Figure 6-19, the two series of peaks correspond to the $Q = 0.17Å^{-1}$ and $Q = 0.24Å^{-1}$ series of peaks. In both cases the pure C_{16}TAB sample shows only peaks from the $0.24Å^{-1}$ series. Interestingly the 5:5 sample, not studied with SPEI, shows only peaks for the $0.17Å^{-1}$ series, which also supports the theory that the two series of peaks are from different structures.

If it is assumed that the two structures are lamellar structures and one of them is just C_{16}TAB and the other is C_{16}TAB with SDS, then it is possible say that if there are equal amount of both structures then the ratio of the peak intensities should be

around 50:50. Using this assumption, it was calculated that if the most favoured mix of C_{16}TAB to SDS was 70:30 for example, as was suggested from the solution scattering results, then an 80:20 mixture would have a peak ratio of the 0.17Å^{-1} peak to the 0.24Å^{-1} peak of 67:33. All the possible peak ratios were calculated and the closest to those observed in Figure 6-19 came out being a mixture of 60:40 C_{16}TAB:SDS, the measured and calculated values are shown in Table 6-4.

Sample	Peak	Relative Intensity	Calculated Peak Ratios				
			50:50	**60:40**	70:30	80:20	90:10
60:40	0.17Å^{-1}	**97**	80	**100**	100	100	100
	0.24Å^{-1}	**3**	20	**0**	0	0	0
70:30	0.17Å^{-1}	**79**	60	**75**	100	100	100
	0.24Å^{-1}	**21**	40	**25**	0	0	0
80:20	0.17Å^{-1}	**50**	40	**50**	67	100	100
	0.24Å^{-1}	**50**	60	**50**	33	0	0
90:10	0.17Å^{-1}	**22**	20	**25**	33	50	100
	0.24Å^{-1}	**78**	80	**75**	67	50	0

Table 6-4. Real and calculated peak intensities for the first two peaks in the line profiles of spray coated C_{16}TAB:SDS films with no polymer.

The same analysis was attempted for films with SPEI however the peak intensities could not be matched up suggesting that for those films the structure is not a simple co-existence of two lamellar phases. This suggests that although the polymer does not have an obvious effect on the structure of the film it does influence how the surfactants mix within the structure. With no extra peak visible in any of these patterns that are not visible in the air/solution films no other details can be extracted from these patterns.

6.3 Conclusions and discussion

Previous work by O'Driscoll et al[71] has shown that as well as forming films with cationic surfactants it was also possible using a mixture of C_{16}TAB and SDS. These films had two advantages over the cationic surfactant films, firstly they were much thicker and secondly they could be formed with polymers other than PEI. Therefore part of this thesis was dedicated to studying the cat-anionic surfactant system to enhance the understanding of these surfactant/polymer thin films.

The method chosen to study these films was to first understand the solutions that make up the films then study the films themselves. In chapter 5 the solution studies

were reported. This study focused on two main regions, firstly the effect of changing the ratio of C_{16}TAB to SDS on the aggregates, and secondly the effect of adding different polymers to solutions. In summary the results showed that the aggregates are very large and that they are not really affected by changing the ratio of C_{16}TAB to SDS. However the addition of polymer does affect the aggregate structures.

From these results the aim of this chapter was to develop understanding of the films formed from the cat-anionic system by studying the films made from the solutions studied in chapter 5. Given the results discussed in chapter 5, the main aim of this chapter was to study the effect of different polymers on the structure and the properties of the films. However, given the difference in viscosity of the 6:4 C_{16}TAB:SDS solution compared to the 7:3 solution, determining the effect on the films of the different ratios of C_{16}TAB:SDS in the solutions is also an aim of this study.

A summary of the results presented in this chapter show that there is a difference in film structure caused by changing the ratios of C_{16}TAB to SDS in the solutions. However this effect is related to the ability of the surfactant to interact with the polymer in the system, therefore it is mainly the polymer that can alter the film structure. It is probably the complexity of the large aggregates that is able to minimise any effect of changing the surfactant ratio on its own.

The current model for film formation suggests the surfactant solution is predominantly made up of vesicles, particularly at surfactant ratios of 60:40 and 70:30 C_{16}TAB:SDS. In making the films the two surfactants were mixed before the polymer was added. The polymer will therefore partition, with the water into and around the vesicles. If there is an interaction between the polymer and the surfactant then the shape of the vesicles may change and the polymer will also be able to bind the vesicles into a larger polymer/surfactant complex. Even if the polymer and surfactant don't interact there should still be enough polymer in solution to bind the vesicles together by interacting with polymer between vesicles and within the vesicles, again forming a polymer-surfactant complex. As this polymer/surfactant complex grows it will become more surface active effectively causing a phase separation to the surface of the solution. At the surface of the solution the rate of evaporation from the solution coupled with a slow diffusion caused by a high concentration of surfactant and polymer at the interface will lead the polymer/surfactant complex to start drying out. As the polymer/surfactant complex dries the concentration of the different species will gradually get higher until the complex appears to have formed a film. Within this film the structure is held in place by the polymer linking the surfactant vesicles.

It had been proposed, within the group, that the cat-anionic films appeared to form slower than the cationic surfactant films. The results here show that although contiguous film formation, visible to the naked eye, might be slower the formation of structure at the interface occurs much quicker. The trend in the data, from the view of changing the surfactant ratios, shows that the more C_{16}TAB in the system the slower the formation appears to be. Given this it may be concluded that the C_{16}TAB only films would take a very long time to form, if they formed at all. Given the cationic surfactant films visually form quicker than the cat-anionic surfactant films it suggests that there may be a different film formation mechanism in the two different systems.

Although a general understanding about the film formation mechanism is apparently fairly straightforward, the more important question in this study is what is the structure of the films? From the earlier work on CTAB-PEI films, there is a sufficient interaction between PEI and cationic surfactants to cause film formation when PEI is almost neutral, although only a weak interaction in the bulk solution was observed.[66] Attempts to prepare similar films using PEI and SDS alone were not successful, so there is no apparent interaction between this pair that induces film formation despite the fact that association between PEI and SDS is well established, even when the polymer is not charged, in bulk solution[157] and multilayer adsorption of a polymer-surfactant complex is observed at interfaces.[36] Nevertheless, no solid film formation is observed in this system, only thin liquid-like adsorbed layers at the interface. PEO does not produce films with either surfactant on its own but is known to have a relatively strong interaction with SDS in solution,[7, 21, 158] forming "beads-on-a-string"-type structures in dilute solutions, although there is only weak cooperatively of adsorption at the air-solution interface.[7, 31] PAAm, however, is thought to have little interaction with SDS or CTAB in solution or toward co-adsorption at the interface.[23]

Given that the d-spacing of the lamella does not appear to change on changing the molar ratio of C_{16}TAB:SDS from 60:40 to 90:10, it is possible that this is an equi-molar mixture of C_{16}TAB:SDS that has precipitated but has been caught up in the film during the formation. This is possible as the two surfactants are mixed together when they are both relatively warm, ~30°C, due to the need to keep the C_{16}TAB solution above its Kraft point of 28°C.[159] The vial the solutions are mixed into is at room temperature along with the polymer solution and this will decrease the temperature of the surfactant solutions rapidly causing small crystallites to precipitate. Given the opaque nature of these solutions these crystallites are not visible to the naked eye.

This formation of a C_{16}TAB:SDS phase and a secondary C_{16}TAB rich phase is supported in two new pieces of work reported here. This first piece of work was the study of films with made with surfactants of varying tail lengths discussed above in the commercial PEI section. This study showed that altering the tail length of the C_nTAB surfactant altered the position of both the two common peaks, at $Q = 0.17Å^{-1}$ and $Q = 0.24Å^{-1}$, whereas the alteration of the sodium alkyl sulfate tail length only really altered the position of the $Q = 0.17Å^{-1}$ peak. As this study was only performed using SAXS of dried films the results are not accurate enough to definitively say that the $0.24Å^{-1}$ peak does not move on the alteration of the sodium alkyl sulfate tail length. The second study that supports this is the spray coated surfactant only film where it can be clearly seen that as the ratio of C_{16}TAB:SDS is altered the relative intensity of the $0.17Å^{-1}$ peak and the $0.24Å^{-1}$ vary as well.

If these two peaks, at $Q = 0.17Å^{-1}$ and $Q = 0.24Å^{-1}$, are part of different structures then the reason that only these two series are consistently seen in most samples may be due to their orientation. Due to the movement of liquid to the interface caused by evaporation the pressure to order perpendicular to the surface is greater than the pressure to form parallel to the surface.[160] This leads to well ordered lamella like structures with less ordering parallel to the interface. When reflectometry is performed the intensity of the scattering from the lamella like layers is much stronger than the scattering from the more disordered structure within the layers. Therefore the intensity and sharpness of the peaks related to the structure orientated with the interface will be much greater than any other peaks.

In the solution data discussed in chapter 5, it was suggested that the solution structures were dependant on the molecular weight of the polymer with the high molecular weight polymers showing multi-lamellar vesicles instead of bilayer vesicles. In the results discussed in this chapter, which are summarised in Table 6-5, the LPEI is not as well structured as the SPEI. The LPEO film however is much more structured than the SPEO film. Given the molecular weight of LPEI is so much higher than the other polymers it appears this polymer cannot rearrange to form well ordered structure. The SPEI however is a lower molecular weight than the SPEO therefore the SPEI must be interacting better with the aggregates than the SPEO. In all cases the 60:40 films are visually thicker than the 75:25 films that are in turn thicker than the 90:10 films.

Surfactant Ratio	SPEI	LPEI	SPEO	LPEO
60:40	$Ia\bar{3}d$	$Ia\bar{3}d$	Lamellar[a]	$Ia\bar{3}d$ [c]
75:25	Distorted $Ia\bar{3}d$ [a]	$Im\bar{3}m$	[b]	[b]
90:10	2D hexagonal	2D hexagonal	$Im\bar{3}m$	$Im\bar{3}m$

Table 6-5. Structural assignments for the films with different molar ratios of surfactant and different polymers as taken from text. All structures apart from those marked with an (a) also contain a series of peaks corresponding to a lamellar phase. (b) These films were not measured.

From this it is then possible to say that the strongest interacting samples lead to an $Ia\bar{3}d$ structure. These structures are the 60:40 films with SPEI, LPEI and LPEO. The SPEO does not interact strongly enough to form any particular structure. The next strongest interacting samples are then probably the SPEI and LPEI with 75:25 ratio of C_{16}TAB:SDS. This can be seen particularly in the SPEI sample as it shows peaks similar to an $Im\bar{3}m$ but they fit more closely to an $Ia\bar{3}d$. This has been suggested to be due to uniaxial compression altering the GIXD patter although it could also be because this sample is on the phase boundary. Following this explanation the next strongest interacting samples are the SPEO and LPEO samples with 90:10 C_{16}TAB:SDS as they show $Im\bar{3}m$ structures, while the SPEI and LPEI samples with the same surfactant show a 2D hexagonal pattern that is very similar to the previously studied C_{16}TAB/PEI films. It is therefore possible that the alteration in aggregate charge density changes the ability of the two polymers to interact with the aggregates to form the films.

These structural assignments were based heavily on data from the publication[102] that was supported by fitting performed with the Garstecki and Holyst model[94, 95] discussed previously. The fitting using the Garstecki and Holyst model has not been included in this report, this is due to the lack of a large number of potential reflections in the real data meaning all the model patterns created have excess peaks which do not line up with any peaks in the real data. Also the models are only written for seven different bi-continuous cubic phases therefore there are a number of other potential non-bicontinuous cubic structures that may also be indexed to the same peaks.

The formation of films from the synthesised polymers adds an extra layer to the understanding. It was expected that the branching of the polymer would help with the formation of film structure based on the ability of the polymer to interact with multiple surfactant aggregates. However what appears to be happening in these results is that the linear polymer is able to form films better than the branched polymers. It appears that the densely branched polymer will have more steric hindrance around the parts of the polymer that interact best with the surfactant

aggregates leading to a weaker interaction between the polymer and the surfactant. In all the synthesised graft polymers the branches are linear chain, this means that they may be able to interact with neighbouring branches limiting their interaction with the surfactant in solution. A similar result has been seen with linear PEI, which is able to hydrogen bond to with other PEI chains making it insoluble at room temperature.[161] This therefore supports the conclusion that it is the chemical nature of the polymer that is most important for film formation even though the surfactant determines the film structure.

Taking these results and trying to determine the parameters that are needed for the best structure and thickest films yields these conclusions. In C_{16}TAB:SDS the films form mostly due to the large surfactant aggregates therefore the polymer needs to be able to interact with multiple surfactant aggregates to bind them all together. This means that the interaction of the polymer and the surfactant is the most important point of the polymer. However with a strongly interacting polymer, such as PEI or PEtOx, a linear polymer will give the least hindrance to interactions between the surfactant and the polymer. A sufficiently high molecular weight of polymer is also required to span across multiple surfactant aggregates however this is also dependent on the ability of the polymer to diffuse in solution. As has been seen with the commercial LPEI, the molecular weight is so high that the film formation is hindered because the polymer is not able to rearrange to give good structure.

If a polymer that has these properties can be found then there is potential to use these polymers for pharmaceutical purposes. Although fairly limited so far, the study of film formation with encapsulated Nile red shows that it is possible to encapsulate small hydrophobic species. The use of Nile red as the dye and PNIPAM as the responsive polymer shows that there is the basis for a more detailed study into potential applications within pharmaceutical industry.

Another area of further study it would be useful to extend is the study of spray coating to include films with PEO and PAAm. Although our main interest is in films formed at the air/solution interface the structural results collected from spray coating are much clearer. Performing the experiments is also much easier as the samples can be prepared in advance, and reflectivity measurements become much quicker as the data collection does not have to wait for the solution surface to become smooth after moving the instrument. Spray coating would also allow much more control over the film formation conditions because the films would be prepared before the experiment allowing the use of chambers to control the ambient conditions during the deposition process.

Using spray coating, a useful experiment would be a repeat of the study of the different tail length surfactants. Using spray coating on ID10B would provide a higher resolution for peak position analysis to determine more accurately any movement of peaks from the altering of the surfactants. This should also be extended to making films with deuterated surfactants and studying these films with neutron reflectivity. Although the neutron data shown in this chapter is not very conclusive, the stronger structure visible in the spray-coated films should increase the chances of seeing structure variation with contrast using neutrons. Also the spray coated films are much more structurally stable therefore comparison of hydrogenated and deuterated samples should be much simpler, as previous chapters have shown that the time resolved nature of the previous neutron data causes problems for comparisons.

Although spray coating appears to be a simpler, quicker, and more reliable method of studying the films, the study of the air/solution interface films is still important because for some applications freestanding films are essential. If the structures of the air/solution interface films are the same as the spray coated films, which they appear to be, then the air/solution films still represent the quickest way to create multi-micron thick films. Also the spray-coated films have yet to be removed from the substrate therefore for potential applications the ease of removal and drying of the air/solution interface films is advantageous. However for rapid fabrication of nanostructured coatings, for example for responsive or self-healing, surfaces spray coating has important potential for extending use of these films to new applications.

7 Conclusions and Future Work

The overall aim of this project was to develop the understanding of nanostructured hydrogel films that had previously been discovered within the group. The starting point for this was the work previously published by Edler et al and O'Drsicoll et al.[8, 59, 66-68, 71] The majority of the work performed by O'Drsicoll et al concentrated on using a cationic surfactant along with the polymer polyethylenimine (PEI) to form a thin nanostructured film at air/water interface. However one publication also showed that it was also possible to create these nanostructured hydrogel films from a mixed cat-anionic surfactant system.

The studies of the cationic films suggested that the structure of these films could be controlled by variation of the surfactant species used to form the films. If these films could be developed into a usable product then any control over the properties could be used to tailor the films to their use. The studies of the cat-anionic surfactant system were much less advanced and therefore it was not clear as to what control there was over these films. However one major advantage of the cat-anionic system was discovered, which was that it allowed film formation with a range of different polymers, instead of just PEI. The use of different polymers could then be used to make the films more biocompatible.

7.1 The Cationic Surfactant System

The cationic surfactant system, discussed in chapters 3 and 4, built on the work by O'Driscoll et al to understand the role of the surfactant in film formation by trying to show control over the film structure. Previously it had been seen that the films of hexadecyltrimethylammonium bromide (C_{16}TAB)/PEI were made up of an array of hexagonal rods, which has been attributed to rod like C_{16}TAB micelles held in a polymer matrix.[67]

The aim of chapter 3 was to show that it was possible to control the structure of the films through rational selection of the surfactants based on the packing parameters. Using two pure surfactant solutions and two mixed surfactant solutions a range of solution structures was created. These solution structures were spheres, ellipses and lamellar sheets. These structures were confirmed using SANS and the effect of adding polymer to the solutions was determined. Following this, films were created from these solutions and studied using x-ray and neutron reflectivity. The results from these films showed that the solutions containing elliptical micelles formed films with structures indicative of a hexagonal array of rods. The solutions with

lamellar structures formed films with structures indicative of repeating bilayers. The films containing roughly spherical micelles formed films with a cubic structure probably indicating a 3-dimensional packing of the micelles.

From these results it was then possible to say that the aim for chapter 3 was achieved and it is possible to control the mesostructure of these films by careful choice of the surfactants being used. Building on this work the next step would be to study a wider range of surfactants. So far these films have only been formed using surfactants with a small quaternary ammonium head group. The next study should therefore be based around variations of the quaternary ammonium head group, such as pyridinium head group surfactants. A further study that may be of interest is a single surfactant through a concentration gradient that includes a phase change. A particular surfactant phase that would of interest to study is a bicontinuous phase[162] as this has previously not been attempted.

For this project, after showing control of the film nanostructure was possible, the next step to was to determine the potential of any applications. The application decided for study was the encapsulation and release of additives. The main reason for this was continuity with previous work by O'Driscoll et al.[68] However the interest in encapsulation and release is due to the uses of thin films as a drug delivery device.[62-64, 118]

The aim of chapter 4 was therefore to use the solutions and films discussed in chapter 3 and show that it was possible to encapsulate small partially soluble species within the surfactant core in the solutions and also into the films. If encapsulation into the films was possible then the next aim was to test whether it could then be released. This data could then be compared and studied in terms of the different structures within the films to determine whether films with different structures are better for encapsulation and release of different species.

The results described in chapter 4 show that it is indeed possible to encapsulate small species into the surfactant solutions, in this case cyclohexane and cyclohexanol. However the encapsulated amounts are fairly low. The films made from these solutions are also believed to contain cyclohexane and cyclohexanol, however it is difficult to determine the quantity. Nile red was also used as a small species for encapsulation and these results, like the cyclohexane and cyclohexanol results, also show encapsulation into the surfactant micelles in small quantities. However in the Nile red samples a phase separation was seen due to the strong colour of the Nile red solution suggesting the full encapsulation of Nile red into the surfactant solutions is higher than determined by SANS. As with the cyclohexane and cyclohexanol results,

the reflectivity was unable to accurately determine the amount of Nile red in the films, however as Nile red is not volatile it was possible to do this using other techniques. The other technique to determine the encapsulation of Nile red in the films was fluorescence spectroscopy, which showed that Nile red was encapsulated in the films and the rate of encapsulation was similar to that seen in the solutions. This technique was also used to study the release, which showed that the Nile red could be released from the film into an aqueous solution but only in small quantities. In relation to the film structure, it was found that the more elongated the structure the more Nile red was encapsulated and also released from the films.

To extend this work in the future, the idea of drug encapsulation and delivery should be put to one side. While the films are made from cationic surfactants they are not very biocompatible. Also to make them strong enough to use they need crosslinking, which is also not biocompatible. Therefore the use of these films for drug encapsulation and release will not be possible until more biocompatible materials can be found. A suggestion for a more biocompatible system would be the use of zwitterionic surfactants, which generally have better biocompatibility. However there is still a use for encapsulation within these films. Although the films are not strong enough on there own for uses such as molecular sieves, if small reactive monomeric species could by encapsulated into the film and then polymerised, it may be possible to create highly ordered polymeric materials for use as molecular sieves.

7.2 The Cat-anionic Surfactant System

The cat-anionic surfactant system, discussed in chapters 5 and 6, was very different to the cationic surfactant system, discussed in chapters 3 and 4, mostly due to the lack of previous studies performed on the system. Apart from a small amount of unpublished work, the main knowledge about this system was taken from a single publication by O'Driscoll et al.[71] Due to this, the main aim of both chapters 5 and 6 was to increase the understanding of the cat-anionic surfactant system.

As with the study of the cationic surfactant system it was decided to study the cat-anionic surfactant system firstly by trying to understand the solutions and then by trying to understand the films and determine how the solutions lead to the films. As O'Drsicoll et al had used a 6:4 ratio of C_{16}TAB to sodium dodecyl sulfate (SDS) it was decided that that should be the starting point of these studies. However early on it was decided to also use a 7:3 ratio as this proved more stable and easier to handle than the 6:4 ratio. Therefore the aim in chapter 5 was to understand the solutions of the mixtures of 6:4 and 7:3 C_{16}TAB:SDS. Particularly, the aims were to study the

effect of changing the surfactant ratio and the effect of adding polymer to the solutions.

Right from the outset this was more complicated than had been expected, as some unpublished scanning electron microscopy images suggested aggregates as large as 2μm. Large aggregates were also seen in the initial small angle neutron scattering (SANS) study of the solutions. Therefore to study these solutions properly both SANS and ultra-small angle neutron scattering (USANS) measurements were made. These measurements showed that large aggregates did exist in the C_{16}TAB:SDS solutions, with sizes in the range 2-4μm. It was determined that the aggregates were large elliptical bilayer vesicles, with the scattering being made up of two patterns, one from the large ellipse, at low Q, and the other from the bilayers, at high Q, which appear to scatter as lamellar structures. Interestingly the alteration of surfactant ratio from 6:4 to 7:3 did not appear to have a large effect on the aggregates. However the addition of polymer did alter the aggregate structures and this alteration was attributed to the strength of the interaction between the polymer and the surfactant.

As well as studying these solutions a few extra studies were also undertaken. The first was with mixing the surfactants at high temperature. This study was performed to determine whether the high viscosity of the room temperature surfactants hindered the surfactant mixing. A study was also performed at one fifth of the standard concentration for the same reason. Both raising the temperature and lowering the concentration lowered the viscosity of the solutions. Both studies lead to smaller aggregates, however it was unclear what effect they had on the surfactant mixing. Also studied was the encapsulation of cyclohexane and cyclohexanol, to provide some comparison with the study in chapter 4. The results of this study were similar to those seen in chapter 4. Finally a study was performed using spin-echo SANS (SESANS) as a comparison and potential alternative to USANS. SESANS appeared to be a useful technique, however without well-developed analysis tools only rough comparisons were possible.

Building on the work in chapter 5, chapter 6 went on to study the films. As with the studies in chapter 5, the main aim is to further the knowledge of these films, with particular attention paid to the effect of different polymers on the films, and the effect of changing the ratio of C_{16}TAB to SDS in the films.

The main result was that the polymer had a major role on the structure of the films, dependant on its interaction with the surfactant aggregates. As the ratio of C_{16}TAB to SDS was varied by increasing the C_{16}TAB and decreasing the SDS, the structure was

seen to change, however this can also be explained by the interaction between the polymer and the surfactant aggregate with stronger interactions occurring when more SDS is present. Overall the films showed two structures, one was determined to be a lamellar structure, probably due to precipitation of equi-molar C_{16}TAB:SDS bilayers. The second structure was determined to be a cubic, however this was difficult due to lack of peaks in the scattering pattern. The reason for the lack of peaks is probably due to the strength of a single series of peaks that represent reflections from a structure well ordered parallel to the air/solution interface. Overall from these studies and those described in chapter 5, the aim of increasing the understanding of the cat-anionic surfactant solutions and film has been achieved. However no definitive conclusions are possible as the system is much more complex than previously anticipated.

Further study of these systems, either as a more detailed study of the surfactant ratios or by using different surfactants or polymers, may help further the understanding more. However to build on what is currently known about these films then a potential next step would be to look at more biocompatible surfactants. For instance a single molecule that may behave in a similar fashion to a C_{16}TAB:SDS pair would be a phosphatidylcholine molecule.

Once again, along with the main study some smaller studies were carried out. One was using specially synthesised poly(2-ethyl-2-oxazoline) polymers and similar branched PEI polymers. However due to the small quantities of these polymers available proper comparisons are difficult.

The other small study was based around using spray coating and spin coating to form films instead of evaporation at the air/solution interface. Spray coating was performed successfully and the films showed similar structures to the films created at the air/water interface. It is this study that exhibits the most potential for future studies into these films. The spray-coated films were more laborious to form than the air/solution films, however as they are created from a single solution they are less labour intensive than current spray coated thin films in the literature.[38] The reason they exhibit the most potential for further study is three fold. The first reason is that the structures are similar to those seen at the air/solution interface. The second reason is that they are quicker to study at facilities as they are already formed on the substrate. The third reason is that because they are formed on a substrate they can be prepared prior to an experiment and transported to the facility. These three reasons mean that spray-coated films could replace air/solution studies but give similar results and more samples could be studied during each facility experiment where time is at a premium.

7.3 Summary

Overall the aim of this project was to increase the understanding of these films. It is possible to say that this aim has been met. The cationic films appear to behave as predicted, which means that the development of these films for a specific application should be straightforward. However as the components are not biocompatible the proposed application discussed of a drug delivery device may not be immediately relevant. The cat-anionic films are much closer to being biocompatible with films already formed out of biocompatible polymers. Also, as mentioned above, it may be possible to use a single biocompatible molecule in place of the C_{16}TAB:SDS pair to also form films. Although, while more is now known about the cat-anionic system as a whole, this system is far more complicated than the cationic surfactant system and still needs more work for proper clarification.

8 References

1. A. L. Lehninger, D. L. Nelson and M. M. Cox, *Lehninger principles of biochemistry*, 4th ed. edn., W.H. Freeman, New York, N.Y. ; Basingstoke, 2005.
2. P. W. Atkins and J. De Paula, *Atkins' Physical chemistry*, Oxford University Press, Oxford, 2002.
3. "Polymers and People" D. J. Tenenbaum, in *Beyond Discovery: The Path from Research to Human Benefit*, by, The National Academy of Sciences, Washington D.C., 2009.
4. D. Myers, *Surfactant science and technology*, 3rd edn., J. Wiley, Hoboken, N.J., 2006.
5. H. M. C. de Azeredo, *Food Res Int*, 2009, **42**, 1240-1253.
6. O. Sonneville-Aubrun, J. T. Simonnet and F. L'Alloret, *Adv Colloid Interfac*, 2004, **108**, 145-149.
7. D. J. F. Taylor, R. K. Thomas and J. Penfold, *Adv Colloid Interfac*, 2007, **132**, 69-110.
8. K. J. Edler, A. Goldar, T. Brennan and S. J. Roser, *Chem Commun*, 2003, 1724-1725.
9. D. J. Shaw, *Introduction to colloid and surface chemistry*, Butterworth Heinemann, 1992.
10. I. Gentle and G. Barnes, *Interfacial science : an introduction*, Oxford University Press, Oxford, 2005.
11. H. Comas-Rojas, E. Aluicio-Sarduy, S. Rodriguez-Calvo, A. Perez-Gramatges, S. J. Roser and K. J. Edler, *Soft Matter*, 2007, **3**, 747-753.
12. "Water-Soluble Polymers" J. E. Glass, in *Kirk-Othmer Encyclopedia of Chemical Technology*, by, John Wiley & Sons, Inc., 2000.
13. "Water-Soluble Polymers" C. L. McCormick, A. B. Lowe and N. Ayres, in *Encyclopedia of Polymer Science and Technology*, by, John Wiley & Sons, Inc., 2002.
14. G. Swift, 1994, **45**, 215-231.
15. D. Schmaljohann, 2006, **58**, 1655-1670.
16. K. Kratz, T. Hellweg and W. Eimer, 2001, **42**, 6631-6639.
17. S. Dai, P. Ravi, K. C. Tam, B. W. Mao and L. H. Gang, *Langmuir*, 2003, **19**, 5175-5177.
18. G. G. Odian, *Principles of polymerization*, 4th edn., Wiley-Interscience, Hoboken, N.J., 2004.
19. G. J. M. Koper, R. C. van Duijvenbode, D. D. P. W. Stam, U. Steuerle and A. Borkovec, *Macromolecules*, 2003, **36**, 2500-2507.
20. A. Jabbarzadeh, J. D. Atkinson and R. I. Tanner, *Macromolecules*, 2003, **36**, 5020-5031.
21. E. D. Goddard, *Colloid Surface*, 1986, **19**, 255-300.
22. E. D. Goddard, *Colloid Surface*, 1986, **19**, 301-329.
23. E. D. Goddard, *J Colloid Interf Sci*, 2002, **256**, 228-235.
24. D. Langevin, *Adv Colloid Interfac*, 2009, **147-48**, 170-177.
25. J. Kwak, *Polymer-surfactant systems*, M. Dekker, 1998.
26. M. N. Jones, *J Colloid Interf Sci*, 1967, **23**, 36-&.
27. H. Lange, *Kolloid Z Z Polym*, 1971, **243**, 101-&.
28. B. M. Folmer and B. Kronberg, *Langmuir*, 2000, **16**, 5987-5992.

29. Y. Moroi, H. Akisada, M. Saito and R. Matuura, *J Colloid Interf Sci*, 1977, **61**, 233-238.
30. E. D. Goddard and R. B. Hannan, *J Colloid Interf Sci*, 1976, **55**, 73-79.
31. D. J. Cooke, C. C. Dong, J. R. Lu, R. K. Thomas, E. A. Simister and J. Penfold, *J Phys Chem B*, 1998, **102**, 4912-4917.
32. M. W. Kim, *Colloid Surface A*, 1997, **128**, 145-154.
33. D. J. F. Taylor, R. K. Thomas, J. D. Hines, K. Humphreys and J. Penfold, *Langmuir*, 2002, **18**, 9783-9791.
34. D. J. F. Taylor, J. Zhang, P. X. Li, R. K. Thomas, J. B. Wang and J. Penfold, *Langmuir*, 2008, **24**, 1863-1872.
35. J. Zhang, R. K. Thomas and J. Penfold, *Soft Matter*, 2005, **1**, 310-318.
36. J. Penfold, I. Tucker, R. K. Thomas and J. Zhang, *Langmuir*, 2005, **21**, 10061-10073.
37. E. Staples, I. Tucker, J. Penfold, N. Warren, R. K. Thomas and D. J. F. Taylor, *Langmuir*, 2002, **18**, 5147-5153.
38. K. Ariga, J. P. Hill and Q. M. Ji, *Phys Chem Chem Phys*, 2007, **9**, 2319-2340.
39. G. Decher, *Science*, 1997, **277**, 1232-1237.
40. Y. Hu, H. Sun and N. F. Hu, *J Colloid Interf Sci*, 2007, **314**, 131-140.
41. F. Caruso, R. A. Caruso and H. Mohwald, *Science*, 1998, **282**, 1111-1114.
42. K. Ariga, J. P. Hill, M. V. Lee, A. Vinu, R. Charvet and S. Acharya, *Sci Technol Adv Mat*, 2008, **9**, -.
43. A. Izquierdo, S. S. Ono, J. C. Voegel, P. Schaaf and G. Decher, *Langmuir*, 2005, **21**, 7558-7567.
44. Z. Q. Lin, D. H. Kim, X. D. Wu, L. Boosahda, D. Stone, L. LaRose and T. P. Russell, *Adv Mater*, 2002, **14**, 1373-1376.
45. M. Michel, A. Izquierdo, G. Decher, J. C. Voegel, P. Schaaf and V. Ball, *Langmuir*, 2005, **21**, 7854-7859.
46. M. Michel, D. Vautier, J. C. Voegel, P. Schaaf and V. Ball, *Langmuir*, 2004, **20**, 4835-4839.
47. J. B. Schlenoff, S. T. Dubas and T. Farhat, *Langmuir*, 2000, **16**, 9968-9969.
48. D. B. Hall, P. Underhill and J. M. Torkelson, *Polym Eng Sci*, 1998, **38**, 2039-2045.
49. F. Marken, A. Vuorema, M. Sillanpaa, L. Rassaei, M. J. Wasbrough, K. J. Edler, W. Thielemans, S. E. C. Dale, S. Bending and D. Wolverson, *Electroanal*, 2010, **22**, 619-624.
50. J. Chluba, J. C. Voegel, G. Decher, P. Erbacher, P. Schaaf and J. Ogier, *Biomacromolecules*, 2001, **2**, 800-805.
51. H. Ai, S. A. Jones and Y. M. Lvov, *Cell Biochem Biophys*, 2003, **39**, 23-43.
52. J. N. Israelachvili, D. J. Mitchell and B. W. Ninham, *J Chem Soc Farad T 2*, 1976, **72**, 1525-1568.
53. G. G. Warr, R. Sen, D. F. Evans and J. E. Trend, *J Phys Chem-Us*, 1988, **92**, 774-783.
54. G. Garg, P. A. Hassan, V. K. Aswal and S. K. Kulshreshtha, *J Phys Chem B*, 2005, **109**, 1340-1346.
55. C. Tanford, *J Phys Chem-Us*, 1972, **76**, 3020-&.
56. P. A. Hassan, S. S. Bhagwat and C. Manohar, *Langmuir*, 1995, **11**, 470-473.
57. H. Hoffmann and G. Possnecker, *Langmuir*, 1994, **10**, 381-389.
58. P. M. Holland and D. N. Rubingh, *J Phys Chem-Us*, 1983, **87**, 1984-1990.
59. B. M. D. O'Driscoll, C. Fernandez-Martin, R. D. Wilson, S. J. Roser and K. J. Edler, *J Phys Chem B*, 2006, **110**, 5330-5336.

60. D. N. Rubingh, *Solution chemistry of surfactants*, Plenum, New York ; London, 1979.
61. M. Corazza, M. M. Lauriola, M. Zappaterra, A. Bianchi and A. Virgili, *J Eur Acad Dermatol*, 2010, **24**, 1-6.
62. M. J. Lawrence, *Chem Soc Rev*, 1994, **23**, 417-424.
63. P. T. Hammond, R. C. Smith, M. Riollano and A. Leung, *Angew Chem Int Edit*, 2009, **48**, 8974-8977.
64. P. T. Hammond, K. C. Wood, H. F. Chuang, R. D. Batten and D. M. Lynn, *P Natl Acad Sci USA*, 2006, **103**, 10207-10212.
65. K. J. Edler, *Aust J Chem*, 2005, **58**, 627-643.
66. B. M. D. O'Driscoll, E. Milsom, C. Fernandez-Martin, L. White, S. J. Roser and K. J. Edler, *Macromolecules*, 2005, **38**, 8785-8794.
67. B. M. D. O'Driscoll, C. Fernandez-Martin, R. D. Wilson, J. Knott, S. J. Roser and K. J. Edler, *Langmuir*, 2007, **23**, 4589-4598.
68. B. M. D. O'Driscoll, A. M. Hawley and K. J. Edler, *J Colloid Interf Sci*, 2008, **317**, 585-592.
69. H. Comas-Rojas, G. Fernandez-Cata, K. J. Edler, S. J. Roser and A. Perez-Gramatges, *J Colloid Interf Sci*, 2009, **339**, 495-501.
70. C. Aberg, E. Sparr, K. J. Edler and H. Wennerstrom, *Langmuir*, 2009, **25**, 12177-12184.
71. B. M. D. O'Driscoll, E. A. Nickels and K. J. Edler, *Chem Commun*, 2007, 1068-1070.
72. M. J. Kim and R. Ryoo, *Chem Mater*, 1999, **11**, 487-491.
73. S. Kripotou, P. Maroulas, P. Sysel, R. Hobzova, J. Kotek and P. Pissis, *J Non-Cryst Solids*, 2006, **352**, 4800-4803.
74. V. A. Bershtein, L. M. Egorova, P. N. Yakushev, P. Sysel, R. Hobzova, J. Kotek, P. Pissis, S. Kripotou and P. Maroulas, *Polymer*, 2006, **47**, 6765-6772.
75. O. Glatter and O. Kratky, *Small angle x-ray scattering*, Academic Press, London, 1982.
76. A. Jackson, in *Introduction to Small-Angle Neutron Scattering and Neutron Reflectometry [online]*, NIST Center for Neutron Research, 2008; Available from http://www.ncnr.nist.gov/summerschool/ss10/pdf/SANS_NR_Intro.pdf
77. R. Pynn, in *Neutron Scattering - A Primer [online]*, Los Alamos Science, 1990; Available from http://www.ncnr.nist.gov/summerschool/ss10/pdf/NeutronScatteringPrimer.pdf
78. B. Hammouda, in *The SANS Toolbox [online]*, NIST Centre for Neutron Research, 2008; Available from http://www.ncnr.nist.gov/staff/hammouda/the_sans_toolbox.pdf
79. Neutron scattering lengths and cross sections, *National Institute of Standards and Technology*, http://www.ncnr.nist.gov/resources/n-lengths/, Last Accessed on 20/10/2010
80. V. Sears, *Neutron News*, 1992, **3**, 26-37.
81. L. Van Hove, *Phys Rev*, 1954, **95**, 249-262.
82. A. Guinier, G. Fournet, C. B. Walker and K. L. Yudowitch, *Small-angle scattering of X-rays*, Wiley ; London : Chapman and Hall, New York, 1955.
83. J. B. Hayter and J. Penfold, *Mol Phys*, 1981, **42**, 109-118.
84. U. Bonse and M. Hart, *Appl Phys Lett*, 1965, **7**, 238-&.

85. J. G. Barker, C. J. Glinka, J. J. Moyer, M. H. Kim, A. R. Drews and M. Agamalian, *J Appl Crystallogr*, 2005, **38**, 1004-1011.
86. C. Vautier-Giongo and B. L. Bales, *J Phys Chem B*, 2003, **107**, 5398-5403.
87. S. R. Kline, *J Appl Crystallogr*, 2006, **39**, 895-900.
88. M. T. Rekveldt, *Nucl Instrum Meth B*, 1996, **114**, 366-370.
89. V. de Haan, *Coherence approach to neutron propagation in spin echo instruments*, Delft University of Technology, Delft, 2007.
90. J. Plomp, *Spin-echo development for a time-of-flight neutron reflectometer*, TU Delft Institutional Repository, Delft, 2009.
91. M. T. Rekveldt, J. Plomp, W. G. Bouwman, W. H. Kraan, S. Grigoriev and M. Blaauw, *Rev Sci Instrum*, 2005, **76**, -.
92. R. Andersson, L. F. van Heijkamp, I. M. de Schepper and W. G. Bouwman, *J Appl Crystallogr*, 2008, **41**, 868-885.
93. A. Nelson, *J Appl Crystallogr*, 2006, **39**, 273-276.
94. P. Garstecki and R. Holyst, *Langmuir*, 2002, **18**, 2519-2528.
95. P. Garstecki and R. Holyst, *Langmuir*, 2002, **18**, 2529-2537.
96. P. Sakya, J. M. Seddon, R. H. Templer, R. J. Mirkin and G. J. T. Tiddy, *Langmuir*, 1997, **13**, 3706-3714.
97. C. Suryanarayana and M. G. Norton, *X-Ray diffraction : a practical approach*, Plenum Press, New York ; London, 1998.
98. H. W. Hillhouse, J. W. van Egmond, M. Tsapatsis, J. C. Hanson and J. Z. Larese, *Micropor Mesopor Mat*, 2001, **44**, 639-643.
99. M. P. Tate and H. W. Hillhouse, *J Phys Chem C*, 2007, **111**, 7645-7654.
100. M. W. Anderson, C. C. Egger, G. J. T. Tiddy, J. L. Casci and K. A. Brakke, *Angew Chem Int Edit*, 2005, **44**, 3243-3248.
101. C. C. Egger, M. W. Anderson, G. J. T. Tiddy and J. L. Casci, *Phys Chem Chem Phys*, 2005, **7**, 1845-1855.
102. K. J. Edler, M. J. Wasbrough, J. A. Holdaway and B. M. D. O'Driscoll, *Langmuir*, 2009, **25**, 4047-4055.
103. T. S. Light, S. Licht, A. C. Bevilacqua and K. R. Morash, *Electrochem Solid St*, 2005, **8**, E16-E19.
104. A. Chatterjee, S. P. Moulik, R. Majhi and S. K. Sanyal, *Biophys Chem*, 2002, **98**, 313-327.
105. P. Greenspan and S. D. Fowler, *J Lipid Res*, 1985, **26**, 781-789.
106. S. A. Buckingham, C. J. Garvey and G. G. Warr, *J Phys Chem-Us*, 1993, **97**, 10236-10244.
107. Y. Ono, H. Kawasaki, M. Annaka and H. Maeda, *J Colloid Interf Sci*, 2005, **287**, 685-693.
108. S. S. Berr, E. Caponetti, J. S. Johnson, R. R. M. Jones and L. J. Magid, *J Phys Chem-Us*, 1986, **90**, 5766-5770.
109. J. F. A. Soltero, F. Bautista, E. Pecina, J. E. Puig, O. Manero, Z. Proverbio and P. C. Schulz, *Colloid Polym Sci*, 2000, **278**, 37-47.
110. N. Jain, S. Trabelsi, S. Guillot, D. McLouglilin, D. Langevin, P. Letellier and M. Turmine, *Langmuir*, 2004, **20**, 8496-8503.
111. D. I. Svergun, L. A. Feigin and G. W. Taylor, *Structure analysis by small-angle x-ray and neutron scattering*, Plenum Press, New York, 1987.
112. M. Bergstrom, J. S. Pedersen, P. Schurtenberger and S. U. Egelhaaf, *J Phys Chem B*, 1999, **103**, 9888-9897.
113. F. Nallet, R. Laversanne and D. Roux, *J Phys Ii*, 1993, **3**, 487-502.
114. F. H. Drake, G. W. Pierce and M. T. Dow, 1930, **35**, 613.

115. K. M. Lusvardi, A. P. Full and E. W. Kaler, *Langmuir*, 1995, **11**, 487-492.
116. C. Fernandez-Martin, S. J. Roser and K. J. Edler, *J Mater Chem*, 2008, **18**, 1222-1231.
117. C. Sanchez, C. Boissiere, D. Grosso, C. Laberty and L. Nicole, *Chem Mater*, 2008, **20**, 682-737.
118. D. J. Irvine, X. F. Su, B. S. Kim, S. R. Kim and P. T. Hammond, *Acs Nano*, 2009, **3**, 3719-3729.
119. T. Bramer, N. Dew and K. Edsman, *J Pharm Pharmacol*, 2007, **59**, 1319-1334.
120. M. Tornblom and U. Henriksson, *J Phys Chem B*, 1997, **101**, 6028-6035.
121. C. Y. Lin, J. X. Zhao and R. Jiang, *Chem Phys Lett*, 2008, **464**, 77-81.
122. http://www.thermoscientific.com/ecomm/servlet/productsdetail_11152_L10497_81967_11957884_-1, Last Accessed on 19/06/2011
123. Y. Kondo, H. Uchiyama, N. Yoshino, K. Nishiyama and M. Abe, *Langmuir*, 1995, **11**, 2380-2384.
124. S. Williams-Daryn and R. K. Thomas, *J Colloid Interf Sci*, 2002, **255**, 303-311.
125. P. Greenspan, E. P. Mayer and S. D. Fowler, *J Cell Biol*, 1985, **100**, 965-973.
126. J. X. Zhao and C. Y. Lin, *Dyes Pigments*, 2010, **84**, 223-228.
127. J. X. Zhao, C. Y. Lin and L. Song, *Acta Chim Sinica*, 2009, **67**, 381-386.
128. T. Zemb, M. Dubois, B. Deme and T. Gulik-Krzywicki, *Science*, 1999, **283**, 816-819.
129. E. S. Kooij, H. Wormeester, E. A. M. Brouwer, E. van Vroonhoven, A. van Silfhout and B. Poelsema, *Langmuir*, 2002, **18**, 4401-4413.
130. M. Bergstrom and J. S. Pedersen, *Phys Chem Chem Phys*, 1999, **1**, 4437-4446.
131. K. L. Herrington, E. W. Kaler, D. D. Miller, J. A. Zasadzinski and S. Chiruvolu, *J Phys Chem-Us*, 1993, **97**, 13792-13802.
132. R. Talhout and B. F. N. Engberts, *Langmuir*, 1997, **13**, 5001-5006.
133. P. Andreozzi, S. S. Funari, C. La Mesa, P. Mariani, M. G. Ortore, R. Sinibaldi and F. Spinozzi, *J Phys Chem B*, 2010, **114**, 8056-8060.
134. V. Tomasic, I. Stefanic and N. Filipovic-Vincekovic, *Colloid Polym Sci*, 1999, **277**, 153-163.
135. C. Letizia, P. Andreozzi, A. Scipioni, C. La Mesa, A. Bonincontro and E. Spigone, *J Phys Chem B*, 2007, **111**, 898-908.
136. B. Tah, P. Pal, M. Mahato and G. B. Talapatra, *J Phys Chem B*, 2011, **115**, 8493-8499.
137. M. T. Yatcilla, K. L. Herrington, L. L. Brasher, E. W. Kaler, S. Chiruvolu and J. A. Zasadzinski, *J Phys Chem-Us*, 1996, **100**, 5874-5879.
138. P. K. Yuet and D. Blankschtein, *Langmuir*, 1996, **12**, 3819-3827.
139. T. Wolff, C. S. Emming, G. Vonbunau and K. Zierold, *Colloid Polym Sci*, 1992, **270**, 822-824.
140. A. Patist, S. Devi and D. O. Shah, *Langmuir*, 1999, **15**, 7403-7405.
141. H. Q. Yin, M. Mao, J. B. Huang and H. L. Fu, *Langmuir*, 2002, **18**, 9198-9203.
142. X. Auvray, T. Perche, R. Anthore, C. Petipas, I. Rico and A. Lattes, *Langmuir*, 1991, **7**, 2385-2393.
143. E. F. Marques, O. Regev, A. Khan, M. D. Miguel and B. Lindman, *Macromolecules*, 1999, **32**, 6626-6637.

144. O. Regev, E. F. Marques and A. Khan, *Langmuir*, 1999, **15**, 642-645.
145. L. F. van Heijkamp, I. M. de Schepper, M. Strobl, R. H. Tromp, J. R. Heringa and W. G. Bouwman, *J Phys Chem A*, 2010, **114**, 2412-2426.
146. X. Wang, E. J. Danoff, N. A. Sinkov, J. H. Lee, S. R. Raghavan and D. S. English, *Langmuir*, 2006, **22**, 6461-6464.
147. E. H. Lucassenreynders, J. Lucassen and D. Giles, *J Colloid Interf Sci*, 1981, **81**, 150-157.
148. S. Kutsumizu, T. Ichikawa, S. Nojima and S. Yano, *Chem Commun*, 1999, 1181-1182.
149. S. Besson, C. Ricolleau, T. Gacoin, C. Jacquiod and J. P. Boilot, *Micropor Mesopor Mat*, 2003, **60**, 43-49.
150. G. E. S. Toombes, A. C. Finnefrock, M. W. Tate, R. Ulrich, U. Wiesner and S. M. Gruner, *Macromolecules*, 2007, **40**, 8974-8982.
151. X. Z. Zhang and R. X. Zhuo, *Langmuir*, 2001, **17**, 12-16.
152. S. Halacheva, G. J. Price, M. J. Wasbrough and K. J. Edler, *Polish J. Appl. Chem*, 2009, **LIII**, 23-30.
153. J. F. Liu and W. A. Ducker, *J Phys Chem B*, 1999, **103**, 8558-8567.
154. C. J. Lawrence, *Phys Fluids*, 1988, **31**, 2786-2795.
155. W. Kern, *Handbook of semiconductor wafer cleaning technology : science, technology, and applications*, Noyes Publications, Park Ridge, N.J., U.S.A., 1993.
156. J. L. Vossen and W. Kern, *Thin film processes*, Academic Press, New York, 1978.
157. M. A. Winnik, S. M. Bystryak, C. Chassenieux, V. Strashko, P. M. Macdonald and J. Siddiqui, *Langmuir*, 2000, **16**, 4495-4510.
158. E. Pettersson, D. Topgaard, P. Stilbs and O. Soderman, *Langmuir*, 2004, **20**, 1138-1143.
159. C. Oelsehlaeger, E. Buhler, G. Waton and S. J. Candau, *Eur Phys J E*, 2003, **11**, 7-20.
160. L. K. Teh, N. K. Tan, C. C. Wong and S. Li, *Appl Phys a-Mater*, 2005, **81**, 1399-1404.
161. S. I. Aksyonov, G. M. Nikolaev, N. A. Klescheva and P. A. Gembitsky, 1977, **62**, 127-139.
162. M. L. Lynch, A. Ofori-Boateng, A. Hippe, K. Kochvar and P. T. Spicer, *J Colloid Interf Sci*, 2003, **260**, 404-413.

Appendix 1. Chemicals used in this thesis.

Surfactants

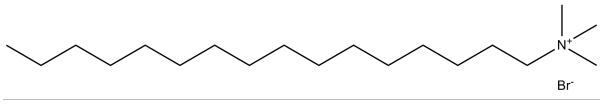

Hexadecyltrimethylammonium Bromide (C_{16}TAB)

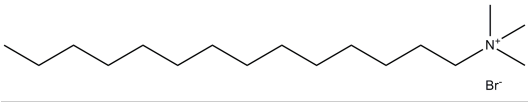

Tetradecyltrimethylammonium Bromide (C_{14}TAB)

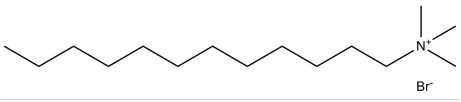

Dodecyltrimethylammonium Bromide (C_{12}TAB)

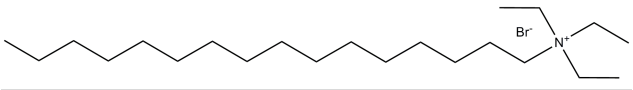

Hexadecyltriethylammonium Bromide (CTEAB)

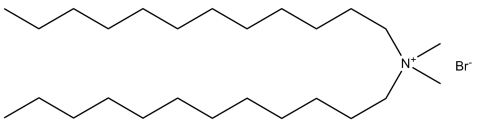

Didodecyldimethylammonium Bromide (DDAB)

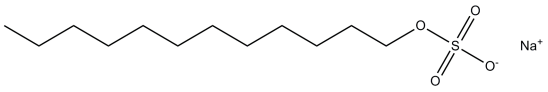

Sodium Dodecyl Sulfate (SDS)

Polymers

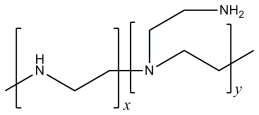

Poly(ethylenimine) (PEI). According to O'Driscoll et al (B. M. D. O'Driscoll, C. Fernandez-Martin, R. D. Wilson, J. Knott, S. J. Roser and K. J. Edler, *Langmuir*, 2007, **23**, 4589-4598.) this is the structure of SPEI although the ratios of x and y are unknown.

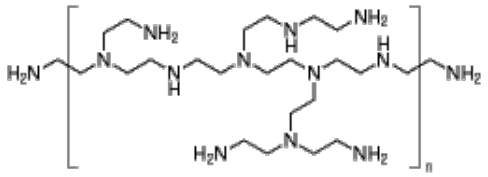

Poly(ethylenimine) (PEI). According to Sigma-Aldrich this is the structure of LPEI. The exact structure is unknown however the ratios of primary, secondary and tertiary amines are 1:2:1.

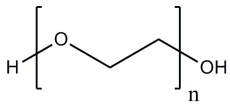

Poly(ethylene oxide) (PEO)

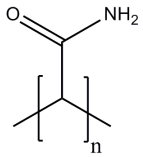

Poly(acrylamide) (PAAm)

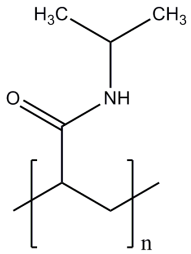

Poly(*N*-Isopropyl acrylamide) (PNIPAM)

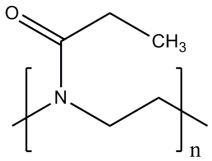

Poly(2-ethyl-2-oxazoline)

Additives

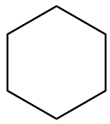

Cyclohexane

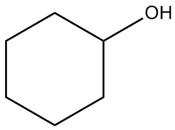

Cyclohexanol

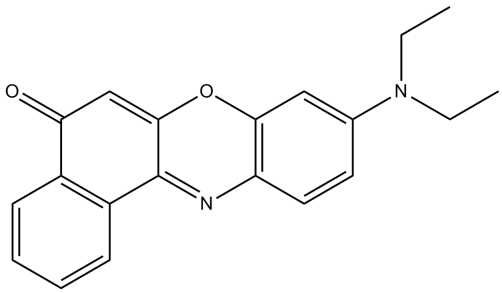

Nile Red

Appendix 2. Fitting model created from papers by Garstecki and Holyst.

This model has been created from P. Garstecki and R. Holyst, *Langmuir*, 2002, **18**, 2519-2528. and P. Garstecki and R. Holyst, *Langmuir*, 2002, **18**, 2529-2537.

Seven procedures have been written, one for each structure described in P. Garstecki and R. Holyst, *Langmuir*, 2002, **18**, 2519-2528. All of the procedures including a loading procedure are available on the supplementary information CD. An example of one of the procedure files is included below. The structure in the procedure is the P surface that has $Im\bar{3}m$ symmetry. The procedure works by calculating the position and intensity and width of peaks corresponding to reflections allowed from the given structure. The parameters needed to determine the position, intensity and width of the peaks are the unit cell dimension, the layer width, the experimental width of a peak at half its maximum intensity, the experimental intensity of the primary peak and the reflection number of the primary peak. The calculated peak positions, intensities, and widths are then converted into Gaussian peaks and appended to a curve for comparison with the experimental data.

```
#pragma rtGlobals=1     // Use modern global access method.


//implements method of Garstecki & Holyst Langmuir 2001 for calculating peak intensities
//note doing lorentz polarization correction to data seems to make small difference to relative peak intensities.

Function PSetup ()

    Make/O Ph ={1,2,2,3,2,3,4,4,3,4,3,4,5,4,5,5,6,5,5,5}
    Make/O Pk ={1,0,1,1,2,2,0,1,3,2,3,2,2,3,3,3,1,4,4,5}
    Make/O Pl  ={0,0,1,0,2,1,0,1,0,0,2,2,1,3,0,2,1,1,3,4}
    Make/O PMhkl ={12,6,24,24,8,48,6,24,12,24,24,24,48,24,24,48,24,48,48,24}
    Make/O PFhkl
…   ={-0.4496,-0.5444,0.4565,0.0985,-0.4056,-0.2177,0.2454,-0.2425,0.2155,0.158,0.2795,0.2536,0.0861,-0.268,-0.1693,-0.1356,0.
…   1577,0.1449,0.1795,-0.207}
    Make/O Palphahkl ={1.14,1,1.03,1,1,1,1,1,1,1,1,1,1,1,1,1,1,1,1,1}

    String Pbwave, Px, Pinten
    Prompt Pbwave, "Background Wave", popup, WaveList("*",";","")+";_none_"
    Prompt Px, "X Wave", popup, WaveList("*",";","")+";_none_"
    Prompt Pinten, "Ywave",popup, WaveList("*",";","")+";_none_"
    Doprompt "Enter Waves",Pbwave, Px, Pinten
    if(V_flag==1)
        KillWaves Ph,Pk,Pl,PMhkl,PFhkl,Palphahkl
        abort
    endif

    Execute "PParamsTable()"

    Duplicate/O $Pbwave Pdata
    Duplicate/O $Pbwave Pbackwave
    Duplicate/O $Px Pxval
    Execute "Pdata:=PFit(Pw,Pxval)"

    Display $Pinten,Pbackwave, Pdata vs Pxval
    ModifyGraph log(left)=1
    ModifyGraph rgb(Pbackwave)=(0,0,0),rgb(Pdata)=(0,52224,0)
    TextBox/C/N=text0/A=MT "P Type"
    TextBox/C/N=AreaVals/A=MB/X=0/Y=0 "\{\"Volume Fraction = %g \"PVolFrac()}\r\{\"Direct Area =
…   %g\"PareaDir()}\r\{\"Inverse Area = %g\"PAreaInv()}"
End

Function PParamsTable ()
    DoWindow/F Pparameters
    if (V_Flag != 0)
        return 0
    endif
    Make /T/O paraPw ={"Unit cell dimension","Layer width","peak full width half maximum","expt intensity 1st peak","Primary
…   Peak","Surfactant Mw"}
    Make /O Pw ={100,20,0.005,0.275,1,334}
    Edit /M/W=(5,5,15,10) paraPw,Pw
    DoWindow/C Pparameters
End

Function PCalc(ww,xx,p)
    Wave ww
    Variable xx, p

    Variable Pint, Pamp
    Variable Pexpt, PLayer,Paa,Psigma,Pprim
    Wave Pw

    Paa = Pw[0]       //Unit Cell Dimension
    PLayer = Pw[1]      //Layer Width
    Psigma = Pw[2]      //Peak full width half max
```

```
    Pexpt = Pw[3]        //experimental intensity of primary peak
    Pprim = Pw[4]        //Primary Peak

    Wave Palphahkl, PFhkl, PMhkl
       Pamp= (((PFhkl[p]*Paa^2)*2*1)/(Palphahkl[p]*xx))*sin(Palphahkl[p]*xx*(PLayer/2))
       Pint= PMhkl[p]*(Pamp^2)
    return Pint
End

Function PFit(wP,xP) : FitFunc
    Wave wP
    Variable xP

    Wave Ph, Pk, Pl, Pbackwave, Pintexpt
    Variable Pexpt, PLayer,Paa,Psigma,Pprim, Pzz,Pout
    Wave Pw

    Paa = Pw[0]        //Unit Cell Dimension
    PLayer = Pw[1]      //Layer Width
    Psigma = Pw[2]      //Peak full width half max
    Pexpt = Pw[3]       //experimental intensity of primary peak
    Pprim = Pw[4]       //Primary Peak

    make/O/N=20 Pintexpt, Pqhkl

    Pqhkl = (2*pi*sqrt(Ph[p]^2+Pk[p]^2+Pl[p]^2))
    Pintexpt = (PCalc(w,(Pqhkl/Paa),p))

    Pzz= Pexpt/Pintexpt[Pprim-1]

       Pout = exp((-((Pqhkl[0]/Paa)-xP)^2)/(2*Psigma^2))*(Pzz*Pintexpt[0])
       Pout = Pout+ exp((-((Pqhkl[1]/Paa)-xP)^2)/(2*Psigma^2))*(Pzz*Pintexpt[1])
       Pout =Pout+  exp((-((Pqhkl[2]/Paa)-xP)^2)/(2*Psigma^2))*(Pzz*Pintexpt[2])
       Pout =Pout+  exp((-((Pqhkl[3]/Paa)-xP)^2)/(2*Psigma^2))*(Pzz*Pintexpt[3])
       Pout =Pout+  exp((-((Pqhkl[4]/Paa)-xP)^2)/(2*Psigma^2))*(Pzz*Pintexpt[4])
       Pout = Pout+ exp((-((Pqhkl[5]/Paa)-xP)^2)/(2*Psigma^2))*(Pzz*Pintexpt[5])
       Pout =Pout+  exp((-((Pqhkl[6]/Paa)-xP)^2)/(2*Psigma^2))*(Pzz*Pintexpt[6])
       Pout =Pout+  exp((-((Pqhkl[7]/Paa)-xP)^2)/(2*Psigma^2))*(Pzz*Pintexpt[7])
       Pout =Pout+  exp((-((Pqhkl[8]/Paa)-xP)^2)/(2*Psigma^2))*(Pzz*Pintexpt[8])
       Pout = Pout+ exp((-((Pqhkl[9]/Paa)-xP)^2)/(2*Psigma^2))*(Pzz*Pintexpt[9])
       Pout =Pout+  exp((-((Pqhkl[10]/Paa)-xP)^2)/(2*Psigma^2))*(Pzz*Pintexpt[10])
       Pout =Pout+  exp((-((Pqhkl[11]/Paa)-xP)^2)/(2*Psigma^2))*(Pzz*Pintexpt[11])
       Pout =Pout+  exp((-((Pqhkl[12]/Paa)-xP)^2)/(2*Psigma^2))*(Pzz*Pintexpt[12])
       Pout = Pout+ exp((-((Pqhkl[13]/Paa)-xP)^2)/(2*Psigma^2))*(Pzz*Pintexpt[13])
       Pout =Pout+  exp((-((Pqhkl[14]/Paa)-xP)^2)/(2*Psigma^2))*(Pzz*Pintexpt[14])
       Pout =Pout+  exp((-((Pqhkl[15]/Paa)-xP)^2)/(2*Psigma^2))*(Pzz*Pintexpt[15])
       Pout =Pout+  exp((-((Pqhkl[16]/Paa)-xP)^2)/(2*Psigma^2))*(Pzz*Pintexpt[16])
       Pout = Pout+ exp((-((Pqhkl[17]/Paa)-xP)^2)/(2*Psigma^2))*(Pzz*Pintexpt[17])
       Pout =Pout+  exp((-((Pqhkl[18]/Paa)-xP)^2)/(2*Psigma^2))*(Pzz*Pintexpt[18])
       Pout =Pout+  exp((-((Pqhkl[19]/Paa)-xP)^2)/(2*Psigma^2))*(Pzz*Pintexpt[19])

    return Pout+Pbackwave
End

Function PVolFrac ()
    Variable Paa, PLayer, PLstar, Pvolfrac, PSparallel, PVdir, PNdir, PAdir
    Wave Pw
    Paa = Pw[0]
    PLayer = Pw[1]
    PLstar = PLayer/Paa
    Pvolfrac = (2.3458*PLstar)+((PI/6)*(-4)*(PLstar^3))
    Return Pvolfrac
End

Function PAreaDir ()
```

```
127     Variable Paa, PLayer, PLstar, Pvolfrac, PSparallel, PVdir, PNdir, PAdir, PMw
128     Wave Pw
129     Paa = Pw[0]
130     PLayer = Pw[1]
131     PMw = Pw[5]
132     PLstar = PLayer/Paa
133     Pvolfrac = (2.3458*PLstar)+((PI/6)*(-4)*(PLstar^3))
134     PSparallel = (2*2.3458*(Paa^2))+(PI*(-4)*(PLayer^2))
135     PVdir = (1-Pvolfrac)*(Paa^3)
136     PNdir = PVdir*(6.022E23/PMw)*1E-24
137     PAdir = PSparallel/PNdir
138     Return PAdir
139 End
140
141 Function PAreaInv ()
142     Variable Paa, PLayer, PLstar, Pvolfrac, PSparallel, PVinv, PNinv, PAinv, PMw
143     Wave Pw
144     Paa = Pw[0]
145     PLayer = Pw[1]
146     PMw = Pw[5]
147     PLstar = PLayer/Paa
148     Pvolfrac = (2.3458*PLstar)+((PI/6)*(-4)*(PLstar^3))
149     PSparallel = (2*2.3458*(Paa^2))+(PI*(-4)*(PLayer^2))
150     PVInv = (Pvolfrac)*(Paa^3)
151     PNInv = PVInv*(6.022E23/PMw)*1E-24
152     PAInv = PSparallel/PNInv
153     Return PAInv
154 End
```

Appendix 3. Alterations made to the SANS model to allow fitting of the percentage additive.

As discussed in chapter 2, scattering is related to the scattering length density contrast between the micelle and the solvent, $\Delta\varrho$. In the fitting functions used in this thesis this is calculated according to:

$$\Delta\varrho = SLD_m - SLD_s$$

Where SLD_m is the scattering length density of the micelle and SLD_s is the scattering length density of the solvent. If you have a binary mixture in the micelle then the scattering is related to the an average of the two components:

$$SLD_m = pSLD_1 + (1\text{-}p)SLD_2$$

Where p is the percentage of component 1 in the micelle and SLD_1 and SLD_2 are the SLDs of the two components. Therefore it is possible to calculate the contrast as

$$\Delta\varrho = (pSLD_1 + (1-p)SLD_2) - SLD_s$$

Changing the equation meant adding some extra parameters as well. An example of the changes is shown below for the uniform ellipse model. The original is shown on the left while the altered version is shown on the right. The full re-written procedure files are available on the supplementary information CD.

```
//The input variables are (and output)
    //[0] scale
    //[1] Axis of rotation
    //[2] two equal radii
    //[3] sld ellipsoid
    //[3] sld solvent (A^-2)
    //[4] background (cm^-1)
    Variable scale, ra,vra,delrho,bkg,slde,slds
    scale = w[0]
    vra = w[1]
    ra = w[2]
    slde = w[3]
    slds = w[4]
    bkg = w[5]

    delrho = slde - slds
//
```

```
//The input variables are (and output)
    //[0] Scale
    //[1] Axis of rotation
    //[2] two equal radii
    //[3] Surfactant SLD (A^-2)
    //[4] Solvent SLD (A^-2)
    //[5] Additive SLD (A^-2)
    //[6] Percent Added
    //[7] background (cm^-1)
    Variable/G scale
    Variable ra,vra,delrho,bkg
    scale = w[0]
    vra = w[1]
    ra = w[2]
    delrho = (w[4]-(((1-(w[6]/100))*w[3])+((w[6]/100)*w[5])))
    bkg = w[7]
    //if vra < ra, OBLATE
    //if vra > ra, PROLATE
//
```

Appendix 4. The model created for SESANS Fitting.

The mathematical model used to simulate the scattering of an ellipse by SESANS was taken from equation 74 in R. Andersson, L. F. van Heijkamp, I. M. de Schepper, and W. G. Bouwman, J. Appl. Crystallogr., 2008, 41, 868–885. Due to the multiple nestled integrals it was quicker for the mathematical function to be performed outside of IgorPro by creating an XOP. An XOP allows the user to extend the programming language of IgorPro to include C++.

The original code for this fit function was written by R. Dalgleish, the OFFSPEC instrument scientist at ISIS. The candidate then adapted it for use as an XOP with IgorPro. The main code for used in the XOP is included here and on the supplementary information CD.

```
/*  SESANS_Ellipse.c

 Notes in here??

*/

#include "XOPStandardHeaders.h"         // Include ANSI headers, Mac headers,
…IgorXOP.h, XOP.h and XOPSupport.h
#include <stdio.h>
#include <stdlib.h>
#include <math.h>
#include <gsl/gsl_integration.h>

// Prototypes
HOST_IMPORT int main(IORecHandle ioRecHandle);


// Custom error codes
#define OLD_IGOR 1 + FIRST_XOP_ERR
#define NON_EXISTENT_WAVE 2 + FIRST_XOP_ERR
#define REQUIRES_SP_OR_DP_WAVE 3 + FIRST_XOP_ERR

#pragma pack(2)     // All structures passed to Igor are two-byte aligned.
typedef struct FitParams {
    double x;               // Independent variable.
    waveHndl waveHandle;    // Coefficient wave.
    double result;
} FitParams, *FitParamsPtr;
#pragma pack()      // Restore default structure alignment

/*

 I might want to put some notes in here.

*/

/*
 ================================================================================
 */
// work with a=b and therefore remove the phi integral
// this introduces an extra factor of pi/2
double p4 (double k, void * params) {
    double r,a;
    double *pars=(double*)params;
    r=pars[0];
    a=pars[1];

    double fa;
    fa=sqrt(a*a*sin(k)*sin(k)+cos(k)*cos(k));
    double x=r/fa;
    double Px;
    if(x<2.0){
        Px=x*x-0.75*x*x*x+0.0625*x*x*x*x*x;
    }else{
        Px=0.0;
    }
    double f=M_PI*Px*sin(k)/(2.0*fa);
    return f;
}
/*
 ================================================================================
 */
double p3(double k, void * params){
    double *pars1=(double*)params;
    double pars[3];
```

```
    pars[0]=k;
    pars[1]=pars1[0];
    pars[2]=pars1[1];
    double z=pars1[2]*2.0;

    gsl_integration_workspace * w = gsl_integration_workspace_alloc (2000);
    double result, error;
    gsl_function F;
    F.function = &p4;
    F.params = &pars;

    double gam;
    if(k!=0.0){
        gsl_integration_qags (&F, 0,  M_PI/2.0, 0, 1e-2, 2000,w, &result, &error);
        gam=2.0*result/(M_PI*k*k);
    }else{
        // the integral divided by k^2 tends to 1 at k=0
        gam=2.0/M_PI;
    }

    double f;
    if(k*k-z*z >= 0.0){
        f=gam*k*pars[1]/sqrt(k*k-z*z);
    }else{
        f=0.0;
    }
    gsl_integration_workspace_free (w);
    return f;
}
/*
 ******************************************************************************************
 */

double SELength(double lambda,double pAngle,double B){
    double h=6.62607e-34;
    double m=1.67493e-27;
    double L=1.0;
    double Gl=1.83247e8;
    double th0=2.31e-3*pAngle*pAngle+5.15e-1*pAngle+2.37e1;
    double c1=Gl*m*2.0*B*L/(2.0*M_PI*h*tan(th0*M_PI/180.0));
    double selength=c1*lambda*lambda*1.0e-9;

    return selength;
}
/*
 ******************************************************************************************
 */

extern "C" int
SESANS_Ellipse(FitParamsPtr p)
{
    double *cp;             // Pointer to coefficient wave.
    double *ip;             // Pointer to instrumental wave.
    double x,r;

    if (p->waveHandle == NULL) {
        SetNaN64(&p->result);
        return NON_EXISTENT_WAVE;
    }
    cp= (double*)WaveData(p->waveHandle);

    gsl_integration_workspace * w = gsl_integration_workspace_alloc (2000);

    double result, error;
    double pars[3] = {1.0,1.0,0.0};
```

```
130     double r1,eta1,rsc,rmax,corrl,volfrac,contrast,sthick,sec;
131     double poleShoeAngle,B,pz,pz2,sigmat,lam;
132     double a;
133 
134     gsl_function F;
135     F.function = &p4;
136     F.params = &pars;
137 
138     volfrac=cp[0];
139     rmax=cp[1];
140     a=cp[2];
141     contrast=cp[3]*1e20;
142     sthick=cp[4]*1e-3;
143 
144     B=cp[5];
145     poleShoeAngle= cp[6];
146     sec=SELength(1.0,poleShoeAngle,B);
147 
148     x=(p->x)/(2.0*rmax);
149 
150     // calculate gamma(0) for normalisation using eqn(7)
151 
152     // r = not quite 0
153     pars[0]=1e-8;
154     // a
155     pars[1]=a;
156     gsl_integration_qags (&F, 0.0, M_PI/2.0, 0, 1e-2, 2000,w, &result, &error);
157     r1=2.0*result/(M_PI*pars[0]*pars[0]);
158 
159     // Caluclate pre factor for G(z) integral (eqn(8))
160     F.function = &p3;
161     // a
162     pars[0]=a;
163     // gamma(0) for normalisation
164     pars[1]=1.0/r1;
165     pars[2]=0.0;
166     gsl_integration_qagiu (&F, 0.0, 0.0, 1e-2, 2000,w, &result, &error);
167     eta1=2.0*result;
168 
169     if(a>1.0)
170     {
171         rsc=2.0*rmax/a;
172         corrl=eta1/2.0;
173     }else{
174         rsc=2.0*rmax;
175         corrl=eta1*a/2.0;
176     }
177 
178         lam=sqrt(x*rsc/sec)+1e-8;
179         pars[2]=x;
180         gsl_integration_qagiu (&F, pars[2],0, 1e-2, 2000,w, &result, &error);
181         r1=2.0*result/eta1;
182 
  … sigmat=(lam*lam*1.0e-18)*sthick*contrast*contrast*volfrac*(1.0-volfrac)*corrl*2.0*rmax*
  … 1.0e-9;
183         pz=exp(sigmat*(r1-1.0));
184         pz2=exp((log(pz)/(lam*lam))*0.209*0.209);
185 
186     gsl_integration_workspace_free (w);
187 
188     r=pz2;
189 
190     p->result= r;
191 
192     return 0;
```

```
193 }
194
195 static XOPIORecResult
196 RegisterFunction()
197 {
198     int funcIndex;
199
200     funcIndex = (int)GetXOPItem(0);         // Which function invoked ?
201     switch (funcIndex) {
202         case 0:                                 // y = SimpleGaussFit(w,x) (curve
  … fitting function).
203             return (XOPIORecResult)SESANS_Ellipse;  // This function is called using
  … the direct method.
204             break;
205     }
206     return 0;
207 }
208
209 /*  XOPEntry()
210
211     This is the entry point from the host application to the XOP for all
212     messages after the INIT message.
213 */
214 extern "C" void
215 XOPEntry(void)
216 {
217     XOPIORecResult result = 0;
218
219     switch (GetXOPMessage()) {
220         case FUNCADDRS:
221             result = RegisterFunction();    // This tells Igor the address of our
  … function.
222             break;
223     }
224     SetXOPResult(result);
225 }
226
227 /*  main(ioRecHandle)
228
229     This is the initial entry point at which the host application calls XOP.
230     The message sent by the host must be INIT.
231     main() does any necessary initialization and then sets the XOPEntry field of the
232     ioRecHandle to the address to be called for future messages.
233 */
234 HOST_IMPORT int
235 main(IORecHandle ioRecHandle)
236 {
237     XOPInit(ioRecHandle);                           // Do standard XOP initialization.
238     SetXOPEntry(XOPEntry);                          // Set entry point for future
  … calls.
239
240     if (igorVersion < 600) {
241         SetXOPResult(OLD_IGOR);
242         return EXIT_FAILURE;
243     }
244
245     SetXOPResult(0);
246     return EXIT_SUCCESS;
247 }
248
```